Monocyte-Derived Osteoclasts as a Platform for Investigating Standard and Novel Treatments for Multiple Myeloma Bone Disease

Hamsa Naser, BSc

Swansea University
Prifysgol Abertawe

Medical School
Ysgol Feddygaeth

Submitted to Swansea University in fulfilment of the requirements for the degree of Doctor of Philosophy (PhD) 2023

Summary

Multiple myeloma is a type of blood cancer originating in the plasma cells of the bone marrow, affecting over 6,000 individuals in the UK annually. As a haematological malignancy, its incidence has increased by 11% in the UK over the past decade, making it the 19th most common cancer in the region. Myeloma bone disease, a severe complication of multiple myeloma, impacts more than 80% of patients, leading to osteolytic lesions, pain, mobility issues, fractures, and neurological deficits. Although not classified as bone cancer, myeloma significantly affects bone health. Current treatments for myeloma bone disease focus on pain management, surgical fracture repair, and radiation therapy to shrink bone lesions, with most therapies aimed at controlling and reducing bone pain. Preventive treatments are needed to mitigate the risk of developing myeloma bone disease.

Direct interactions between myeloma cells and osteoclasts have been shown to increase myeloma cell proliferation and osteoclastic differentiation. This study employs an *in vitro* osteoclast model to explore the mechanisms of osteoclast differentiation and activation. The model serves as a valuable tool for investigating the effects of current myeloma therapies, such as immunomodulatory imide drugs, and for examining potential new treatments like interleukin-4, -10, and -13. The study showcases the use of various endpoint techniques and the development of real-time cell analysis systems to monitor osteoclast differentiation and fusion. Additionally, it demonstrates the application of impedance and clustering to further investigate these changes in response to treatments.

The research provides insights into the differences between peripheral blood and bone marrow-derived mononuclear cells and examines the impact of immunomodulatory imide drugs and interleukins-4, -10, and -13 on the production of pro-inflammatory cytokines by these cells.

Declarations

This work has not previously been accepted in substance for any degree and is not being concurrently submitted in candidature for any degree.

Signed.....[redacted].....

Date.....27/03/2023.....

This thesis is the result of my own investigations, except where otherwise stated. Other sources are acknowledged by footnotes giving explicit references. A bibliography is appended.

Signed.....[redacted].....

Date.....27/03/2023.....

I hereby give consent for my thesis, if accepted, to be available for photocopying and for inter-library loan, and for the title and summary to be made available to outside organisations.

Signed.....[redacted].....

Date.....27/03/2023.....

The University's ethical procedures have been followed and, where appropriate, that ethical approval has been granted.

Signed.....[redacted].....

Date.....27/03/2023.....

Table of Contents

List of Figure

List of Tables

Abbreviations

ANOVA	analysis of variance
ASCT2	Alanine, Serine, Cysteine Transporter
ASIC	Acid sensing ion channel
ATCC	American type culture collection
ATP	Adenosine triphosphate
BD	Becton Dickinson
BF	Bright field
BLIMP	B lymphocyte-induced maturation protein
BM	Bone marrow
BMI	Body mass index
BMM	Bone marrow microenvironment
BMP	Basic metabolic panel
BSA	Bovine serum albumin
CCL	Chemokine ligand
CCR	Chemokine receptor
CD	Cluster of differentiation
CI	Cell index
CK,	creatine kinase
CO_2	Carbon dioxide
COVID	Coronavirus disease
CRAB	Calcium, renal failure, anaemia, bone lesions
CRBN	Cereblon
CT	computerised tomography
CTSK	Cathepsin K
CUL4	Cullin-4 A
CXC	C-X-C motif chemokine
CXCL	C-X3-C motif chemokine ligand
CXCR1	C-X3-C motif chemokine receptor
DAMP	Damage associated molecular pattern
DC	Dendritic cell
DCSTAMP	The dendritic cell-specific transmembrane protein
DDB1	DNA damage-binding protein 1
DKK	Dickkopf1
DMSO	Dimethyl sulphoxide
DNA	Deoxyribonucleic acid
DR	Death receptor
DSMZ	Deutsche Sammlung von Mikroorganismen und Zellkulturen
ECL	electrochemiluminescence
ECM	Extracellular matrix

ELISA	Enzyme-linked immunosorbent assay
FACS	Fluorescence activated cell sorting
FBS	Fetal bovine serum
FISH	Fluorescence In Situ Hybridization
FITC	Fluorescein isothiocyanate
FSC	Forward scatter
GAPDH	Glyceraldehyde 3-phosphate dehydrogenase
H_2SO_4	Sulfuric acid
HCL	Hydrochloric acid
HGF	Hepatocyte growth factor
HIF	Hypoxia-inducible factor
HRP	Horseradish peroxidase
HSC	Haematopoietic stem cell
HSPC	Haematopoietic stem and progenitor cell
ICAM	Intercellular Adhesion Molecule
IFN	Interferon
IGF	Insulin-like growth factor
IKZF	The Ikaros Zinc Finger
IL	Interleukin
IL10R	IL-10 receptor
IL13R	IL-13 receptor
IL4R	IL-4 receptor
IMID	Immunomodulatory imide drug
IRF4	interferon regulatory factor 4
JAK	Janus kinase
LAT	Large amino acid transporter 1
LCDD	Light chain deposition disease
LDH,	Lactate dehydrogenase
LPS	Lipid polysaccharide
MACS	Magnetic activated cell sorting
MALT	Mucosa-associated lymphoid tissue
MAPK	Mitogen-activated protein kinase
MCL	Mantle cell lymphoma
MCP	Monocyte chemoattractant protein-1
MEK	Mitogen-activated protein kinase kinase
MFI	Median fluorescence intensity
MGUS	Monoclonal gammopathy of undetermined significance
MHC	Major histocompatibility complex
MIP	Macrophage inflammatory proteins
MIP	Macrophage Inflammatory Proteins

MM	Multiple myeloma
MMP	Matrix metallopeptidase
MNCs	Mononuclear cells
MRI	Magnetic resonance imaging
MTG	MitoTracker Green
mTOR	Mammalian target of rapamycin
MTR	MitoTracker Red
MW	Molecular weight
NFAT	Nuclear factor of activated T-cells
NK cell	Natural killer cell
OPG	Osteoprotegerin
PAMP	Pathogen-associated molecular patterns
PB	Peripheral blood
PBMCs	Peripheral blood mononuclear cells
PBS	Phosphate buffer saline
PET	Positron emission tomography
PI3K	Phosphoinositide 3-kinase
PRR	Pattern recognition receptors
RANK	Receptor activator of nuclear factor kappa B
RANKL	Receptor activator of nuclear factor kappa B ligand
RNA	Ribonucleic acid
ROS	Reactive oxygen species
RPMI	Roswell Park Memorial Institute medium
RTCA	Real-time cell analyser
RUNX	Runt-related transcription factor
RUO	Research use only
SDF	Stromal cell-derived factor
SDS	Sodium dodecyl sulphate
SEM	Standard error of the mean
SMM	Smoldering multiple myeloma
SOCS	Suppressors of cytokine signalling
SSC	Side scatter
STAT	Signal transducer and activator of transcription
TBS	Tris-buffered saline
TBST	TBS with tween
TEMED	Tetramethyl ethylenediamine
TGF	Transforming growth factor
Th	T helper cell
TIMP	Tissue inhibitors of metalloproteinases
TLR4	Toll-like receptor
TNF	Tumour necrosis factor
TOMM20	Translocase of outer mitochondrial membrane 20
TRAF	Tumour necrosis factor receptor–associated factor

TRAIL	tumour necrosis factor–related apoptosis–inducing ligand
TRAP	Tartrate-resistant acid phosphatase
TYK2	Non-receptor tyrosine-protein kinase
VCAM	Vascular cell adhesion protein
VEGF	Vascular endothelial growth factor

Acknowledgement

I have enjoyed the whole experience and I have learnt so much through the years of doing my PhD at Swansea University. I would like to express my deepest appreciation to my supervisor Professor Cathy Thornton for always believing in me and always pushing me to reach my goal and for supporting me at every stage of the research project. I am also thankful for the support that was provided by my two other supervisors, Dr James Cronin and Dr Nick Jones, who encouraged me and provided technical support on my study. Finally, I would like to extend my sincere thanks to everyone in the CT group and everyone in the PhD office.

And finally, I would like to express my gratitude to my family and friends; I really couldn't have done it without your tremendous understanding and support throughout these years.

Chapter One

Introduction

1.1 General aspects of multiple myeloma

Multiple myeloma (MM) is a haematological cancer that originates in the bone marrow (BM)[1]. It affects plasma cells that differentiate from a type of leukocyte known as B-lymphocytes[2]. The main function of plasma cells is the production of antibodies that provide a specific and remembered defence to the host against foreign bodies and other threats[3]. Despite treatment progress, multiple myeloma is considered an incurable disease, with most patients relapsing after chemotherapy/radiotherapy. In addition, the epidemiology of MM remains unclear. However, risk factors have been identified, such as ageing and obesity.

1.2 Multiple myeloma classification

1.2.1 Revised International Staging System

According to the Revised International Staging System (R-ISS), MM can be classified into three stages based on the measurement of serum albumin, lactate dehydrogenase (LDH), and serum beta-2 immunoglobulin **(**β2-M) and whether high-risk chromosomes are found using fluorescence in situ hybridisation (FISH) test. The stages of MM are as follows:

Stage I:

- Serum β2-M (a small protein that is important in the immune response as it is essential for the presentation of tumor antigens to T cells as a critical component of the MHC class I molecule.) measured at less than 3.5 mg/L
- Serum albumin (a protein made by the liver that is necessary for maintaining good blood volume and general health. Albumin plays a critical role in upholding the oncotic pressure required for the appropriate distribution of body fluids between blood vessels and body tissues. This is measured at 3.5 g/dL or more
- Normal LDH (The levels ranged from 140 units per liter (U/L) to 280 U/L)
- No high-risk chromosome changes in myeloma cells found using FISH test. This is defined as having certain cytogenetic abnormalities, including immunoglobulin heavy chain translocations t(4;14), t(14;16), and t(14;20), del(17p), p53 mutation, 1q gain/amplification, and 1p deletion.

Stage II: Not stage I or stage III

Stage III:

- Serum β2-M is more than 5.5 mg/L, in addition to the presence of one of the following:
- High LDH
- High-risk chromosome changes in myeloma cells found using FISH test

In the case of relapsed or recurrent myeloma, the cancer may need to be staged again (re-staging) using one of the systems above.

1.2.2 Myeloma-defining events

There are many factors the doctor will rely on for an accurate MM diagnosis. These include the overall health of the patient, symptoms and diagnostics tests of blood, urine, and BM biopsies. The following tests may be used to diagnose MM (data sourced from Cancer Research UK, NHS, and Mayo Clinic):

- **M-protein** – Myeloma cells often produce monoclonal immunoglobulin, known as M protein. Blood and urine tests can determine the levels of M proteins, which gives an indication of the extent of the disease, and disease, as well as monitor the response to treatment and whether the disease has relapsed. Some patients only secret a part of the antibody known as the light chain. The levels of M protein in blood or urine can be detected by serum protein electrophoresis or urine protein electrophoresis.
- **The presence of serum-free light chain** – These can be measured in the blood before being filtered by the kidneys. The test is called serum-free light chain assay; it is considered a more sensitive test than measuring M protein in the urine. When light chains are found in the urine, it is referred to as Bence Jones protein. The amount of light chain is measured as a ratio of 100 or more.
- **Immunoglobulin** – The levels of immunoglobulins are measured to check the levels of antibodies in the body. These antibodies can be immunoglobulin A (IgA), immunoglobulin G (IgG), and immunoglobulin M (IgM).
- **Serum albumin and serum β-2M** – The serum albumin and serum β-2M levels are measured using blood tests, reflecting the liver's biosynthetic capacity for proteins and factors.
- **Lactase dehydrogenase (LDH)** – LDH is an enzyme that is present in almost all the tissues in the body. Damage tissues release LDH into the bloodstream, and therefore it is used as an indicator for injury or the presence of a disease. In MM, LDH levels are used to determine the prognosis and also the stage of the disease.
- **Hypercalcemia** – High levels of calcium in the blood can cause various symptoms, such as dehydration, kidney problems, severe constipation, abdominal pain, weakness and confusion. The levels detected in MM are more than 2.75mmol/L serum calcium (normal range 2.15-2.55 mmol/L).
- **Kidney damage** – In amyloidosis, excess light chains produced by abnormal plasma cells accumulate in the tissue, forming an abnormal protein called amyloid. These proteins can cause damage to the kidneys. At the earlier stages of MM, this does not cause any symptoms; however, blood tests and urine tests can detect kidney damage, which is indicated by serum creatinine of more than 177 μmol/L or creatinine clearance of less than 40 mL/min. As the kidneys begin to fail, it loses the ability to get rid of bodily fluids, excess salt and body waste products. This may lead to symptoms such

as weakness, swelling and shortness of breath. Additionally, MM can lead to cardiac complications such as cardiomyopathy and heart failure, which can be caused by cardiac amyloidosis and/or anaemia.

- **Anaemia** – The lack of red blood cell production in the BM can lead to anaemia in patients with MM. This is indicated by haemoglobin less than 100g/L.
- **Osteolytic lesions** – More than one bone lesion that is at least 5mm or larger in size, as picked by an MRI scan.

The main materials and types of equipment used for the diagnosis of MM include the use of an X-ray, where skeletal X-ray is typically the first step in evaluating bones when myeloma is suspected or diagnosed[4,5]. Magnetic resonance imaging (MRI) is an instrumental test in determining whether normal BM has been replaced by myeloma cells or by plasmacytoma, and those images can also be used to detect compression fractures of the spine. Computed tomography (CT) gives a detailed cross-section view of the tumour in the soft tissue. Positron emission tomography (PET) or PET-CT scan can provide images of organs and tissues inside the body where a small amount of radioactive sugar substance is injected into the patient's body. This sugar substance is taken up by cells that use the most energy, and because cancer cells tend to use more energy, they absorb more of the radioactive substance, where a scanner can detect this substance to produce images of the inside of the body[6,7]. BM aspiration and biopsy, these are very similar procedures often done at the same time, where BM biopsy requires the removal of a small amount of solid tissue using needle, whereas a BM aspiration removes the fluid part of the BM with a needle. In case of suspected amyloidosis, a sample of the abdominal fat pad will be examined under a microscope. Additionally, testing for specific chromosomes (cytogenetics test) or genes (FISH test) is another way to determine the presence of the disease and can also help determine treatment options[8].

1.2.3 Symptoms and complications of MM

In the early stages of the disease, myeloma may not cause any symptoms; it is often suspected or diagnosed after a routine blood or urine test. Eventually, myeloma causes a wide range of symptoms (Figure 1.1), such as (data sourced from Cancer Research UK, NHS, and Mayo Clinic):

1. Myeloma bone disease:

- Bone pain - Mainly in the middle or lower back, the rib cage and the hips are the most affected area. This pain is often persistent and aching, and it is usually worsened by movement.

- Bone fractures - Bones that commonly get fractured include the spine and the ribs. Fractures of the spine can lead to the collapsing of the spine with associated height loss and spinal cord compression.
- Hypercalcemia - This occurs when the calcium levels in the blood are too high. It shows in patients, due to the progression of their bone disease that causes excess calcium is released from the affected bones. Symptoms of hypercalcemia include thirst, nausea, vomiting, confusion and constipation.

2. Low blood cell count, a shortage of red blood cells, white blood cells and platelets are common in multiple myeloma. This is due to the presence of myeloma cells in the BM that can crowd out the healthy BM, which prevents the normal number of blood cells from being produced. Furthermore, common myeloma treatments such as bortezomib, daratumumab and thalidomide can also cause low blood cell count as they can affect the production of blood cells within the BM as a side effect of the treatment. Anaemia is caused by reducing the number of red blood cells or the oxygen-carrying haemoglobin they contain. This could be due to the myeloma itself or the treatments given to the patients. This can cause weakness, fatigue, dizziness and breathlessness. Leukopenia refers to a low white blood cell count, which can lower the resistance to serious infections such as pneumonia. Thrombocytopenia is when blood platelet counts are low, which may cause severe bleeding even with minor injuries.
3. Fatigue - This is a common symptom of myeloma. It is a side effect of the treatments given to myeloma patients. It could be caused by anaemia and other factors.
4. Infection - This is a common symptom and complication of MM as infection occurs due to the disease, and the treatments can interfere with the immune system, which reduces the number of leukocytes, making patients more susceptible to infection. Pneumonia is a common and serious infection commonly seen in myeloma patients.
5. Kidney failure can occur in patients for a variety of reasons, such as the abnormal proteins produced by myeloma cells can damage the kidneys, as can hypercalcemia. Some of the treatments for MM can cause kidney damage.

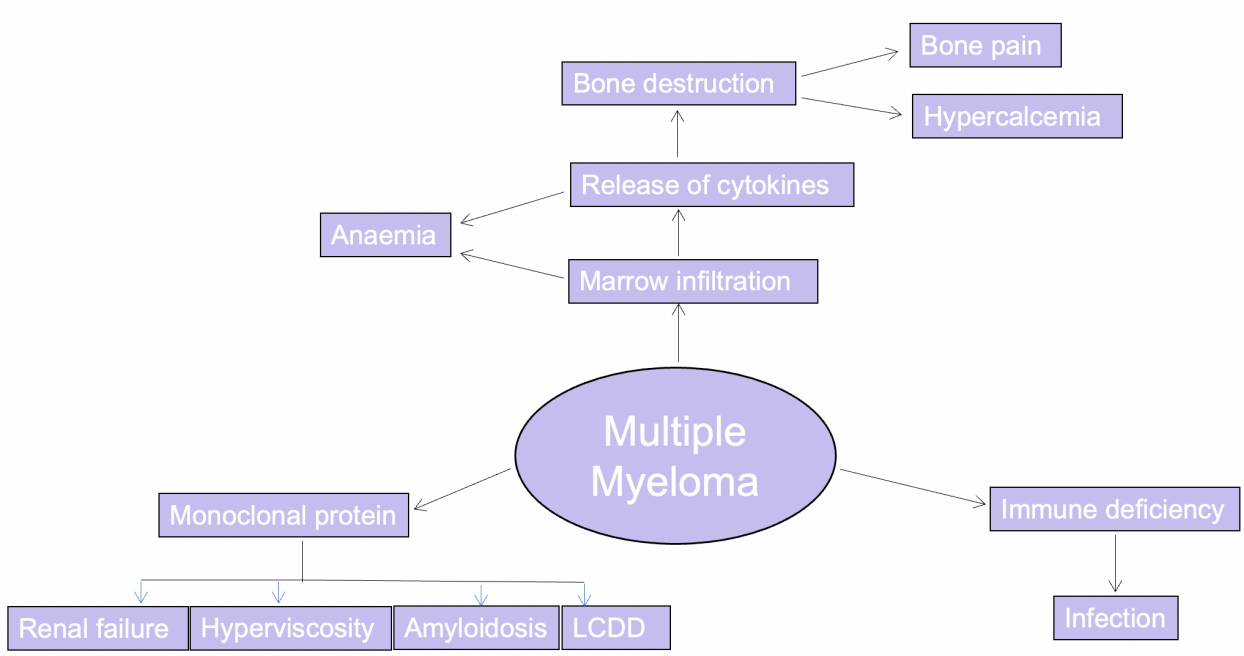

Figure 1.1 Disease manifestations in multiple myeloma

Bone pain and fractures occur due to enhanced bone resorption, usually observed in the lower back, hips and head. Excess bone resorption also leads to the release of calcium into the blood, leading to hypercalcemia and its associated symptoms, such as confusion, weakness, and drowsiness. Lower than normal red blood count can lead to anaemia, causing dizziness and general weakness. M proteins released by myeloma cells can damage the kidneys, causing various complications such as renal failure, hyperviscosity, amyloidosis, and LCDD. Frequent infections occur in patients due to the reduced numbers of immune cells; pneumonia is a common and serious infection commonly seen in myeloma patients. Figure made by the author.

LCDD = light chain deposition disease.

1.2.4 Pre-malignant myeloma-related conditions

In individuals with no symptoms of myeloma but who still have abnormal plasma cells producing M-protein, they must be closely monitored; however, no treatment is prescribed until they show signs and/or experience symptoms of end-organ damage. Pre-malignant disorders can occur prior to developing MM[9]. Individuals diagnosed with these conditions have a high risk of developing MM. Monoclonal gammopathy of undetermined significance (MGUS) is an asymptomatic condition in which M proteins are present in the body, and it is characterised by the presence of serum M protein levels in the blood less than 30 g/L, less than 10% of myeloma cells present in the bone marrow, absence of an end-organ damage (hypercalcemia, anaemia or bone lesions) and absence of B cell lymphoma. MGUS does not

always progress to malignancy. CT scan tests are usually recommended in high-risk patients for the detection of osteolytic bone lesions to rule out MM. The causes of MGUS are unknown. Risk factors that increase the risk of developing this disease include age (diagnosis is usually after 70 years of age)[10], race (African and African Americans are more likely to develop MGUS than are white people)[11], sex (it is more common in men than women)[12,13,] high body mass index (BMI)[14] and family history[13,15]. Due to the increased risk of MGUS developing into multiple myeloma, doctors advise patients to look out for signs and symptoms of multiple myeloma such as bone pain, fatigue, weight loss, bleeding, anaemia and swollen lymph nodes, liver, or spleen.

Smoldering multiple myeloma (SMM) (previously known as asymptomatic MM)[16] is an asymptomatic clonal plasma cell disorder that is often discovered by chance following a routine health check or blood test for another condition. It is considered to be an intermediate stage between MGUS and multiple myeloma[17]. It is regarded as a precancerous condition that alters the levels of certain proteins in the body and increases plasma cells in the BM but does not cause symptoms of the disease. SMM is characterised by the presence of paraprotein levels in the blood at 30 g/L or more and in the urine 500 mg or more per 24 hours and the presence of 10-60% myeloma cells in the bone marrow[18,19]. Over half of the individuals diagnosed with SMM develop MM within 5 years. As no symptoms are presented, high-risk patients are closely monitored for evidence of the progression to active MM, such as end-organ damage. There are other abnormal plasma cell-related disorders; these include solitary plasmacytoma and light chain amyloidosis[20,21]. The abnormal protein in MGUS and SMM begins to form within the BM that dispenses into the blood stream[20].

SMM is distinguished from MGUS in its clinical presentation, as in SMM there is monoclonal protein of more than 3 g/dL and 10-60% clonal bone marrow PCs (BMPCs) and no evidence of any end organ damage. The acronym CRAB refers to the most typical manifestations observed with MM; these being hypercalcemia, renal failure anaemia, and bone disease[22,23.] The presence of CRAB is used to distinguish between symptomatic active MM and MGUS or SMM (Table 1.1). In SMM, abnormal plasma cells can be detected in the bone marrow and abnormal protein can be detected in the blood and urine; patients do not show the typical symptoms of active MM such as those associated with kidney, blood calcium, paraprotein and light chain, immune system, or bone problems[24.] Like MGUS, SMM does not require treatment[25]. However, patients with SMM should be monitored for their progression to active MM as it was shown that there is a direct relation between the risk of progression from SMM to MM and the amount of serum monoclonal protein level along with the number of bone marrow plasma cells[26.]

Disorder	Definition
MGUS	All 3 criteria must be met
	Serum monoclonal protein (non-IgM type) <3 g/dL
	Clonal bone marrow plasma cells <10%
	Absence of end-organ damage, such as hypercalcemia, renal insufficiency, anaemia, and bone lesions that can be attributed to the plasma cell proliferative disorder
SMM	Both criteria must be met:
	Serum monoclonal protein (IgG or IgA) 3 g/dL, or urinary monoclonal protein 500 mg/24 h, and/or clonal bone marrow plasma cells 10% to 60%
	Absence of myeloma-defining events or amyloidosis
Multiple Myeloma	Both criteria must be met:
	Clonal bone marrow plasma cells 10% or biopsy-proven bony or extramedullary plasmacytoma
	Any 1 or more of the following myeloma-defining events:
	Evidence of end-organ damage that can be attributed to the underlying plasma cell proliferative disorder, specifically:
	Hypercalcemia: serum calcium >25 mmol/L (>1 mg/dL) higher than the upper limit of normal or >275 mmol/L (>11 mg/dL)
	Renal insufficiency: creatinine clearance <40 mL/min or serum creatinine >177 µmol/L (>2 mg/dL)
	Anemia: hemoglobin value >2 g/dL below the lower limit of normal or a hemoglobin value <10 g/dL
	Bone lesions: ≥1 osteolytic lesion on skeletal radiography, CT, or PET/CT
	Clonal bone marrow plasma cell percentage 60%
	Involved/uninvolved serum FLC ratio 100 (involved FLC level must be 100 mg/L)
	>1 focal lesion on MRI studies (≥5 mm in size)

Table 1.1 Summary of diagnostic criteria for MM and related disorders.

MGUS = Monoclonal Gammopathy of undetermined significance; SMM = smoldering multiple myeloma; FLC = free light chain; CT = computed tomography; PET = Positron emission tomography.

1.2.5 Role of plasma cells in healthy individuals

Plasma cells are a subset of B lymphocytes developed from B lymphocytes that have become antigen-activated[27]. The differentiation process initiates as vital transcription factors such as B-lymphocyte-induced maturation protein 1 (BLIMP-1)[28], interferon regulatory factor 4 (IRF4) and x-box binding protein (XBP-1) are being induced in the lymphoid organs[29]. Mature plasma cells have a lifespan of 2-3 days, and during this time, they continuously secret antibodies with antigen specificity to the antigen that stimulates the differentiation and proliferation of parental B cells and then plasma cells[30]. With a single plasma cell estimated to produce hundreds of antibodies per second, they are considered antibody factories and are vital contributors to humoral immunity[31] (Figure 1.2). Plasma cells are also important in immune response regulation, as they inhibit the development of follicular T-helper cells by using an antigen-specific negative feedback loop[32,33].

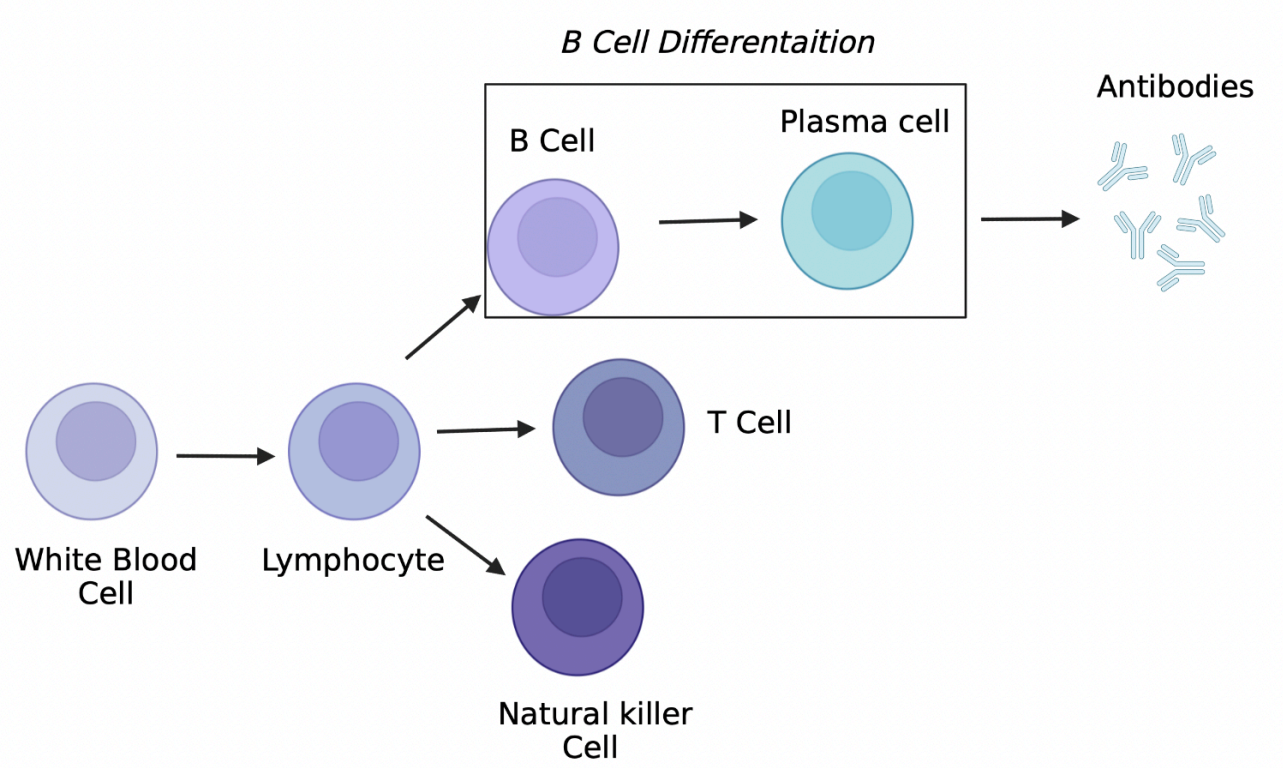

Figure 1.2 Schematic illustration of plasma cell development.

Plasma cells play a significant role in the adaptive immune system. Plasma cells develop from B lymphocyte white blood cells that have been activated. Plasma cells can produce immunoglobulins or antibodies that can attach to and destroy invading viruses or bacteria. T cells can directly fight foreign invasion and produce cytokines that activate the immune system. Figure made using BioRender.

1.2.6 B cell differentiation into memory and plasma cells

B lymphocytes develop from the BM multipotent stem cells. When naïve B cells navigate through secondary lymphoid tissues and encounter foreign antigens, they differentiate into multiple fates depending on the type, strength and timing of signals received within the lymphoid microenvironment[34,35]. Within the germinal centre (GC), B cells undergo somatic hypermutation, isotype switching and affinity-based selection, which results in the generation of long-lived memory B cells and plasma cells. These two cell types can migrate from the GC to specific sites such as splenic red pulp, medullary cords of lymph nodes or mucosal-associated lymphoid tissues (MALT) of the guts for long-lived plasma cells, or splenic marginal zone or tonsillar epithelium for memory B cells[36–38]. T cell-dependent antigens induce naïve B cells to become short-lived antibody-producing plasma cells that localise to extrafollicular regions of lymphoid tissues. Plasma cells can depart from the tissue of origin and enter the circulatory system and reside mainly in the bone marrow. The migration of plasma cells from

the GC requires several changes in the expression of chemokine receptors as they downregulate the B zone and the T zone homing receptors chemokine CXC receptor (CXCR) 5 and chemokine CC receptor (CCR) 7 as well as increasing CXCR4 expression. The CXCR4-CXCL12 axis is essential for plasma cell migration into the BM[38]. Additionally, plasma cells can be generated from memory B cells upon exposure to the initial antigen. Therefore, plasma cells can be generated from several precursors at different stages during an immune response: naïve B cells can generate short-lived plasmablasts that provide the first line of protection; GC B cells can yield high-affinity long-lived plasma cells, and finally, B memory cells can generate long-lived plasma cells upon encounter with specific antigens[37] (Figure 1.3).

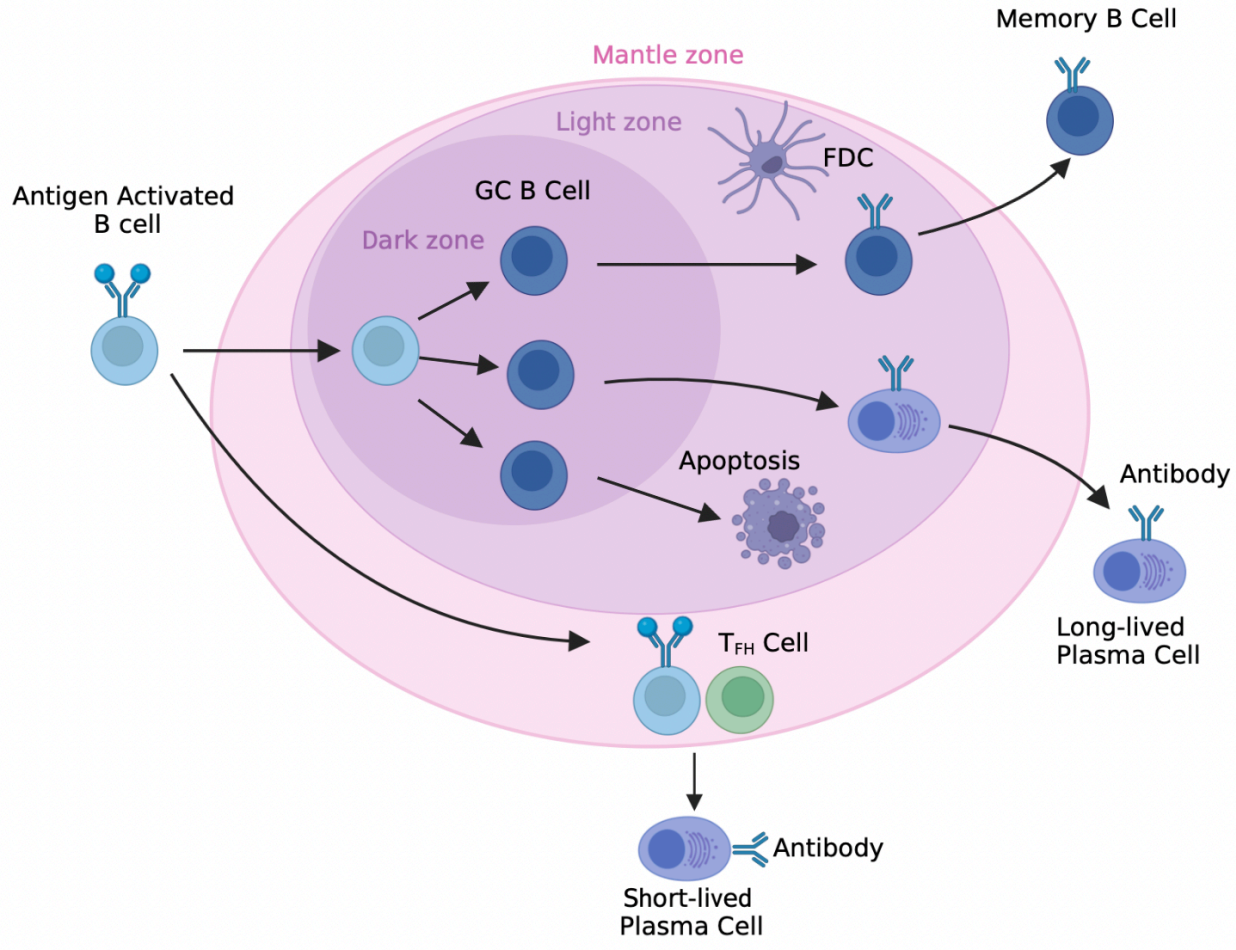

Figure 1.3 B cell development and differentiation.

B cells develop from multipotent stem cells present in the bone marrow. Encounters with antigens cause naïve B cells to differentiate into short-lived plasmablasts, secreting mainly IgM. These cells provide the first line of defence against infection. Activated naïve B cells can

also reside in a germinal centre, where they mature and differentiate into long-lived memory and plasma cells. Memory B cells and plasma cells can then travel into specific sites such as MALT, BM, and splenic red pulp, where they receive signals from neighbouring cells. Figure made using BioRender.

1.2.7 From plasma cells to myeloma cells

Myeloma cells form when plasma cells grow out of control. Myeloma cells happen when healthy cells turn into abnormal cells that multiply, causing various issues within the body[27]. These myeloma cells produce abnormal immunoglobulins that are known by several names, including monoclonal proteins (M-protein), monoclonal immunoglobulins, M-spike and paraprotein[39]. The uncontrollable proliferation of myeloma cells in the bone marrow can prevent normal cell production, such as red blood cells, platelets and other white blood cells. They affect bones and the ability to produce healthy white blood cells, red blood cells and platelets. The causes of MM are still unclear; however, it is known that MM begins with abnormal plasma cells in the bone marrow that multiply rapidly (see Table 1.2 for the most occurring mutation in MM) [1,12]. Acquired mutations can cause multiple myeloma; risk factors such as family history, age, race, lifestyle and exposure to radiation and chemicals can also increase the risk of developing MM. As explained in *1.2.4 pre-malignant myeloma-related conditions,* Multiple myeloma can also develop from asymptomatic pre-malignant disorders such as MGUS and SMM[12,13].

Gene	Mutation Type	Impact on Disease
KRAS	Point mutations	Activates MAPK pathway, increasing proliferation and survival
NRAS	Point mutations	Similar to KRAS, leads to increased cell growth and survival
BRAF	Point mutations	Activates MAPK pathway, promoting cell proliferation and survival
TP53	Deletions, point mutations	Loss of tumour suppressor function, leads to genomic instability
CCND1	Translocations	Overexpression leads to cell cycle dysregulation and increased proliferation
MYC	Translocations, amplifications	Drives cell growth, proliferation, and metabolism
FGFR3	Translocations, point mutations	Activates signalling pathways leading to cell proliferation
MMSET (WHSC1)	Translocations	Epigenetic modifications leading to altered gene expression
TRAF3	Deletions	Loss leads to increased NF-kB activity, promoting cell survival
CYLD	Mutations, deletions	Negative regulator of NF-kB pathway, mutations lead to pathway activation

Table 1.2 A table highlighting the main mutations occurring in MM[40-49].

1.3 Bone marrow microenvironment in healthy individuals

The bone marrow microenvironment (BMM) is a cellular system within the marrow that serves as a vital and dynamic support system for hematopoiesis[50]. It consists of different cell types as well as cytokines and matrix proteins that are vital for the proliferation and differentiation of hematopoietic stem cells (HSC) and the maturation of lineage-specific precursor cells[51,52]. The BMM represents a complex system that comprises of several niches which communicate precisely with each other to regulate the development of the cells belonging to each hematopoietic lineage[53].

In the adult human bone marrow, about 500 billion mature blood cells of different types are produced daily by a pool of hematopoietic stem cells (HSC)[54]. Hematopoiesis is the process by which HSCs differentiate into blood cells that belong to myeloid and lymphoid lineages[55]. Myeloid lineage cells include megakaryocytes, erythrocytes, dendritic cells, mast cells, granulocytes (basophils, neutrophils, eosinophils) and monocytes[56]. Lymphoid lineage cells include T and B lymphocytes, natural killer cells, and plasma cells[57]. The HSC pool serves to concurrently replace the number of all blood cells that are consumed daily while maintaining a pool of HSCs that will allow the individual to maintain hematopoiesis throughout their life[58]. As HSCs have the ability to replicate themselves and regenerate multiple different blood cell types, they are considered multipotent[59]. The potency of cells refers to the ability of a cell to differentiate into other cell types. Totipotent cells have the ability to differentiate into subtypes of cells, such as extraembryonic and placental cells[60,61]. Pluripotent cells can differentiate into any cell type that can make up the body[62]. The HSC compartment consists mainly of long-term repopulating HSCs (LT-HSC), short-term repopulating HSCs (ST-HSC) and multipotent progenitor (MPP) cells[63]. LT-HSCs are located near the endosteum of the bone marrow in a hypoxic environment where most of them are in a quiescent state. Upon stress, LT-HSCs enter the cell cycle and differentiate into all types of blood cells[64]. The fate of HSCs is controlled by intrinsic and extrinsic factors[65,66]. Intrinsic factors utilise transcription factors, epigenetic modifiers and non-coding RNAs[67]; extrinsic factors include the changes in stem cell fate dictated by the microenvironment, such as the release of cytokines and growth factors, as well as physical interactions with the cells within the niche[68]. Transcription factors are thought to be responsible for the regulation of HSC renewal and differentiation. The two essential transcriptional factors involved in HSC specification are RUNX1 and GATA1[69,70]. RUNX1 plays a role in early embryonic blood cell lineage development alongside CBF-b

through several mechanisms to allow the transition from hemogenic endothelium to HSCs[71,72]. GATA1 plays an important role in the differentiation of hematopoietic progenitors to erythrocytes, megakaryocytes, mast cells, eosinophils, and basophils[73,74]. GATA2 is important to the expression of all hematopoietic lineages, and high levels of GATA2 prevent differentiation which helps in preserving the immature HSC pool whereby low GATA2 levels initiate HSC commitment[75]. Epigenetic modifiers allow either the activation or deactivation of gene expression without altering the genetic sequence. These include histone modification (e.g., methylation and acetylation), chromatin remodeling and DNA methylation, which is responsible for the repression of the methylated genes that are necessary for HSC[76,77].

1.3.1 Extrinsic factors that affect the HSC niche

1. Hypoxia **-** The adult BM is hypoxic with an absolute level of pO2 less than 32mmHg and 10 mmHg in the deeper peri-sinusoidal regions in the BM of live animals[78]. BM is hypoxic due to the limited afferent arterioles and the active consumption of oxygen during hematopoiesis[79]. Hypoxia is associated with HSC quiescence and retention[80]. Low oxygen tension induces the stabilisation of hypoxia-inducible factor (HIF)1-α which promotes the quiescence of HSC preventing their exhaustion by reducing the proliferation rate via modulating CDK1 function[81]. HSCs in the BM niche contain less reactive oxygen species (ROS) and are therefore, less susceptible to oxidative stress. Additionally, the difference in oxygen tension of the BM significantly affects and regulates the interactions of HSCs and the niche environment in a co-culture system[82].
2. The nervous system - hematopoietic stress can be triggered by the innervation of autonomic and sensory nerves throughout the BM[83,84]. HSC mobilisation can occur due to the stimulation of the β_3-adrenergic receptor[85], which activates the sympathetic nervous system. In addition, nonmyelinated Schwann cells have been shown to play a role in HSC quiescence[85].

1.3.2 intrinsic factors that affect the HSPC niche

Epigenetics modifications- these include the changes in the chromatin structure underlie the differentiation of HSCs into their committed progenies. Important examples of these include EZH2, which controls gene repression through the recruitment of histone deacetylases followed by chromatin deacetylation and methylation of histone H3 lysine 27; BMI-1 is recruited for the methylation of histone H3 lysine 27 and has a role in the maintenance of the epigenetic memory.

1.3.3 Components of HSC microenvironment

Most of the time, HSCs reside in the BM niche, which is composed of multiple cell types, including endothelial, osteoblastic, and stromal cells that emanate signals which play an important role in regulating HSC behaviour.

Osteoclasts - whereas osteoblasts are derived from MSCs, osteoclasts are derived from monocytes which are of hematopoietic origin. These cells are multinucleated and considered polykaryons[86,87]. They exhibit phenotypic variability and may derive from distinct progenitors, contingent upon their environmental conditions, the stimuli they are exposed to, and their developmental phase[88].

They are precisely located in the lacunae on the bone surface and are close to the stem cell niche[89]. These cells provide important proteolytic enzymes that are essential for the breakdown of bone and subsequent bone remodeling[90,91], providing space into which the hematopoietic tissue expands[92]. Under stress, osteoclasts produce proteases which promote stem cell mobilisation[93,94]. Some work shows osteoclasts being dispensable in maintaining and mobilising HSCs by G-CSF[95], and that they might function as negative regulators in the hematopoietic system[96]

Endothelial cells- these cells line the vasculature and play an essential role in the homing of the HSCs[97]. The two types of endothelial cells in the BM are arteriolar and sinusoidal endothelial cells[98]. They release an array of cytokines and express adhesion molecules such as intercellular adhesion molecule-1 (ICAM-1), vascular cell adhesion molecule (VCAM-1), E-selectin and P-selectin[99]. Another important protein produced by endothelial cells is C-X-C motif chemokine ligand 12 (CXCL12, also known as the stromal cell-derived factor (SDF)-1[100,101], which is required for the maintenance of the HSC pool. E-selectin is important in preventing HSC quiescence and promotes HSC proliferation, so it negatively regulates stem cell quiescence[101,102]. Therefore, endothelial cells are important in hematopoietic regeneration and can aid in myelosuppressive injuries through the release of factors mentioned above, including pleiotrophin[103].

Bone marrow macrophages- these are large phagocytic cells that are part of the immune system that respond to infection and tissue damage[104,105.] In the BM niche, they help to retain HSCs, as a reduction in their levels in the BM causes HSC egress to the blood tream[106,107].

Megakaryocytes- these are the largest of the hematopoietic cells and are platelets precursors essential in maintaining the HSC pool size[108]. These cells promote the quiescence of HSC through the expression of adhesion proteins such as CXCL4 and growth factors such as TGFb[109,110]. The interaction of thrombopoietin (THPO) and its receptor MPL triggers megakaryocytes to produce an extracellular matrix composed of collagens and fibronectin, which allows the self-renewal and quiescence of HSCs in adult BM. In addition, THPO/MPL is important in the maintenance of quiescent HSCs and the megakaryocyte niche[111,112].

Regulatory T cells (Tregs)- are subsets of T cells that express transcription factors such as Foxp3 and are highly important in maintaining immune homeostasis[113,114]. The main type of Tregs present in the BM is a $CD150^{high}$ subset in close proximity to HSCs where they promote and maintain HSC quiescence via the secretion CD73[115]. In addition, Tregs support the plasma cell population in the BM and prevent loss of the plasma cell population during infection[116].

1.3.4 Components of HSC microenvironment-mesenchymal stem cells (MSCs)

Mesenchymal stem cells (MSCs) are non-hematopoietic stem cells which are located in the bone marrow and have the ability to differentiate into different types of stromal cells, adipose cells and osteoblasts, amongst others[117]. These cells are limited in their presence in the bone marrow to approximately 1 per 10,000 cells. MSCs express definitive cell surface markers, including CD73, CD90 and CD105 but do not express classical hematopoietic cell surface markers such as CD11b, CD14, CD34, CD45 and CD14[118,119,120]. They also lack expression of MHC-II, CD40, CD80, and CD86[120], which is considered to make them hypoimmunogenic[120,121]. The main types of mesenchymal cells within the BM include osteolineage progenitors[122,123], perivascular cells and adipocytes. Immature mesenchymal stem cells also regulate HSCs. Types of mesenchymal stem cells are as follows:

Osteolineage cells- these support hematopoiesis through their release of cytokines, such as granulocyte colony-stimulating factor (G-CSF)[123], interleukin-6 (IL-6)[124] and hepatocyte growth factor (HGF)[125]. These cells reside on the endosteal surfaces of trabecular and flat bones were bone and BM contact[126]. When these cells become terminally differentiated, they reside permanently within the bone matrix[127]. In osteoblasts, transcription factors such as RUNX2 and osterix promote their differentiation, which allows osteoblasts to exclusively express the extracellular matrix protein osteocalcin[128,129].

In addition, osteoclasts originate from the myeloid cell lineage that can promote HSC quiescence through the production of thrombopoietin, angiopoietin 1, CXCL12, the ECM protein osteopontin and Wnt pathway regulators. The signalling from these cells promotes the retention of HSCs in the BM. In the absence of osteoclast activity, a defective form of the HSC niche in the BM, which leads to the accumulation of undifferentiated HSCs in the spleen. This defect includes a modification of the phenotype of the mesenchymal cells involved in the HSPC niche, which has a negative effect on the differentiation of osteoblasts[130,131].

Perivascular cells- these cells and HSCs co-localize near the sinusoids and the balance between maintenance and differentiation depends on the perivascular niche of the HSC[132]. These cells support the HSC in vitro and are able to form a highly organised BM niche where active hematopoiesis is taking place[133]. Three types of perivascular cells have been identified.

These include CXCL12-abundant reticular cells (CAR cells), nestin-GFPdim/leptinR+ mesenchymal stem cells and nestin-GFPbright/NG2+ pericytes, which all contribute to HSC differentiation[134,135,136].

Adipocytes-these are fat cells that infiltrate the BM as it ages. Adipocytes were thought to be negative regulators of the BM niche and osteoblasts as adipocyte number was inversely proportional with hematopoietic activity in the BM and osteoblasts [137]. However, this theory is challenged by identifying the role of adipocytes in resorting stem cell regeneration and hematopoiesis upon chemotherapy and radiotherapy[138,139].

1.4 Pathogenesis of bone pain in multiple myeloma

As mentioned earlier, multiple myeloma (MM) is a type of blood cancer characterised by the abnormal growth of plasma cells, leading to bone disease. The most common complication of multiple myeloma is the development of osteolytic bone lesions, primarily found in the skull, spine, and hips.

Over recent years, many studies have been conducted to help elucidate the mechanisms and factors that promote the development of bone pain in MM (Figure 1.4). These include clinical studies that investigate the type, location and intensity of pain in myeloma patients[140]. However, a greater understanding of the mechanisms underpinning the development of bone lesions and fractures in patients with MM is still required.

Interactions between MM cells and bone marrow stromal cells (BMSC) are crucial for the development of bone disease[141]. Adhesion molecules, such as vascular cell adhesion molecule 1 (VCAM-1) on BMSCs and α4β1 integrin on MM cells allow cell-cell interactions that lead to the upregulation of autocrine and paracrine factors. These factors promote the development of MM cells and stimulate osteoclast activity particularly by reducing the effect of negative regulators of osteoclast activation/differentiation[142,143]. These stimulators include interleukin-6 (IL-6), interleukin-1α (IL-1α), interleukin-1β (IL-1β), interleukin- 3 (IL-3), tumour necrosis factor (TNF) α, macrophage inflammatory protein-1α (MIP-1α) and MIP-1b, hepatocyte growth factor (HGF), Stromal cell-derived factor-1α (SDF-1α), Annexin II, and vascular endothelial growth factor (VEGF). These factors stimulate the differentiation and activation of osteoclasts directly and indirectly[142,144].

IL-6 is a multifunctional cytokine that is upregulated in MM and stimulates the growth of osteoclasts and myeloma cells as well as blocking apoptosis in myeloma cells, therefore increasing bone loss[145,146]. IL-6 is mainly expressed and secreted by cells in the bone marrow microenvironment, such as BMSC (via direct interactions with MM cells) and macrophages, and it acts through the phosphatidylinositol 3-kinase (PI3k/Akt) pathway in the target cell[147].

Simultaneously, osteoblasts can secrete IL-6, promoting bone destruction and, therefore, bone pain. IL-6 increases the pool of early osteoclast precursors, which eventually develop into mature osteoclasts[147,148]. IL-6 is elevated *in vivo* and has been shown to induce bone resorption, which is related to bone disease[149,150].

IL-1 is a proinflammatory cytokine present at elevated levels in highly inflammatory conditions such as rheumatoid arthritis and osteoporosis[151]. It has two main isoforms: IL-1α and IL-1β, which activate different signalling pathways within osteoclasts[152]. Both isoforms increase the number and the resorption activity of osteoclasts in the presence of RANKL. However, IL-1α mainly stimulates the formation of large osteoclasts and increases the number of resorptive pits, while IL-1β changes the morphology of large osteoclasts, such as promoting the expression of ruffled edges[153,154]. IL-1α binds with high affinity to IL-1 receptor I (IL-1RI), an activating receptor expressed on the osteoclast cell surface, activating downstream signalling molecules that induce osteoclast formation from osteoclast precursors, thereby enhancing bone resorption[155]. Additionally, IL1α is a classic danger-associated molecular pattern (DAMP) and has been shown to trigger many inflammatory responses upon its release from necrotic cells[155,156].

IL-1β is a highly pleiotropic cytokine which acts as a potent inflammatory mediator as well as playing a role in haematopoiesis[157,158]. It has a potent effect on osteoclastogenesis. The main biological effect of IL-1β in MM is to enhance the expression of adhesion molecules and stimulate paracrine IL-6 production, which in turn leads to bone disease and bone painClick or tap here to enter text.'[159]. High levels of IL-1β have been found in monoclonal plasma samples from patients with MM[159,160].

IL-3 levels have been shown to be increased in bone marrow samples[161] and serum samples[161] of individuals with MM in comparison to healthy donors and to be associated with poor prognosis. IL-3 stimulates the formation of osteoclasts from osteoclast precursors and was found to increase osteoclast bone resorption in combination with MIP-1α and RANKL when these cytokines were added to osteoclasts in culture[162,163].

TNFα is found in high levels in the plasma of MM patients. This cytokine acts in synergy with RANKL to induce osteoclastogenesis by enabling NFκB-mediated stimulation of the transcription of IL-6 and adhesion molecules which promote the breakdown of bone[164,165]. Moreover, TNFα inhibits the differentiation of osteoblast precursors from progenitor cells via inhibiting osteoblast-specific transcription factors RUNX2 and osterix, which are responsible for osteoblast differentiation[166].

MIP-1α and MIP-1β are important chemokines secreted by myeloma cells that play a crucial role in MM bone disease and, therefore, bone pain[167,168]. MIP-1α and MIP-1β belong to the C-C family of chemokines, which is responsible for the adhesion of MM to BMSCs, bone

resorption, and myeloma cell migration[167]. MIP-1α binds to C-C chemokine receptor type 1 (CCR1), a receptor expressed on monocytes, T-cells, neutrophils, and dendritic cells, whereas MIP-1β binds to C-C chemokine receptor type 5 (CCR5), which is expressed on monocytes, T-cells, dendritic cells, eosinophils and microglia[169,170]. Both chemokines are potent chemoattractants for monocytes/macrophages and are expressed and secreted by MM cells. They attract osteoclast precursors and induce osteoclastogenesis while suppressing osteoblast activity by downregulating RUNX2[171,172]. High levels of both chemokines have been detected in the bone marrow and serum of MM patients[173,174].

HGF is involved in angiogenesis, the proliferation of epithelial cells and osteoclast activation[175]. HGF and HGF-receptor are expressed in high concentrations by myeloma cells in the bone marrow. Like TNFα, HGF inhibits osteoblastogenesis transcription factors RUNX2 and osterix by suppressing the expression of bone morphogenetic proteins (BMP), important signalling molecules for inducing bone formation via promoting mesenchymal stem cell differentiation into osteoblasts[175,176]. Myeloma-derived HGF was found to upregulate interleukin-11 (IL-11). IL-11 is a factor produced by osteoblasts to recruit and activate osteoclasts as well as suppress bone formation by osteoblasts[177]. Therefore, HGF is thought to indirectly promote bone disease in patients with MM[178]. It is also upregulated in the serum of MM patients and these high levels are associated negatively with disease prognosis[178,179].

SDF-1α is a chemokine expressed by BMSCs and myeloma cells. Levels of SDF-1α are elevated in the plasma of patients with MM in comparison to those without. SDF-1α levels correlate positively to the presence of bone lesions in patients with MM. This chemokine facilitates the movement and embedding of myeloma cells in the bone marrow by binding to multiple receptors, such as CXC chemokine receptor type 4 (CXCR4) and CXCR7[180] which are widely expressed on leukocytes, activated endothelial cells, dendritic cells, osteoclast precursors and myeloma cells[181,182]. SDF-1α also induces the expression of MMPs such as MMP-9 and other matrix-degrading enzymes, which promote osteoclast migration, recruitment, and activation. This suggests that the inhibitors of CXCR4 could reduce osteoclast activation to reduce bone pain[183].

Annexin II is a calcium-dependent phospholipid-binding protein belonging to the annexin family and is expressed by endothelial cells, BMSCs, macrophages, and myeloma cells. This pleiotropic protein is upregulated in MM patients and promotes MM cell adhesion, angiogenesis, osteoblast suppression, and osteoclastogenesis[184].

VEGF is another multifunctional cytokine expressed by myeloma cells. It binds to surface receptors expressed predominantly on osteoclasts, stimulating osteoclastogenesis and osteoclast activity to enhance bone resorption and osteoclast survival. In M-CSF deficient mice, VEGF can substitute for M-CSF in inducing osteoclasts[185]. VEGF also can enhance IL-6 production from BMSCs. This creates a vicious cycle as IL-6, in turn, stimulates the

expression of VEGF by MM, suggesting a paracrine interaction between BMSCs and MM cells driven by VEGF and IL-6[185].

Other mediators have a major role through more direct effects on osteoclastogenesis in MM. These include receptor activators of nuclear factor-kappa B (NFκB) (RANK), RANK ligand (RANKL) and osteoprotegerin (OPG). RANK is a transmembrane signalling receptor belonging to the TNFα receptor superfamily expressed on the surface of osteoclast precursors. RANKL is a cytokine expressed as a membrane-bound protein on the cell surface of BMSCs and osteoblasts that can be shed to form a soluble protein via the action of a metalloprotease-disintegrinTNF-converting enzyme (ADAM17)[186]. Osteoblasts and stromal cells are the main sites of production of RANKL[187]. RANKL expression is upregulated in response to various mediators and chemokines to stimulate bone resorption. These factors include parathyroid hormone, prostaglandins, and 1,25-dihydroxyvitamin D3[188]. The binding of RANKL to RANK on osteoclast precursors induces multinucleation that results in the formation of mature osteoclasts. OPG is a soluble decoy receptor for RANKL and also belongs to the TNF receptor superfamily. Produced by osteoblasts and BMSCs, OPG blocks the interaction of RANKL with RANK, thereby limiting osteoclastogenesis[188]. Like RANK/RANKL, knockout of the *Opg* gene in mice confirmed the importance of OPG in the regulation of bone remodelling. *Opg-/-* mice developed osteopenia and osteoporosis. OPG can be captured by syndecan-1 expressed by MM cells, leading to decreased availability and increased bone resorption[189]. OPG also attracts macrophages by binding to syndecan-1[189].

The importance of OPG in bone lesions in MM is supported by the abnormal ratio of OPG to RANKL found in the serum of MM patients[190]. The RANKL-RANK-OPG pathway holds significant importance in the realm of T cell biology[191]. Additionally, the RANKL-RANK axis plays a crucial role in modulating the immune system during the development and functioning of dendritic cells[192].

1.4.1 Role of inflammation in bone pain

Osteoclasts degrade bone minerals by secreting protons via the α3 isoform vacuolar-type H+ATPase (V-ATPase), creating an acidic microenvironment (acidosis) of around pH 5. Protons are potent mediators of pain as they create a low pH environment which activates the nociceptors[193].

Inflammation is a well-characterised stimulus of pain that can result in either acute or chronic pain[194]. It is triggered by a variety of mediators resulting in inflammatory responses throughout the body. Increased production of pro-inflammatory cytokines such as IL-6 and TNFα with MM promotes osteoclastic bone resorption, as discussed above, which contributes to bone pain and increased sensitivity/hypersensitivity to pain (hyperalgesia). However, MM-associated inflammatory bone pain is thought to be due predominantly to the activation of acid-sensing receptors, such as acid-sensing ion channels (ASICs) and the transit receptor potential channel vanilloid 1 (TRPV1), by creating acidosis[195]. ASIC3 is an acid-sensing nociceptor that sends pain signals to the brain and the spinal cord via the central nervous system. If the brain decides the threat is viable, it creates a sensation of pain that is experienced at the point where the signal originated[196]. Acidosis results from an increase in secreted protons normally essential for bone mineralisation. Bone resorption occurs when osteoclasts attach to the surface of bone and secrete protons into an extracellular compartment formed between the osteoclast and the bone surface[197]. Increased release of protons causes an acidic microenvironment within close proximity to sensory neurons, such as calcitonin gene-related peptide-positive (CGRP+) neurons, innervating the periosteum and marrow cavity. CGRP and ASIC3 are highly important for physiological and pathological processes and are widely associated with pain[195]. An acidic pH activates these channels and sensitises primary afferent nociceptors that contribute to pain in MM[194].

Injection of bafilomycin A1, a highly selective and potent inhibitor of V-ATPase, has been shown to decrease the activation of CGRP+ neurons and the phosphorylation of ERK1/2, whereas injection of APEXx2, a selective antagonist of ASIC3, decreases function ASIC3. Both injections reduce MM bone pain, with the combination having a synergistic effect. This shows that protons released from osteoclasts to resorb bone activate pH-sensitive nociceptors and sensory neurons to stimulate bone pain. Therefore, molecules that inhibit osteoclast release of protons could be effective in reducing bone pain in patients. Furthermore, solid tumours formed by MM cells also contribute to pain through increased acidity in the bone marrow microenvironment by the release of H+ via various plasma membrane pH regulators[195].

The microenvironment of inflamed tissue is more acidic than surrounding normal tissue, and since inflammation is a cause of pain and hyperalgesia[198], pro-inflammatory cytokines are, therefore, mediators of pain with their expression in turn enhanced by acidosis in the human

body. Acidosis enhances ASIC1 and ASIC3 expression on innate immune cells such as macrophages and dendritic cells[199,200] and promotes expression of IL-6, IL-1β and TNFα by human monocytes [201,202]. These pro-inflammatory cytokines have a paracrine effect on ASICs as they increase the number of ASIC-expressing neurons as well as enhancing ASIC-like current amplitude on nociceptive neurons, which in turn leads to a higher sensory neuron excitability[198]. This signalling mechanism on the nerve cells maintains inflammation-evoked pain, which impacts the nervous system. Overall, these studies provide evidence that pro-inflammatory cytokines are not only involved in the maintenance and promotion of inflammation but also with the generation and maintenance of inflammatory pain through direct effects on sensory neurons and nociceptors[190].

1.4.2 Hypercalcemia

Hypercalcemia is a secondary effect of bone pathology in MM. It is a serious condition whereby calcium levels in the blood are increased to above normal[203]. The causes of hypercalcemia are many. However, in MM, the main cause of hypercalcemia is the resorption of bone, which causes the excess release of calcium from bone[204]. This negatively affects many parts of the body, including the brain, kidneys and the digestive system. The effect of hypercalcemia on the brain is particularly important, as it can cause low mood and/or depression[204]. This, in turn, has been shown to exaggerate pain perception, decrease pain tolerance and reduce the effectiveness of chronic pain management in patients with MM[205]. Furthermore, hypercalcemia can cause non-bone-related pain in patients with MM by affecting the digestive system, where it can cause stomach upset and constipation[206].

1.4.3 Apoptosis

Upregulation of apoptosis in osteoblasts contributes to bone loss and, thus bone pain in MM[207]. Pathways, such as TNF-related apoptosis-induced ligand (TRAIL), and Fas/Fas ligand (Fas-L), all members of the TNF superfamily, regulate osteoblast apoptosis[208,209]. Fas-L is a transmembrane protein that induces apoptosis by clustering Fas and activating a caspase cascade that leads to Fas-induces apoptosis. Fas-L is overexpressed by myeloma cells to promote metastasis in the bone marrow. Osteoblasts were shown to be susceptible to stimuli that promote apoptosis *in vitro* when co-cultured with myeloma cells. This includes TNFα, IFNγ, IL-1β and IL-6 that are overexpressed in patients with bone disease in comparison to control osteoblasts from patients without bone disease and normal donors. Osteoblasts overexpress activation markers, such as Fas, death receptor 4 and 5 (DR4/DR5), intercellular adhesion molecule 1 (ICAM-1) and monocyte chemoattractant protein (MCP-1)[210]. These chemokines and adhesion molecules regulate contact between MM cells and osteoblasts[209,

and this direct cellular contact leads to the activation of Fas/Fas-L or DR4-DR5/TRAIL pathways[210]. Evidence from myeloma cell models (MCC-2 and MCC-4 myeloma cell lines) supports this mechanism of osteoblast apoptosis as co-culturing primary osteoblasts from patients overnight with MCC-2 and MCC-4 and MM cells isolated from patients increased osteoblast cell death, therefore, preventing bone formation[210]. This supports the idea of osteoblasts being programmed for cell death due to the release of inhibiting factors in the local microenvironment[207,210,211].

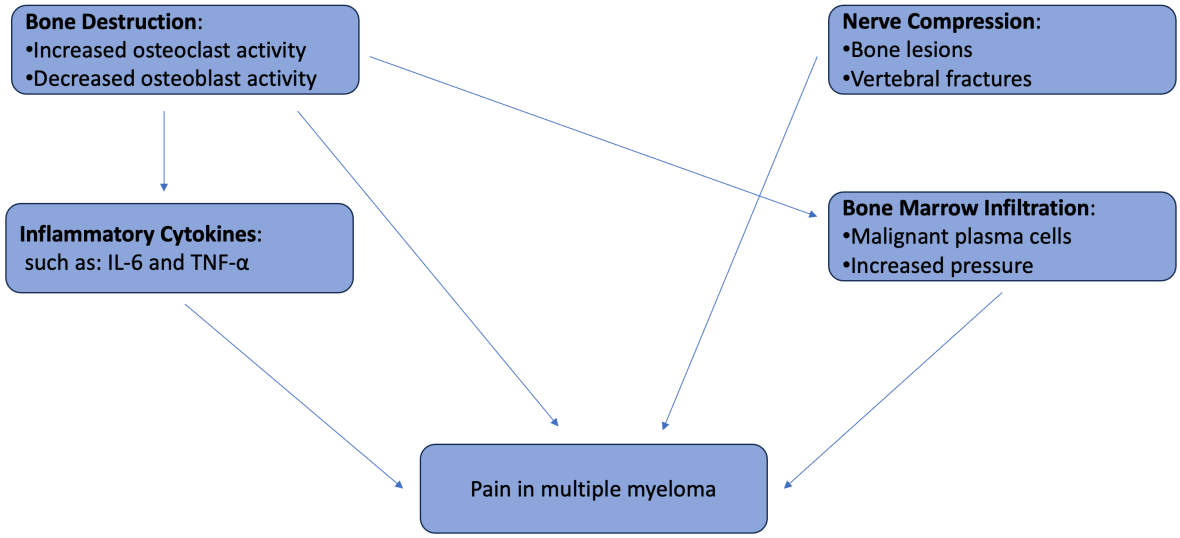

Figure 1.4. A schematic diagram illustrating the various factors contributing to pain in multiple myeloma. *Each of these factors is interconnected and collectively contributes to the pain experienced by patients with multiple myeloma.*

Pathophysiology of osteoblast impairment

Osteoblasts are mononuclear cells originating from mesenchymal stem cells[212](Figure 1.5). Usually located near the bone surface, they form new bone via a process that requires the transcription factors RUNX2 and osterix[213]. Different factors prevent osteoblast differentiation and maturation through the inhibition of the Wnt pathway, contributing to an imbalance of bone remodelling and affecting bone disease in MM[214]. Wnt signalling pathway plays a significant role in osteoblast maturation and function[215]. Wnts are a group of cysteine-rich signalling glycoprotein molecules that activate intracellular signalling pathways to regulate various cellular processes[214]. Wnt glycoproteins bind to the Wnt receptor complex that comprises the Wnt molecule, lipoprotein receptor-related protein-5/6 (LRP5/LRP6) and a member of the frizzled family, leading to β-catenin stabilisation and, therefore accumulation in the cell[216]. β-catenin translocates to the nucleus and associates with transcription factors, such as the T-

cell factor/lymphoid enhancer factor (TCF/LEF) family, activating the expression of target genes that regulate osteoblast commitment and maturation.

Extracellular antagonists, such as secreted frizzled-related proteins (sFRPs), and co-receptor inhibitors, such as Dickkopfs (DKKs), prevent the binding of Wnt glycoproteins to the receptor complex. The DKK family bind to the LRP5/6 component of the Wnt receptor complex, and the sFRPs bind to Wnt proteins, preventing them from binding to the Wnt receptor complex[217]. Both result in the suppression of Wnt-signaling and reduce osteoblast production.

Secreted Frizzled-related protein-2 (sFRP2) is expressed by myeloma cells and suppresses bone formation by inhibiting osteoblast differentiation induced by bone morphogenetic protein 2 (BMP2)[218]. MM cell lines and primary myeloma cells from individuals with MM have been shown to inhibit both early and terminal stages of osteoblast differentiation and, therefore bone formation by producing sFRP-2[219]. IL-3 also has been shown to block BMP-2 stimulation of osteoblast differentiation[220] thereby indirectly inhibiting osteoblast formation.

DKK1 is produced by MM cells[221] and by osteoblasts and BMSCs[222]. DKK1 inhibits differentiation and maturation of osteoblast precursors by antagonising the Wnt pathway[223 224]. Elevated levels of serum DKK1 were found in patients with MM and have been related to the progression of myeloma bone disease[225]. DKK1 is overexpressed in those with lytic bone lesions, with levels reduced in patients who respond to therapy[225].

RUNX2 is a transcription factor that is essential for the proliferation of pre-osteoblasts and for the commitment of mesenchymal stem cells to the osteoblast lineage. In vitro study has shown that MM cells block the activity and differentiation of osteoblasts from osteoprogenitor cells[226], and many of the mediators discussed above, such as TNFα and HGF, mediate their effects via inhibiting RUNX2.

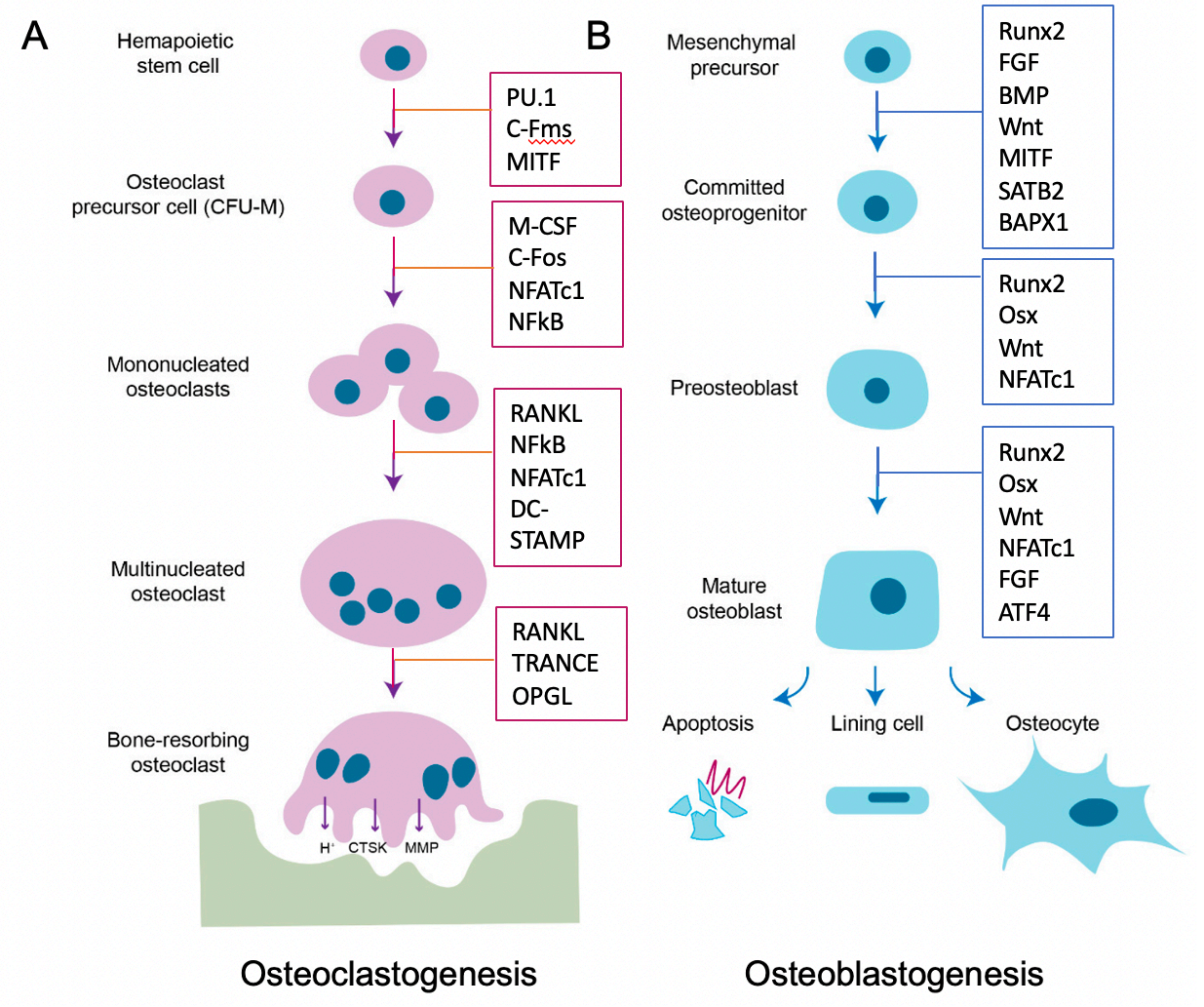

Figure 1.5 Illustration of osteoclastogenesis and osteoblastogenesis.

Osteoclasts are derived from haematopoietic stem cells. In the presence of M-CSF, haematopoietic stem cells (HSC) are committed to macrophage colony-forming units (CFU-M), which are the common precursor cells of osteoclasts. RANK-RANKL interaction activated CFU-M to further differentiate into mononucleated osteoclasts that ultimately fuse to form multinucleated osteoclasts. Multinucleated osteoclasts are fully matured upon interactions with osteoblast and activated upon interactions with the bone matrix, secreting acids (H+), proteases (e.g., CTSK), and matrix metalloproteases (MMP, e.g., MMP-9) to resorb bone (A). Osteoblasts are derived from multipotent mesenchymal precursors and differentiate into osteoblast lineage through the expression of transcription factors such as RUNX2 and Osterix. Osteoblasts continue to differentiate further until they either become lining cells or osteocytes or commit to apoptosis (B). Figure adapted from[227 and 228].

Other negative regulators of osteoblast differentiation include sclerostin and various members of the transforming growth factor-beta (TGFβ) and bone morphogenetic protein (BMP) family. Sclerostin inhibits the Wnt pathway. It is produced by osteocytes (osteoblasts when attached to bone matrix) and is also overexpressed by MM cells. Serum levels of sclerostin are elevated in individuals with MM who suffer from bone disease in comparison to individuals with monoclonal gammopathy of undetermined significance (a premalignant non-symptomatic condition that can progress to MM)[229,230]. Furthermore, high sclerostin mRNA and protein levels were expressed by four different human myeloma cell lines and in myeloma cells isolated from MM patients with bone disease[230]. The TGFβ and BMP pathways downregulate osteoblasts through transducing intracellular signals via Smad complex or mitogen-activated protein kinase (MAPK) as cytokines expressed through these pathways regulate osteoblast maturation and bone mineralisation. TGFβ proteins bind to a tetrameric receptor complex comprised of TGFβ type I and II receptors that induce Smad-dependent or Smad-independent signalling. In Smad-dependent signalling, the recruitment of intracellular Smad complexes regulates target gene expression. In the Smad-independent pathway, activation of the MAPK/ERK signalling cascade initiates the expression of target genes that regulate osteoblast differentiation and activation. BMP signalling is initiated through the binding of BMP ligands to type I and II BMP receptors, inducing transphosphorylation of the type I receptors. This leads to the activation of either Smad or MAPK signalling pathways that induce the transcription of target genes regulating osteoblast differentiation and activation. Both TGFβ and BMP pathways regulate osteoblasts under both physiological and pathological conditions and studying their pathways will provide novel therapeutic approaches for controlling bone disease. In MM, $TGF\beta_1$ is released predominantly by MM cells, BMSCs and osteoblast[231,232,233], and it has been shown to be elevated in serum in individuals with MM.

Factor	Osteoclast Differentiation	Osteoblast Differentiation
Key Transcription Factors	- NFATc1	- Runx2
	- c-Fos	- Osterix
Cytokines/Growth Factors	- RANKL (Receptor Activator of Nuclear Factor κB Ligand)	- BMPs (Bone Morphogenetic Proteins)
	- M-CSF (Macrophage Colony-Stimulating Factor)	- Wnt/β-catenin signalling
	- TNF-α (Tumour Necrosis Factor alpha)	- IGF-1 (Insulin-like Growth Factor 1)
Signalling Pathways	- RANK/RANKL/OPG signalling	- Wnt/β-catenin signalling
	- NF-κB signalling	- TGF-β (Transforming Growth Factor beta) signalling
	- c-Fos/AP-1 signalling	- MAPK (Mitogen-Activated Protein Kinase) signalling
	- Calcium signalling (via NFATc1 activation)	- Hedgehog signalling
Hormones	- Parathyroid hormone (PTH)	- Parathyroid hormone (PTH)
	- Vitamin D3	- Vitamin D3
	- Calcitonin (inhibitory effect)	- Oestrogen (indirect positive effect by inhibiting osteoclasts)
Cell Surface Receptors	- RANK (Receptor Activator of Nuclear Factor κB)	- LRP5/6 (Low-Density Lipoprotein Receptor-Related Protein 5/6)
	- c-Fms (Colony Stimulating Factor 1 Receptor)	- Frizzled receptors
Environmental Factors	- Hypoxia (can promote differentiation)	- Mechanical loading (promotes differentiation)
	- Acidic environment (promotes activity)	
Inhibitors	- Osteoprotegerin (OPG)	- Sclerostin (inhibits Wnt signalling)
	- Interferon-gamma (IFN-γ)	- Dkk1 (Dickkopf-1, inhibits Wnt signalling)

Table 1.3. A table summarising the main factors in osteoclast and osteoblast differentiation*. References used for osteoclast differentiation [142,143, 164, 165, 184-190] and references used for osteoblast differentiation [213-233].*

1.4.4 Current treatments for myeloma bone disease and myeloma bone pain.

Bone pain MM treatment- Bone pain in MM is one of the most significant factors resulting in reduced quality of life for individuals with MM, so its management is of paramount importance. Pharmaceuticals remain an important therapeutic approach in the management of MM bone pain, and research in the pharmaceutical management of MM bone pain has yielded great advances in the last ten years. However, most patients will require a multimodal approach where physical therapies (including surgical procedures and radiotherapy) will be considered for individuals with significant bone lesions and at high risk of bone fracture. Treatment of MM bone pain is best tailor-made for the individual, with a balance of various approaches, and this will depend on various factors, including the age of the individual with MM and the existence of co-morbidities.

Radiation therapy is utilised to treat lytic lesions and to prevent pathological fractures. The aim of radiotherapy is to cure plasmacytoma. About 20% of MM patients require radiation therapy[234]. For painful bone lesions, pain relief is usually obtained with a radiation dose of 30-36 Gy in 10-15 sessions[235]. This therapy has its downfalls as it can cause permanent damage

to the treated areas in the bone marrow, so it is particularly a concern for patients of older age and who are already receiving cytotoxic therapy[236].
Vertebroplasty is used to treat painful vertebral compression fractures and involves the injection of polymethyl methacrylate using fluoroscopy. It is very effective in relieving pain in MM patients[237]. Kyphoplasty involves a thin tube with an inflation balloon at one end being inserted into the collapsed vertebra prior to the injection[238].

Bone loss MM treatment- Bisphosphonates are analogues of pyrophosphate that inhibit osteoclasts specifically and have been shown to reduce bone pain in MM patients as well as reduce pain in rheumatoid arthritis patients[239]. They bind to the exposed areas of the bone where they are taken up by osteoclasts during bone resorption, impairing the ability of osteoclasts to form the ruffled border and adhere to bone[240] thereby preventing bone resorption. The aim of bisphosphonate treatment is to prevent the differentiation of monocytes/macrophages to osteoclasts and to inhibit osteoclast maturation[241]. Furthermore, bisphosphonates induce apoptosis in osteoclasts and disrupt their linkage to the bone by binding to and inhibiting the activity of farnesyl pyrophosphate synthase, a crucial regulatory enzyme in osteoclasts[,242]. Possible mechanisms of bisphosphonates include reducing IL-6 from BMSCs[242, 243]. The following compounds, alendronate, neridronate, ibandronate, pamidronate, risedronate, and zoledronic acid, belong to the category of nitrogen-containing bisphosphonates, whereas etidronate and tiludronate do not possess a nitrogen group and are referred to as non-nitrogen containing bisphosphonates[244].

Bortezomib is a first-generation proteasome inhibitor essential for treating refractory/relapsed MM. It affects the differentiation and activation of osteoclasts in a dose-dependent manner, reducing bone resorption through the reduction of RANKL and DKK1, restoring normal bone remodeling[245]. While particularly effective at limiting the early stage of osteoclast differentiation, bortezomib also affects the late phase of osteoclast differentiation by inhibiting NFκB and activator protein-1 (AP-1), disrupting the regulation of important downstream effectors in osteoclast differentiation[246]. Overall, normalisation of bone remodelling is achieved through the reduction of bone resorption and increased bone formation[247].
IMiDs, including thalidomide, lenalidomide and pomalidomide, are effective in the treatment of newly diagnosed and refractory/relapsed MM (Figure 1.6). They modify the interactions of MM cells with the bone marrow microenvironment and also alter bone metabolism in MM[248]. Thalidomide inhibits RANKL-induced osteoclast formation *in vitro*[249]. In combination with dexamethasone, thalidomide reduces bone resorption markers such as c-telopeptide of collagen type-1 (CTX) and TRACP-5b in patients with relapsed/refractory myeloma[250,251].

There is also a strong correlation between RANKL/OPG ratio and TRACP-5b and CTX in patients, which suggests that thalidomide works by reducing the levels of RANKL[252]. In contrast, many studies suggest that thalidomide does not affect osteoblasts and bone formation[253].

Lenalidomide inhibits osteoclast formation by targeting PU.1, a transcription factor for osteoclast development, and downregulates cathepsin K[254,255]. The downregulation of this transcription factor in hematopoietic progenitors results in a change in lineage towards granulocytes. Similar to thalidomide, lenalidomide inhibits angiogenesis by inhibiting VEGF, altering the bone marrow microenvironment and suppressing the growth and proliferation of MM cells. This drug has been shown to reduce serum RANKL/OPG ratio in patients and in vitro[251].

Pomalidomide is a third-generation IMiD that blocks RANKL-induced osteoclastogenesis, normalising the RANKL/OPG ratio[254]. Additionally, it downregulates PU.1, which shifts the commitment of osteoclast precursors in granulocytes instead of mature osteoclasts[256].

Chimeric antigen receptor T (CAR-T) cell therapy targeting B cell maturation antigen (BCMA) has demonstrated notable success in addressing relapsed/refractory (R/R) MM, presenting a new outlook for patients with this condition in recent years[257]. There are presently two FDA-approved CAR T-cell products for the treatment of relapsed/refractory MM (RRMM): idecabtagene vicleucel (ide-cel) and cilta-cel. Both medications are authorized for use in RRMM following four or more lines of therapy, including a proteasome inhibitor (PI), immunomodulatory agent, and anti-CD38 directed therapy[258].

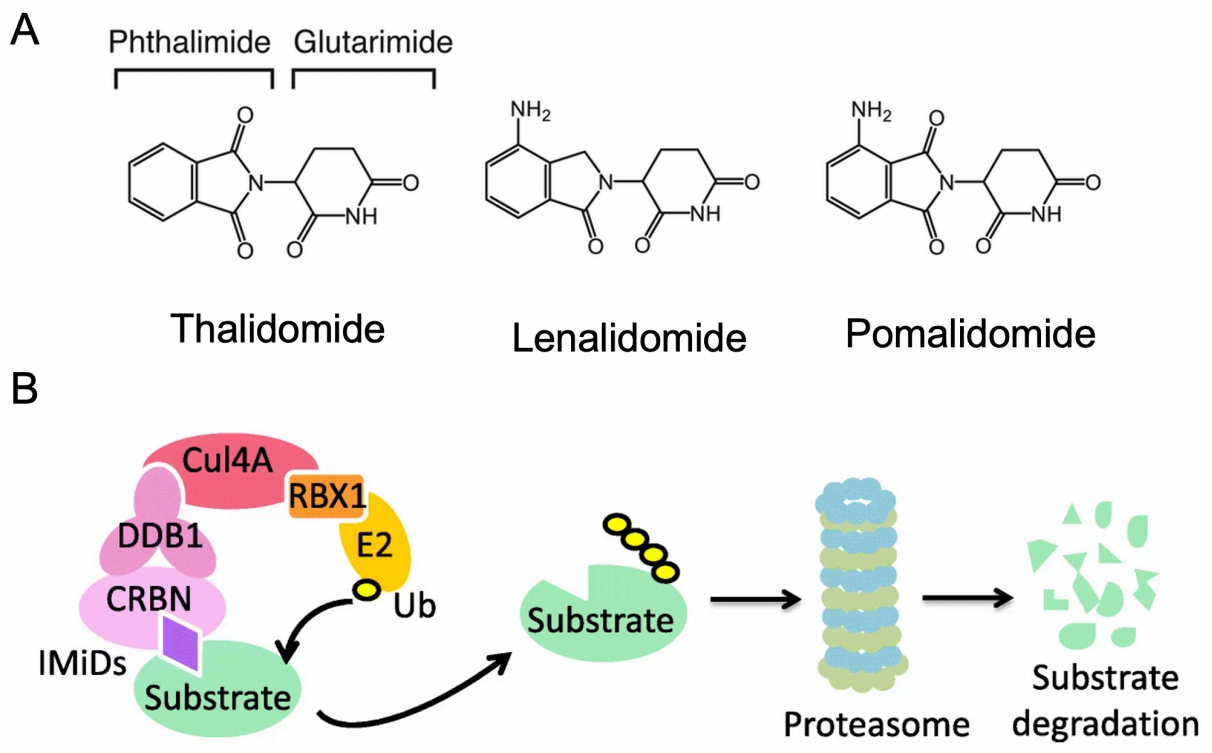

Figure 1.6 Chemical structure and mechanism of action of IMiDs.

Chemical structure of thalidomide, lenalidomide, and pomalidomide are collectively referred to as IMiDs. Thalidomide is composed of phthalimide and glutarimide (A). IMiDs (purple parallelogram) bind to CRBN, a substrate receptor of CDL4 E3 ligase, to recruit substrates for ubiquitination and proteasomal degradation (B). Ub = ubiquitination; E2 = ubiquitin-conjugating enzyme; RBX1 = ring box 1; Cul4A = Cullin 4 Ring E 3 ubiquitin ligase; DDB1 = DNA damage-binding protein 1; CRBN = cereblon; IMiDs = immunomodulatory Imide drugs. Figure adapted from Gao, S., Wang, S. & Song, Y. 2020.

Although many treatments are available to prolong the life of patients with MM, many suffer from chronic pain. While the priority is to treat the myeloma malignancy itself, treatments are available to provide pain relief/palliative care resulting from myeloma bone disease (Figure 1.7). However, current therapies do not provide the necessary pain relief for many patients with MM, and more research is required to identify new therapies that will improve patients' outcomes.

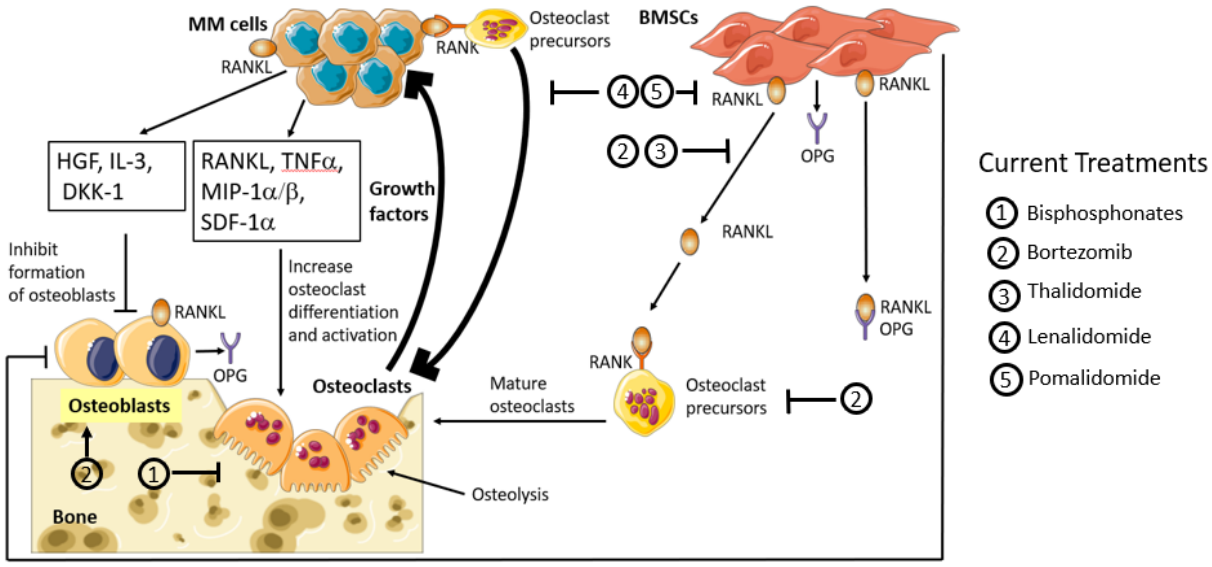

Figure 1.7 Pathophysiology of osteolytic bone disease and sites of action of current treatments.

Bisphosphonates inhibit osteolytic bone resorption by interrupting osteoclast binding to bone, preventing osteoclasts from forming the ruffled border. Bortezomib inhibits osteoclast maturation and differentiation by reducing the levels of RANKL to suppress osteoclast precursors, induce osteoblast differentiation and increase osteoblast activity. IMiDs are potent inhibitors of osteoclastogenesis, inhibiting the differentiation and activation of osteoclasts. This restores the RANKL/OPG ratio in the bone marrow microenvironment, allowing normal bone remodelling.

Bone pain has a detrimental impact on the physical capacity and quality of life of patients with MM causing increased morbidity and disability. Imbalanced bone remodelling is the main cause of bone disease in myeloma, with various mechanisms and factors contributing thereto, such as Wnt/DKK1, RANKL/OPG, IL-6, TNFα and TGFβ, amongst others, as illustrated in this review. However, more research into the neuropathic pathways in myeloma bone disease are required to identify the pathophysiological mechanisms underlying both chronic and acute pain to provide more targeted therapy. Nevertheless, much progress has been made recently to further our understanding of myeloma bone disease. Osteoclasts play a role in the development of drug resistance in multiple myeloma by providing cytoprotective signals in the bone marrow[259]. This insight could potentially lead to the development of new strategies to overcome drug resistance in MM. This has led to the development of targeted therapies which, when used in combination with anti-myeloma therapies, have improved the median survival of patients with MM[260,261,262].

1.5 Aims and objectives

Over the last decade, survival outcomes for patients with MM have increased significantly. Nevertheless, the disease remains incurable, with many patients developing bone disease, often leading to chronic pain. Better therapeutic regimes which inhibit osteoclastogenesis, promote osteoblast-driven bone formation and control neuropathic pain are required. Overall, this would likely achieve more effective analgesic control in patients with MM, improving health outcomes and patients' quality of life. The main aim of this thesis is to improve our understanding of osteoclastogenesis and to investigate the effects of current and novel myeloma therapies on the differentiation and activation of osteoclasts and myeloma cells by:

1. Using an osteoclast model *in vitro* to monitor the differentiation of osteoclasts using real-time assays.
2. Determining the effects of IMiDs and IL-4, IL-10 and IL-13 on the differentiation and activation of osteoclasts using endpoint and real-time assays.
3. Investigating the effects of IMiDs and IL-4, IL-10, IL-13 on MNCs derived from early diagnosed patients.

Chapter Two

Experimental Procedures

Experimental procedures

2.1 Overview:

This chapter contains a general overview of the materials and methods used for the experimental chapters within the thesis. Specific methodologies and experimental designs are described in detail within the relevant chapters. Experimental outlines and concepts are described below.

2.2 Laboratories consumables, chemicals and reagents

Cell culture multi-well and other plastic consumables were purchased from Greiner Bio-One (Stonehouse, UK). Monocyte separation reagents for the autoMACS separator, including specific microbeads and magnetic columns, were purchased from Miltenyi Biotec (Cologne, Germany). Chamber slides used for confocal microscopy were purchased from Merck Millipore (Massachusetts, USA). All cell culture media and supplements, including phosphate buffered saline (PBS), RPMI 1640, sodium pyruvate and 2-mercaptoethanol, were purchased from ThermoFisher Scientific (Massachusetts, USA).

2.3 Antibodies, agonists and antagonists

The flow cytometry antibody for monocyte purity monitoring was an anti-CD14 antibody eFluor® 450 (isotype mIgG1, clone 61D3, eBioscience™; 48-0149-42). Anti-CD36 antibody (anti-human, REAfinity™, clone REA760, isotype IgG1; 130-110-739) and anti-CD98 antibody (anti-human, REAfinity™, Clone REA387, isotype IgG1; 130-120-051) were both purchased from Miltenyi Biotec. The agonist lipopolysaccharide (LPS; ultrapure) was purchased from InvivoGen (San Diego, USA). Dimethyl Sulfoxide (DMSO) Hybri-Max™ was purchased from (Sigma-Aldrich; Poole; UK).

Cytokines needed for osteoclast differentiation: Macrophage colony-stimulating factor (M-CSF) and receptor activator of nuclear factor kappa β ligand (RANKL), purchased from Miltenyi Biotec, Cologne, Germany.

Treatments used in this study: lenalidomide (brand name: Revlimid), pomalidomide (brand name: Pomalyst) and thalidomide (brand name: Thalomid) were all obtained from Celgene (now part of Bristol Myers Squibb); New Jersey, USA.

Anti-inflammatory cytokines used in this study: human interleukin 4 (IL-4) research grade, human interleukin 10 (IL-10) research grade, and human interleukin 13 (IL-13) research grade were purchased from Miltenyi Biotec, Cologne, Germany.

Primary antibodies used in confocal microscopy included anti-TOMM20 mouse monoclonal (ab56783; isotype IgG1), and anti-tartrate resistant acid phosphatase (TRAP) mouse monoclonal antibody (ab238033; isotype IgG1) that were both purchased from Abcam, Cambridge, UK. Anti-receptor activator of nuclear factor kappa β (RANK) monoclonal mouse antibody (Clone 80707; isotype IgG_{2A}) was purchased from R&D systems (Biotechne; Minneapolis; Minnesota, USA). The secondary antibody used in confocal microscopy was a goat anti-mouse H&L polyclonal antibody (Alexa Fluor 488; ab150113, isotype IgG) purchased from Abcam Cambridge, UK.

Antibodies used in western blotting: Integrin αV polyclonal antibody (Cell Signalling; 4711), integrin β3 antibody (Cell Signalling; (D7X3P) XP® Rabbit IgG mAb 13166), α5 integrin polyclonal antibody (Cell Signalling; 4705), integrin β1 (Cell Signalling (D2E5) Rabbit IgG mAb 9699), integrin β5 (Cell Signalling (D24A5) Rabbit IgG mAb 13629) and integrin α4 (Cell Signalling; (D2E1) XP® Rabbit IgG mAb 8440). The monoclonal mouse β-actin was purchased from Abcam (8226; isotype IgG1), Cereblon (CRBN) (abcam; mouse IgG1 mAb;ab244223). GAPDH (Biotechne; monoclonal mouse IgG1; MAB5718; clone 686613). (see ***Table 2.1*** for summary of antibodies used).

Antibody	Application	Company	Catalogue Number	Dilution
Anti-CD14 (eFluor® 450, mIgG1, clone 61D3)	Flow Cytometry	eBioscience™	48-0149-42	1/100
Anti-CD36 (REAfinity™, IgG1, clone REA760)	Flow Cytometry	Miltenyi Biotec	130-110-739	1/100
Anti-CD98 (REAfinity™, IgG1, clone REA387)	Flow Cytometry	Miltenyi Biotec	130-120-051	1/100
Anti-TOMM20 (mouse monoclonal, IgG1)	Confocal Microscopy	Abcam	ab56783	1/1000
Anti-TRAP (mouse monoclonal, IgG1)	Confocal Microscopy	Abcam	ab238033	1/1000
Anti-RANK (monoclonal mouse, IgG2A, clone 80707)	Confocal Microscopy	R&D Systems (Biotechne)	MAB6831	1/1000
Goat anti-mouse H&L (Alexa Fluor 488, IgG)	Confocal Microscopy	Abcam	ab150113	1/800
Integrin αV (polyclonal antibody)	Western Blotting	Cell Signaling	4711	1/1000
Integrin β3 (D7X3P) XP® Rabbit IgG mAb	Western Blotting	Cell Signaling	13166	1/1000
Integrin α5 (polyclonal antibody)	Western Blotting	Cell Signaling	4705	1/1000
Integrin β1 (D2E5) Rabbit IgG mAb	Western Blotting	Cell Signaling	9699	1/1000
Integrin β5 (D24A5) Rabbit IgG mAb	Western Blotting	Cell Signaling	13629	1/1000
Integrin α4 (D2E1) XP® Rabbit IgG mAb	Western Blotting	Cell Signaling	8440	1/1000
β-actin (monoclonal mouse, IgG1)	Western Blotting	Abcam	8226	1/1000
Cereblon (CRBN) (mouse IgG1 mAb)	Western Blotting	Abcam	ab244223	1/1000
GAPDH (monoclonal mouse IgG1, clone 686613)	Western Blotting	Biotechne	MAB5718	1/500

Table 2.1. A table summarising the antibodies used, along with the company, catalogue numbers, and dilutions for immunostaining, Western blotting (WB), or flow cytometry.

2.4 Sample collection and preparation

All samples were collected with informed written consent. Ethical approval was obtained from Wales Research Ethics Committee 6 (REC number 13/WA/0190) initially and then Swansea University Medical School (SUMS) Research Ethics Committee (REC), project reference 2022-0029. Human venous blood samples were collected between 0830 and 1000 from healthy non-fasted participants into sterile sodium heparinised Vacuettes™ (Greiner Bio-one, Frickenhausen, Germany). The volume of samples would vary, but in general, 12 tubes of blood would be collected from individuals of different age groups – this is around 110 mLs. The samples were processed *ex vivo* within 10-15 minutes of collection to avoid the potential activation of cells.

2.4.1 Blood separation

All primary cell culture procedures were implemented under sterile conditions within a Biological Safety Class II Scanlaf Mars Hood (Labo, Lynge, Denmark) using sterile equipment. All media used for cell culture was sterile and endotoxin-free. Any non-sterile media was filter sterilized using a 0.22 µL filter unit (Millipore, USA) and a 20 mL syringe (BD Biosceince, USA). Cell incubation unless specified otherwise, was carried out at 37 °C under atmospheric pressure accompanied by 5% CO_2-in-air (CO_2 air-jacketed incubator NuAire, Plymouth, USA).

2.4.2 Mononuclear cell isolation

Mononuclear cells (MNCs) were isolated by layering whole blood (1:1 ratio) onto sterile Histopaque (density 1.077g/mL, Sigma-Aldrich; Poole; UK) prior to centrifugation at 805 x *g* for 20 minutes at room temperature, no brake. Centrifugation resulted in four distinct layers according to density; plasma, MNC layer, Histopaque and red blood cells combined with the polymorphonuclear cells (Figure 2.1). After discarding the plasma layer (yellow colour), MNCs (buff colour) were carefully removed with a sterile plastic Pasteur pipette and washed with RPMI 1640 (Life Technologies, Paisley, UK) twice by centrifugation at 515 x *g*. The MNC pellet was resuspended in media specific for the downstream assay, and cell count was determined using the Countess® automated cell counter (Life Technologies) as described in section 2.5.

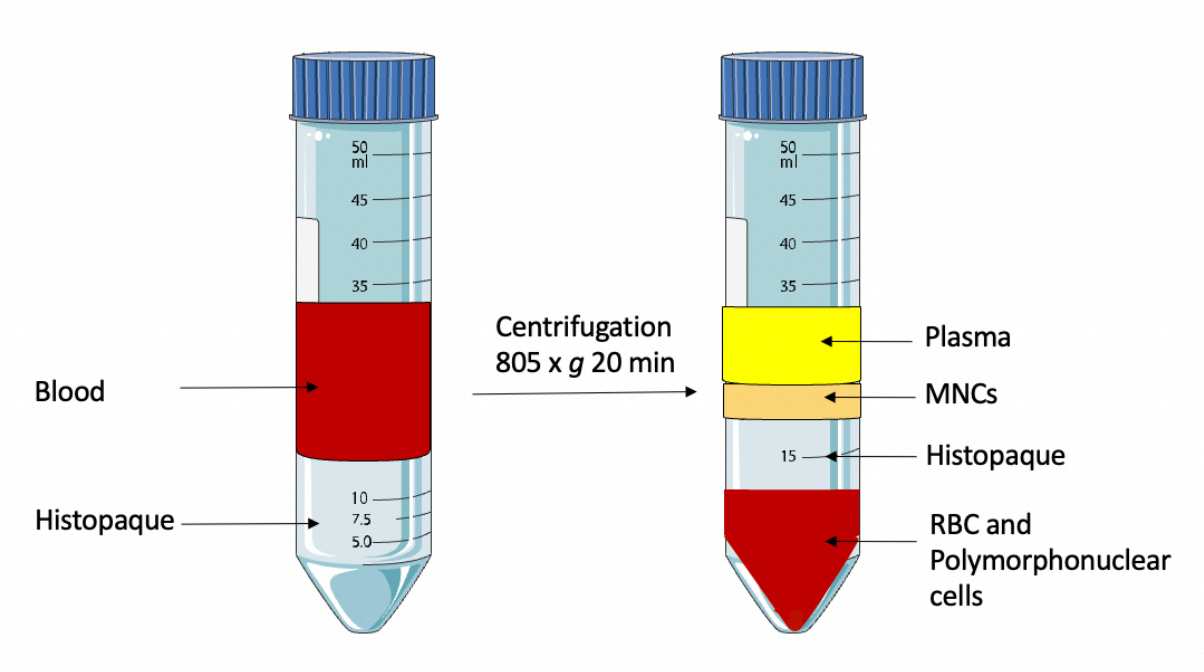

Figure 2.1 Mononuclear cell isolation from whole blood.

Human blood was layered onto a Histopaque gradient at a 1:1 ratio. Density gradient centrifugation separation resulted in four distinct layers: plasma, mononuclear cells (MNC), Histopaque, and red blood cells (RBC)/polymorphonuclear cells.

2.4.3 Monocyte isolation.

Classical monocytes represent about 80 - 90% of all monocytes, and they are characterised by high expression of CD14[263]. On monocytes, CD14 is bound to the membrane via a glycosylphosphatidylinositol anchor[264]. Initially, MNCs isolated as in section 2.4.2 were counted and then centrifuged at 300 x *g* for 10 minutes and the pellet was resuspended in 80 µL of MACS buffer (2% fetal calf serum (FCS HyClone, ThermoFisher Scientific, Massachusetts USA) in PBS (Life Technologies)) per 10^7 cells and 20 µL of CD14 specific microbeads per 10^7 cells. The MNC-microbead cocktail is incubated in the fridge for 15 minutes and then washed with MACS buffer (1 mL per 10^7 cells) and centrifuged at 300 x *g* for 10 minutes. The supernatant was discarded, and the pellet was resuspended in 1 mL of MACS buffer. This solution was then applied to the autoMACS separator (Miltenyi Biotec) twice; monocytes were isolated through positive magnetic selection. Monocyte numbers were determined using the Countess® automated cell counter (Life Technologies) as described in section 2.5.

2.4.4 Cell counting

Cell counting and viability were accomplished using the Countess™ automated cell counter (Life Technologies). Isolated cells were diluted accordingly (based on the cell type and the anticipated cell number), and a 1:1 ratio of diluted cells to trypan blue (0.4%; Life Technologies) (usually 10µL of cells in suspension is mixed with 10µL of Trypan blue) was applied to the Countess™ cell counting slide (Life Technologies). The density was determined via the equivalent counting of four 1 mm x1 mm squares on a standard haemocytometer. The total live cell count (via trypan blue exclusion) was used for calculations for downstream experiments, inclusive of the application dilution factor.

2.4.5 Monocyte purity

Flow cytometry was used to determine the purity of isolated monocytes. For purity monitoring, 100,000 cells were incubated with anti-CD14 eFluor 450 in the dark at 4 °C for 30 minutes. Cells were then washed once with FACS buffer (0.2% w/v bovine serum albumin (BSA), 0.05% sodium azide (Sigma-Aldrich; Poole; UK) in PBS) and centrifuged at 515 x *g* at 4 °C for 7 minutes. Cells were then resuspended in 100 µL of the FACs buffer and analysed using the NovoCyte flow cytometer and the NovoExpress software, version 1.4.1 (Agilent; California; USA). The lasers and wavelengths used were blue (488 nm), red (633 nm), and violet (405 nm). Initially, forward scatter (FSC) and side scatter (SSC) parameters were set and then the individual fluorophore channel was set with the use of an isotype control sample; typically, a relative fluorescence intensity of above 10^4 was set as a positive signal. FSC is a measure of the cell size, and SSC is a measure of cellular granularity. Cells were then acquired at 10,000 events of the population of interest. The flow cytometer's quality control (QC) was monitored using BD Cytometer and Tracking beads (BD Biosciences). Briefly, one drop of the beads was added to 0.5 mL of PBS, and the QC programme was initialised. The data acquired were compared to a previously set baseline to ensure laser functionality.

2.4.6 Data analysis

All cells were initially acquired using the NovoExpress Software (Agilent; California; USA). All data post-acquisition were analysed using FlowJo 10.8.1 (Tree star, Oregon, USA). Initially, histograms of the single stained sample or quadrants of dual stained samples were created for the specific fluorophores of interest. Example gating strategies are provided for each experimental use of flow cytometry throughout the results chapters. Purity data are expressed as a percentage (Figure 2.2).

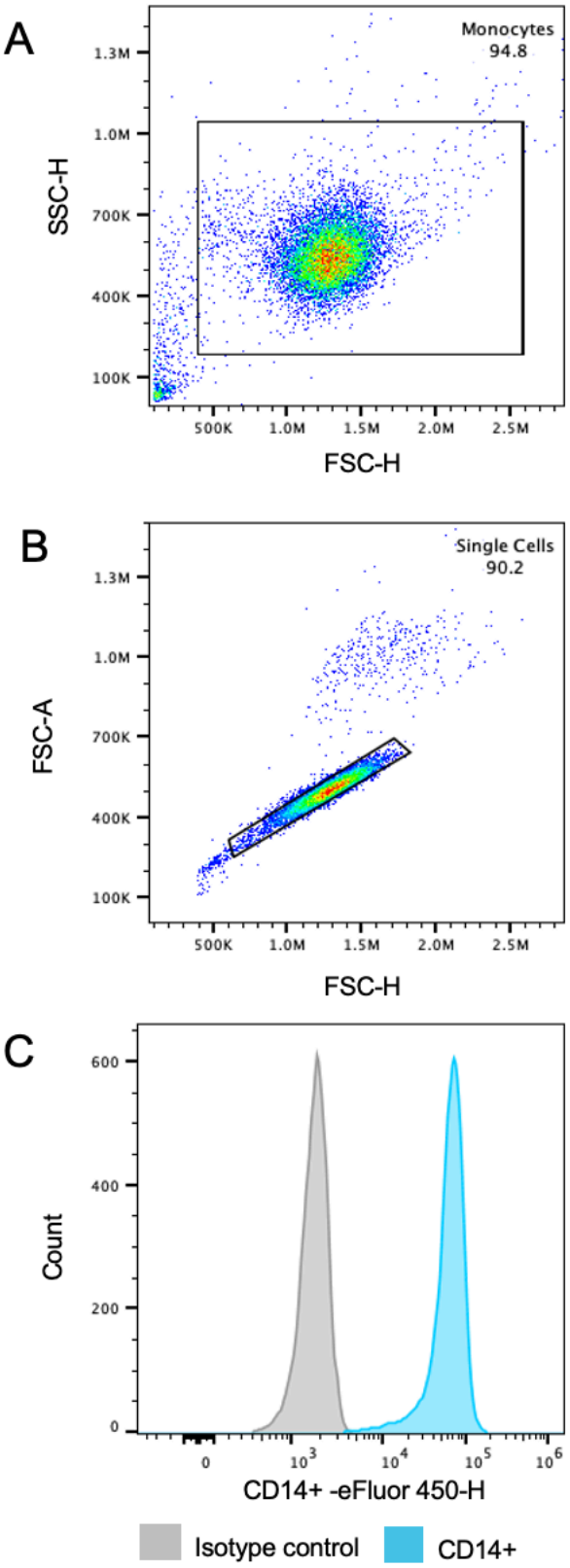

Figure 2.2 Example of CD14 monocyte purity monitoring.

Flow cytometry revealed the purity of a magnetic microbead-isolated CD14+ monocytes. An example of a rectangular gated monocyte population acquired on the Novocyte flow cytometer according to forward scatter (FSC), and side scatter (SSC) properties (Figure 2.2 A). Exclusion

of doublet cells using FSC height (FSC-H) versus FSC area (FSC-A) (Figure 2.2 B). A histogram of isolated monocytes with isotype control (grey) and stained (blue) with anti-human CD14 eFluor 450 (Figure 2.2 C).

2.5 Compensation

The presence of two or more fluorophores within the same tube required compensation to adjust the potential spectral overlap upon emission. Any spectral overlap could cause false positive results upon data collection. Compensation was performed using a single stained tube for each fluorophore with a distinct positive and negative population within. In the case where all events were positively stained, a mix of the positively stained sample and the unstained control sample was run. Gates and labels were applied to the positive and negative events, and a compensation matrix was calculated using FlowJo 10.8.1 (Tree Star, Oregon, USA). The compensation matrix specifies any percentage spill over of the primary fluorophore into the other channels of interest. The compensation matrix was applied to all downstream-acquired tubes prior to data analysis.

2.6 Enzyme-Linked Immunosorbent Assay (ELISA)

ELISA is a technique used to quantify proteins and other mediators, typically in the supernatant of samples. Here it is used to measure specific cytokines or chemokines from the cell-free culture supernatant. A sandwich ELISA was used in this project according to the manufacturer's instructions (R&D Systems Duo-Set; Bio-Techne; Figure 2.3). Initially, the ELISA plate is coated with the capture antibody that is specific for the targeted protein. The antibody is diluted to a working concentration in PBS and 50 µL added to each well of half area 96-well plates (Greiner Bio-One; Stonehouse; UK); these are used to minimise reagent use and increase the number of assays per purchased kit. The coated plate was left overnight at 4 °C. The next day, the excess capture antibody was discarded, and the remaining protein binding sites on the plate were blocked with 150 µL of blocking buffer that consisted of 1% BSA (Sigma-Aldrich; Poole; UK) dissolved in PBS. The plate was incubated in the block buffer for one hour at room temperature with gentle agitation on a Heidolph Titramax 1000 plate shaker (Heidolph instrument; Schwabach; Germany) at 450 RPM. The blocking buffer was discarded, and the plate was washed three times with 200 µL/well of the washing buffer (0.05% of Tween 20 (Sigma-Aldrich; Poole; UK) in PBS). Samples were thawed and either used neat or diluted accordingly with the block buffer. The standards were also diluted according to the protocol and the datasheet provided with the kit. The samples were added in

duplicates to the plate along with duplicates of a specific standard curve for the cytokine of interest, which included a blank (block buffer only; negative control) to analyse the contribution of the background absorbance of the plate and the block buffer to the signal.

The plate was incubated at room temperature for at least two hours with gentle agitation. After discarding the samples, the plate was then washed with the washing buffer four times. The detection antibody was diluted to a working concentration and added to the plate for two hours at room temperature with gentle agitation. The plate was then washed four times with the wash buffer. A working concentration of streptavidin-horseradish peroxidase (HRP) was applied to the plate for exactly 20 minutes at room temperature with gentle agitation. The plate was washed for a final six times with the wash buffer. A 1:1 solution of hydrogen peroxide and tetramethylbenzidine (TMB; BD Biosciences) was prepared, and 50 µL of the solution was applied to the plate. A blue colour was allowed to develop in the dark at room temperature. A final 50µL of 1M sulphuric acid (H_2SO_4) was added, turning the blue solution into a yellow solution. The absorbance of the plate was measured at 450 nm using a plate reader (POLARstar Omega, BMG, Germany), and the final protein concentration was calculated using the standard curve using Excel Version 16.70 (Microsoft, USA) (Figure 2.3).

The cytokines analysed for this project: Human MMP-9 DuoSet (DY911), Human MMP-2 DuoSet (DY902), Human IL-6 DuoSet (DY206), Human TNFα DuoSet (DY210). All ELISA kits were purchased from Bio-techne (R&D Systems; Minneapolis; Minnesota; USA).

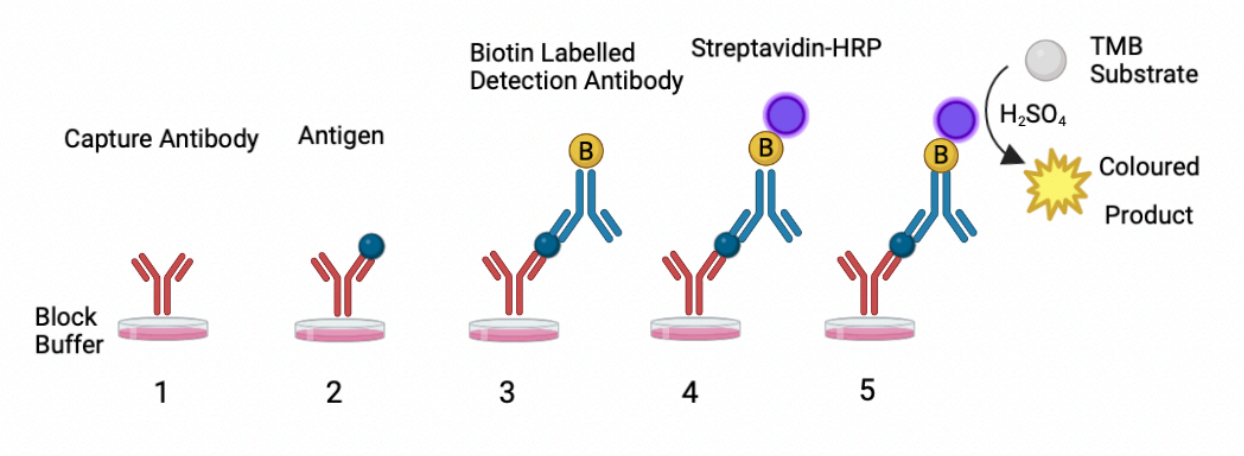

Figure 2.3 Overview of enzyme-linked immunosorbent assay (ELISA).

An overview of the five-step experimental procedure of a sandwich ELISA. (1) 50 µL of diluted capture antibody was applied to the plate, and the plate was sealed and incubated overnight at 4 °C. The plate was then washed three times with PBS/tween using a multichannel pipette. The plate was then blocked for 1 hour. (2) The samples were diluted to the desired concentrations using the blocking buffer or appropriate diluent. The plate was sealed and

incubated for 2 hours at room temperature. The plate was then washed four times with PBS/Tween. (3) Detection antibody was diluted accordingly and added to the plate for 2 hours, then the plate was washed four times with PBS/Tween. (4) Streptavidin horseradish peroxidase (HRP) conjugate was added for 20 minutes, and then the plate was washed six times. (5) The addition of tetramethylbenzidine (TMB) allows blue colour development before stopping the reaction with the addition of sulphuric acid (H_2SO_4). The plate was read at 450 nm. Diagram made with BioRender (Toronto; Ontario; Canada).

2.7 Protein estimation

Protein estimation was performed using a detergent-compatible (DC) protein assay (Bio-Rad, Hemel Hempstead, UK). The assay is designed to measure protein concentrations using coulometric techniques following detergent solubilisation. Briefly, cell lysates were centrifuged at 20,817 x g at 4^{o}C for 10 minutes. Samples were diluted and applied in duplicates to a 96-well plate along with the BSA protein standard curve (Sigma-Aldrich; Poole; UK). Dilutions of protein standards were prepared each time the assay was performed to create a standard curve, from 0-2 mg/mL. The diluted cell lysates and the standards were pipetted onto the plate at 5 µL/well and then 20 µL of reagent S (surfactant solution) was added to each 1 mL of reagent A (alkaline copper tartrate solution) and 25 µL of this mix was applied to the plate. Reagent B (dilute folin reagent; Bio-Rad) was added to the plate at 200 µL/well. The plate was gently mixed and placed in the dark to incubate for 15 minutes at room temperature with gentle agitation. Optical density was measured at 650-759 nm with a microplate reader (POLARstar, BMG), and protein quantity was calculated then normalised to a final volume of 45 µL for loading using Excel Version 16.70 (Microsoft, USA).

2.8 Sodium dodecyl sulphate-polyacrylamide gel electrophoresis (SDS-PAGE)

Normalised protein lysate samples were added to x 5 loading buffer (10% w/v SDS, 10 mM β-mercaptoethanol, 20% v/v glycerol, 0.2M Tris-HCl (pH 6.8) and 0.05% w/v bromophenol blue) and heated at 95°C for 5 min. Samples were carefully applied to a 10% (v/v) SDS-polyacrylamide gel and separated by gel electrophoresis, which was performed using a Bio-Rad Mini-PROTEAN Tetra system (Bio-Rad) (see Table 2.2 for separating gel and stacking gel recipe). The system was submerged in x 1 SDS-PAGE running buffer (25 mM Tris- HCl, 200 mM glycine and 0.1% w/v SDS; all purchased from Sigma-Aldrich; Poole; UK), and samples were carefully loaded onto the gel. A Precision Plus Protein All Blue Standard (Bio-Rad) molecular weight marker (10-250 kD) was used in two lanes, on either side of the gel, to aid in the cutting of the membranes. Gel electrophoresis was performed at 200 V for 40 min using a Power Pack 300 (Bio-Rad).

Table 2.2 Separating (running) gel and stacking gel recipes used western blot.

Separating gel	**Required volume**	**Stacking gel**	**Required volume**
1.5M Tris pH 8.8	3.75 mL	0.5M Tris pH 8.8	1.25mL
30% acrylamide	5mL	30% acrylamide	650µL
H_2O	6mL	H_2O	3mL
10% SDS	150µL	10% SDS	50µL
10% APS	75µL	10% APS	25µL
TEMED	15µL	TEMED	5µL

2.9 Semi-dry membrane transfer

Prior to completion of the gel electrophoresis, Amersham™ Hybond®-P polyvinylidene difluoride (PVDF) membrane (GE HealthCare, Technologies Inc; Chicago, USA) was activated in methanol for 20 seconds and then transferred to cold x 1 transfer buffer (10% x 10 Tris-glycine and 20% methanol). Blot absorbent filter paper (Bio-Rad) was allowed to equilibrate in transfer buffer for 10 min. The SDS-PAGE gel was carefully transferred to a filter paper – PVDF sandwich, and another layer of filter paper was applied on top. A Trans-Blot Turbo transfer system (Bio-Rad) was used to transfer the proteins from the gel to the PVDF membrane at 25 V for 30 min. Once removed from the transfer system, the membrane was placed into 5% (w/v) bovine serum albumin (BSA; Sigma-Aldrich; Poole; UK) in Tris-buffered saline (TBS; Sigma-Aldrich; Poole; UK) for 1 h at room temperature with gentle agitation for non-specific blocking.

2.10 Immunoblotting

Membranes were probed with antibodies targeting different integrin subunits: integrin αV polyclonal antibody (Cell Signalling; 4711), integrin β3 antibody (Cell Signalling; (D7X3P) XP®

Rabbit IgG mAb 13166), α5 integrin polyclonal antibody (Cell Signalling; 4705), integrin β1 (Cell Signalling (D2E5) Rabbit IgG mAb 9699), integrin β5 (Cell Signalling (D24A5) Rabbit IgG mAb 13629) and integrin α4 (Cell Signalling; (D2E1) XP® Rabbit IgG mAb 8440). The protein loading was evaluated and normalised using monoclonal mouse β-actin Abcam (8226; isotype IgG1). All primary antibodies were used at 1:1000 dilutions in 5% (w/c) BSA, TBS, 0.1 Tween 20 (pH 7.6; Sigma-Aldrich; Poole; UK) overnight at 4 °C with gentle agitation.

The primary antibody solution was carefully discarded, and the PVDF membrane was washed three times with x1 TBS/0.05% Tween 20 and incubated in horseradish peroxidase conjugated (HRP) secondary antibody. The secondary antibody used was either anti-rabbit or anti-mouse IgG, HRP linked (7074S or 7076S respectively; both Cell Signalling) in x1 TBS/0.05% Tween 20 for 1.5 hours and then washed a further three times. The levels of immune reactive proteins were visualised using enhanced chemiluminescence (ECL; ChemiDoc XRS, Bio-Rad). Depending on the expression levels of the protein of interest, PVDF membranes were incubated for a period of 1 - 240 seconds with Amersham ECL Select Western blotting detection reagents (GE HealthCare Technologies Inc). Immunoblots were then saved for downstream densitometric analysis.

2.11 Densitometry

Semi-quantification of immune reactive proteins was performed using densitometry. Images of non-saturated immunoblots were transferred to ImageJ software 1.53k (Java 1.8.0; Wayne Rasband and contributors National Institutes of Health, USA). Briefly, a rectangular selection was employed to capture all specific immunoblots and lanes were consistently selected using the straight-line tool. The area of the histogram was then determined and normalised to the corresponding area of the β-actin loading control.

2.12 Adhesion of cells using Cell-Tak

To visualise monocytes on day zero of the differentiation, Cell-Tak (Corning, Massachusetts, USA), a specifically formulated protein solution extracted from the marine mussel, *Mytilus edulis,* was used at 3.5 µg/cm^2 per well to attach them to the chamber slides used for confocal microscopy. Cell-Tak was applied to the plate and was allowed to be absorbed onto the plate with the addition of 0.1 M sodium bicarbonate (Gibco; ThermoFisher Scientific;

Massachusetts, USA). After 20 minutes, the liquid was removed, and each individual well was washed once with sterile, endotoxin-free water. The chamber slide was left to dry at room temperature before being used immediately.

2.13 Confocal microscopy

Isolated monocytes were either adhered with Cell-Tak on a Millicell EZ 8-well chamber slides (Merck Millipore, Massachusetts, USA) or seeded onto the slides for culture in differentiation media. To visualise the nuclei and the cytoplasm, all the media was removed from the chamber slide. The chambers were washed twice with 1 X PBS before fixing with 10% neutral buffered formalin (Sigma-Aldrich; Poole; UK) for 15 minutes at room temperature. The cells were then washed twice with 1 X PBS (ThermoFisher Scientific; Massachusetts, USA) before adding 1 µg/mL of Hoechst 33342 Solution (ThermoFisher Scientific; Massachusetts, USA) and 0.1 % CellMask™ Orange plasma membrane stain (ThermoFisher Scientific; Massachusetts, USA), as per manufacturer's instructions. Cells were then incubated in the dark for 15-30 minutes at room temperature. The cells were washed a final two times with 1 X PBS before removing the chamber and adding VECTASHIELD® Mounting Medium for Fluorescence (Vector Laboratories, Burlingame, USA). Fixed cells were visualised at a range of magnifications using a laser scanning confocal microscope (Zeiss LSM720, Oberkochen, Germany). Image analysis was performed using ImageJ Software.

2.14 Mitochondria, RANK and TRAP visualisation

Prior to applying the primary antibodies to the cells, different fixing techniques were tested, and the best-suited fixing and permeabilisation method was used for each antibody (these data are shown in Appendix 10.1-10.3). Isolated monocytes grown on chamber slides were removed from the incubator and chilled for 5 minutes in the cold room before aspirating the media. Tris Buffered Saline (TBS; Thermo Scientific; Massachusetts, USA) was used to wash the cells three times before fixing them, using three different methods: 80% acetone (Thermo Scientific; Massachusetts, USA) was used to fix the cells at 4°C for 10-15 minutes (acetone 99% + 1 X TBS solution). The second method used 80% methanol (Fisher Scientific; UK), diluted with 1 X TBS, the cells were fixed at 4°C for 10-15 minutes. Finally, cells were fixed in 4% Paraformaldehyde (PFA) for 5-10 minutes. In all cases, the cells were then washed three times with 1 X TBS and then permeabilised with 0.01% Triton X-100 diluted in 1 X TBS for 10 minutes. After the fixing and permeabilising steps, the cells were washed three times with 1 X

TBS. The cells were then blocked with 5% normal goat serum (ab7481; Abcam, Cambridge, UK) for 60 minutes at room temperature.

All the primary antibodies were optimised to a suitable dilution and accordingly: diluted in 5 % normal goat serum, applied to the wells, and incubated overnight at 4°C. The next day, the cells were washed three times with 1 X TBS, and then the secondary antibody was added to the cells at an optimised dilution of 1:800 in block solution for one hour in the dark at room temperature. The cells were then washed three times with 1 X TBS for 5-10 minutes each time. Counterstains, such as the Hoechst and CellMask Orange, were applied (see Section 2.14). Finally, VECTASHIELD® Mounting Medium for Fluorescence (Vector Laboratories; Burlingame USA) before gently placing coverslips onto the slides. The sealed slides were stored at 4°C for at least 24 hours before imaging.

2.15 *In gel* zymography

Gelatine zymography is a method used to detect the activity of gelatinase enzymes, such as the matrix metalloproteases (MMPs) MMP-2 and MMP-9 here. *In-gel* zymography is an SDS-PAGE-based enzyme assay in which MMPs were analysed based on their ability to degrade gelatine. MMPs were electrophoretically separated on a 7.5% (v/v) SDS running gel that incorporated gelatine co-polymerised with acrylamide. MMPs hydrolyse the substrate dose-dependently, and this reaction is visualised as a zone of clearing after staining the gel with the Coomassie stain. Protein estimation methods were used to determine total protein concentration; equal protein concentrations for each sample were then loaded onto the gel. Sample preparation was then finalised by the addition of 5 X non-reducing sample buffer (see Table 2.3 for sample buffer recipe). MMPs were initially denatured with sodium dodecyl sulphate (SDS) to abolish the effects of charge and structure on migration. This way, they were separated based only on their mass. A Precision Plus Protein All Blue Standard (Bio-Rad) molecular weight marker (10-250 kD) was used in two lanes, on either side of the gel, to aid in the visualisation and the identity of MMPs (see Table 2.4 for separating and stacking gel recipes). To restore the activity of MMPs, the gel was incubated in a non-ionic detergent with a neutral pH, Triton™ X-100 (1 % diluted in distilled water) (Sigma-Aldrich; Poole; UK), which allowed the exchange of the SDS with the detergent. The gel was then incubated at 37 °C overnight in the incubation buffer that contains the co-factors (see Table 2.5 and 2.6 for the zymography washing and incubation buffer recipes). MMP-9 would need to be refolded to an active conformation to digest the co-polymerized gelatine. The gel is then stained with Coomassie Blue (see Table 2.7 for recipe) for 1 hour before applying a de-staining solution (see Table 2.8 for recipe) for 4-6 hours until clear bands are visible. The gel stains dark blue with the proteolytically cleaved sites remaining lightly stained/unstained (Figure 2.4).

Recombinant human MMP-9 was used as a positive control to further identify MMP-9 on the zymography gel (Biolegend; San Diego, USA). The gel was visualised using the ChemiDoc Imaging System (Bio-Rad, Hemel Hempstead, UK). Analysis of the gels was performed using densitometry. Images obtained were transferred to ImageJ software. Briefly, a rectangular selection was employed to capture all the lanes that were consistently selected using the straight-line tool. The area of the histogram was then calculated and plotted as either raw data or normalised to the control specific to the experiment.

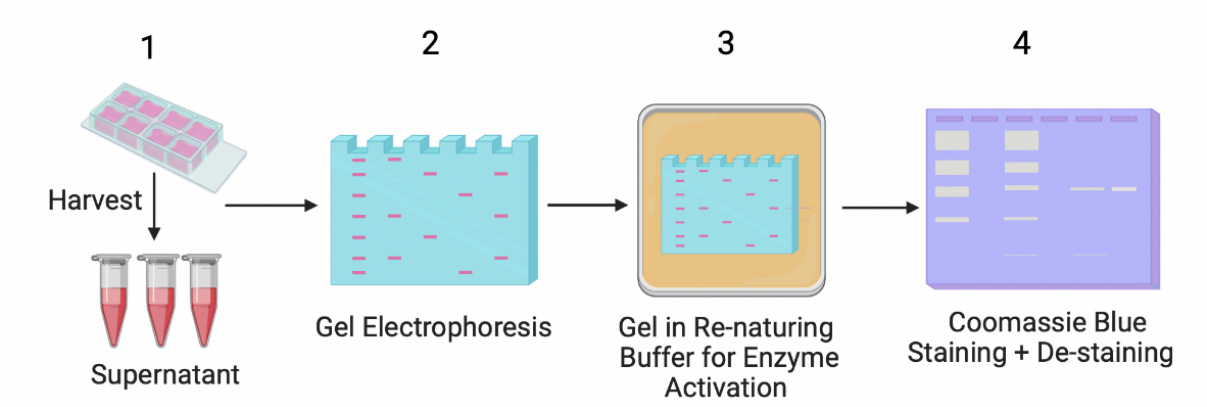

Figure 2.4 Gelatine zymography of MMPs.

The total protein concentration of harvested supernatants (1) was determined and run through gel electrophoresis (2). The gel was incubated in renaturing and assay buffer (3). The gel was stained with Coomassie Blue; bright bands of cleared zones indicated the activity of MMPs after de-staining (4).

Table 2.3 Complete recipe for the 5 X non-reducing sample buffer.

Non-reducing sample buffer (Final concentration)	**For 250 mL of sample buffer**
4% SDS	10g
20% glycerol	50mL of 100%
0.01% bromophenol blue	0.025g
125mM Tris-HCL, pH 6.8	4.91g

Table 2.4 Separating (running) gel and stacking gel recipes used in gel zymography.

Separating gel	**Required volume**	**Stacking gel**	**Required volume**
1.5M Tris pH 8.8	2mL	0.5M Tris pH 8.8	1.25mL
30% acrylamide	2mL	30% acrylamide	0.670mL
H_2O	2mL	H_2O	3.075mL
Gelatine (4mg/mL)	2mL	10% SDS	50µL
10% SDS	80µL	10% APS	50µL
10% APS	80µL	TEMED	10µL
TEMED	10µL		

Table 2.5 Recipe of the washing buffer used for in gel zymography.

Washing Buffer (Final concentration)	**For 250mL**
2.5% Triton X-100	6.25mL of 100%
50mM Tris-HCl	12.5mL of 1M stock
5mM $CaCl_2$	625µL of 2M stock
1µM $ZnCl_2$	2.5µL of 0.1M stock

Table 2.6 Recipe of the incubation buffer used for in gel zymography.

Incubation Buffer (Final Concentration)	**For 250 mL**
1% Triton X-100	2.5mL of 1M
Tris HCL 50 mM pH 7.5	12.5mL of 1M
5mM $CaCl_2$	625µL of 2M
1µM $ZnCl_2$	2.5µL of 0.1M

Table 2.7 Staining solution recipe used for in gel zymography.

Staining Solution (Final concentration)	**For 100 mL**
Methanol	40mL
Acetic acid	10mL
H_2O	50mL
Coomassie Blue	0.5g

Table 2.8 De-staining solution recipe used for in gel zymography.

De-staining solution (Final concentration)	**For 1L**
Methanol	400mL
Acetic acid	100mL
H_2O	500mL

2.16 The differentiation of monocytes into osteoclasts on the RTCA E-plates

The xCELLigence RTCA E-plate (Agilent, California, USA) was prepared by adding 50 µL of media to every well. The plate was inserted into the xCELLigence chamber, where the baseline impedance was measured to establish the Cell Index value as zero and to ensure that the wells were connected. Monocytes were counted and seeded onto the 96-well microplates (E-Plates) (initially, without any matrix coating) embedded with the gold biosensors at the bottom of each well (Figure 2.5). The total volume was increased to 200 µL by adding more media, and the volume was kept constant throughout all experiments. The plates were placed on the eSight in the incubator. The specific acquisition schedule for data and imaging was set up using the RTCA eSight software version 1.1.2. For all the experiments conducted in this thesis, three images were taken of each well every 1 hour. Over the duration of the experiment, the biosensors monitored the differentiation, recording changes in morphology and adhesion of cells. Every 2-3 days, the experiment was paused for approximately 15 minutes to allow media change and then resumed.

The RTCA eSight software (Research Use Only (RUO); version 1.1.2 Agilent, California, USA) was used in these experiments. The software presents the strength of cell adhesion as the Cell Index (no unit available). The Cell Index increases from zero as cells adhere to the plate. All experimental data in the files are permanent and cannot be altered or changed by the user. Data analysis was performed on the CI data taken at specific time points for all treatment conditions. The CI data was normalised to the control used in the experiment using Excel version 16.70 (Microsoft, USA), and the normalised CI data was plotted on GraphPad Prism version 9 (La Jolla, USA).

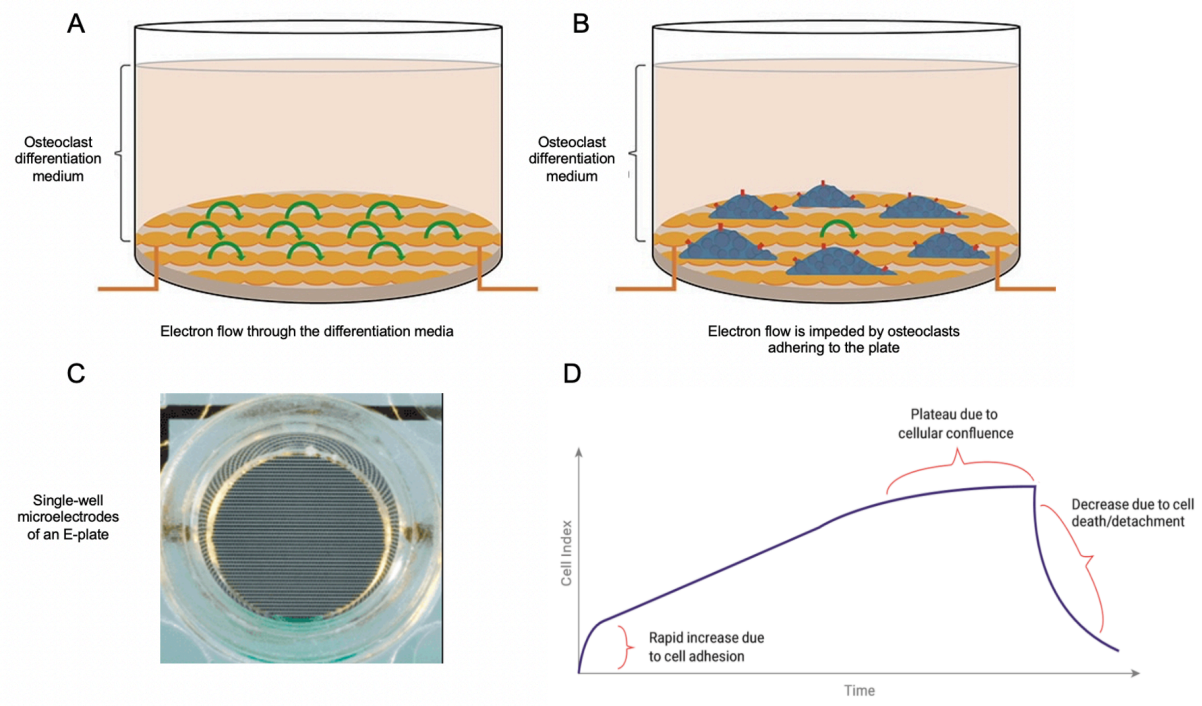

Figure 2.5 Electron flow in a single well of an E-plate

The xCELLigence RTCA label-free technology assesses cell number by measuring the changes in impedance through gold electrodes impeded in propriety E-plates. Impedance was measured in the absence of cells to establish the baseline value at CI zero (Figure 2.5A). Monocytes were then seeded onto an electronic microtiter plate (E-plate) wells. Differentiation of monocytes into osteoclasts causes the adhesion of cells to the gold microelectrode, impeding the flow of electric current between electrodes (Figure 2.5B, C). This impedance value, plotted as a unitless parameter called "Cell Index", increases as cells adhere more and then plateaus as the well reaches 100% coverage by cells (Figure 2.5 D). Figure adapted from Agilent.com.

2.17 Data analysis

Statistical analysis was performed using GraphPad version 9 (La Jolla, USA). Data are represented as the mean ± standard error of the mean (SEM) unless otherwise stated. Kolmogorov-Smirnoff test was used to test for normality. Any substantial deviation from normality resulted in a non-parametric test being used; otherwise, it was considered appropriate to use parametric statistics. Analysis of variance (ANOVA) was used to compare two or more group means with one variable (one-way ANOVA). For multiple comparisons, a two-way ANOVA or three-way ANOVA was used. All experiments have a replicate sample

size of at least n=3, and significant values were taken as $p < 0.05$ graphically denoted as * $p \leq 0.05$, ** $p \leq 0.01$, *** $p \leq 0.001$, and ****$p \leq 0.0001$. More detail is provided in each results chapter.

Chapter Three

The Optimisation of an Osteoclast Model Derived from Human Peripheral Blood Monocytes

3 The optimisation of an osteoclast model derived from human peripheral blood monocytes

3.1.1 Introduction

Bone remodelling is the process by which old bone is replaced by new bone; it helps maintain mineral homeostasis by releasing calcium and phosphorus into the circulation[265]. Bone remodelling occurs at specific sites on bone surfaces. The remodelling process involves two types of bone cells: osteoclasts and osteoblasts[266]. Osteoclasts are multinucleated cells that attach to the bone surface to enable bone resorption, whereas osteoblasts are responsible for bone formation as well as regulating bone mineralisation[267]. Osteoclasts are derived from the monocyte/macrophage lineage. Osteoclasts can originate from hematopoietic stem cells (HSCs) directly and from mature cells of the monocyte-macrophage lineage when a suitable bone marrow microenvironment is provided[268]. Osteoclast precursors also reside in the human mononuclear fraction of peripheral blood[269]. Human peripheral blood monocytes consist of classical (CD14++CD16-), intermediate (CD14++CD16+), and nonclassical (CD14+CD16++)[270,271] subunits. The three subunits are phenotypically and functionally different in migration, cytokine production and differentiation[272]. It has been suggested that human osteoclast precursors reside within the classical subset of peripheral blood monocytes but not in the CD16+ subsets[273]. Osteoclasts have been shown to originate from CD14+CD16- monocytes *in vitro* in the presence of M-CSF and RANKL[274]. In response to these cytokines, cells of the monocyte or macrophage lineage differentiate into osteoclast precursors that ultimately fuse to form multinucleated osteoclasts[275,276]. This is the canonical differentiation pathway. The non canonical pathway corresponds to the differentiation of osteoclast when exposed to M-CSF and alternative substances for RANKL (e.g., TNFα, TGFβ, IL-6, IL-11, IL-8), or when exposed to RANKL and alternative substances for M-CSF (e.g., HGF, VEGF, Flt3 ligand)[277]. Osteoclasts are the only cells in the bone marrow microenvironment known to cause bone resorption.

The mechanism of bone resorption was unknown until the 1980s, when cathepsins and matrix metalloproteases (MMPs) were identified as the proteases most involved in bone resorption[278]. To resorb bone effectively, osteoclasts must attach themselves to the bone surface. Upon attachment, they form tight seals with the underlying bone matrix by extending the cytoplasm and forming ruffled border membranes, an intensely convoluted membrane inside the sealing zone[279–281]. This ruffling of the cytoplasm increases the surface area of the cells for secretion of the proteolytic enzymes[282,283]. This sealing and secretory mechanism allow the degradation of the matrix and the dissolving of the mineral of the bone while protecting adjacent cells from the harmful acidified microenvironment secreted by osteoclasts

during bone resorption[284]. Hydrochloric acid is released by mature osteoclasts close to the ruffled border, leading to the dissolution of the organic bone matrix. Osteoclasts also produce cathepsin K and matrix metalloproteases (MMPs), which degrade the residual bone matrix[285,286]. Cathepsin K is a potent cysteine proteinase that degrades the type I collagen matrix[287]. MMPs are a class of zymogens that have shared and unique properties; osteoclasts predominantly express MMP-9 *in vitro* and *in vivo*[288]. MMP-9 is a zinc-dependent endopeptidase that is secreted as an inactive enzyme (pro-MMP-9) with a molecular weight of 92 kDa[288]. Activation of MMM-9 requires the disruption of the cysteine interaction with the zinc atom, exposing the catalytic site[289,290]. The most studied mechanism of MMP-9 activation is enzyme proteolysis by the pro-domain[289]. MMP-9 is responsible for the degradation and remodelling of the extracellular matrix proteins during normal developmental processes and pathological processes[291,292]. MMP-9 initiates osteoclast-mediated bone resorption by removing collagen and demineralised bone, which is vital for bone resorption[292,293]. Substrates for MMP-9 include type IV collagen, gelatine, and laminin[293,294].

RANKL and integrins, such as $\alpha V\beta 3$, mediate cell-to-cell and cell-to-matrix recognition[295,296]. Interactions with the bone matrix via $\beta 3$ and RANKL activates osteoclasts[297]. Osteoclast precursors fuse together under the influence of RANKL. RANKL is a member of the TNFα ligand family, which also induces the expression of tartrate-resistant acid phosphatase (TRAP) and cathepsin K in osteoclasts through the nuclear factor of activated T cells (NFAT-c1), which is a member of the nuclear factor of activated T cells (NFAT) family of transcription factors[298]. RANKL is a type II heterotrimeric transmembrane protein that is typically expressed on the membrane of osteoblasts and stromal cells and activates T cells. RANKL is also found in a soluble form secreted into the bone marrow microenvironment by some cells, such as activated T cells, to induce osteoclastogenesis[299,300]. RANKL is also produced by osteoblasts and the main source of RANKL in bone are osteocytes[301]. RANKL binds to a receptor activator of nuclear factor κB (RANK), which is a homotrimeric transmembrane protein that belongs to the TNF receptor superfamily[302]. RANKL-RANK interactions induced the recruitment and activation of major adaptor proteins that promote osteoclast precursors differentiation to osteoclasts[303,304]. One of the major adaptor proteins involved in the RANKL-RANK-mediated differentiation is TNF receptor-associated factor 6 (TRAF 6) to certain sites within the intracellular domain of RANK. TRAF 6 then acts as a second messenger, which activates multiple protein kinase pathways as well as transcription factors, such as nuclear factor kappa B (NF-κB). The activated NF-κB translocates into the nucleus and upregulates the expression of c-fos, which in turn interacts with NFAT-c1. This induces the transcription of osteoclastogenic genes (Figure 3.1)[304–306]. Osteoprotegerin (OPG) is another protein that belongs to the TNF receptor family. It is a soluble decoy receptor that binds to RANKL, thereby

inhibiting the interaction of RANKL with RANK. OPG is produced by osteoblast and bone marrow stromal cells. OPG inhibits osteoclast differentiation and maturation, thereby promoting their apoptosis (Figure 3.2).

Multiple myeloma is a plasma cell disorder whereby clonal plasma cells infiltrate the bone marrow, causing the production of monoclonal immunoglobulins[307] in conjunction with the development of end-organ damage, including hypercalcemia, anaemia and renal impairment[308]. The presence of end-organ damage is what differentiates symptomatic from asymptomatic MM[309]. Myeloma bone disease is a devastating complication of MM and one of the main contributors to symptoms in MM, with up to 60% of patients experiencing bone pain and 60% developing pathological fractures during the disease[309,310]. Typically, bone lesions are associated with decreased quality of life and complications of such lesions are associated with around a 20% increase in mortality in MM[311,312]. In myeloma bone disease, lesions could be in the form of a classic discrete lytic lesion such as plasmacytoma and radiolucent, widespread osteopenia[313], or multiple lytic lesions affecting many parts of the skeleton; the most common location is the axial skeleton[314]. With $\geq$ 3 large focal lesions, the poorer the prognosis in newly diagnosed myeloma patients[313,315].

The main mechanism associated with myeloma bone disease is the upregulation of osteoclastogenesis along with osteoblastogenesis inhibition[316]. The main factors involved in the hyperactivation of osteoclasts and reduction of osteoblast proliferation are the elevated levels and secretion of RANKL[317] and the reduction in OPG formation and secretion by stromal and osteoblastic lineage cells[318,319]. Typically, patients with MM will require anti-myeloma treatment; however, with the presence of myeloma bone disease, patients will require additional treatments, such as bisphosphonates[320 321], radiotherapy, and in some instances, surgical interventions (such as vertebroplasty) that are required as early as possible[320]. In normal bone remodelling, osteoclastic activity is responsible for the degradation of mineralised bone during bone development, homeostasis and repair, and osteoblastic activity is responsible for new bone formation in the developing skeleton and during bone remodelling[322,323]. In healthy individuals, this process is well-regulated and well-balanced to keep bones in healthy condition. Cytokine and hormone release in the bone marrow microenvironment is responsible for this regulation[324,325]. In healthy individuals, the RANKL/OPG ratio is low. On the contrary, in MM patients, OPG is reduced and correlates significantly with the severity of the bone disease. In MM, the coupling of osteoclast and osteoblast function is absent, and an increase in osteoclastic activity is observed, resulting in elevated bone resorption accompanied by a decrease in bone formation due to the suppressed activity of osteoblasts. Myeloma bone disease, where there is a decrease in bone

formation and an increase in bone resorption, differs from other metastatic diseases as in other cancers such as prostate cancer, osteoblastic and osteoclastic activity is increasedClick or tap here to enter text.'[326]. The increased activity of osteoclasts in myeloma bone disease results in the elevated secretion of resorptive markers that are recognised to be elevated in patients with MM, such as urinary N-telopeptide (U-Ntx) and serum carboxy-terminal telopeptide of type I collagen (S-ICTP)[327,328]. The interactions between myeloma cells and bone marrow stromal cells within the bone marrow microenvironment contribute largely to the development of myeloma bone disease[329]. Myeloma bone disease not only increases the disability and morbidity in patients with MM but also increases the cost of treatment for these patients. Therefore, interventions that control such complications will positively impact their quality of life.

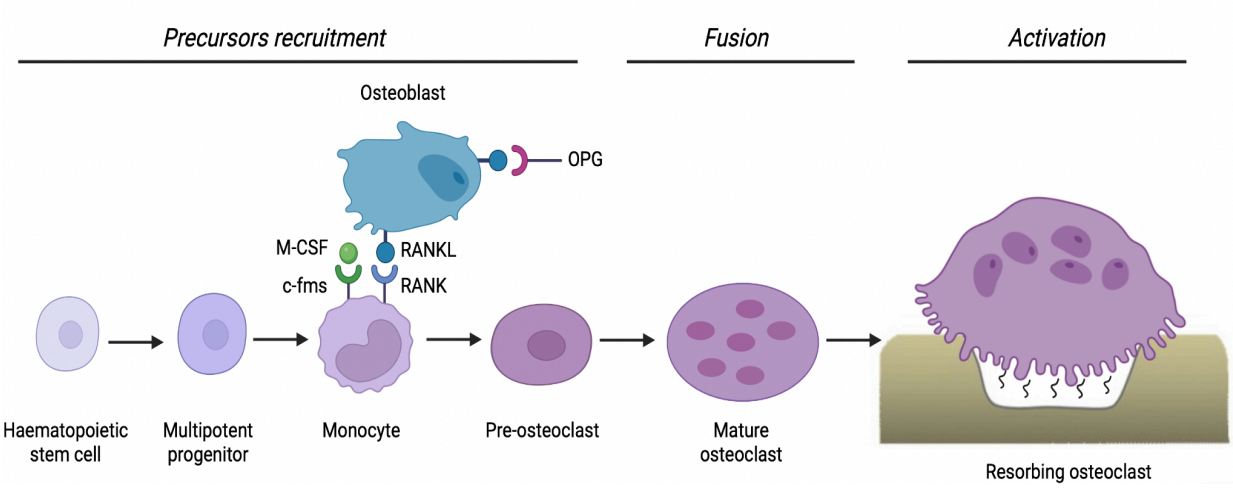

Figure 3.1 Schematic illustration of the cells and molecules involved in osteoclastogenesis.

Osteoclasts originate from hematopoietic cells of the monocyte-macrophage lineage under the control of bone-forming osteoblasts. M-CSF and RANKL are the two main factors controlling their differentiation. M-CSF is necessary for precursor recruitment and RANKL expression on pre-osteoclasts. RANKL enables the fusion of pre-osteoclasts into polykaryon and the final differentiation into mature osteoclasts. Bone resorption occurs with the acidification of the resorption lacuna followed by proteolysis to remove the organic matrix. OPG = osteoprotegerin; M-CSF = macrophage-colony stimulating factor; c-fms = colony-stimulating factor-1 receptor; RANK = receptor activator of NF-κB; RANKL = receptor activator of NF-κB ligand. Figure made using BioRender.

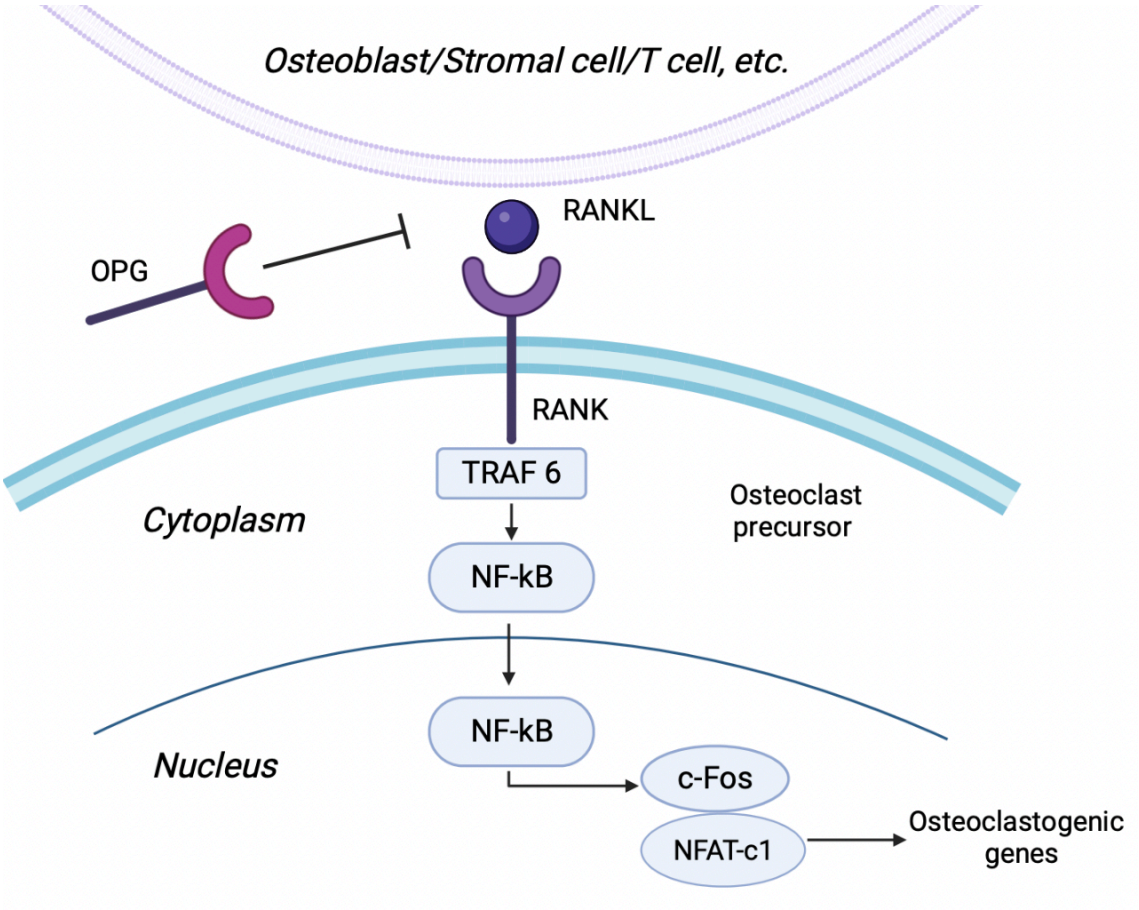

Figure 3.2 Signalling pathways activated by RANK-RANKL interactions.

RANKL can be produced by osteoblasts, stromal cells, T cells and other cells. RANK is a receptor for RANKL present on the surface of osteoclasts and osteoclast precursors. RANK activation leads to the recruitment of the adapter protein TRAF 6, leading to NF-kB activation and, subsequently, translocation to the nucleus. This increases c-Fos expression, which interacts with NFAT-c1 to trigger the transcription of osteogenic genes. This pathway is subjected to inhibition by osteoprotegerin (OPG), which prevents RANKL from interacting with RANK in the extracellular environment. Figure made using BioRender.

3.1.2 Rationale

The study of osteoclasts in humans requires a model of osteoclast differentiation and fusion, as access to primary material is ethically and practically restrictive. Monocytes can be isolated readily from the peripheral blood and differentiated into osteoclasts within a defined cytokine environment. Therefore, a monocyte-derived osteoclast model was utulised using the blood of healthy donors. The reasons for this were (i) to allow a better understanding of their formation and activation as (iii) the understanding of such effects will reveal novel therapeutic targets for the treatment of myeloma bone disease in patients. Recently, the xCELLigence real-time cell analysis (RTCA) system was developed to observe cell morphology and cell adhesion using electrical impedance *in vitro*[330,331]. The core mechanism of the system is composed of microelectronic cell biosensor arrays that are integrated into the bottom of the E-plate[331,332]. It monitors the changes in the cells by measuring the electronic impedance of these biosensors[332]. Biological processes such as cell viability, cell number, cell morphology, and the degree of adhesion can affect electrode impedance[333]. The differentiation of human peripheral blood monocytes into osteoclasts has not been studied in RTCA settings before. Here, real-time changes in osteoclast morphology are captured to track their differentiation in real-time.

3.1.3 Hypothesis

xCELLigence Real-Time Cell Analysis (eSight) can be used to monitor osteoclast differentiation and migration *in vitro.*

3.2 Experimental procedures

3.2.1 Samples

Human peripheral blood from healthy, non-fasted individuals was collected into heparinised Vacuettes™ (Greiner Bio-one, Frickenhausen, Germany). The healthy volunteers gave informed written consented and were over the age of 18 years, as detailed in *chapter 2.4 Sample collection and preparation.*

3.2.2 Monocytes isolation

Monocytes were isolated by positive selection on magnetic microbeads as described in Chapter *2.4.1 Blood* separation and *2.4.2 Mononuclear cell isolation*. Briefly, the pellet containing the monocytes was resuspended in differentiation or complete cell culture media as described in *3.2.3 Differentiation of monocytes into osteoclasts using M-CSF and RANKL differentiation media.* Cell density was determined using the Countess® automated cell counter (Life Technologies). To check monocyte purity, an anti-CD14 antibody (Clone 61D3; fluorophore eFluor®450; isotype mIgG1) was added to 100,000 monocytes. The cells were incubated with the antibody for 30 minutes. The cells were washed twice with FACS buffer (0.2% (w/v) bovine serum albumin (BSA), 0.05% (w/v) sodium azide (Sigma-Aldrich) in PBS) and centrifuged at 515 *x g* at 4 ºC for 7 minutes; the pellet was resuspended in the FACS buffer and checked for purity and acquired using the NovoCyte Flow Cytometer (BD Biosciences). Data analysis post-acquisition was interpreted using FlowJo Version 1.3 (Tree Star, Oregon, USA). Purity $\geq$ 92% was accepted for downstream experiments.

3.2.3 The differentiation of monocytes into osteoclasts using M-CSF and RANKL differentiation media in chamber slides

Monocytes were cultured at a density of 100,000 cells/200 μL of RPMI Glutamax, 10% charcoal-stripped FBS, 100 ng/mL RANKL, 25 ng/mL M-CSF and 1 % penicillin/streptomycin. The cells were put on Millicell EZ 8-well chamber slides (Merck Millipore, Massachusetts, USA) or seeded onto the slides for culture in differentiation media and incubated at 37 °C in 5% CO_2-in-air for the 14 days of differentiation. The media was changed every 2-3 days; around 100 μL of the media was collected from the chamber slides into micro-tubes and stored at -20°C for downstream experiments. Fresh media was added to replace the harvested media (Figure 3.3).

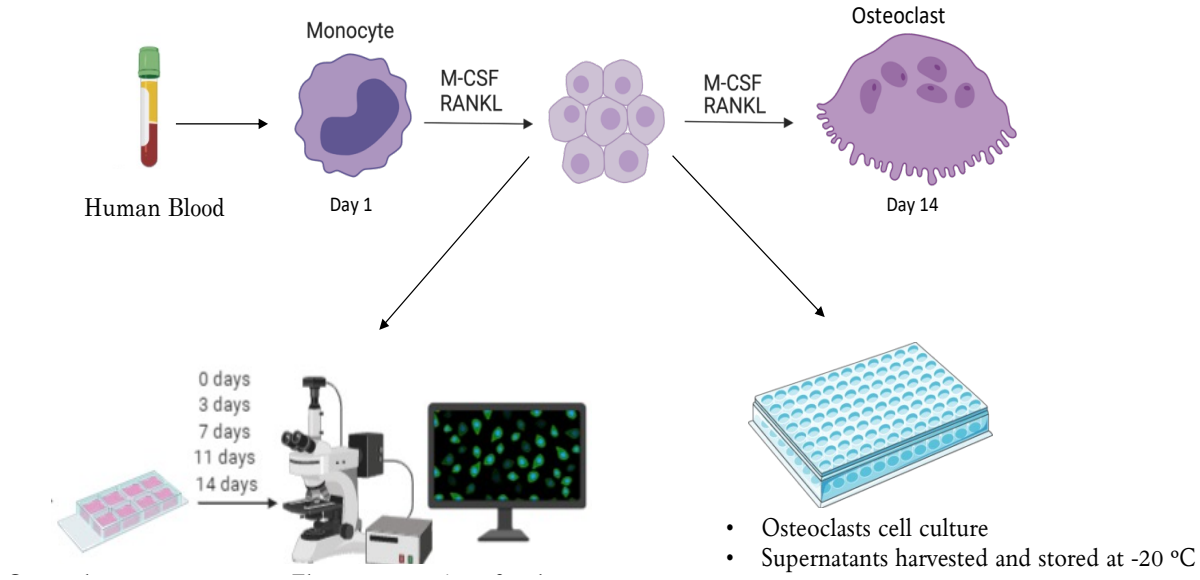

Figure 3.3 The differentiation of osteoclasts from peripheral blood monocytes.
Monocytes were isolated from human peripheral blood using a density gradient technique and positive selection with CD14 microbeads. Cells were seeded on either MilliCell EZ 8-well chamber slides or culture plates at a density of 100,000 cells/200 μL. Media changes occurred every 2-3 days, where half of the volume of media was collected and stored for future analysis, and fresh complete differentiation media was added. Osteoclasts were subjected to various stains and antibodies to determine the changes in morphology and to determine the expression of various marker proteins using confocal microscopy. To visualise the nuclei and the cytoplasm, Hoechst 33342 and CellMask™ Orange plasma membrane stain were used; anti-TOMM20 was used to visualise the mitochondria, anti-tartrate resistant acid phosphatase (TRAP) and anti-RANK were used to identify the presence of osteoclasts. Monocytes were also seeded onto cell culture plates in the presence of M-CSF and RANKL. Supernatants were harvested to be used for various experimental assays, such as ELISA and in gel zymography.

3.2.4 Confocal Microscopy

Isolated monocytes were seeded on Millicell EZ 8-well chamber slides (Merck Millipore, Massachusetts, USA) and cultured in differentiation media. Slides were fixed for visualisation on various days throughout the differentiation period to determine the changes in morphology as the cells differentiate. Since the media was changed every 2-3 days, slides were harvested on day 3, day 7, day 9, day 11, and day 14 (Figure 3.4). Sample preparation was performed as per chapter *2.13 Confocal microscopy*. The stains used in this chapter were Hoechst 33342 Solution (ThermoFisher Scientific; Massachusetts, USA) and 0.1 % CellMask™ Orange plasma membrane stain (ThermoFisher Scientific; Massachusetts, USA). Primary antibodies

used in confocal microscopy included anti-TOMM20 mouse monoclonal (ab56783; isotype IgG1), and anti- TRAP mouse monoclonal antibody [rACP5/1070] (ab238033; isotype IgG1) that were both purchased from Abcam, Cambridge, UK. Anti- RANK monoclonal mouse antibody (Clone 80707; isotype IgG_{2A}) was purchased from R&D systems (Biotechne; Minneapolis; Minnesota, USA). The secondary antibody used in confocal microscopy was a goat anti-mouse H&L polyclonal antibody (Alexa Fluor 488; ab150113, isotype IgG) purchased from Abcam Cambridge, UK. Fixed cells were visualised at 20X and 63X magnification using a laser scanning confocal microscope (Zeiss LSM720, Oberkochen, Germany). Image analysis was performed using ImageJ Software 1.53k (Java 1.8.0; Wayne Rasband and contributors National Institutes of Health, USA).

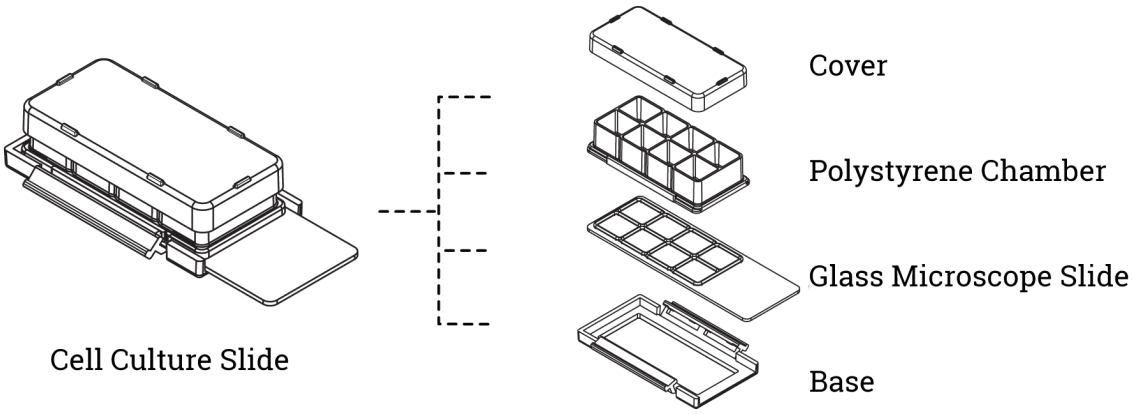

Figure 3.4 The utilisation of Millicell EZ Slides to monitor osteoclast differentiation from healthy peripheral blood monocytes.

The chamber slides consist of 4 different components. On the day of harvest, upon fixing and staining the cells, the cover, the polystyrene chamber, and the base parts were removed. The VECTASHIELD® Mounting Medium was added directly to the glass microscope slide; coverslips were added, and slides were stored at 4℃ until imaging. The usage of such chamber slides allowed the monitoring of the differentiation of osteoclasts without the need to detach the cells from the culture well.

3.2.5 Enzyme-linked immunosorbent assay (ELISA)

Analysis of cytokines using ELISA was as per the manufacturer's instructions (DuoSet; Biotechne). See Chapter *2.6 Enzyme-Linked Immunosorbent assay (ELISA)*. The ELISA kits used in this chapter were to detect the levels of matrix metalloprotease 2 (MMP-2) and MMP-9 secreted by osteoclasts into the supernatants during differentiation.

3.2.6 *In-gel* Zymography

Gelatine zymography is a method used to detect the activity of gelatinase enzymes, such as the matrix metalloproteases (MMPs) MMP-2 and MMP-9. *In gel* zymography was performed as detailed in Chapter *2.15 In gel zymography*. See *Table 2.4 Recipe of the washing buffer used for in gel zymography* and *Table 2.5 Recipe of the incubation buffer used for in gel zymography* for the zymography washing and incubation buffer recipes. For the Coomassie Blue staining and de-staining solution, see *Table 2.6 Staining solution recipe used for in gel zymography* and *Table 2.7 De-staining solution recipe used for in gel zymography.* The gel stains dark blue with the proteolytically cleaved sites remaining lightly stained/unstained. Recombinant human MMP-9 was used as a positive control to further identify MMP-9 on the zymography gel (Biolegend; San Diego, USA).

3.2.7 xCELLigence Real-Time Cell Analysis-eSight model

Monocyte differentiation into osteoclasts on the E-plates was performed as detailed in Chapter *2.16 The differentiation of monocytes into osteoclasts on the RTCA E-plates*. Every 2-3 days, the experiment was paused for approximately 15 minutes to allow media change and then resumed. The RTCA eSight software (Research Use Only (RUO); version 1.1.2 Agilent, California, USA) was used in these experiments. All experimental data in the files are permanent and cannot be altered or changed by the user.

3.2.8 Statistics

Statistical analysis was performed using GraphPad Prism version 9.4.1 (USA). Data are presented as the mean +/- standard error of the mean. A two-way ANOVA was used to compare the means of MMP-9 and MMP-2 levels during the differentiation time course. A two-way ANOVA was used to compare the activity of osteoclast derived MMP-9 using *in gel* zymography. All experiments have sample sizes of at least n=3, and significant values were taken as $p < 0.05$ graphically denoted as * $p \leq 0.05$, ** $p \leq 0.01$, *** $p \leq 0.001$ and **** $p \leq 0.0001$.

The xCELLigence graphs shown in this chapter are representative of several repeated experiments. The CI data were averaged and presented as a ratio of DMSO (VC) $n \geq 4$. Two-way ANOVA was used to compare the effects of the different treatments; significant values were taken as $p < 0.05$ graphically denoted as * $p \leq 0.05$ and ** $p \leq 0.01$.

3.3 Results

3.3.4 Osteoclast differentiation from peripheral blood monocytes

Before a detailed investigation of the formation and activation of the *in vitro* osteoclast model, confocal microscopy was first used to determine the changes in morphology and structure of monocytes on day 0 (Figure 3.5 A) in comparison to osteoclasts on day 14 (Figure 3.5 B). Monocytes were grown on the Millicell EZ chamber slide in the presence of M-CSF and RANKL, which promoted the differentiation of monocytes into osteoclasts with multi-nucleated cells with ruffled edges. (See Appendix 10.6 for confocal images of the differentiation on days 0, 3, 5, 7, 10, and 14) The example shown is representative of 6 repeated experiments taken at X63 magnification.

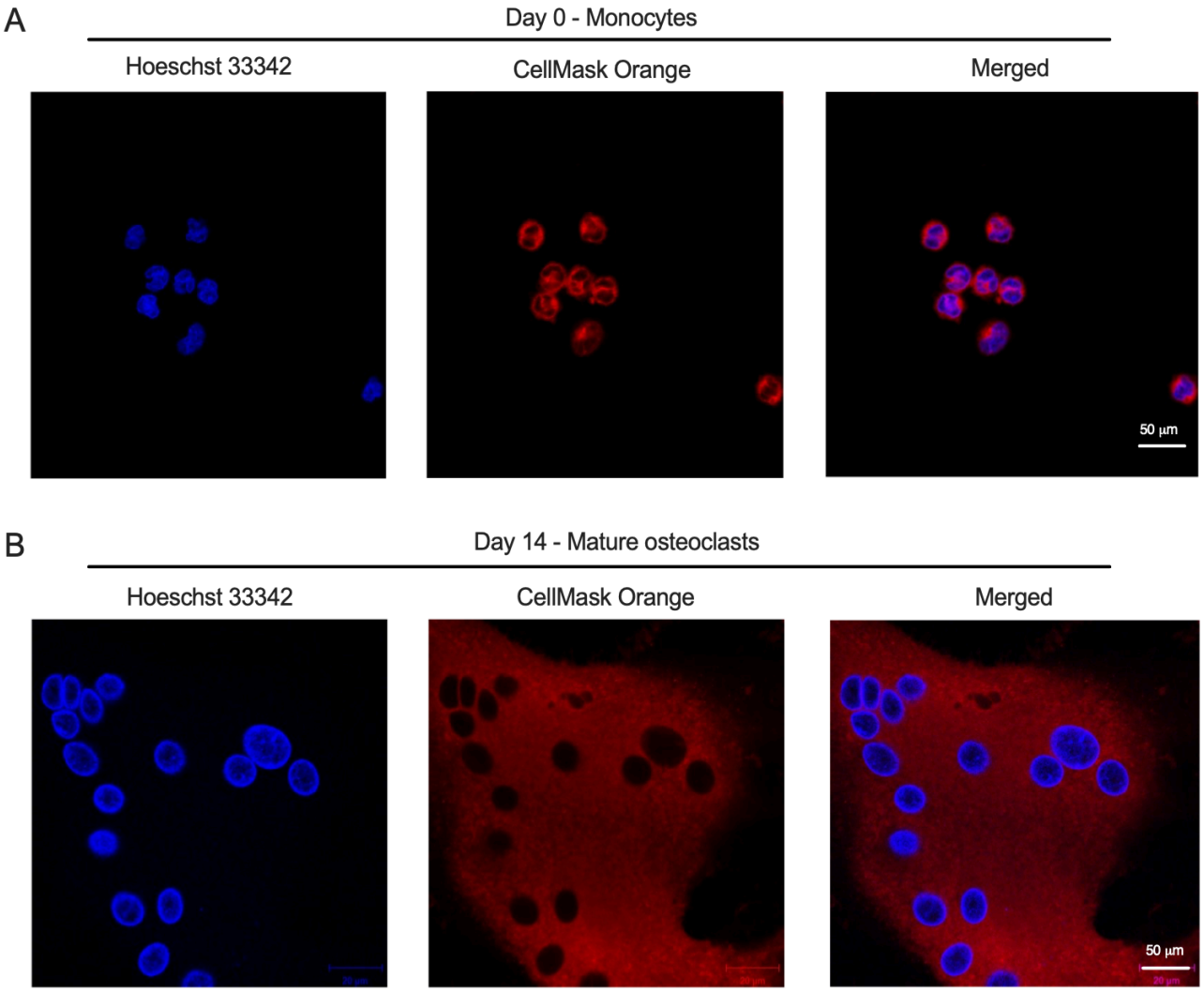

Figure 3.5 Monocyte-derived osteoclast differentiation with M-CSF and RANKL.

M-CSF and RANKL were used to drive the differentiation of monocytes isolated from healthy donors into osteoclasts. Confocal microscopy was used to determine the differentiation of

monocytes on day 0 (A) into mature osteoclasts on day 14 (B). Nuclei were stained with Hoechst 33342 Solution and the plasma membrane was stained with CellMask™ Orange. Images were taken at X63 magnification, and a 50 μm scale bar was included. Representative images from n= 6 experiments.

To further explore this and to further confirm the identity of the differentiated cells as osteoclasts, the expression of osteoclast markers, such as TRAP and RANK, was examined. Mature osteoclasts express TRAP, and it is considered to be a histochemical marker to identify the presence of osteoclasts[334]. It plays a critical role in the degradation and mineralisation of bone due to its ability to degrade bone matrix phosphoproteins, including osteopontin and bone sialoprotein[335–337]. As previously discussed, osteoclast precursors and mature osteoclasts express RANK on their surface and, therefore, are likely to express RANK in the *in vitro* model. Probing the cells with anti-TRAP and anti-RANK on day 0 and day 14 revealed that TRAP and RANK expression was enhanced on day 14 in comparison to day 0 (Figure 3.6 A-B and Figure 3.6 C-D, respectively). The example shown is representative of six repeated experiments (See Appendix 10.4 and 10.5 for X63 confocal images of TRAP and RANK expression).

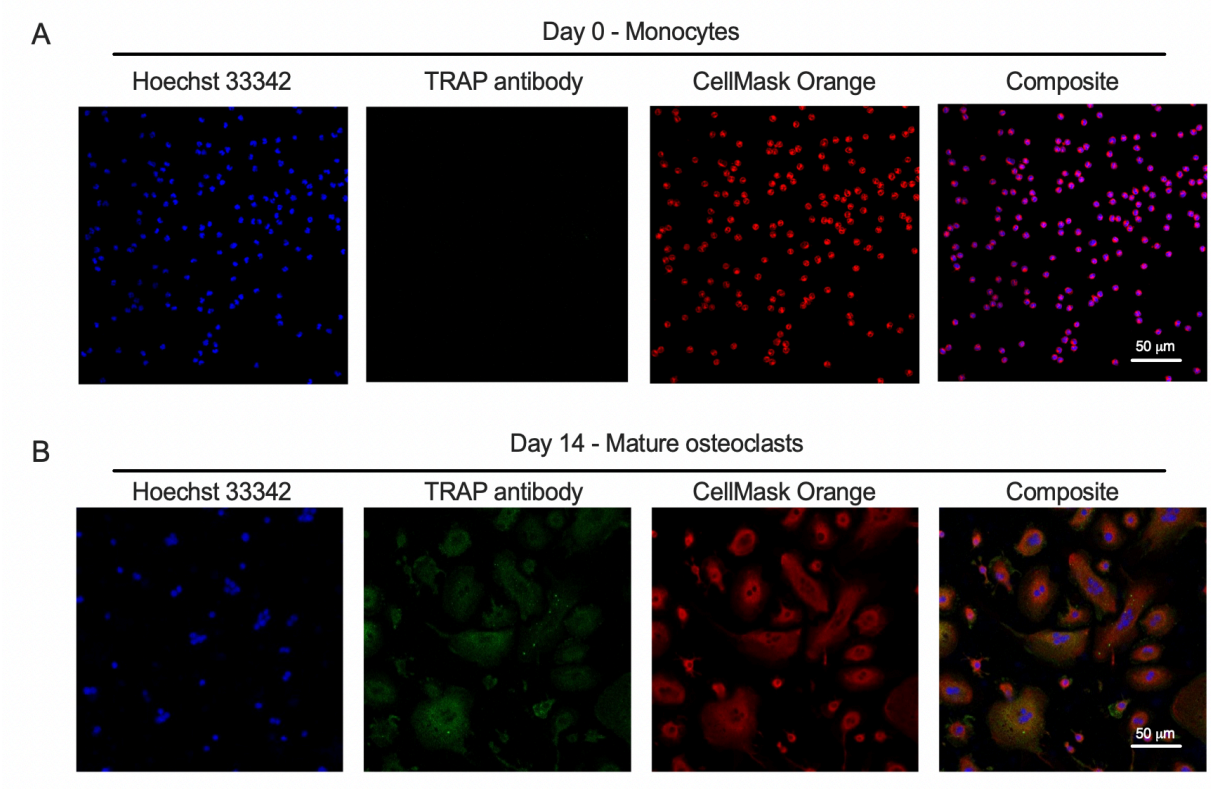

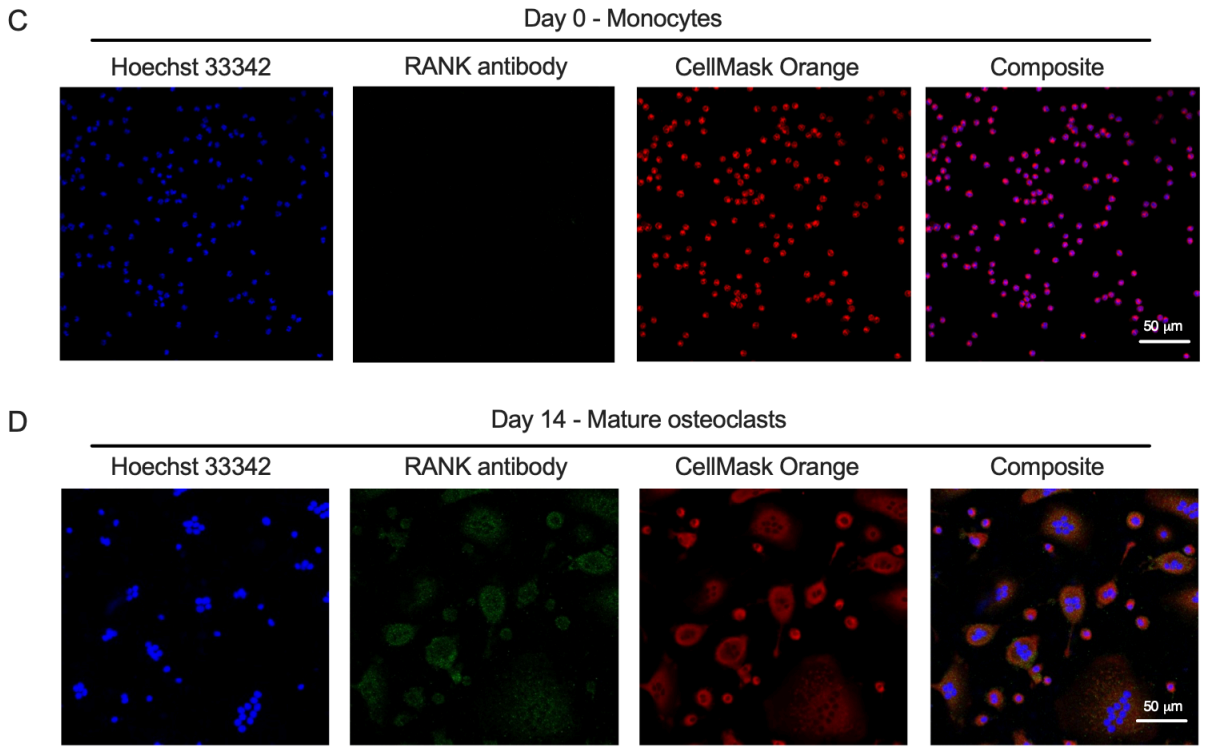

Figure 3.6 TRAP and RANK expression on monocyte-derived osteoclasts differentiated with M-CSF and RANKL.

M-CSF and RANKL were used to drive the differentiation of monocytes isolated from healthy donors into osteoclasts. Confocal microscopy was used to determine the expression of TRAP and RANK on day 0 (A and C, respectively) and day 14 (B and D, respectively). Nuclei were stained with Hoechst 33342 Solution and the plasma membrane was stained with CellMask™ Orange. TRAP and RANK were stained with FITC-labelled antibodies. Images were taken at X20 magnification, and a 50 µm scale bar was included. Representative images from n= 6 experiments.

The differentiation process of monocytes into mature osteoclasts is regulated by many factors *in vivo* that causes changes in their metabolism. There is enhanced glucose/glutamine uptake during osteoclastogenesis and bone resorption[338,339]. Osteoclast differentiation in murine bone marrow macrophages revealed that both glycolysis and oxidative phosphorylation were found to be increased. This is accompanied by an increase in the number, the size and the cristae abundance of mitochondria[340,341]. Therefore, the changes in mitochondria during differentiation were visualised using confocal microscopy. TOMM20 antibody was used to probe the mitochondrial in monocytes (Figure 3.7 A) and mature osteoclasts at two magnifications: X20 (Figure 3.7 B) and X63 (Figure 3.7 C). There appears to be a change in

the distribution of the mitochondria in monocytes in comparison to mature osteoclasts. In images captured on day 0, the distribution of the mitochondria in a compact manner, and as they differentiate into osteoclasts, an increase in their distribution , which can suggest mitochondrial fusion. The example shown is representative of 6 repeated experiments taken at X20 and X63 magnification.

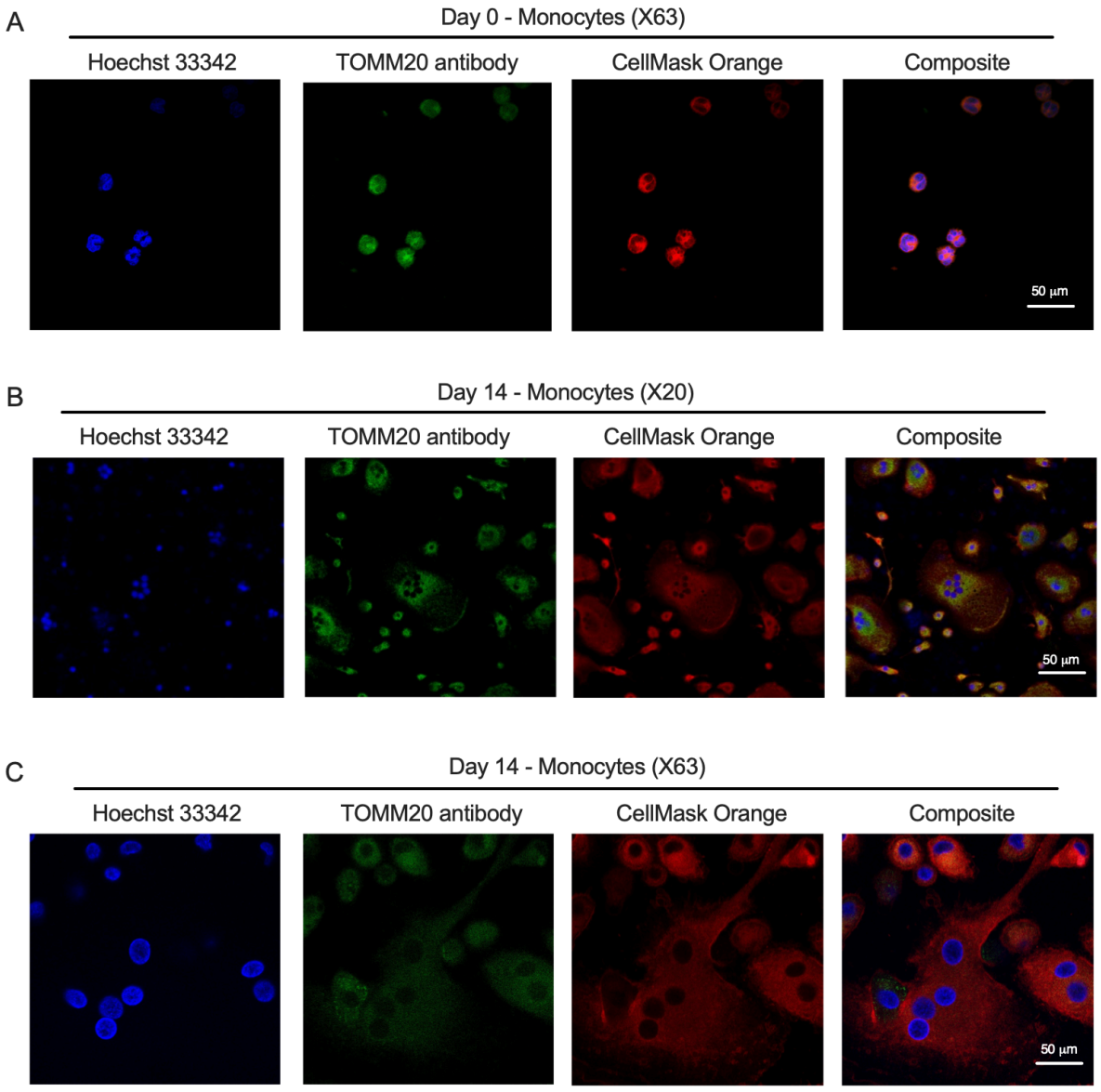

Figure 3.7 Expression of mitochondria in monocyte-derived osteoclasts differentiated with M-CSF and RANKL.

M-CSF and RANKL were used to drive the differentiation of monocytes isolated from healthy donors into osteoclasts. A mitochondria-specific antibody, TOMM20, was used to visualise the changes in shape and size of the mitochondria in monocytes at X63 (A) as they differentiated into mature osteoclasts at X20 (B) and X63 (C). Nuclei were stained with Hoechst 33342

Solution and the plasma membrane was stained with CellMask™ Orange, and the mitochondria were stained with FITC-labelled antibodies. Images were taken at X20 and X63 magnification, and a 50 μm scale bar was included. Representative images from n= 6 experiments.

Using the X20 images, the number of osteoclasts per image and the average number of nuclei per osteoclast were scored manually and presented in Figure 3.8A and 3.8B respectfully. Counting the number of osteoclasts revealed that osteoclasts appear from day 5 (3+ nuclei per cell). Then number of osteoclasts increases rapidly and significantly when compared to day 0 from day 7 (**** $p \leq 0.0001$) and remained high on day 11 (**** $p \leq 0.0001$) and day 14 (**** $p \leq 0.0001$). The average number of nuclei per osteoclast appeared to be increasing significantly from day 7 (**** $p \leq 0.0001$) and remained elevated on day 11 (**** $p \leq 0.0001$) and day 14 (**** $p \leq 0.0001$).

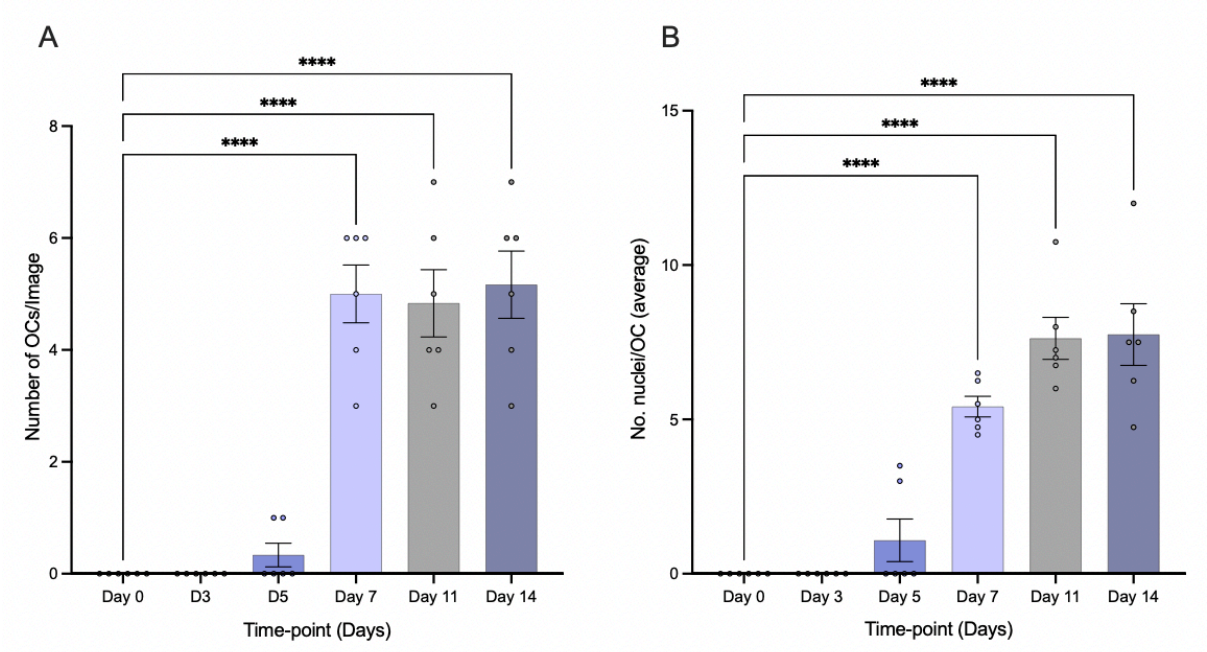

Figure 3.8. M-CSF and RANKL were used to drive the differentiation of monocytes isolated from healthy donors into osteoclasts. *Confocal images at X20 were used to score the number of osteoclasts per image (A) and the number of nuclei per osteoclast (B). Statistics were performed with a one-way ANOVA and Turkey's multiple comparisons test. Data are from n= 6 independent experiments expressed as the mean ± SEM: **** $p \leq 0.0001$.*

3.3.5 MMP-9 expression and proteolytic activity of monocyte-derived osteoclasts

Supernatants were harvested during the differentiation time course. The quantity of MMP-2 and MMP-9 secreted by monocytes as they differentiate was determined over the 14 days of differentiation using a specific ELISA. Upon incubation in the differentiation media, monocytes produce increasingly more MMP-2 (Figure 3.9 A) and MMP-9 (Figure 3.9 B) with levels significantly higher than baseline from day 7 for MMP-2 (n = 4; p = 0.0122) and from day 7, day 11 and day 14 for MMP-9 (n= 5; p = 0.0001, p = 0.0002, and p = 0.0003, respectively).

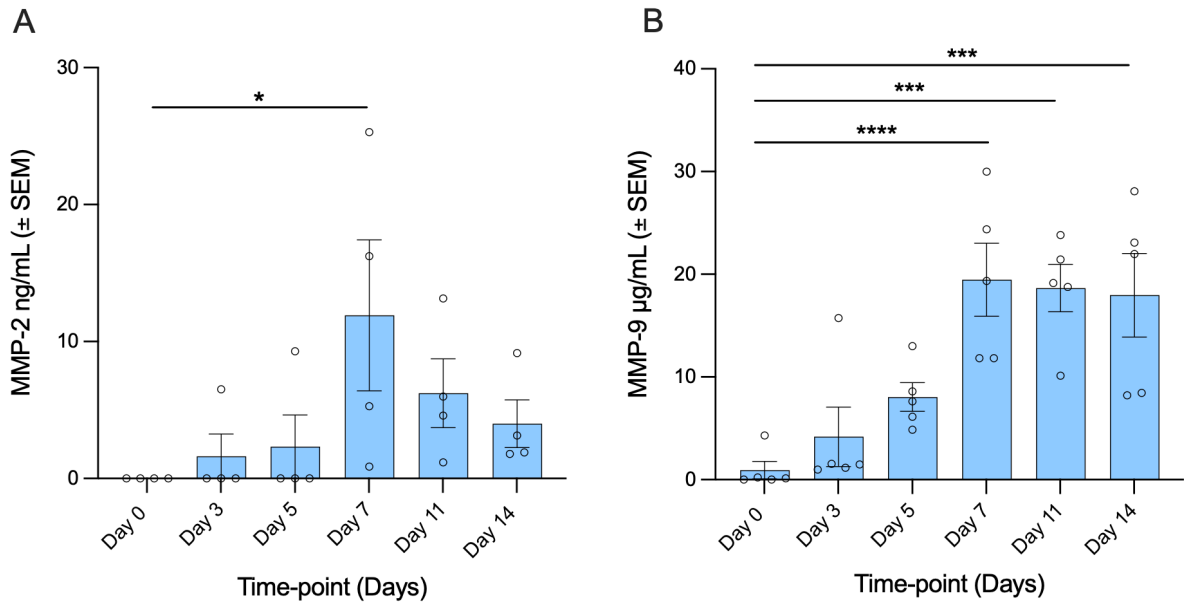

Figure 3.9 Expression of MMP-2 and MMP-9 in monocyte-derived osteoclasts differentiated with M-CSF and RANKL.

*Human peripheral monocytes were differentiated in the presence of M-CSF and RANKL. Supernatants were harvested during the media change, which took place every 2-3 days, throughout the differentiation process and analysed for levels of MMP-2 (A) and MMP-9 (B) using specific ELISAs. Statistics were performed with a two-way ANOVA and Dunnett's multiple comparisons test. Data are from n ≥ 4 independent experiments expressed as the mean ± SEM; * p ≤ 0.05, *** p ≤ 0.001 and **** p ≤ 0.0001.*

Given the pattern of differentiation of osteoclasts *in vitro*, we next assessed their MMP-2 and MMP-9 secretion as it is relevant for the resorptive activity *in vitro,* focussing on MMP-9 as detailed in *3.1 Introduction*; MMP-9 is highly expressed in osteoclast cells and plays a major role in the degradation of the extracellular matrix. Testing the secretion and activity of MMP-2 and MMP-9 by osteoclasts required the employment of an *in-gel* zymography method that

depends on the renaturing of the MMP-9 enzyme in an incubation buffer containing essential factors for the digestion of the gelatine embedded/co-polymerised in the SDS gel. The areas of gelatine digestion on the zymography gel appear as unstained against a dark-blue background. The samples used in this experiment were supernatants harvested as the monocytes differentiated into osteoclasts. An example of a zymography gel is shown in Figure 3.10 A, alongside intensity measures of these bands when analysed on ImageJ (Figure 3.10 B). The raw data of n = 5 repeated experiments show the pattern of digestion calculated as the band intensity of the raw data. When compared to day 0, a significant increase of the area of digestion was observed with day 5 ($p = 0.0009$), day 7 ($p \leq 0.0001$), and day 11 ($p = 0.0003$), (Figure 3.9 C).

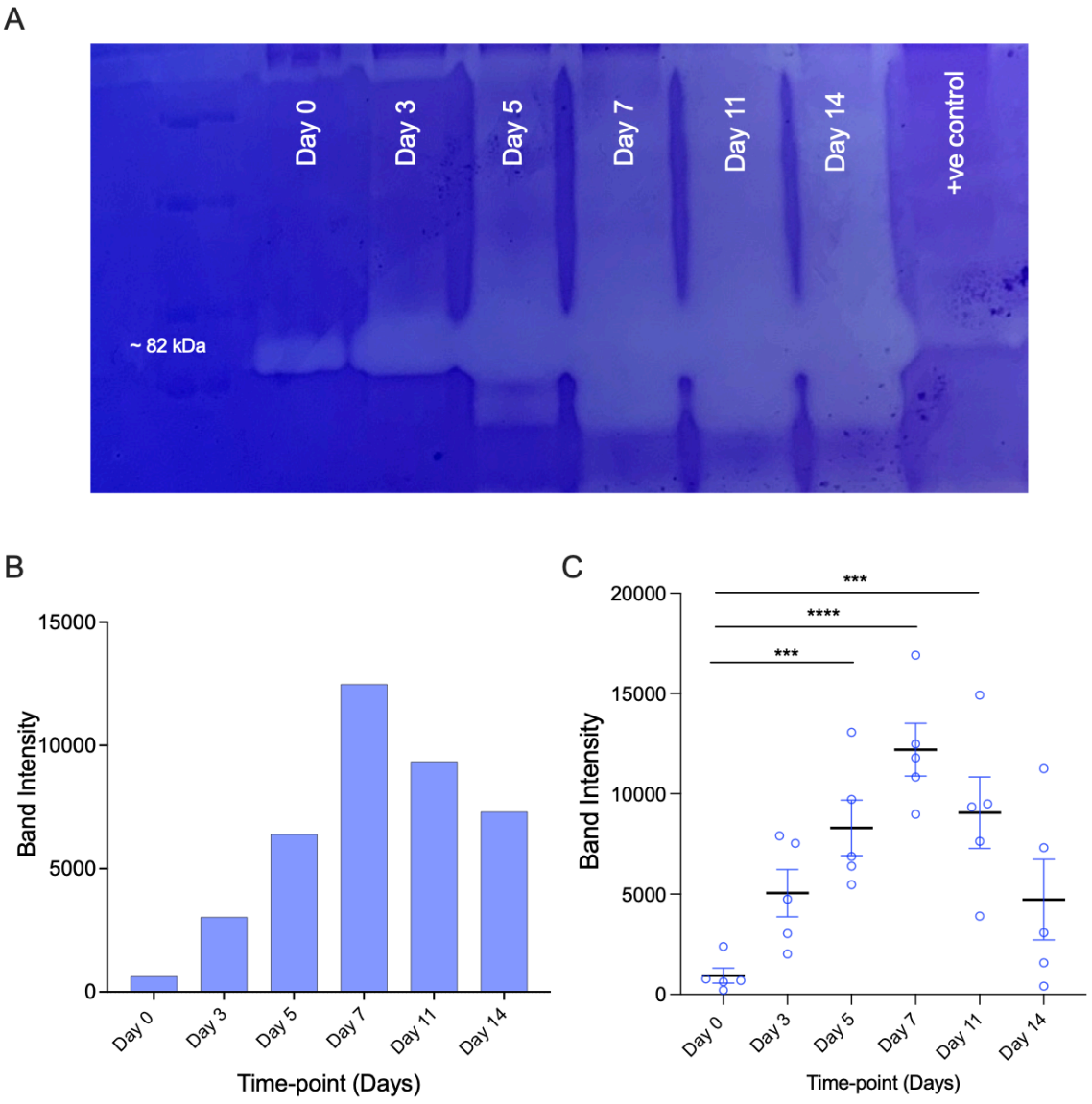

Figure 3.10 Activity of MMP-9 in monocyte-derived osteoclasts differentiated with M-CSF and RANKL.

*Human peripheral monocytes were differentiated in the presence of M-CSF and RANKL. Supernatants were harvested during the media changes, which took place every 2-3 days, throughout the differentiation process and used for gelatine zymography. An example of one zymography gel showing the digestion of the gel throughout the differentiation process (A) with the densitometry values of proteolytic bands corresponding to MMP-9 presented as raw data of that same experiment (B) and from five donors (C). Statistics were performed with a one-way ANOVA and Turkey's multiple comparisons test. Data are from n = 5 independent experiments expressed as the mean ± SEM; * $p \leq 0.05$, *** $p \leq 0.001$ and **** $p \leq 0.0001$.*

3.3.6 Application of the xCELLigence real-time cell analysis (RTCA) biosensor technology to measure monocyte-derived osteoclast differentiation.

After investigating osteoclast differentiation using end-point analysis methods, a more detailed kinetic approach to the analysis of monocyte differentiation into osteoclasts was then undertaken using the xCELLigence real-time cell analysis (RTCA). Figure 3.11 shows images captured by the RTCA xCELLigence system from the video produced during an experiment of osteoclast differentiation from human peripheral blood monocytes (see Appendix 10.7 for the link to the video obtained from the RTCA). Clustering of cells was observed around as early as 4-50 hours after seeding. Fusion of cells was observed from 100-150 hours. Apoptotic osteoclasts were observed by their change in appearance, and cell death was observed in the culture plate after 300 hours.

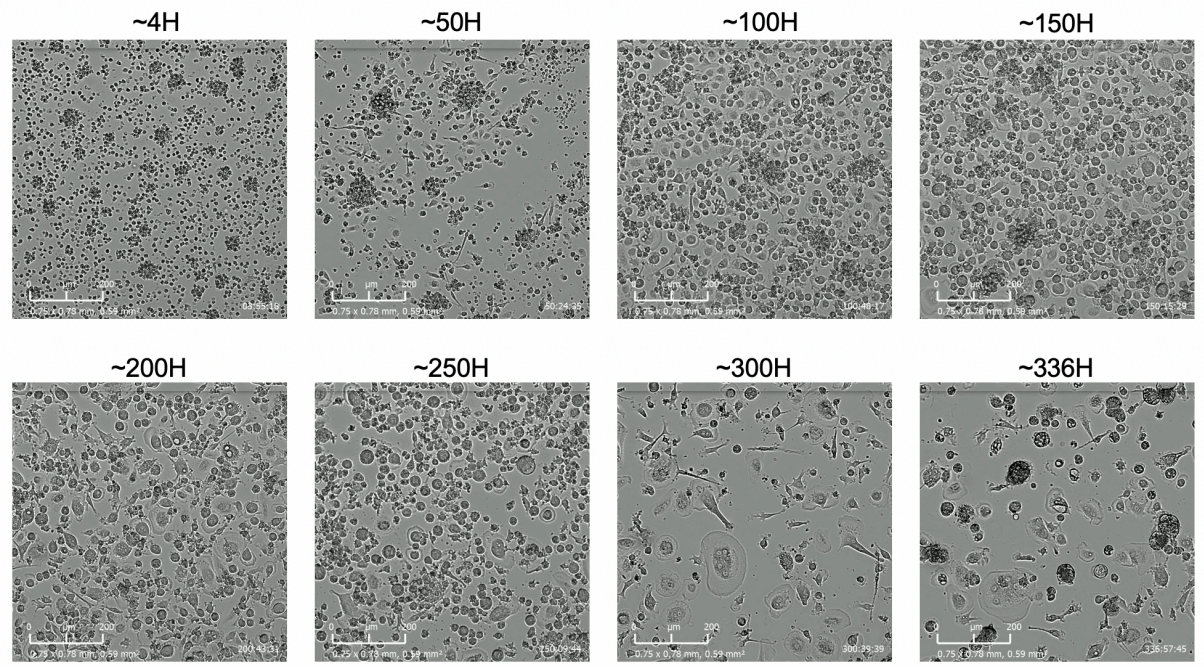

Figure 3.11 Real-time monitoring of osteoclast differentiation from human peripheral blood-derived monocytes.

Osteoclast differentiation was initiated with the addition of M-CSF and RANKL to monocytes. Images showing the progression of osteoclast differentiation at different time points: 4 hours, 50 hours, 100 hours, 150 hours, 200 hours, 250 hours, 300 hours and 336 hours. Images were obtained from one experiment. Similar results were observed with three independent experiments.

To gain a greater number of mature osteoclasts, we initially investigated osteoclast differentiation in two cell populations, MNCs and monocytes. The same range of the number of cells for the two cell populations were seeded on the E-pate (10,000-200,000 cells/well) in the presence of M-CSF and RANKL to drive osteoclast differentiation. This was done initially to determine the best cell type for optimal osteoclast differentiation. This was done for the first time here using human peripheral blood MNCs – a heterogeneous cell mix that contains about 10% monocytes - and monocytes. Using the percentage confluency of MNCs (Figure 3.12 A) and monocytes (3.12 B) at different seeding densities revealed different differentiation patterns. The percentage confluency of the MNCs population seems similar for the first 50 hours (100 % confluency of the plate for the 200,000 and 150,000 cells); however, after a media change occurred ~ 50 hours, the percentage confluency was observed to reduce slightly to ~ 70 % when compared to the initial 50 hours. This decrease could be due to the removal of non-differentiated cells in the MNCs cell population. After a second media change

took place ~ 120 hours, the percentage confluency of the MNCs population was observed to decrease further to ~ 60-50 % when compared to the previous time points; the percentage confluency plateauing from 120 hours onwards. Bright-field confluence is due to the cells' adhesion and cell spreading at the surface of the chip. Bright-field confluency was defined as the area of the plate covered by the cells that can be detected using a bright-field microscope. A bright-field confluency of 100% has been calculated when the cells have fully covered the microchip and the CI index have reached a plateau (see Figure 2.5 for the impedance peak). The percentage confluency of monocytes was observed to be different to that observed with MNCs. For the initial 50 hours, the confluency percentage was observed to slightly reduce from ~ 50 % percentage confluency (for the 200,000 cells); however, after the first media change, the percentage confluency enhanced rapidly to ~ 70 %. The percentage confluency appears to be similar from ~ 120 hours onwards. Interestingly, a similar percentage confluency pattern was observed with 150,000 and 100,000 cells, where a decrease was initially observed, followed by an increase after the first media change, plateauing after ~ 120 hours; in contrast, cell numbers of 50,000, 25,000, and 20,000 cells displayed a continuous increase of the percentage confluency throughout the differentiation period.

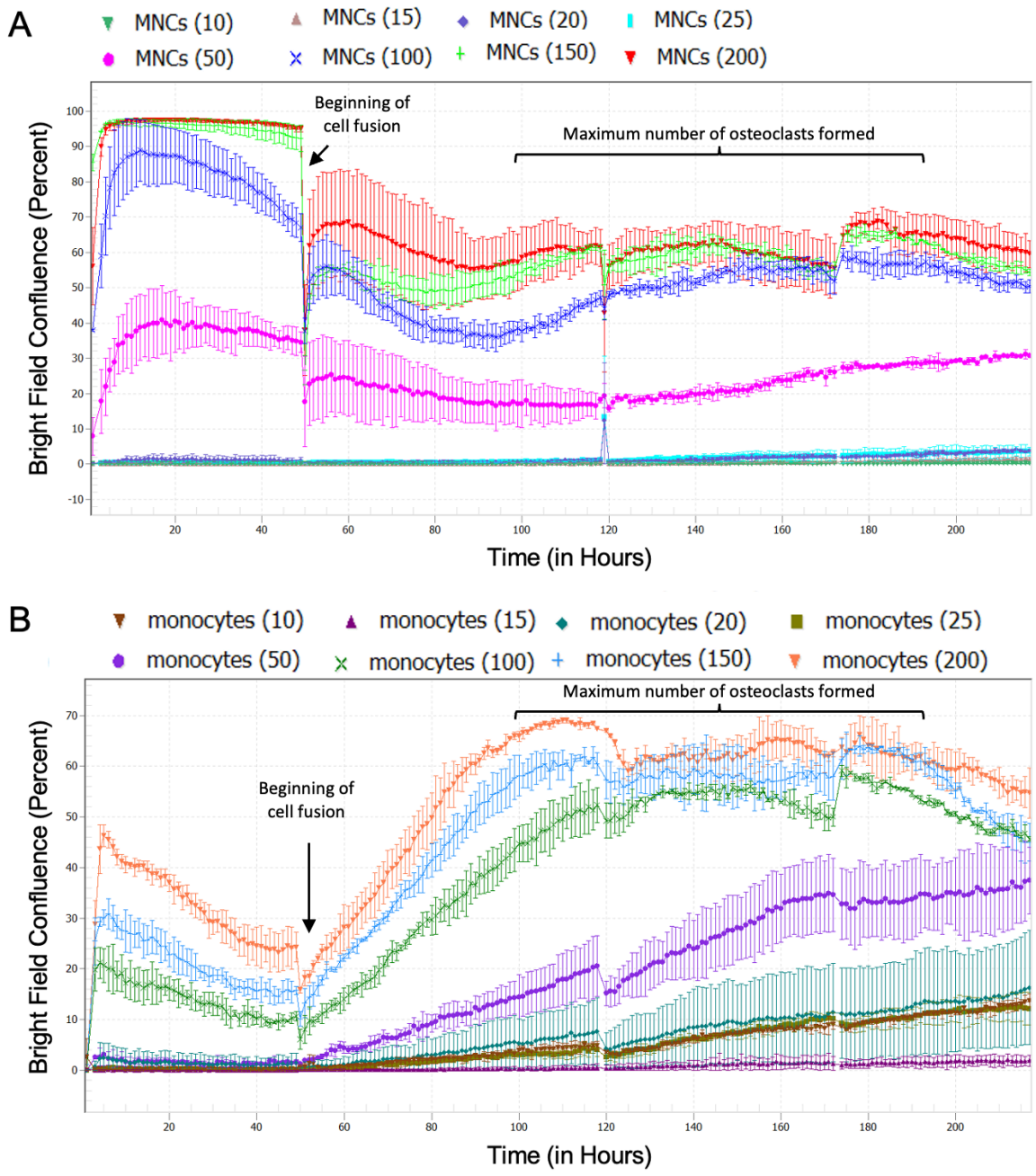

Figure 3.12 Percentage confluency profiles of MNCs and monocyte differentiation in vitro.

Various cell densities of MNCs and monocytes were seeded on the E-plate. The cells were incubated in M-CSF and RANKL to differentiate into osteoclasts. Different cells densities of MNCs and monocytes were seeded 200= 200,000, 150= 150,000, 100= 100,000, 50= 50,000, 25= 25,000, 20= 20,000, 15= 15,000, and 10= 10,000. Graphs are representative of 1 experiment.

The E-96 xCELLigence plates were prepared by adding complete media (50 µL) to every well to establish the baseline reading to calibrate the RTCA (media only). After equilibration to 37 ºC, plates were inserted into the xCELLigence chambers and baseline measurements and connections of the plates were established. Different cell densities were added to the wells (200 µL total volume). Figure 3.13 A shows examples of growth curves obtained from different monocyte seeding densities; these values were also shown normalised to the baseline Cell Index (CI) CI signal, zero monocytes (Figure 3.13 B). The initial increase (0-50h) in the CI is associated with the attachment and adhesion of the cells, followed by spreading and a brief plateau phase (70-100h). The cells were grown for 10-11 days; this was done as previous endpoint assays used within this chapter revealed that MMP-9 secretion and the number of osteoclasts per image was observed to plateau or decrease after day 10/11. Therefore, cells were monitored for 10/11 days to identify the ideal cell number for the monitoring of osteoclast differentiation and proliferation *in vitro*. In addition to providing live images and impedance changes of the cells, this technique also allows the production of live videos from cell differentiation and migration, making it a very powerful technique for determining treatment responses on osteoclast differentiation and potentially migration.

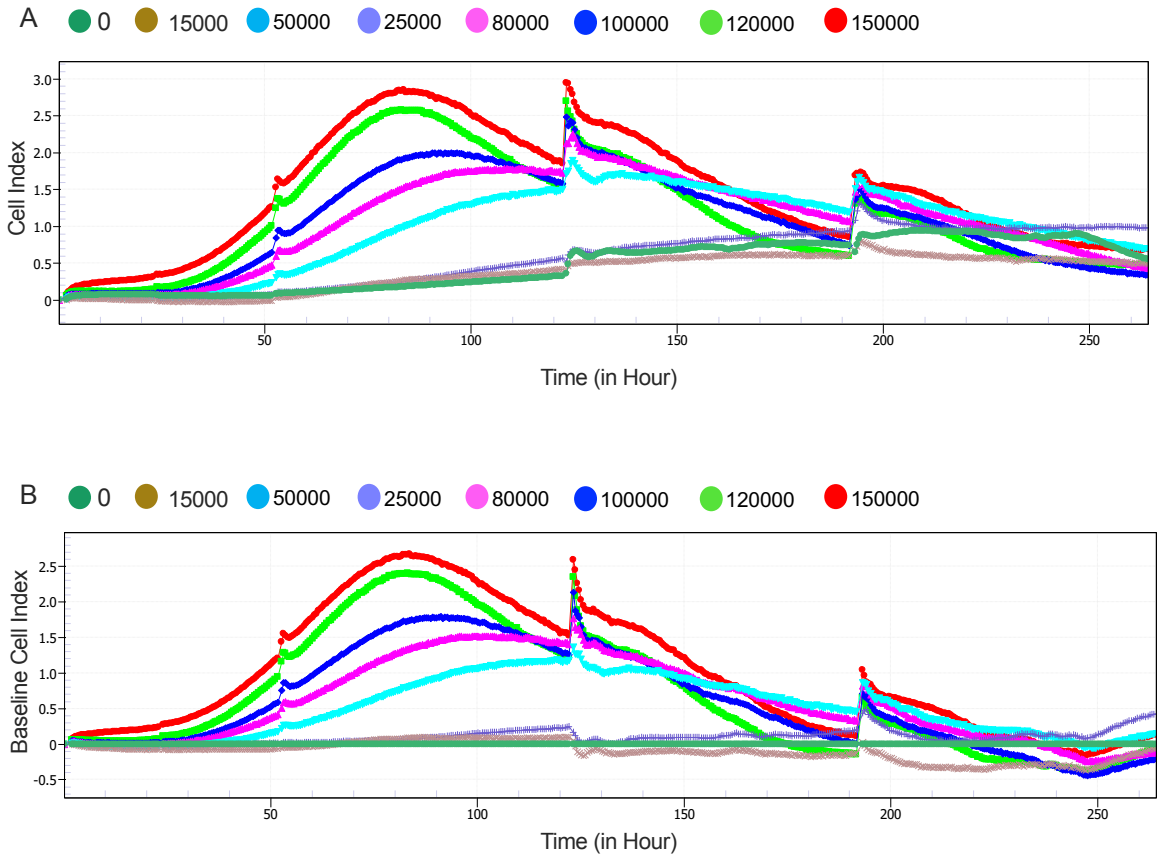

Figure 3.13 Real-time cell analysis (RTCA) of monocyte-derived osteoclasts differentiated with M-CSF and RANKL.

Monocytes were seeded at different densities (0; 15,000; 25,000; 50,000; 80,000; 100,000, 120000 , and 150,000 cells) on a 96-well E-plate. Three images were taken for each well every hour. The optimisation of cell density required monocytes to be seeded at a range of cell numbers to identify the ideal seeding density for obtaining a good Cell Index (CI) signal as well as a clear image on the View Window of the E-plate. The cells were seeded onto the 96-well plates with an equal volume of media (200 µL total). The graph presents triplicates of wells of monocytes derived from the same donor. Impendence recording was measured every hour. Different cell index curves are obtained from different cell densities of monocytes. Curves present the mean CI value from ≥ 3 wells. The highest CI was observed at the highest cell density of monocyte cell titration. The impedance of osteoclasts shown as raw data (A) and normalised to zero monocytes (B). Similar to that observed with repeated experiments obtained from n=3 independent repeats. Quantitative analysis of the CI signal in the presence of RANKL and M-CSF is shown in the upcoming figure.

The CI is a unitless parameter, and it is the result of the impedance induced by adherent cells to the electron flow; it is defined as the measurement of the electrical impedance at a time point minus the initial impedance (no cells present impedance = 0)/nominal impedance value[342]. The CI values increase progressively as cells become more attached to the electrodes. The representative graph gives a remarkable insight into the impedance of osteoclasts throughout the differentiation process. The ability to reproduce and quantify such data is something that has not been shown in previous reports, as many current studies would show a representative graph of repeated experiments[342–345]. The impedance data shown in Figure 3.14 illustrates the effects of different cell densities on the CI data reproduced in three independent experiments. The CI variations are displayed in a real-time plot by the software. An increase was observed in the CI signal with higher cell numbers when compared to the lowest cell number seeded on the E-plate. Using a two-way ANOVA statistical test, a significant increase was observed in the CI signal was observed in comparison to the lowest cell number (15,000) at 100 hours (150,000, $p = 0.0001$; 120,000, $p = 0.0007$; 100,000; $p = 0.0138$), 150 hours (150,000, $p < 0.0001$; 120,000, $p = 0.0066$; 100,000; $p = 0.0157$, 80,000; $p = 0.0399$); 200 hours (150,000, $p = 0.0051$) and 250 hours (150,000, $p = 0.0429$).

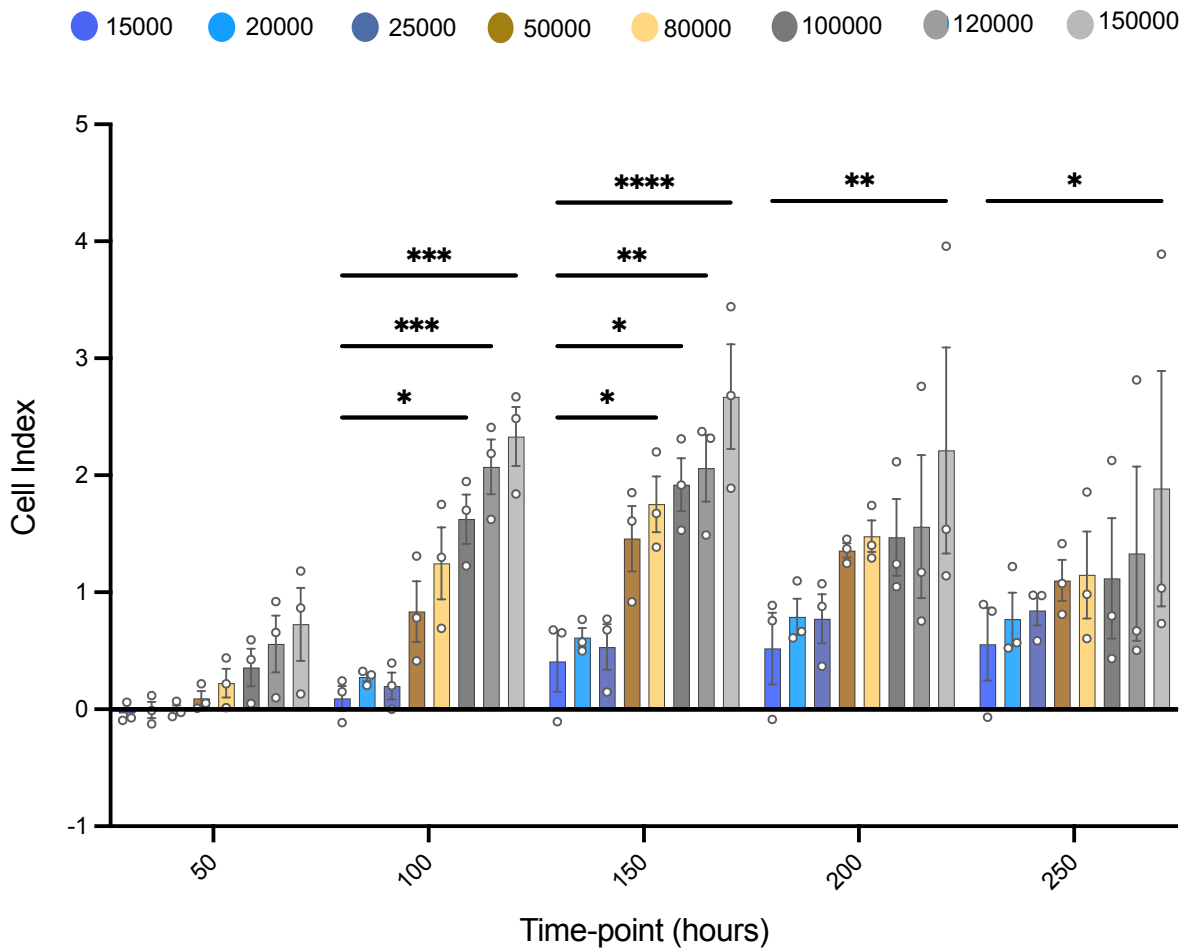

Figure 3.14 CI signal displaying the impedance of osteoclasts at different seeding densities in repeated experiments.

*Monocytes were seeded on E-plates and differentiated into osteoclasts in the presence of M-CSF and RANKL. Quantitative measures of the impedance are displayed as a CI signal at different seeding densities; 15,000, 20,000, 25,000, 50,000, 80,000, 100,000, , 120,000, and 150,000. The impedance was monitored continuously for the 10/11 days of osteoclast differentiation. Statistics were performed with a two-way ANOVA and Dunnett's multiple comparisons test. Bar graphs represent means +/- SEM, n=3 and significant values were taken as $p < 0.05$ graphically denoted as * $p \leq 0.05$, ** $p \leq 0.01$, *** $p \leq 0.001$ and **** $p \leq 0.0001$.*

A novel software feature of the xCELLigence eSight RTCA is the ability to determine the number of clustering objects per image. In osteoclasts, the number of objects per image could correspond to the clustering formed by pre-osteoclasts before they start fusing to form mature multinucleated giant cells (mature osteoclasts). Previous observation of osteoclast differentiation has been already done many years ago (by time lapse microscopy). Using real-

time imaging and videos from RTCA and referring to previous endpoint assays testing the differentiation and activation within this chapter, osteoclasts were observed after 5 days of seeding. Therefore, we determined the cluster formation of pre-osteoclasts until ~ 130 hours post-seeding. Figure 3.15 illustrates the masking strategy used to determine the highest number (quantified in upcoming figures) of clusters formed (~ 60 hours), where the masking displayed the most extensive coverage within the image. This was done as it would be a powerful approach to test the formation of pre-osteoclasts *in vitro*.

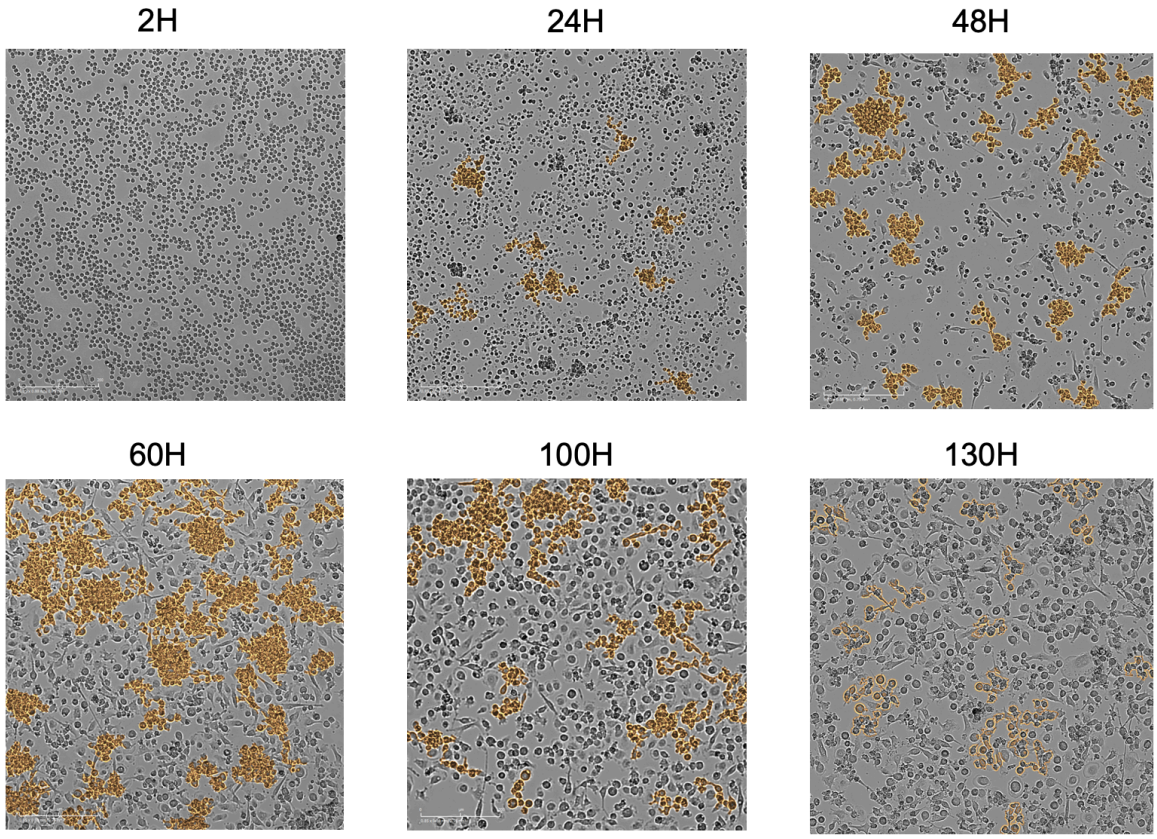

Figure 3.15 Label-free monitoring of osteoclast differentiation using an xCELLigence RTCA eSight analyser.

Images tracking the progression of cell spreading and the aggregation displaying clusters forming over time. Images from 2-, 24-, 48-, 60-, 100-, and 130-hour time points highlight the formation of clusters at early time points, displaying the higher intensity and larger surface area of masking (displayed in orange) after 48 and 60 hours of seeding. Clustering of osteoclasts (which is a characteristic of differentiation) becomes more robust. At later time points, these osteoclast clusters contain less of the orange masking, which displays an increase in CI and cytoplasm elongation and appears to be progressing into mature osteoclasts. Finally, after 120 hours of seeding, the masking of aggregates slowly disappears

with the emergence of multinucleated cells. An outline of the masking was selected using bright field microscopy images. H=Hour

Figure 3.16 shows an example of a single experiment where the clusters formed at the different cell densities at ~ 60 and ~ 130 hours post-seeding. To quantify the formation of pre-osteoclastic clusters, the object count per image, along with the CI signal measured at 60 hours (Figure 3.16 A) and 130 (Figure 3.16 B) hours post-seeding was determined. At ~ 60 hours, a more distinctive object count and CI signal for the different cell densities were observed; in contrast, fewer differences were observed within the different seeding densities for the object count and the CI signal at ~ 130 hours.

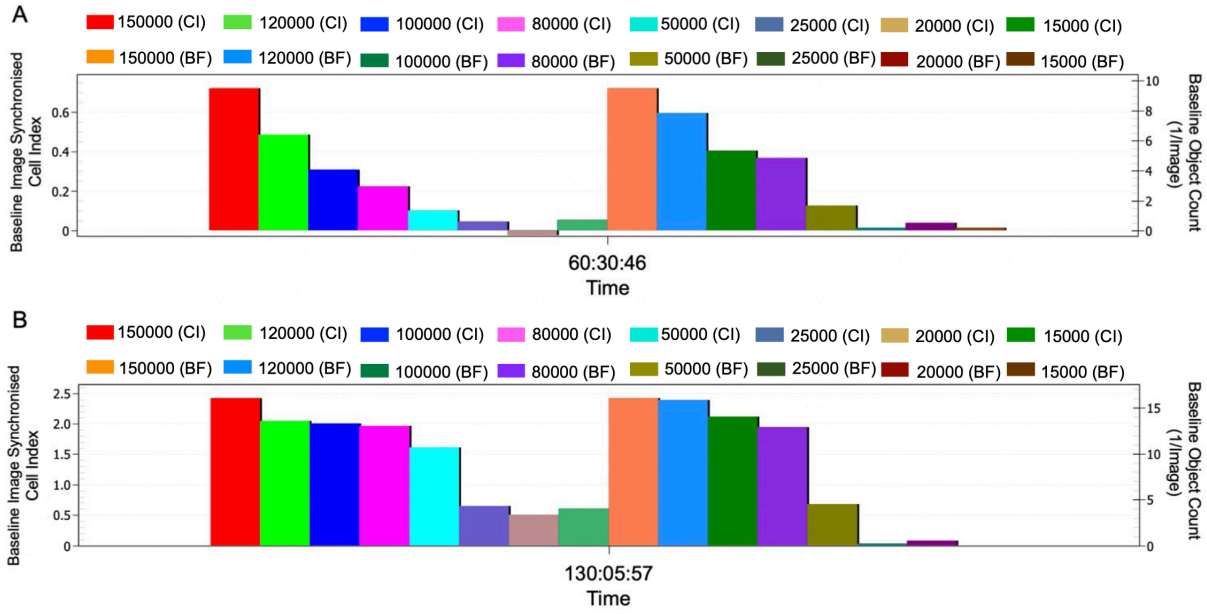

Figure 3.16 CI signal and the object count per image of pre-osteoclasts.

M-CSF and RANKL were used to differentiate monocytes into osteoclasts. The object count per image and the CI signal for pre-osteoclasts of the different cell densities at ~ 60 hours (A); and ~ 130 hours (B) from one individual experiment. CI-S = Image Synchronised Cell Index; BF = Object count per image (Bright Field).

Repeated experiments (n = 3) showing the two measurements at 60 and 130 hours display similar results. Figure 3.17 A shows the object counts and the CI signal at 60 hours to be more distinctive for the different cell numbers; Figure 3.16 B shows the object count per image and the CI signal at 130 hours with less distinctive changes within the object count and the CI signal measurements. A significant decrease was observed with the CI signal at ~ 60 hours with 150,000 cells and 15,000 cell numbers ($p = 0.0455$); with the object count with 150,000 cells ($p \leq 0.0001$), 120,000 cells ($p \leq 0.0001$), 100,000 cells ($p \leq 0.0001$), 80,000 cells ($p \leq$

0.0001), 50,000 cells ($p = 0.0442$), and 20,000 cells ($p = 0.0136$) when compared to the least number of monocytes seeded (Figure 3.17 A). A significant decrease was also observed at ~ 130 hours with the CI signal of 150,000 in comparison to 15,000 cells ($p = 0.0322$); and with the object count per image with 150,000 cells ($p \leq 0.0001$), 120,000 cells ($p \leq 0.0001$), 100,000 cells ($p \leq 0.0001$), 80,000 cells ($p \leq 0.0001$), 50,000 cells, and ($p \leq 0.0001$)) when compared to the least number of monocytes seeded (Figure 3.17 B).

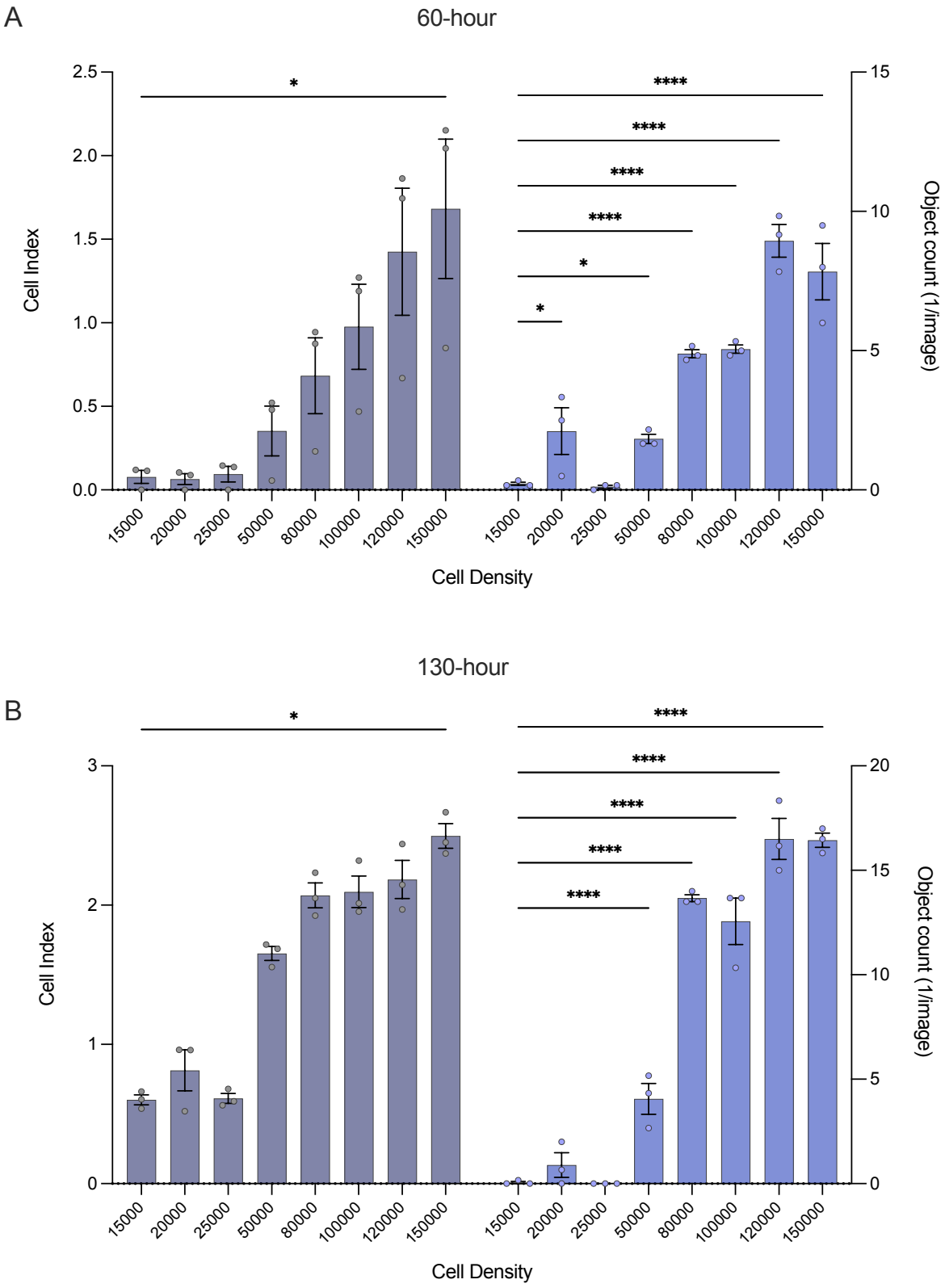

Figure 3.17 CI signal and the object count per image of pre-osteoclasts in repeated experiments.

M-CSF and RANKL were used to differentiate monocytes into osteoclasts. Bar graphs displaying the object count per image and the CI signal obtained at 60 hours (A) and 130 hours

*(B) post-seeding. Statistics were performed with a two-way ANOVA and Dunnett's multiple comparisons test. Bar graphs represent means +/- SEM, n=3 and significant values were taken as $p < 0.05$ graphically denoted as * $p \leq 0.05$ and **** $p \leq 0.0001$.*

3.4 Discussion

We have completed an evaluation of the quantification of the progression over time of changes in the area covered by cells in culture and impedance using live imaging and specific associated equipment. This was compared with alternative methods such as changes in RANKL expression, area of spread of osteoclasts, and the number of nuclei per cell.

Peripheral blood monocytes originate in the bone marrow from hematopoietic stem cells. This involves numerous commitment stages[346,347]. Under the influence of different microenvironmental stimuli, peripheral blood monocytes can migrate into the blood to reach various tissues, where they differentiate further into macrophages, dendritic cells and other specialised cells[348,349]. As previously discussed in *3.1 Introduction*, peripheral blood monocytes can divide into three subunits based on their CD14 and CD16 expression. These subsets display morphological, immunotypic, and physiological heterogeneity. Previous studies have confirmed that treating peripheral blood monocytes with M-CSF and RANKL is sufficient to induce *in vitro* osteoclast differentiation[350,351]. From previous work on osteoclast differentiation, stimulating human peripheral blood monocytes with M-CSF and RANKL, induced monocyte elongation, cell polarity at the early stages of differentiation, multinucleation and an increase in the size of the cell observed at the later stages of differentiation (after day 5), strongly suggesting the presence of mature osteoclasts. The growth factors M-CSF, used at 25 ng/mL, and RANKL, used at 100 ng/mL, were sufficient to drive the differentiation of monocytes into osteoclasts over a culture time of 14 days.

The addition of such growth factors promoted the differentiation towards osteoclasts and expression of prototypic markers such as TRAP and RANK[352,353]. Additionally, TRAP is expressed by macrophages as well as RANK[354.] RANK-deficient mice have been used to demonstrated that RANK is essential for osteoclastogenesis and that CD14+RANK^{high} cells constitute a circulating pre-osteoclast pool[355]. TRAP is regarded as an important biomarker for osteoclasts; its concentration in serum is used as a biochemical marker of mature osteoclast function and degree of bone resorption[356,357]. Therefore, TRAP and RANK were tested for their expression in monocytes (day 0) and after 14 days of differentiation. The absence of RANK expression at Day 0 could be attributed to the low sensitivity of immunocytochemistry and/or the low number of RANK expressed.

The data obtained from quantifying the number of osteoclasts (3+ nuclei per cell) and the number of nuclei per osteoclast, has revealed that osteoclast start to appear from day 5; a significant increase in the number of osteoclasts is observed on day 7, this increase stays

constant for day 11 and day 14. A similar pattern is observed for the number of nuclei per osteoclast as a significant increase is observed with days 7, 11 and 14. These findings support the data obtained from confocal microscopy, confirming the presence of osteoclasts and their maturation throughout the course of differentiation.

MMP-2 and MMP-9 are expressed in mononucleated and multinucleated osteoclasts; they are specialised in the degradation of the extracellular matrix[358,359]. As previously discussed, MMP-9 is a proteolytic enzyme highly expressed in osteoclasts and is vital for osteoclastic degradation of the extracellular matrix during bone resorption and bone remodelling. Many studies have been conducted to interpret the regulatory mechanism involving osteoclastic MMP-9 expression during bone resorption and the other roles of MMP-9[360–366]. Here, to establish the presence of MMP-2 and MMP-9 in osteoclasts, cytokine analysis using ELISA was utilised to detect the amounts throughout the differentiation period. The levels of MMP-2 and MMP-9 increased with the progression of osteoclast differentiation from peripheral monocytes. To further establish the reliability of the osteoclastic *in vitro* model, it was vital to test the secretion of MMP-9 by osteoclasts *in vitro,* as this would provide a powerful method to study the regulatory mechanisms of MMP-9 in bone resorption *in vitro*. In the present study, supernatants harvested from different days throughout the differentiation period were tested for MMP-9 activity using gelatine zymography to reveal increased secreted MMP-9 activity which correlated with the increased levels of MMP-9 release detected by ELISA as differentiation progressed. This further confirms the presence of osteoclasts *in vitro*. Interestingly, the highest levels of MMP-9 were measured at day 7, suggesting the presence of osteoclasts at the peak of their MMP-9 secretion ability.

The next step was to adopt a quantitative approach to analysis of osteoclastogenesis ahead of assessing the responses to different treatments in the following chapters. RTCA offers a new system for real-time cell analysis that measures impedance-based signals in a label-free non-invasive manner[367,368].

The results indicate that the highest levels of impedance align with the highest levels of OC maturation observed through commonly used methods. These findings validate the use of increased cell impedance and changes in RTCA as indicators to easily track OC differentiation over time. These straightforward methods enable the monitoring of changes in OC differentiation in live cultures without the need for cell processing and quantification of parameters at endpoints. This is a significant advantage for the in vitro study of OC biology.

Osteoclasts can adhere to substrates on which they form distinct F-actin structures[369]. *In vitro*, when attached to non-mineralised substrates such as plastic or glass, mature osteoclasts exhibit canonical podosomes similar to monocyte-derived cells such as macrophages or dendritic cells[369,370]. During osteoclast differentiation, podosomes patterning is highly dynamic and it is proposed that it ends up in a sealing zone in mature bone-resorbing osteoclasts[371].

The sealing zone consists of a dense actin core surrounded by kinases such as c-Src and Pyk2 as well as small GTPases Rho, Rac and cdc42[369,370,372]. When stimulated with M-CSF and RANKL, osteoclasts organise an inner actin ring which is the functional unit of the osteoclast membrane at the sealing zone[283]. The previously described dynamics of cytoskeletal and adhesion remodelling during OC differentiation may explain the increased impedance measurements with the xCELLigence system. The xCELLigence system provides a powerful tool for studying osteoclast differentiation as it provides information on the proximity of contact between the cell and the substrate. Using the xCELLigence in this study allowed the combination of endpoint with continuous assays using live rather than fixed cells which presented a more powerful tool for studying osteoclast differentiation and activity *in vitro*. The impedance of osteoclasts at different monocyte cell densities was first studied to optimise seeding densities and revealed increasing impedance with increasing cell densities. For the first time, this was quantifiable across repeated experiments and allowed for statistical analysis.

Other features of the xCELLigence system allow for analysis of other features of osteoclastogenesis. In the presence of M-CSF and RANKL, the monocytic/macrophage cell line RAW264.7 gives rise to TRAP+ cells which fuse together spontaneously within 3 days to form multinucleated osteoclasts expressing the phenotypic markers TRAP and RANK[373]. Given the images obtained from the live cell view here, the next approach was to study the earlier stages of monocyte clustering. Images captured from the RTCA show the formation of pre-osteoclasts around 60 hours after seeding as clustered objects. At later time points, these clusters slowly disappeared as the cells started to fuse to form the multinucleated giant osteoclasts. This is the first time that quantification of pre-osteoclastic clustering has been performed, and it provides an important tool for studying the differentiation mechanisms of osteoclasts at the osteoclast precursors stage and in response to treatments, as demonstrated in the following chapters.

Various other reports have detailed many methods to study osteoclasts *in vitro* using endpoint assays[374-377] along the lines deployed at the outset of this chapter. However, RTCA has been used here for the first time to investigate the differentiation of osteoclasts at the earlier stages (pre-osteoclastic clustering formation measurements), as well as quantify the impedance throughout the differentiation process and display the results of repeated experiments in a unified graph. This is likely to become a new essential tool. The use of RTCA here provided many advantages in determining the differentiation and the proliferation of osteoclasts derived from human peripheral blood monocytes. These advantages include real-time monitoring, high reproducibility, and high correlation with endpoint assays (such as the number of osteoclasts

and the number of nuclei per osteoclast obtained from scoring the cells in the confocal images manually). Furthermore, the impedance signal can be a useful tool to detect compound effects on osteoclast proliferation, adhesion, and invasion. There is suite of other features such as cluster analysis used here that lend themselves to even greater insights. Ideally, osteoclasts directly isolated from human bone tissues should be used to study the underlying mechanisms of hyper-differentiation and hyper-activation of osteoclast in myeloma bone disease. However, the difficulty in obtaining bone tissue specimens in sufficiently large numbers without disrupting osteoclasts from bone tissue specimens is mostly unfeasible. Due to the close relationship between peripheral blood monocytes and osteoclasts, the *in vitro* osteoclast model derived from peripheral blood monocytes is an attractive tool to characterise the altered osteoclastic formation, migration, differentiation and functional activity at the precursor stages of osteoclastogenesis associated with bone disease.

One limitation of this work is not including a control without RANKL to osteoclast differentiation. It affects the overall validity, reliability, and mechanistic understanding of the experimental outcomes. To address these limitations, future studies should include a RANKL-free control to ensure comprehensive and accurate interpretations of osteoclast differentiation processes.

3.5 Conclusion

The RTCA allows for monitoring of osteoclastogenesis using real-time images, videos, impedance and pre-osteoclastic cluster formation. The endpoint assays and the RTCA method could allow the investigation of basic mechanisms underlying the differentiation and activation of monocytes/osteoclast precursors/mature osteoclasts in the presence of treatments obtained from patients with myeloma-related bone disease and potentially other bone disorders such as osteoporosis.

Chapter Four:

Measuring the Effects of Immunomodulatory Imide Drugs on the Differentiation and Activation of Osteoclasts

4.1 Introduction

4.1.1 The biological effects of immunomodulatory imide drugs (IMiDs)

One of the most common therapies used for MM are immunomodulatory imide drugs (IMiDs); they contributed vastly to the improvement in outcomes for patients with MM[378]. IMiDs are proprietary compounds with immunomodulatory properties[379]. They are orally administrated treatments, targeting several biological activities through many mechanisms of action, some of which have yet to be fully characterised and understood[380]. IMiDs are a class of compounds analogous to thalidomide, a glutamic acid derivative with anti-angiogenic properties and potent anti-inflammatory effects due to its anti-tumour necrosis factor (TNF) effects[381]. Thalidomide analogues were first developed to optimise their anti-tumour and anti-inflammatory properties and reduce the devastating side effects of thalidomide toxicity. The two best known analogues of thalidomide are lenalidomide (CC-5013; IMiD3; Revlimid) and pomalidomide (CC-4047; IMiD1; Actimid)[382, 383]. IMiDs are widely used for the treatment of MM along with monoclonal antibodies, proteasome inhibitors and steroids[384, 385, 386]. IMiDs are limited in clinical application due to acquired drug resistance[387,388]. Lenalidomide has been granted approval in combination with dexamethasone for treating patients with relapsed/refractory multiple myeloma[389] in nearly 70 countries, including Europe, America, the middle east and Asia[390].

Cereblon (CRBN) is the primary cellular target of IMiDs. It is a substrate receptor of Cullin-RING ligase 4 (CRL4), an E3 ligase that ubiquitinates and degrades two essential lymphoid transcription factors, Ikaros zinc factor family protein (IKZF) 1 and IKZF3 (Aiolos)[390,391]. The downregulation of these two transcription factors causes a decrease in interferon regulatory factor 4 (IRF4) and MYC production[392], resulting in toxicity to myeloma cells. IMiDs bind to and modulate CRBN at the canonical substrate-binding site; this induces the E3 ligase activity of $CRL4^{CRBN,}$ which results in the ubiquitination and degradation of neo-substrates of IMiDs including casein kinase 1 α (CK1 α) and zinc finger protein 91 (ZFP91)[393, 394].

IMiDs share a similar biological and molecular activity with a decrease effects on adhesion molecules, MM-BM stromal cell interactions (this is due to the ability of IMiDs to disrupt this interaction due a decrease in expression of cell adhesion molecules and decreased cytokine production such as IL-6 and ^{VEGF}[395]), growth factors, angiogenesis and immune cells. The variety of interactions between malignant plasma cells and their microenvironment are vital to tumour growth and progression[396, 397]. The MM-BM stromal cell interaction triggers the production of several growth factors; this includes interleukin 6 (IL-6), vascular endothelial growth factor (VEGF), and TNFα. IL-6 secretion by BM stromal cells plays a significant role in MM cell adhesion[398]. The overproduction of IL-6 is considered to be an important factor in MM

pathogenesis, even though it is crucial for normal B cell development. IL-6 is a multifunctional cytokine implicated in bone metabolism[399]. It is produced by many types of cells and is expressed during cellular stress, such as inflammation, infection and cancer. IL-6 is produced by activated immune cells and stromal cells, including T cells, myeloid precursor cells, endothelial cells and fibroblasts[400]. IL-6 has been identified as a major cytokine involved in the emergence of the tumour clone and in tumour-associated toxicities in patients with MM[401,402]. Furthermore, IL-6 has been shown to increase osteoclast differentiation, in addition to MM cell survival[403, 404, 405]. VEGF isoforms expressed and secreted by myeloma cells stimulate the expression of IL-6 by microvascular endothelial cells and BM stromal cells[406]. In turn, IL-6 stimulates the expression of VEGF isoforms by myeloma cells, suggesting a paracrine role of VEGF in tumour-stroma interactions in MM[407].

The expression of MMPs in human cancers can be enhanced as a result of interactions between tumour cells and stromal cells, including endothelial cells, fibroblasts and inflammatory cells[408]. In a mouse model of pancreatic islet tumorigenesis, MMP-2 and MMP-9 contributed to tumour growth, and stromal MMP-9 had additional effects on the angiogenic switch during multistage pancreatic carcinogenesis[409]. This interaction in myeloma cells has been shown to stimulate osteoclast activation through binding to their receptors[410]. Serum IL-6 and MMP-9 levels have been associated with bone resorption in myeloma patients and may be helpful in disease prognosis[411]. TNFα is a signalling cytokine found to be elevated in myeloma patients and is involved in the pathogenesis of MM bone disease[412]. TNFα has been shown to work with RANKL to induce osteoclastogenesis[413].

Tissue inhibitors of MMPs (TIMPs) are proteins that inhibit MMPs. They are found in the ECM either in a soluble form or bound to the ECM (TIMP-3)[414]. TIMPs inhibit MMPs by forming reversible blockages, creating 1:1 stoichiometric complex. Different TIMPs selectively inhibit various MMPs, as well as members of the ADAM and ADAMTS families. Additionally, TIMPs play a role in the activation and removal of MMPs from the extracellular environment[414]. TIMP function impacts the effect of the ECM on cell behaviour, cell adhesion molecules, cytokines, chemokines, and growth factors. TIMPs consist of an amino-terminal inhibiting domain that binds to the active site of MMPs and domain C, which allows interaction with the hemopexin domain of some MMPs[414].

4.1.2 Rationale

The aim of this chapter is to confirm the use of impedance variations as a non-invasive, label-free, and real-time measuring method for determining the effect of drugs on osteoclast differentiation. This method aims to provide sensitivity similar to well-accepted traditional endpoint methods.

Therefore, the primary purpose of this chapter is (i) to demonstrate the usage of real-time live cell imaging and impedance for studying osteoclast differentiation and function in the presence of IMiDs at different time points as this new technique will (ii) help to understand bone disease progression and identify new treatment targets for its control in MM. This study (iii) can provide comprehensive results that will compare tests from endpoint results and real-time analysis that will reveal new IMiD targets in treating bone disease in MM.

4.1.3 Hypothesis

I. IMiD treatment is able to control osteoclast hyper-differentiation and hyper-activation.
II. xCELLigence real-time cell analysis (RTCA) is a valuable tool for studying the effects of IMiDs on osteoclast differentiation and activation.

4.2 Experimental procedures

4.2.1 Samples

As per section 3.2.1, human peripheral blood was collected from healthy, non-fasted individuals over 18 years old into heparinised Vacuettes™ (Greiner Bio-one, Frickenhausen, Germany). All samples were collected with informed written consent as detailed in *Chapter 2.4 Sample collection and preparation.*

4.2.2 Monocyte isolation

Monocytes were isolated by positive selection on magnetic microbeads as described in Chapter *2.4.1 Blood* separation and *2.4.2 Mononuclear cell isolation*. Briefly, the pellet containing the monocytes was resuspended in differentiation or complete cell culture media as described in *3.2.3 Differentiation of monocytes into osteoclasts using M-CSF and RANKL differentiation media.* Cell density was determined using the Countess® automated cell counter (Life Technologies). To check monocyte purity, an anti-CD14 antibody (Clone 61D3; fluorophore eFluor®450; isotype mIgG1) was added to 100,000 monocytes. The cells were incubated with the antibody for 30 minutes. The cells were washed twice with FACS buffer (0.2% (w/v) bovine serum albumin (BSA), 0.05% (w/v) sodium azide (Sigma-Aldrich) in PBS) and centrifuged at 515 *x g* at 4 ºC for 7 minutes; the pellet was resuspended in FACS buffer and checked for purity and acquired using the NovoCyte Flow Cytometer (BD Biosciences). Data analysis post-acquisition was interpreted using FlowJo Version 1.3 (Tree Star, Oregon, USA). Purity ≥ 92% was accepted for downstream experiments.

4.2.3 Differentiation of monocytes into osteoclasts using M-CSF and RANKL differentiation media

Monocyte differentiation into osteoclasts as detailed in *3.2.3 Differentiation of monocytes into osteoclasts using M-CSF and RANKL differentiation media.* Fresh media was added to replace the media removed. Lenalidomide, pomalidomide, and thalidomide (Celgene; New Jersey, USA) were added every 2-3 days at either 1 µM or 10 µM concentration. These concentrations have been chosen based on the literature[415, 416, 417].

To assess the response to the inflammatory stimulus lipopolysaccharide (LPS), cells were cultured in RPMI 1640 GlutaMAX™ (ThermoFisher Scientific; Massachusetts, USA) supplemented with 10% fetal bovine serum (FBS, HyClone, Cytiva) and 0.5 µM 2-mercaptoethanol (2-ME) (ThermoFisher Scientific; Massachusetts, USA), +/- 10 ng/mL LPS (Ultrapure, InvivoGen (San Diego, USA)). The supernatants were collected after 24 hours and cultures were centrifuged at *515 x g* for 7 minutes, and cell-free supernatants were removed

and stored immediately at -20 °C until analysis of cytokines and enzymes using specific ELISAs.

4.2.4 Confocal Microscopy

Isolated monocytes were seeded on Millicell EZ 8-well chamber slides (Merck Millipore, Massachusetts, USA) and cultured in differentiation media. The day of harvest was chosen to be on day 9/10. This is due to the results in chapter three showing the mature osteoclast differentiation observed on day 10, and a plateau of MMP-9 production after day 9/10. Sample preparation and confocal microscopy were performed as detailed in *Chapter 2.13 Confocal microscopy.*

4.2.5 The differentiation of monocytes into osteoclasts on the RTCA E-plates

Monocyte differentiation into osteoclasts on the E-plates was performed as detailed in chapter *2.16 The differentiation of monocytes into osteoclasts on the RTCA E-plates*. Every 2-3 days, the experiment was paused for approximately 15 minutes to allow media change and then resumed. Lenalidomide, pomalidomide, and thalidomide were added to the cell cultures on the day of seeding and every 2-3 days at either 1μM or 10 μM. The RTCA eSight software (Research Use Only (RUO); version 1.1.2 Agilent, California, USA) was used in these experiments.

4.2.6 Gelatine coating on the RTCA E-plates

Gelatine at 0.02% volume per weight, dissolved in double-distilled water, was purchased from Sigma-Aldrich (Poole, UK) and prepared as a working solution following the manufacturer's instructions. For pre-coating, the well plates were incubated with 40 μL of the gelatine solution for 1 hour at 37 °C. The gelatine solution was then removed, and the wells were washed with 100 μL with 1 X PBS. Once coated, depending on the experiment, cells were seeded, and the protocol was followed as per chapter *2.16 The differentiation of monocytes into osteoclasts on the RTCA E-plates.*

4.2.7 Enzyme-linked immunosorbent assay (ELISA)

Analysis of cytokines using ELISA was as per the manufacturer's instructions (DuoSet; Biotechne). See Chapter *2.6 Enzyme-Linked Immunosorbent assay (ELISA).* The ELISA kits used in this chapter were to detect the levels of matrix metalloprotease 9 (MMP-9) and MMP-2 secreted by osteoclasts into the supernatants during differentiation. ELISA kits specific to IL-6 and TNFα were used to demonstrate the effects of lenalidomide, pomalidomide, and

thalidomide on the production of pro-inflammatory cytokines by osteoclasts upon LPS stimulation.

4.2.8 *In-gel* Zymography

Gelatine zymography is a method used to detect the activity of gelatinase enzymes, such as the matrix metalloproteases (MMPs) MMP-2 and MMP-9. In gel zymography was performed as detailed in Chapter *2.15 In gel zymography*. See *Table 2.4 Recipe of the washing buffer used for in gel zymography* and *Table 2.5 Recipe of the incubation buffer used for in gel zymography* for the zymography washing and incubation buffer recipes. For the Coomassie Blue staining and de-staining solution, see *Table 2.6 Staining solution recipe used for in gel zymography* and *Table 2.7 De-staining solution recipe used for in gel zymography.* The gel stains dark blue with the proteolytically cleaved sites remaining lightly stained/unstained. Recombinant human MMP-9 was used as a positive control to further identify MMP-9 on the zymography gel (Biolegend; San Diego, USA).

4.2.9 Immunoblot

Protein estimation was performed using a detergent-compatible (DC) protein assay (Bio-Rad, Hemel Hempstead, UK) as per Chapter *2.7 Protein estimation.* Freshly isolated osteoclast cell lysates were quantified using a microplate reader (POLARstar, BMG) and Excel (Microsoft, USA). Western blotting technique was perfumed as per Chapter *2.8 Sodium dodecyl sulphate-polyacrylamide gel electrophoresis (SDS-PAGE), 2.9 Semi-dry membrane transfer, and 2.10 Immunoblotting.* Membranes were probed with different integrin subunits antibodies targeting integrin αV polyclonal antibody (Cell Signalling; 4711), integrin β3 antibody (Cell Signalling; (D7X3P) XP® Rabbit IgG mAb 13166), α5 integrin polyclonal antibody (Cell Signalling; 4705), integrin β1 (Cell Signalling (D2E5) Rabbit IgG mAb 9699), integrin β5 (Cell Signalling (D24A5) Rabbit IgG mAb 13629) and integrin α4 (Cell Signalling; (D2E1) XP® Rabbit IgG mAb 8440). The protein loading was evaluated and normalised using monoclonal mouse β-actin Abcam (8226; isotype IgG1). All primary antibodies were previously optimised and used at 1:1000 dilutions in 5% (w/c) BSA, TBS, 0.1 Tween 20 (pH 7.6; MilliporeSigma; Burlington; USA) overnight at 4 C with gentle agitation. Analysis of the band size was determined using ImageJ Software. Densitometry was performed as per Chapter *2.11 Densitometry.*

4.2.10 xCELLigence real-time cell analysis (RTCA) eSight-Imaging and Impedance

Cell-based assays serve as an indispensable tool for basic and applied biological research. However, the utility of many cell-based assays is diminished by the need to use labels,

incompatibility with continuous monitoring (so limited to end-point analysis), and the inability to provide an objective/quantitative readout. These limitations can, however, be overcome by non-invasive, label-free and real-time cellular impedance assay. An RTCA system was developed recently to observe cell morphology and adhesion, including prospectively in kinetic assays[418]. The RTCA system is based on the electronic detection of biological processes[419]. This technique enables label-free, real-time and continuous measurement of adhesion, proliferation, growth, activation, and morphology states. The core principle of the eSight assay is the specialised electronic microplate. The electrical biosensor allows the detection of cellular impedance (denoted as Z); the measurement of impedance depends on the size, cell number and cell attachment. A gold biosensor array that continuously and non-invasively monitors cellular impedance is incorporated into the glass bottom of all 96 wells of the plate[420]. The passage of electrons and ions on the sensor surface is affected by changes in the properties of cells or molecules and is measured as impedance. It is vital to note that the gold microelectrode surfaces, and the weak applied electric potential have no effect on cell health or behaviour[342-345]. Electronic impedance allows the detection of the attachment of the cells to the bottom of the well and monitors their spreading at a particular time, expressed as cell index (CI)[421]. CI is defined as (Zi-Z0Ω /15Ω)[422], where ohm (Ω) is the unit for electrical resistance in the international system of units (IS), Z0 is the background impedance of the well measured with the medium alone at the start of the experiment, and Zi is the impedance at an individual point of time during the experiment, with the cells present; this value is then divided by the frequency for which the impedance is measured (15Ω)[423]. Therefore, measuring CI reflects cell number, cell adhesion quality, and cell morphology, which can change with time. It allows the investigation of the effects of test compounds on cells at any time during the experiment. Cell toxicity of IMiDs has been investigated previously but only using end-point methods that usually require harvesting and fixing cells; RTCA is dedicated to the live-cell analysis and overcomes the limitations of endpoint assays such as antibody-based technologies, including ELISA, western blotting and flow cytometry[424,425]. Protocols for testing non-adherent cells using the RTCA system require covering the wells with a substrate such as fibronectin, laminin, collagen, or gelatineClick or tap here to enter text.. The previous chapter has already reported using RTCA eSight to monitor osteoclast formation. In this chapter, the use of such a technique is used to test the effect of current myeloma treatments.

The adhesion of targeted cells to the biosensors impedes the flow of a microampere electric current, providing an exquisitely sensitive readout of cell attachment and, in this case, cell adhesion. The microelectrodes are incorporated into special cell culture plates, E-plates. The electrical impedance measured is recorded at a defined temporal frequency (every hour for the experiments here). In addition, this is a heterogenous assay, where the impedance signal

exclusively reflects target cell health and behaviour. Along with providing an impedance signal of osteoclasts, a viewing window in the centre of each well's biosensor enables eSight to track the migration and differentiation along with the overall changes in the morphology of osteoclasts. This has allowed the evaluation of the cytotoxicity of existing drugs to improve (Figure 4.1).

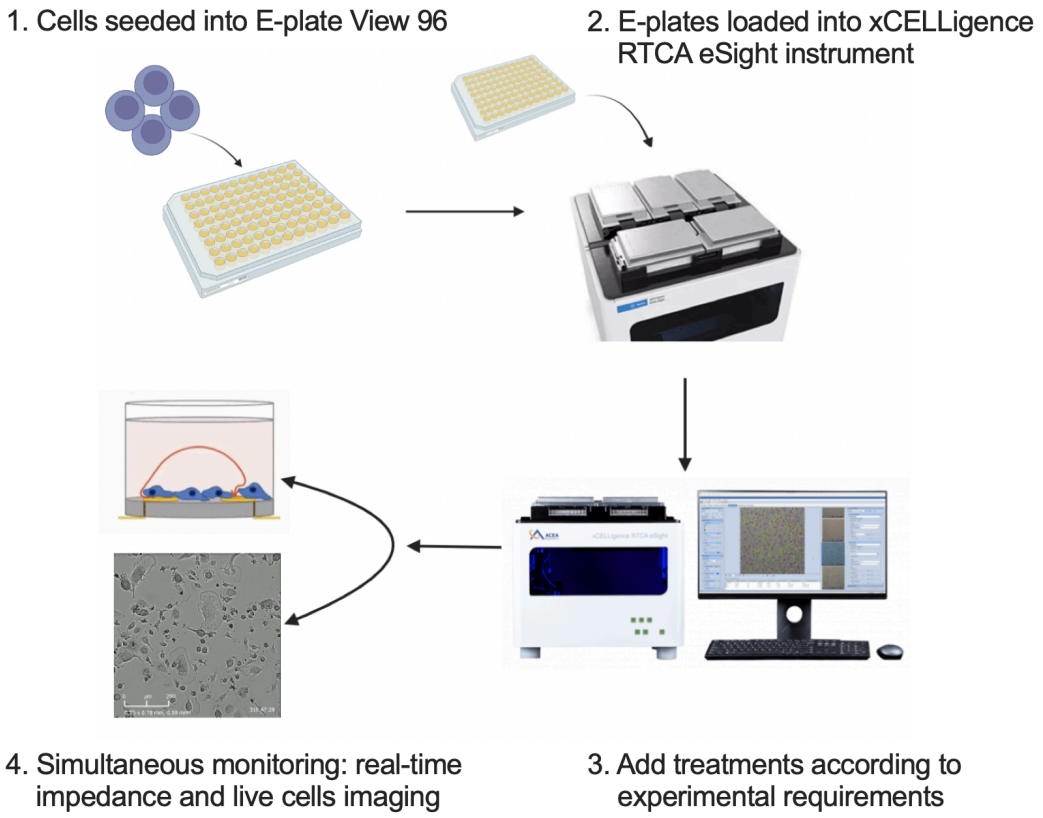

Figure 4.1 Combined impedance and live cell image analysis for enhanced understanding of cell behaviour.

The xCELLigence RTCA eSight enables comprehensive insight into cell behaviour and function using live, simultaneous, and real-time biosensor impedance-based and image-based measurements. The incubator contains a microscope that provides a real-time live cell imaging system that gives two perspectives - the image data and the accurate, real-time kinetics measured by biosensors on the same cell populations, independently and simultaneously.

4.2.11 Statistics

Statistical analysis was performed using GraphPad Prism version 9.4.1 (USA). Data are presented as the mean +/- standard error of the mean (SEM). Two-way ANOVA was used to compare the production of MMP-9 and MMP-2 in the presence of IMiDs over the differentiation period. A one-way ANOVA was used to compare the means of MMP-9 and MMP-2 production by osteoclasts on day 7; +/- LPS upon IMiD treatment. A one-way ANOVA was used to compare MMP-9 proteolytic activity *in gel* zymography upon IMiD treatment. All experiments have replicated sample sizes of at least n = 3 as indicated, and significant values were taken as $p < 0.05$ graphically denoted as * $p \leq 0.05$, ** $p \leq 0.01$, *** $p \leq 0.001$ and **** $p \leq 0.0001$. The xCELLigence graphs shown in this chapter are representative of several repeated experiments. The CI data for IMiDs were averaged and presented as a ratio of DMSO (vehicle control; VC) $n \geq 4$. Two-way ANOVA was used to compare the effects of the different treatments; significant values were taken as $p < 0.05$, graphically denoted as * $p \leq 0.05$, ** $p \leq 0.01$, *** $p \leq 0.001$ and **** $p \leq 0.0001$.

4.3 Results

4.3.1 The direct effects of IMiDs on osteoclast proteolytic activity examined using ELISA and in gel zymography.

Supernatants were harvested from monocyte-derived osteoclasts during the differentiation period in the presence of IMiDs. The IMiDs (10 μM) were added on the day of seeding with the osteoclastogenic medium (day 0) and when the media was changed every 2-3 days. Upon incubation in the differentiation media containing the IMiDs, 10 μM of lenalidomide decreased the overall output of MMP-9; however, the reduction was not statistically significant. Pomalidomide significantly reduced the production of MMP-9 in osteoclasts on day 5 ($p = 0.0131$) and day 7 ($p = 0.0035$) (Figure 4.2 A). Lenalidomide and pomalidomide significantly reduced the production of MMP-2 on day 7 ($p = 0.0486$ and $p < 0.0001$, respectively) and day 10 ($p = 0.0001$ and $p < 0.0001$ respectively) (Figure 4.2 B), where pomalidomide displayed a higher efficacy than lenalidomide in reducing the overall output of MMP-2. Thalidomide did not have a significant effect on either MMP-9 or MMP-2 (Figure 4.2 A and B).

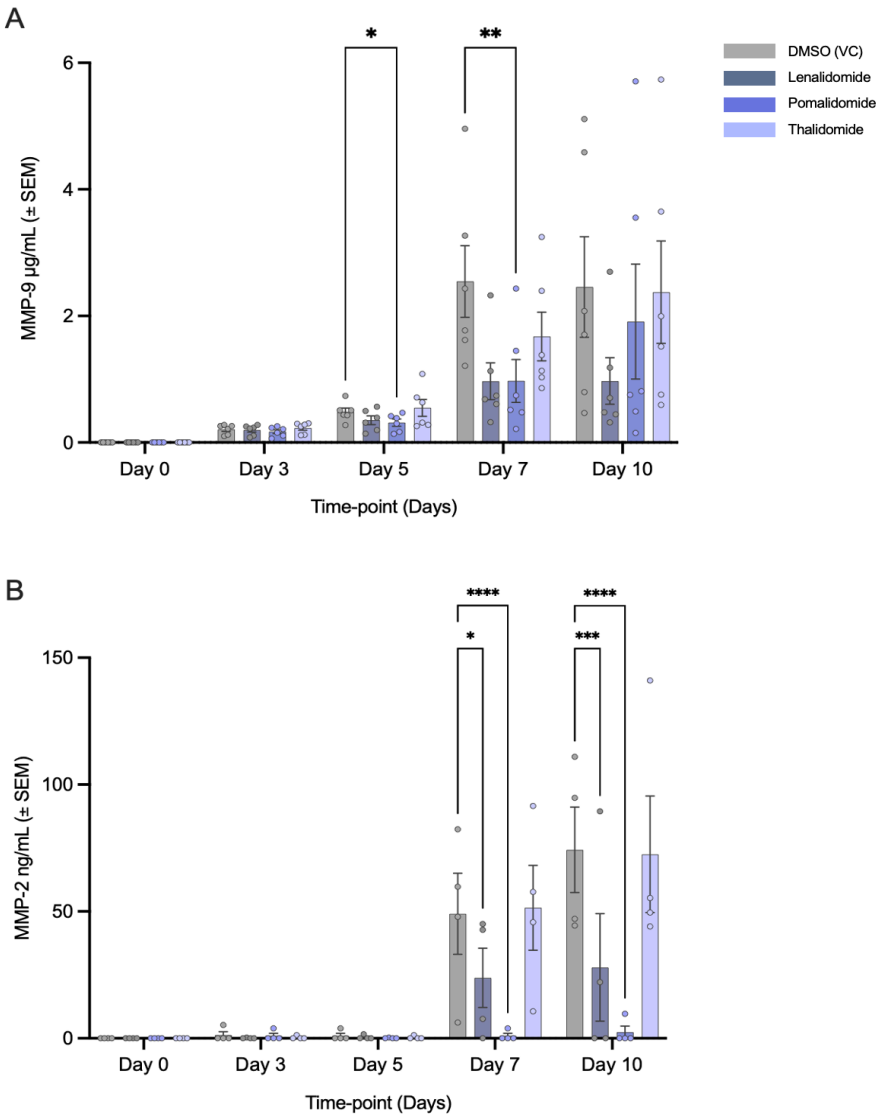

Figure 4.2 MMP-9 and MMP-2 concentrations during monocyte-derived osteoclast differentiation in the presence of IMiDs.

*M-CSF and RANKL were used to differentiate monocytes into osteoclasts. A dose of 10 µM IMiDs (lenalidomide, pomalidomide and thalidomide) or vehicle control (VC; DMSO) was added to the media on the day of seeding and when the media was changed every 2 – 3 days. MMP-9 (A) and MMP-2 (B) in supernatants harvested on days indicated on the x-axis were measured using specific ELISAs. Statistics were performed with a two-way ANOVA and Dunnett's multiple comparisons test. Data are from n ≥ 4 independent experiments expressed as the mean ± SEM: * p ≤ 0.05, ** p ≤ 0.01, *** p ≤ 0.001 and **** p ≤ 0.0001.*

After the initial investigation of the effects of IMiDs on osteoclast differentiation, the impact of IMiDs on MMP-9 and MMP-2 levels at day 7 with the addition of IMiDs on the day of seeding

compared to the addition of IMiDs on the third day after seeding was investigated. This was investigated to demonstrate the effects of early exposure to IMiDs. The addition of 10 μM IMiDs at day three of differentiation was less effective in reducing MMP-9 and MMP-2 levels by osteoclasts compared to the addition at day 0 to the monocyte-derived osteoclasts from the same donors. MMP-9 production was affected by the addition of IMiDs on the day of monocyte seeding compared to their addition on the day of day three. Pomalidomide and lenalidomide displayed a statistically significant reduction of MMP-9 released by cells (osteoclast and undifferentiated mononuclear cells) on day 7 ($p = 0.0080$ and $p = 0.0034$, respectively) when added on day 0 of differentiation (Figure 4.3 A). Only pomalidomide reduced MMP-9 production on day 7 when IMiDs were added on day 3; however, this was not statistically significant (Figure 4.3 B). Comparable results were observed with MMP-2 production, where pomalidomide substantially reduced MMP-2 ($p = 0.0049$) along with lenalidomide ($p = 0.0249$) on day 0 addition (Figure 4.3 C). Both lenalidomide and pomalidomide reduced the overall concentration of MMP-2 on day 3; however, this change was insignificant (Figure 4.3 D).

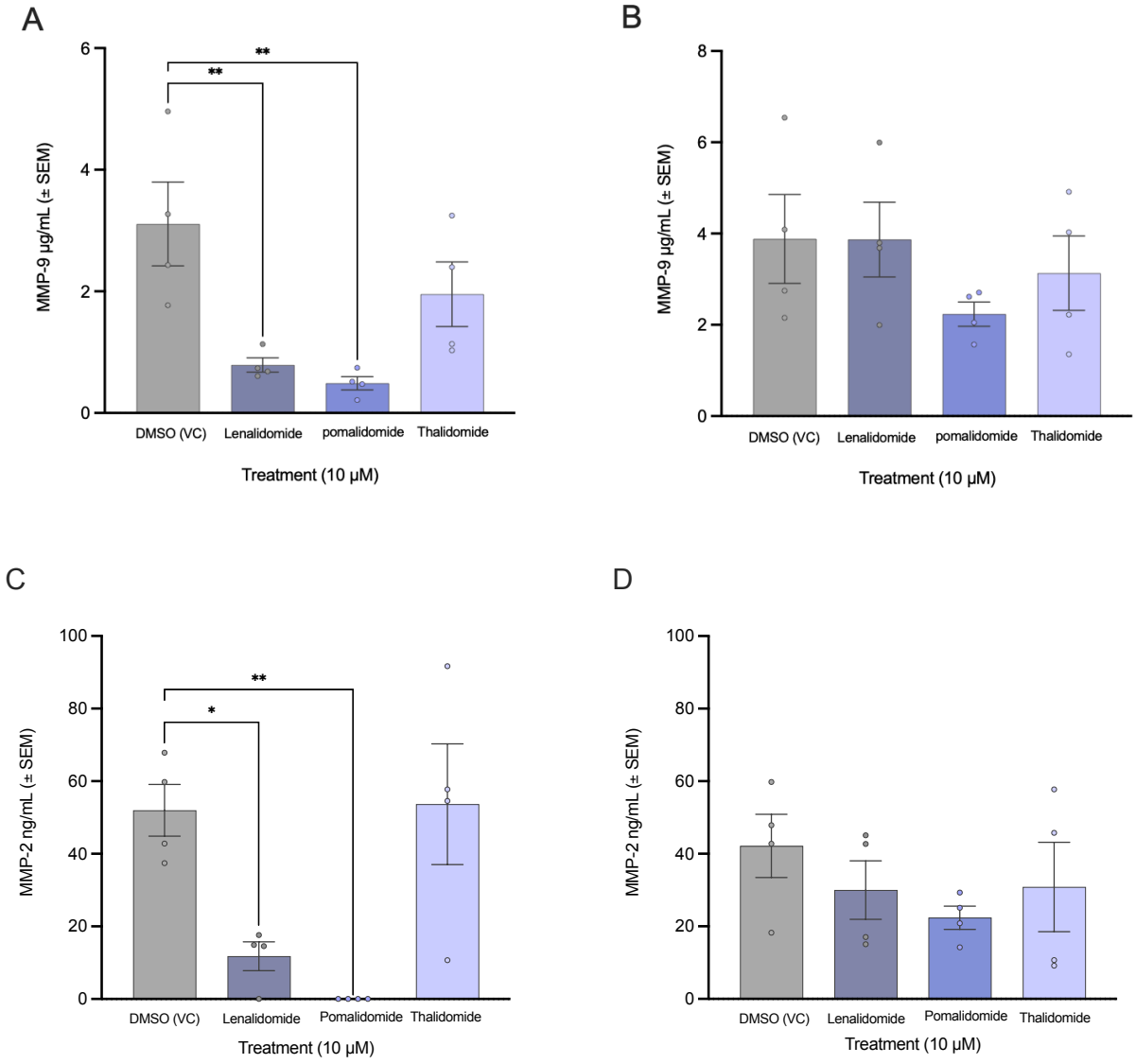

Figure 4.3 Comparison of MMP-9 and MMP-2 concentrations in monocyte-derived osteoclasts with the first addition of IMiDs on day 0 or day 3.

*M-CSF and RANKL were used to differentiate monocytes into osteoclasts. A dosage of 10 µM IMiDs (lenalidomide, pomalidomide and thalidomide) or vehicle control was added to the media on the day of seeding and when the media was changed every 2 – 3 days. MMP-9 with the first addition of IMiDs on day 0 (A) or day 3 (B), and MMP-2 with the first addition of IMiDs on day 0 (C) or day 3 (D) were measured in supernatants harvested on days indicated on the x-axis using specific ELISAs. Statistics were performed with a one-way ANOVA and Dunnett's multiple comparisons test. Data are from n= 4 independent experiments expressed as the mean ± SEM: * $p \leq 0.05$, ** $p \leq 0.01$, *** $p \leq 0.001$ and **** $p \leq 0.0001$.*

Based on these data, the expression of MMP-9 and MMP-2 was then investigated when added on day seven of differentiation. Day seven was chosen to explore this as Chapter three revealed the highest expression and activity of MMP-9 by mature osteoclasts on day seven. The cells were exposed to IMiDs with and without LPS stimulation for 24 hours after this differentiation period. There was no significant difference between DMSO vehicle control treated and IMiDs-treated cells for the expression of either enzyme after 24 hours of treatment (MMP-9; Figure 4.4 A, MMP-2 Figure 4.4 B). Furthermore, no significant difference was observed between LPS-stimulated and unstimulated cells for the expression of MMP-9 and MMP-2 production (Figure 4.4 A-B). The production of pro-inflammatory cytokines, such as TNFα and IL-6, under LPS stimulation was also examined in the presence of IMiDs in osteoclasts. While LPS induced production of both IL-6 and TNFα, the levels of IL-6 and TNFα were unaffected by IMiD treatment, Figure 4.4 C and D, respectively.

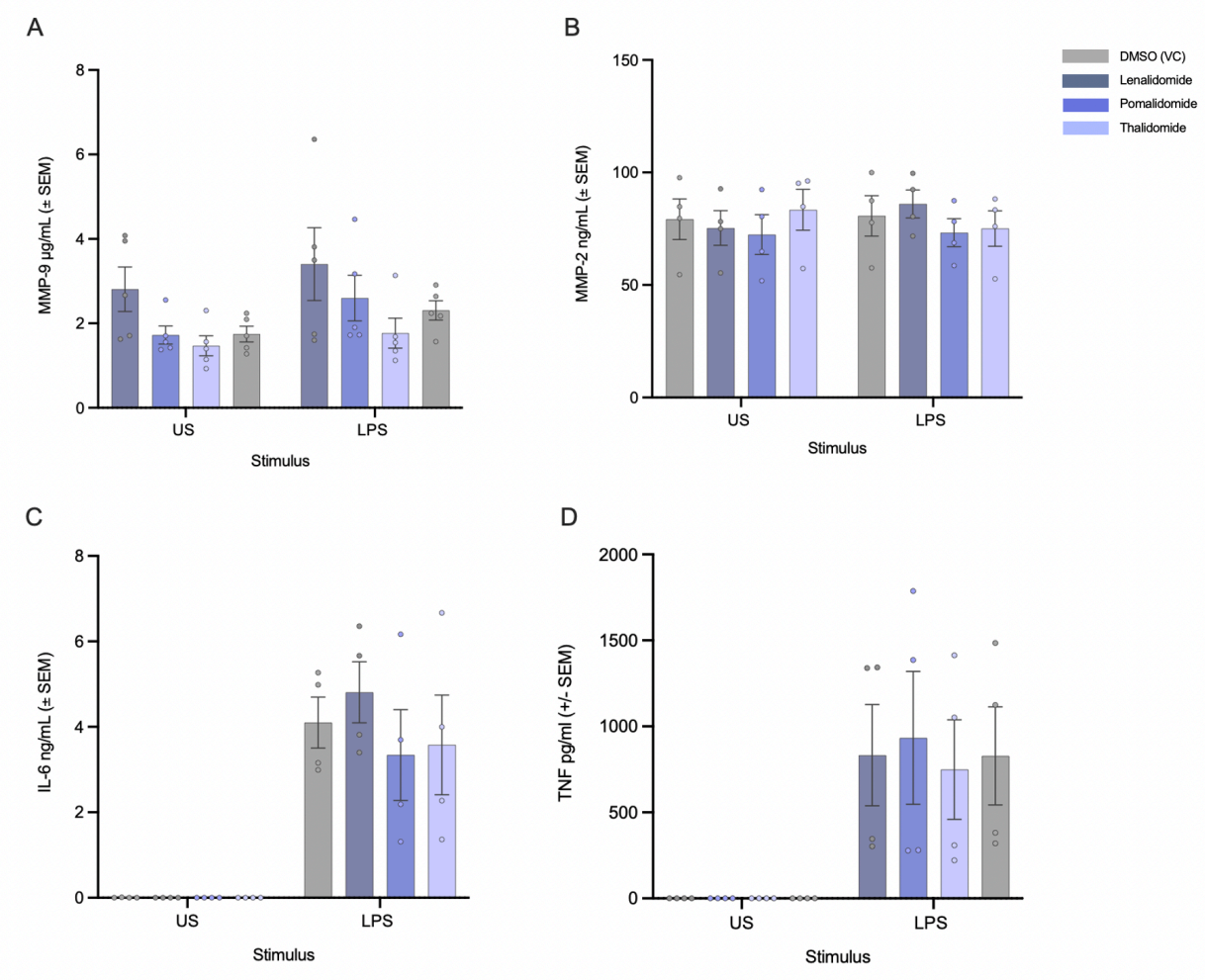

Figure 4.4 Comparison of MMP-9, MMP-2, IL-6 and TNFα concentrations in monocyte-derived osteoclasts with the first addition of IMiDs on day 7.

M-CSF and RANKL were used to differentiate monocytes into osteoclasts. A dose of 10 μM IMiDs (lenalidomide, pomalidomide and thalidomide) or vehicle control (VC; DMSO) was added to the media on day 7 of differentiation for 24 hours, with or without LPS. MMP-9 (A), MMP-2 (B), IL-6 (C), and TNFα (D) were measured in supernatants harvested 24 hours post-treatment with IMiDs using specific ELISAs. Statistics were performed with a two-way ANOVA and Dunnett's multiple comparisons test. Data represented n = 4 independent experiments expressed as the mean ± SEM. US= Unstimulated.

4.3.2 Downregulation of MMP-9 proteolytic activity in osteoclasts upon IMiDs treatment.

As seen in chapter three, the greatest proteolytic activity of osteoclasts is measured within ~7-9 days of differentiation. Having established above that IMiDs reduce MMP-9 production in osteoclasts especially when present form the outset of differentiation, the assessment of MMP-9 activity secreted by osteoclasts upon treatment with IMiDs was investigated next. Gelatine zymography was chosen, where supernatants from day 7 osteoclasts were harvested and used to perform the zymography. The activity of MMP-9 was illustrated in all samples (Figure 4.5A). However, the intensity of the signal and, therefore, the enzyme activity in supernatants decreased when treated with 10 μM of lenalidomide and pomalidomide (Figure 4.5 A and B). There was no significant difference between DMSO (VC) and thalidomide-treated cells. Due to the insufficient amounts of MMP-2 released by osteoclasts, it was unfeasible to detect using *in gel* zymography. Therefore, all *in gel* zymography experiments were conducted on MMP-9 secreted by osteoclasts.

Raw data from zymography analysis (Figure 4.5 C) displays the overall pattern of the IMiD effect on the activity of MMP-9. Values depicted relative to the DMSO vehicle control +/- SEM (n= 5), which shows the overall trend of the effect. The activity was normalised to that produced by DMSO-treated osteoclasts alone and represented as a ratio of the control (Figure 4.5 D), where lenalidomide and pomalidomide significantly reduced the activity of MMP-9 ($p = 0.041$ and $p = 0.0038$, respectively).

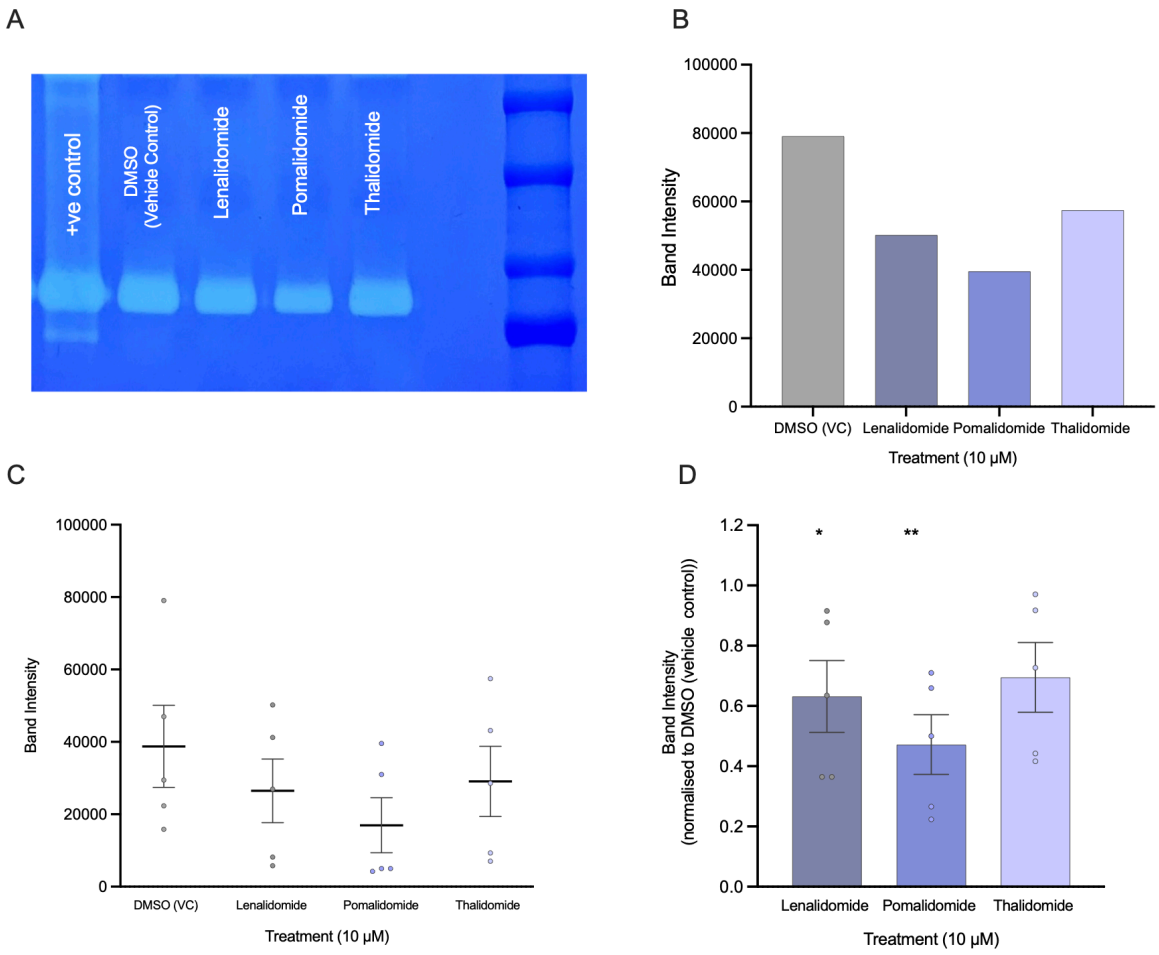

Figure 4.5 The effect of IMiDs on MMP-9 activity of monocyte-derived osteoclasts using in-gel zymography.

*M-CSF and RANKL were utilised to generate monocyte-derived osteoclasts. IMiDs (lenalidomide, pomalidomide and thalidomide) were added to the media on the day of seeding and were added with each media change. A representative zymography gel (A) and its corresponding band intensity (B) from one experiment. The raw data of the band intensity (C) and normalised to DMSO control (D) from n=5 independent experiments expressed as the mean ± SEM. Statistics were performed with a one-way ANOVA and Dunnett's multiple comparisons test. Positive (+ve) control = recombinant human MMP-9; * $p \leq 0.05$, ** $p \leq 0.01$.*

The proteolytic activity of osteoclasts on day seven was then measured with the addition of IMiDs on day three of differentiation. On day seven of differentiation, the supernatants were harvested and tested for the secretion of MMP-9. There was a slight reduction of MMP-9 activity in pomalidomide-treated cells when added three days post-seeding. However, this change was not statistically significant (Figure 4. 6 A). A similar effect was observed when

osteoclasts were treated with IMiDs for 24 hours, seven days into the differentiation period; this was insignificant (Figure 4.6 B). Raw data was displayed for day three addition (Figure 4.6 C) and 24-hour addition (Figure 4.6 D) to show the overall pattern of IMiDs efficacy. The effects of IMiDs on the MMP-9 proteolytic activity was represented as a ratio of the DMSO vehicle control-treated cells (Figure 4.6 E); day seven supernatants when IMiDs was added three days after seeding into the osteogenic medium (Figure 4.6 F;) supernatants harvested on day seven after 24 hours of adding the IMiDs into the cell differentiation medium.

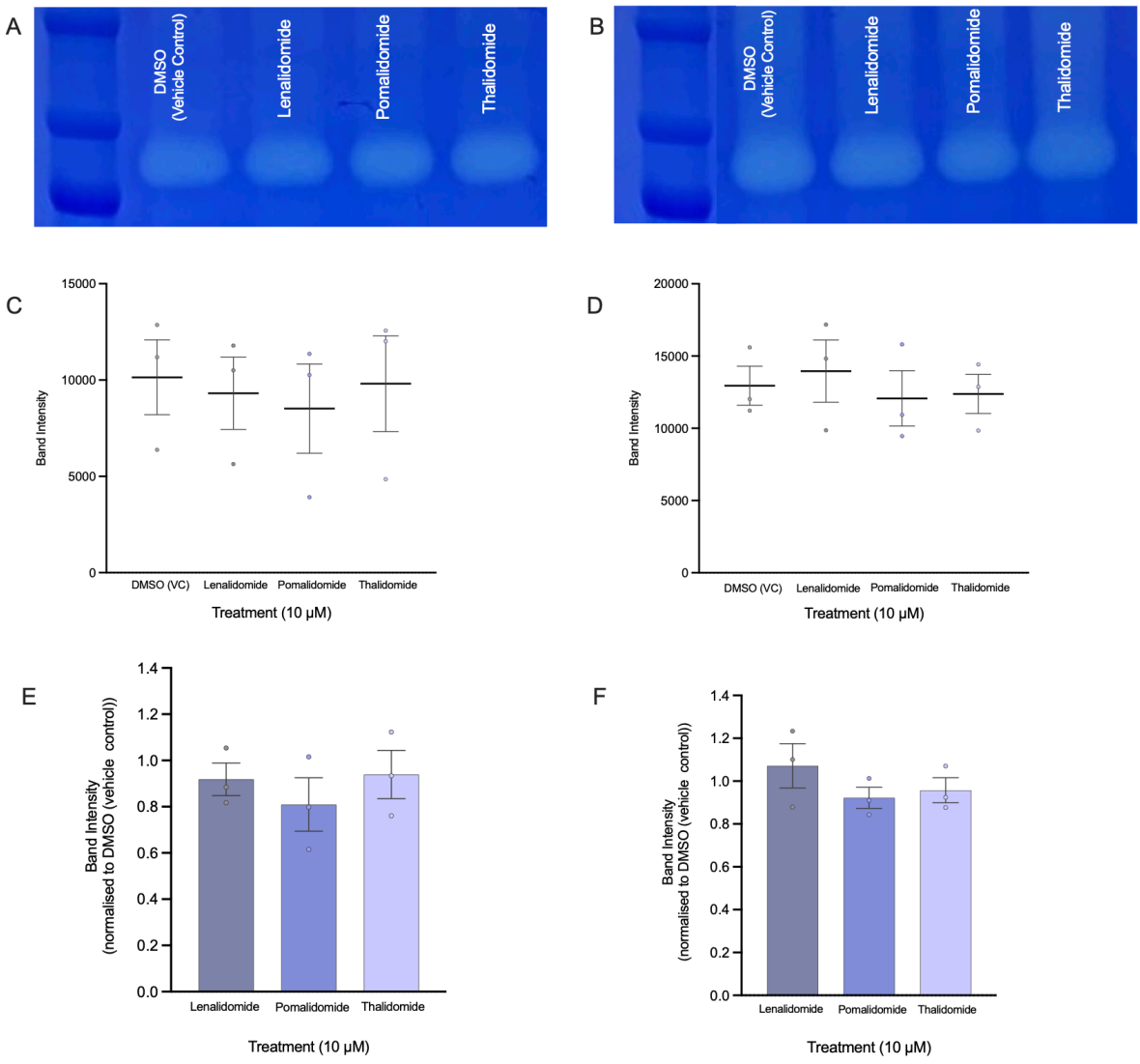

Figure 4.6 The effect of IMiDs on MMP-9 activity of monocyte-derived osteoclasts using in-gel zymography when added after differentiation has commenced.

M-CSF and RANKL were utilised to generate monocyte-derived osteoclasts. IMiDs (lenalidomide, pomalidomide and thalidomide) were added to the media on day 3 of differentiation (A, C and E) and then with each media change or for 24 hours after day 7 of differentiation (B, D and F). A zymography gel showing the effects of IMiDs on day 3 addition

*(A) or the addition of IMiDs on day 7 for 24 hours (B). Raw data for day 3 addition (C) or the addition of IMiDs on day 7 for 24 hours (D). Data normalised to the DMSO vehicle control for day 3 addition of IMiDs (E) or the addition of IMiDs on day 7 for 24 hours (F). Statistics were performed with a one-way ANOVA and Dunnett's multiple comparisons test. Data represent n=3 independent experiments expressed as the mean ± SEM: * $p \leq 0.05$, ** $p \leq 0.01$.*

4.3.3 Qualitative images of osteoclast morphology and differentiation in the presence of IMiDs

Prior to a more detailed examination of the effects of IMiDs on osteoclast differentiation and activation, confocal microscopy was used initially to monitor the changes in the morphology of osteoclasts treated with 10 μM of each IMiD. Monocytes were seeded on the Millicell EZ chamber slides. IMiDs were added to a complete osteoclastogenic medium (consisting of M-CSF and RANKL) that promoted the differentiation of monocytes into osteoclasts. Images captured on day zero displayed the common features of monocytes (Figure 4.7 A), whereas images taken on day seven (Figure 4.7 B) and day ten (Figure 4.2 C) showed multinucleated cells displaying the morphology of mature osteoclasts. The differentiation rate of osteoclasts is marked by the fusion of monocytes and by the number of nuclei within the cells. On average, mature osteoclasts are 15 times larger than monocytes and have more than 8 nuclei[426, 427]. Representative images from one donor from a series of n=6 experiments. IMiDs seemed to delay the differentiation rate of osteoclasts as shown by qualitative analysis of the changes observed to the overall size, shape and multinucleation of cells at the end of the differentiation period.

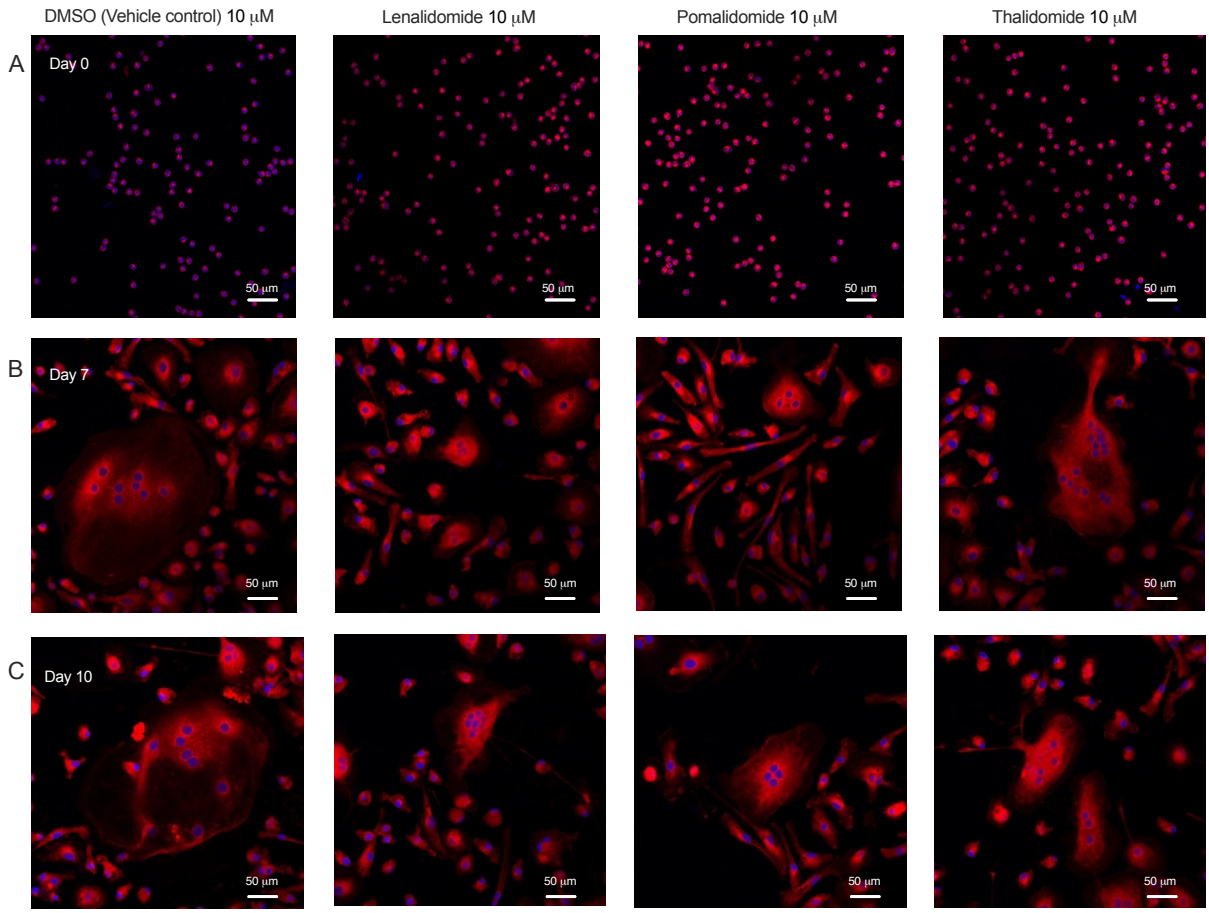

Figure 4.7 The effect of different IMiDs on monocyte-derived osteoclast differentiation using confocal microscopy.

M-CSF and RANKL were used to differentiate monocytes into osteoclasts. A dose of 10 μM IMiDs (lenalidomide, pomalidomide and thalidomide) or equivalent DMSO (vehicle control) was added to the media on the day of seeding and when the media was changed every 2 – 3 days. Nuclei were stained with Hoechst 33342 Solution and the plasma membrane was stained with CellMask™ Orange on day 0 (A), day 7 (B) and day 10 (C). Images were taken at 20X magnification, and a 50 μm scale bar was included. Representative images from n=6 experiments.

Using the X20 images, the number of osteoclasts per image and the average number of nuclei per osteoclast in the presence of IMiDs were scored manually and presented in figure 4.8A and B, respectfully. Counting the number of osteoclasts revealed that osteoclasts have significantly decreased in the presence of lenalidomide ($p= 0.0003$) and pomalidomide ($p <0.0001$) on day 7 and on day 10 (p value for lenalidomide $p= 0.0076$); (p value for pomalidomide $p <0.0001$). The number of nuclei per osteoclast have decreased significantly

in the presence of lenalidomide and pomalidomide on day 7 (p= 0.0015 and p= 0.0003 respectfully) and on day 10 (p value for lenalidomide = 0.0015 and pomalidomide p <0.0001).

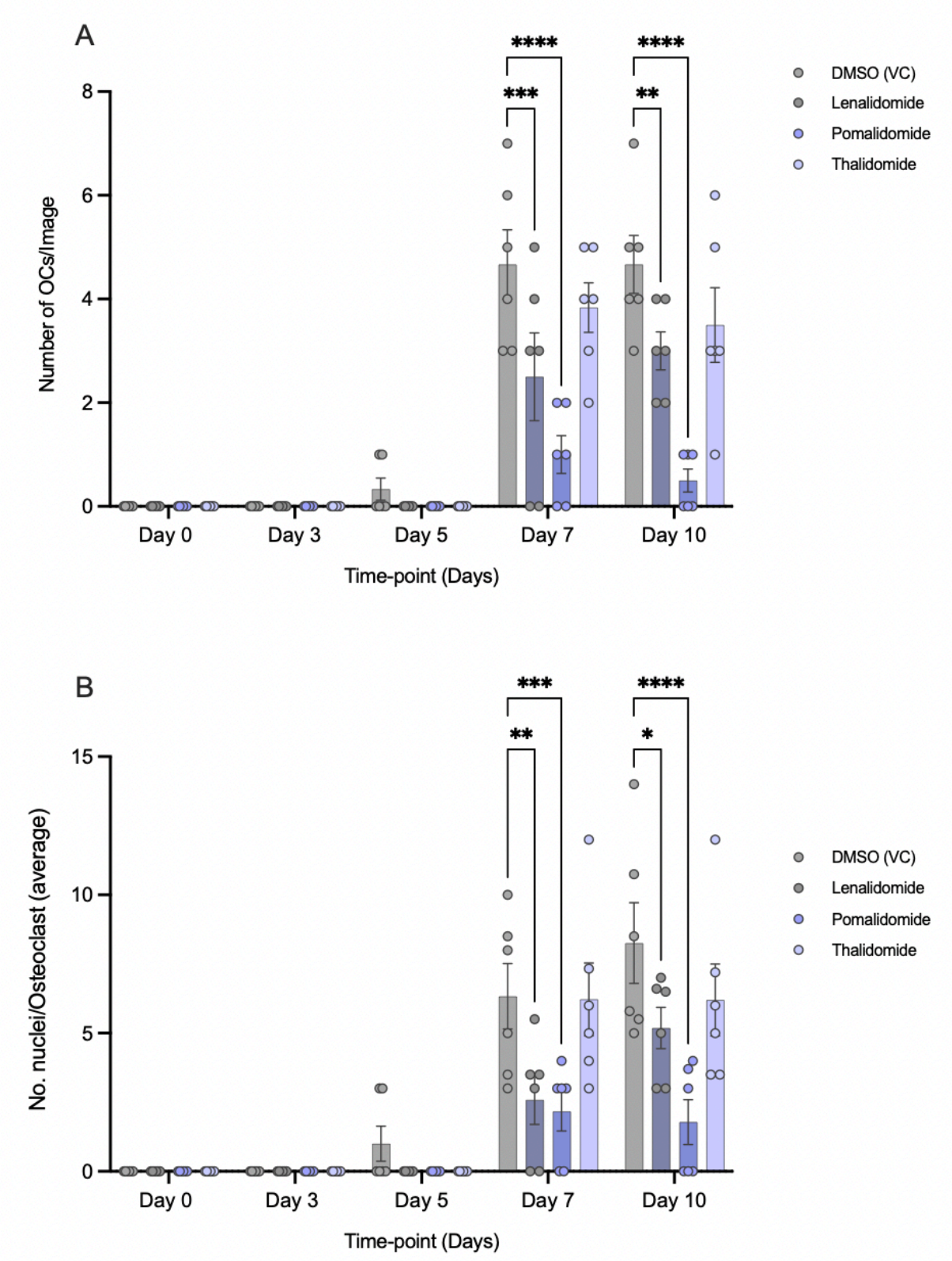

Figure 4.8 Quantification of the effect of different IMiDs on monocyte-derived osteoclast differentiation using confocal microscopy.

*M-CSF and RANKL were used to differentiate monocytes into osteoclasts. A dose of 10 μM IMiDs (lenalidomide, pomalidomide and thalidomide) or equivalent DMSO (vehicle control) was added to the media on the day of seeding and when the media was changed every 2 – 3 days. The number of osteoclasts per image and the number of nuclei were scored manually using X20 day 0, day 5, day 5, day 7 and day 10. Statistics were performed with a two-way ANOVA and Dunnett's multiple comparisons test. Data expressed as the mean ± SEM: * $p \leq 0.05$, ** $p \leq 0.01$, *** $p \leq 0.001$and **** $p \leq 0.0001$.*

4.3.4 Monitoring osteoclasts differentiation upon IMiDs treatment by live-cell imaging (a quantitative approach to imaging)

IMiDs were added on the day of seeding the cells onto the E-plate and with each culture media change as previously. The cells were allowed to differentiate for 14 days. Three images were taken every hour of the differentiation. After 24h (Figure 4.9 A), the clustering of monocytes begins (which is a characteristic of differentiation)[428, 429] and becomes more robust (quantified in upcoming figures). At later time points at 120 hours (day 5) and 170 hours (day 7) (Figure 4.9 B-C), DMSO-treated osteoclasts have differentiated more progressively than IMiD-treated cells, as a higher number of clusters are observed 24 hours post-treatment in the control sample; this accompanied a higher number of multinucleated cells with ruffled edges observed at 315 hours post-treatment. Over the first 24 hours, a decrease in the cellular cluster formation rate in lenalidomide and pomalidomide-treated cells is observed (Figure 4.9 A). Comparison of cell morphology at the final stages of differentiation has revealed the overall downregulation of differentiation rate in lenalidomide and pomalidomide-treated cells. DMSO-treated cells in Figure 4.9 D have the mature osteoclast characteristics of multinucleation with ruffled edges. These characteristics were not observed in pomalidomide and lenalidomide-treated cells as they expressed elongated features, which suggests a delay in the overall differentiation process when treated with such treatments (See Appendix 10.8 for video obtained from RTCA for osteoclast differentiation in the presence of 10 μM DMSO (VC); Appendix 10.9 for video obtained from RTCA for osteoclast differentiation in the presence of 10 μM lenalidomide; Appendix 10.10 for video obtained from RTCA for osteoclast differentiation in the presence of 10 μM pomalidomide; Appendix 10.11 for video obtained from RTCA for osteoclast differentiation in the presence of 10 μM thalidomide).

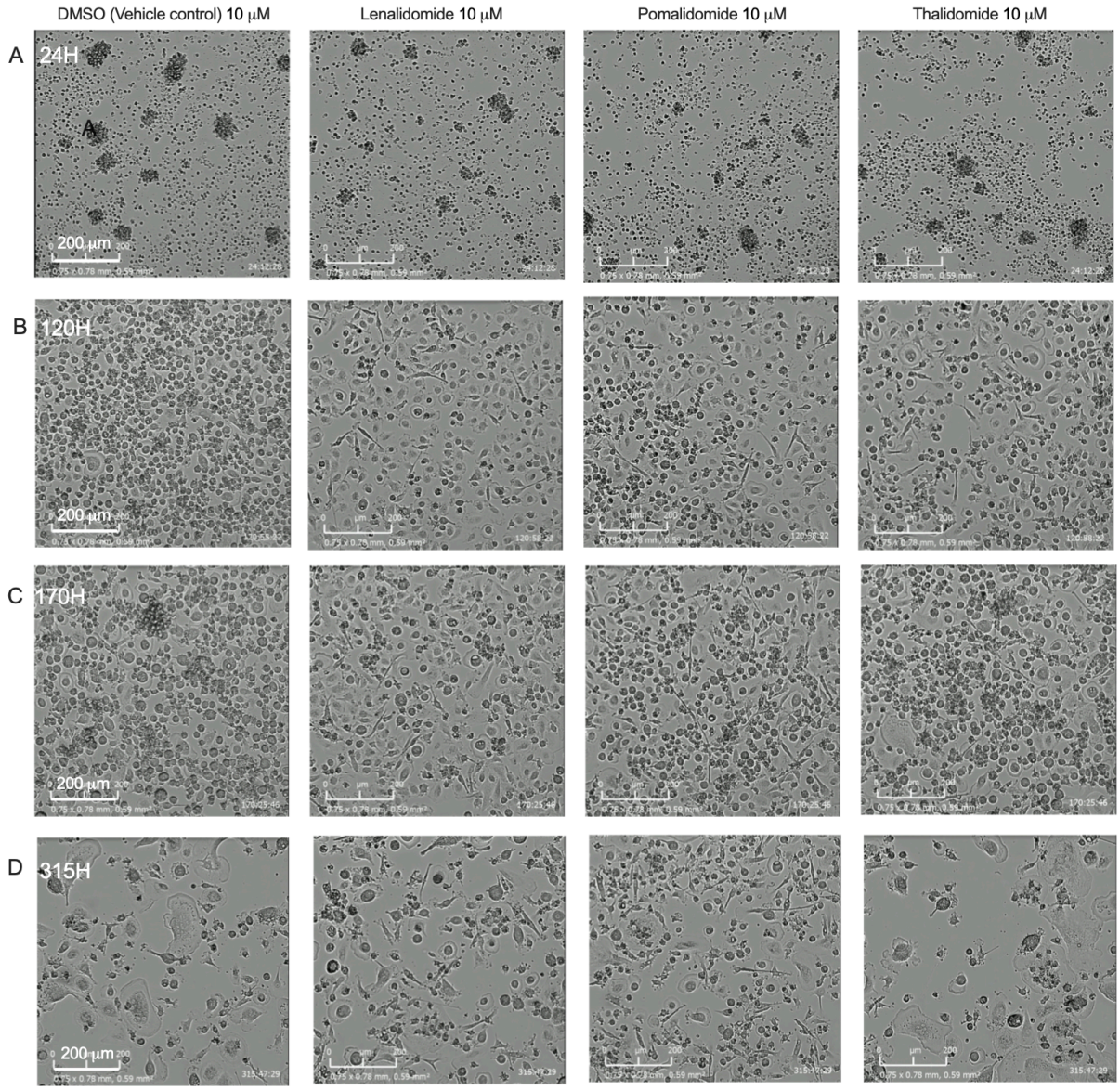

Figure 4.9 Visualisation of osteoclast differentiation in the presence of IMiDs in vitro using real-time imaging.

Monocytes (100,000/well) were differentiated to osteoclasts using M-CSF and RANKL and exposed to 10 μM of IMiDs on the day of seeding. Images show the progression of osteoclast differentiation in the presence of IMiDs at 24H (A), 120H (B), 170H (C) and 315H (D). Images shown were obtained from one experiment. Similar results were observed with three independent and repeated experiments.

The graphs (Figure 4.10) show the bright-field confluence percentage over time (in hours) for cells treated with lenalidomide, pomalidomide, and thalidomide) at two different concentrations (1 μM (A) and 10 μM) (B). This was compared to vehicle control (DMSO). Both concentrations

show similar trends, with Pomalidomide maintaining the highest confluence and Thalidomide showing the lowest confluence. A higher concentration (10 µM) generally results in lower confluence levels compared to a lower concentration (1 µM). The VC shows a moderate confluence decrease, maintaining lower levels compared to lenalidomide and pomalidomide. Lenalidomide shows slightly higher confluency compared to DMSO. Pomalidomide consistently shows the highest confluence levels among all treatments. Thalidomide exhibits the most significant decrease in confluence.

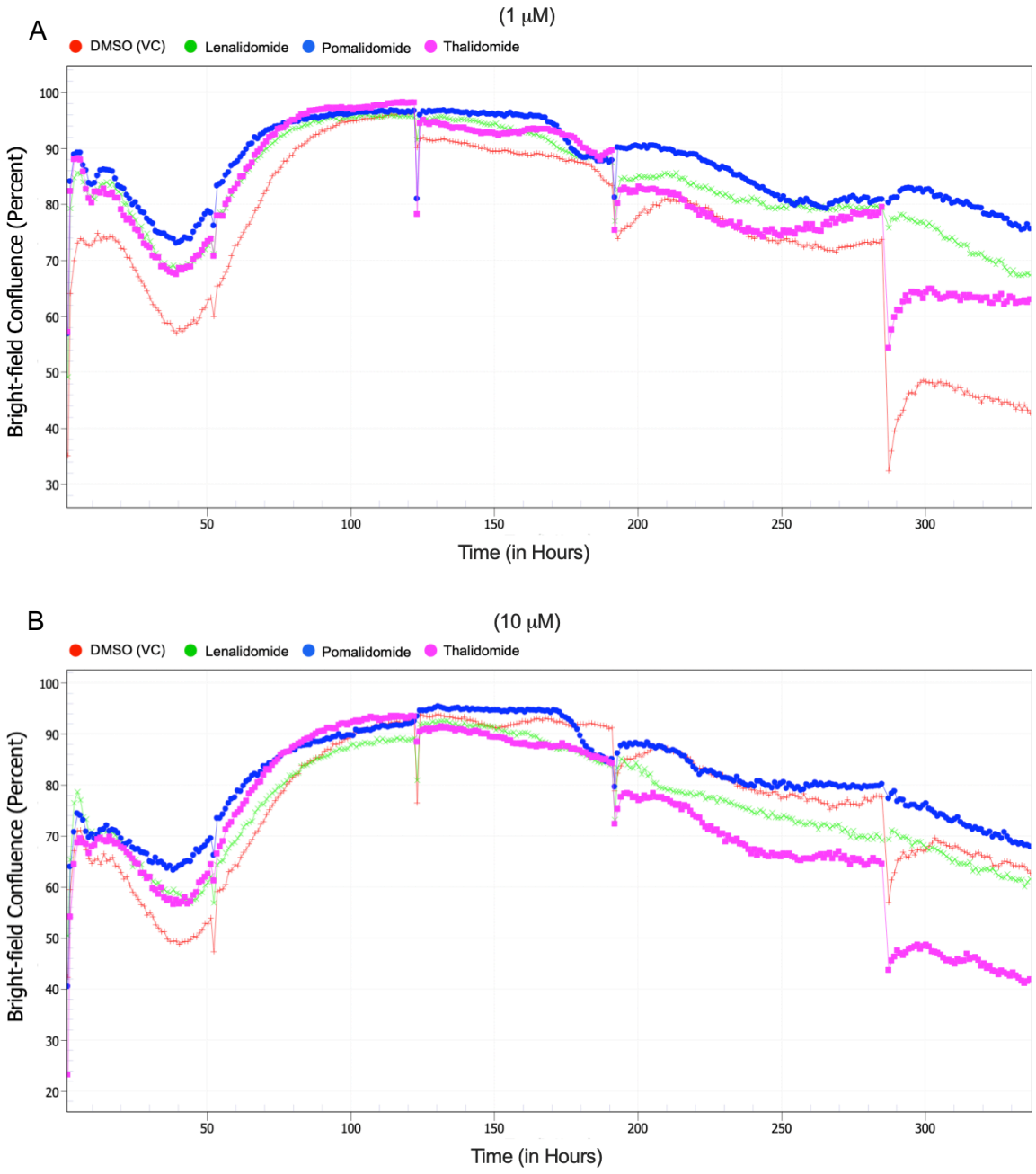

Figure 4.10 Percentage confluency profiles of monocyte differentiation in vitro in the presence of IMiDs. *The cells were incubated in M-CSF and RANKL to differentiate into osteoclasts. A dosage of 1 (A) and 10 µM (B) (lenalidomide, pomalidomide and thalidomide)*

or DMSO (VC) was added to the media on the day of seeding and when the media was changed every 2 – 3 days. The data shown are representative of 1 experiment, similar to that observed with repeated experiments obtained from n=4 independent repeats.

4.3.5 Quantifying the effects of IMiD treatment on osteoclast differentiation using real-time impedance measurements.

Continuing to use 100,000 monocyte cells/well on the E-plate differentiation to osteoclasts with M-CSF and RANKL, the effects of two concentrations of IMiDs: 1 μM (Figure 4.11 A and B) and 10 μM (Figure 4.11 C and D), were studied. According to previous results obtained in this chapter, the progression of differentiation is suggested to be decreased when treated with lenalidomide and pomalidomide, with pomalidomide having a greater impact than lenalidomide. Additionally, thalidomide did not a significant impact on the differentiation progress. The CI signal, dependent upon cells being adhered to the E-plate, increases steadily for all the treatments over the first ~ 70 hours, after which it briefly plateaus ~ 70-120 hours. Overall, the presence of IMiDs significantly increases cell impedance throughout the entire differentiation process. Because impedance is highly sensitive to changes in cell size and adhesion strength, it effectively detects the early stages of differentiation.

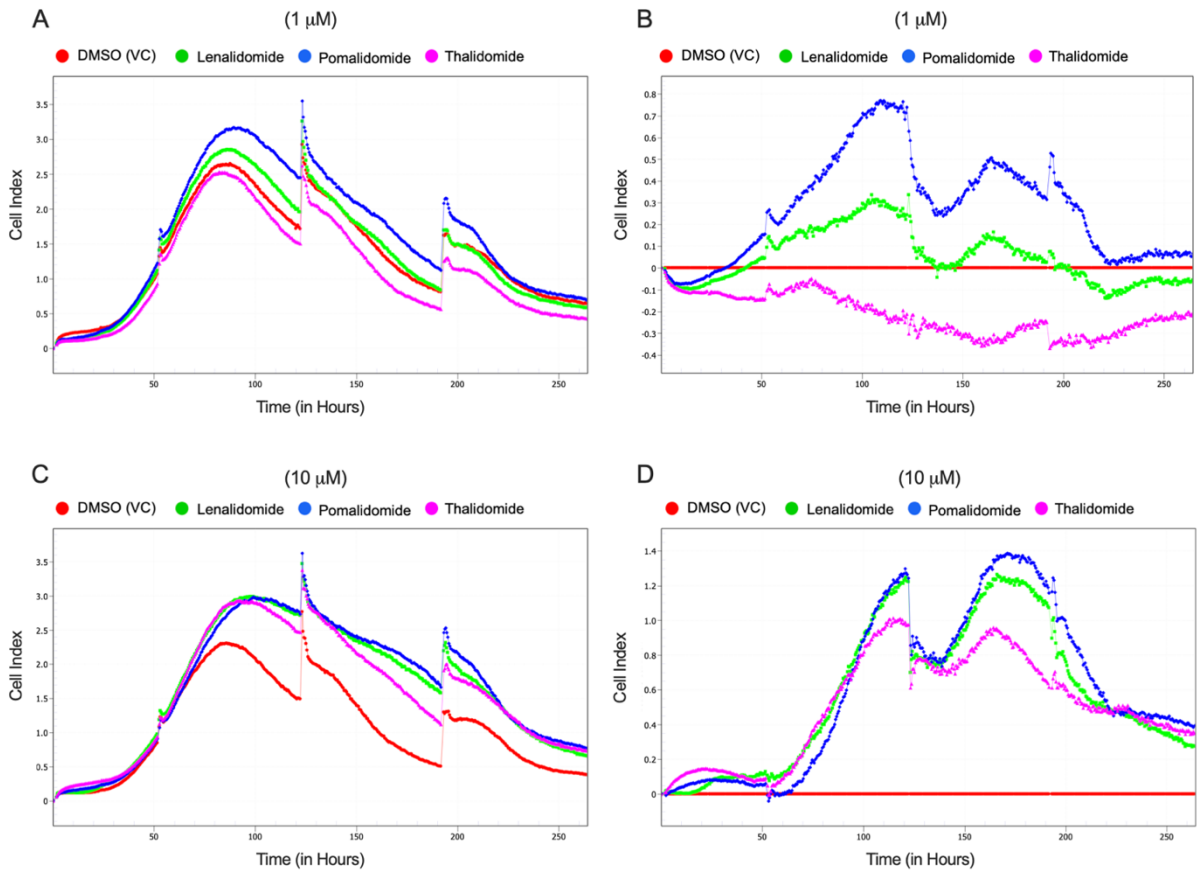

Figure 4.11 CI signal displaying the impedance of osteoclasts in the presence of IMiDs. *M-CSF and RANKL were used to differentiate monocytes into osteoclasts. A dosage of 1 and 10 μM (lenalidomide, pomalidomide and thalidomide) or DMSO (VC) was added to the media on the day of seeding and when the media was changed every 2 – 3 days. The impedance of osteoclasts in the presence of IMiDs showing the CI signal at 1 μM (A); DMSO (VC) as CI baseline (B); the CI signal at 10 μM (C); DMSO (VC) as CI baseline (D). The data shown are representative of 1 experiment, similar to that observed with repeated experiments obtained from n=4 independent repeats. Quantitative analysis of the CI signal in the presence of IMiDs obtained from 4 independent experiments at 1 μM and 10 μM are shown in the upcoming figure.*

The ability to quantify the effects of IMiDs on the impedance of osteoclasts in multiple repeats from real-time live imaging without any additional staining is a unique property of the xCELLigence RTCA. The impedance data shown in Figure 4.10 illustrates the effects on the CI data reproduced in four independent experiments. Pomalidomide has increased the impedance of osteoclasts at a concentration of 1 μM at 200 hours ($p = 0.0011$), 250 hours ($p = 0.0261$), 300 hours ($p = 0.0071$), and 350 hours ($p = 0.0181$) (Figure 4.12 A). Pomalidomide

and thalidomide both displayed a significant increase in the impedance at 10 μM concentration at different time points. Pomalidomide was found to significantly increase the impedance at 250 hours ($p = 0.00312$), pomalidomide and thalidomide significantly increased the impedance at 300 hours ($p < 0.0001$ and $p = 0.0282$, respectively), and pomalidomide significantly increased the impedance at 350 hours ($p = 0.0014$). The most significant increase was observed at 300 hours post-seeding with pomalidomide when compared to the DMSO (VC) (Figure 4.12 B).

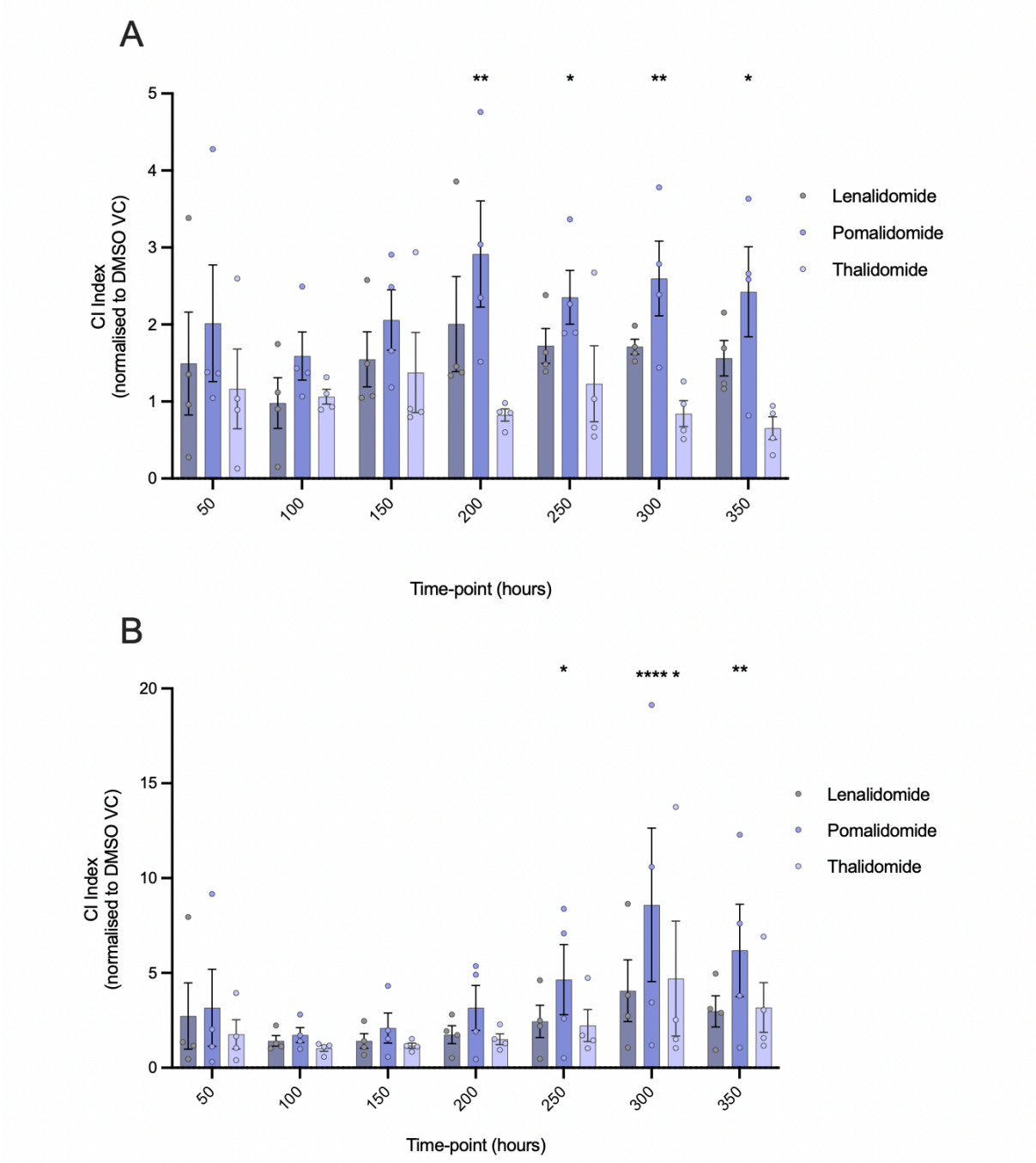

Figure 4.12 The effects of IMiDs on osteoclast differentiation using RTCA impedance measurements.

*M-CSF and RANKL were used to differentiate monocytes into osteoclasts. A dose of 10 μM IMiDs (lenalidomide, pomalidomide and thalidomide) or vehicle control was added to the media on the day of seeding and when the media was changed every 2 – 3 days. The impedance measured as the CI signal of osteoclasts in the presence of IMiDs at 1 μM, normalised to the DMSO control (A), the impedance measured as the CI signal of osteoclasts in the presence of IMiDs at 10 μM, normalised to the DMSO control (B). Quantitative analysis of the CI signal in the presence of IMiDs obtained from 4 independent experiments the 1 μM and 10 μM concentration of IMiDs. Statistics were performed with a two-way ANOVA and Dunnett's multiple comparisons test. Data expressed as the mean ± SEM: * $p \leq 0.05$, ** $p \leq 0.01$, and **** $p \leq 0.0001$.*

4.3.6 The impedance signal in osteoclasts is affected by the addition of IMiDs on the first day of differentiation compared to three days after seeding.

The effects of the time when the IMiDs are added to osteoclasts, using the xCELLigence RTCA, has not been studied before in literature. The addition of lenalidomide, pomalidomide, and thalidomide at either 1 μM or 10 μM on the day of seeding or three days after seeding has impacted the CI signal in osteoclasts. Upon treatment with lenalidomide and pomalidomide on the day of seeding, increased impedance is seen, as already described above. However, there was less of an effect on the impedance when lenalidomide and pomalidomide were added three days after seeding to monocyte, differentiating to osteoclasts isolated from the same donor. IMiDs have increased the impedance of osteoclasts in a dose-dependent manner at 1 μM IMiDs (Figure 4.13 A), this can be seen at when the data is normalised to DMSO (VC) (Figure 4.13 B). At 10 μM IMiDs, there was a greater increase observed with the impedance (Figure 4.13 C). This can be seen when the data is normalised to DMSO (VC) (Figure 4.13 D). The impedance measured as the CI signal did not increase when 1 μM of IMiDs was added after three days of seeding (Figure 4.13 E); this can be seen when the data is normalised to DMSO (VC) (Figure 4.13 F). However, there was a slight increase when 10 μM of IMiDs was added at this time (Figure 4.13 G); this can be seen when the data is normalised to DMSO (VC) (Figure 4.13 F).

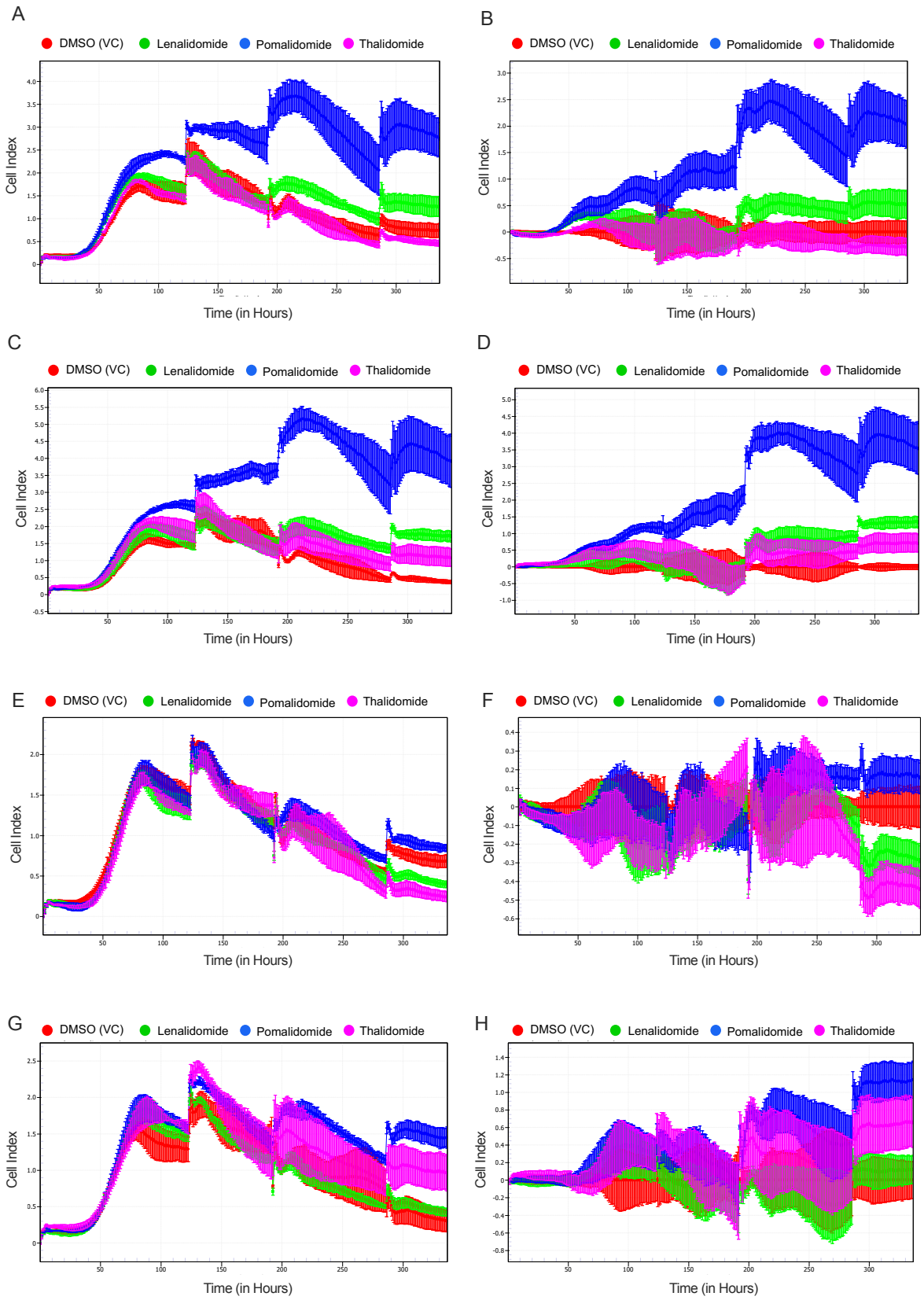

Figure 4.13 The effects of IMiDs on the impedance of monocyte-derived osteoclasts when added on day 3 of differentiation.

M-CSF and RANKL were used to differentiate monocytes into osteoclasts. A dosage of 1 and 10 μM (lenalidomide, pomalidomide and thalidomide) or DMSO (VC) was added to the media either on the day of seeding or after day 3 of differentiation. The media was changed every 2 – 3 days. The impedance of osteoclasts in the presence of IMiDs showing the CI signal at 1 μM (A); DMSO (VC) as CI baseline (B); the CI signal at 10 μM (C); DMSO (VC) as CI baseline (D). The CI signal of osteoclasts at 1 μM IMiDs when added at day 3 (E); DMSO (VC) as CI baseline (F); the CI signal of osteoclasts at 10 μM IMiDs added at day 3 (G); DMSO (VC) as CI baseline (H). The data shown are representative of 1 experiment, similar to that observed with repeated experiments obtained from n=3 independent repeats.

4.3.7 Cluster and activation function of the xCELLigence RTCA

To quantify the effects of IMiDs on the early stages of osteoclastogenesis, we used the Sight confluence masking. This displays the confluency at different time points of differentiation. The measuring of clustered objects was possible due to the parameters set that allowed the isolation of clusters from the background. The parameters used were based on measuring the areas of the clusters from different time points and then using those measures to set the parameters that allowed the differentiation of clusters against single cells and multinucleated cells within an image. Using the images obtained from the control images, the parameters on the RTCA software were set to a minimum area of 2500 μm and a maximum area of 50,000 μm with Adjust Size (pixels) of 1 and a Segmentation Adjustment of 0.2 of cells to background ratio. These parameters allowed the detection of cellular clustering in each if the images obtained. These parameters were then applied to all selected images at all time points in the presence and absence of treatments. Figure 4.14 shows an example of using the eSight confluence masking to identify the cellular clustering of pre-osteoclasts pre-fusion. To demonstrate the masking algorithm, images of six different time points are included in the figure from the same well. The yellow area represents the cells detected by the masking parameters which indicate cellular clustering, whereas the grey area represents the excluded cells which were not counted as part of the clustering. Singular cells and multinucleated cells were excluded from the mask and did not get counted. Cluster formation seems to begin from 24 hours, with the most clusters observed at 48 h and 60h.

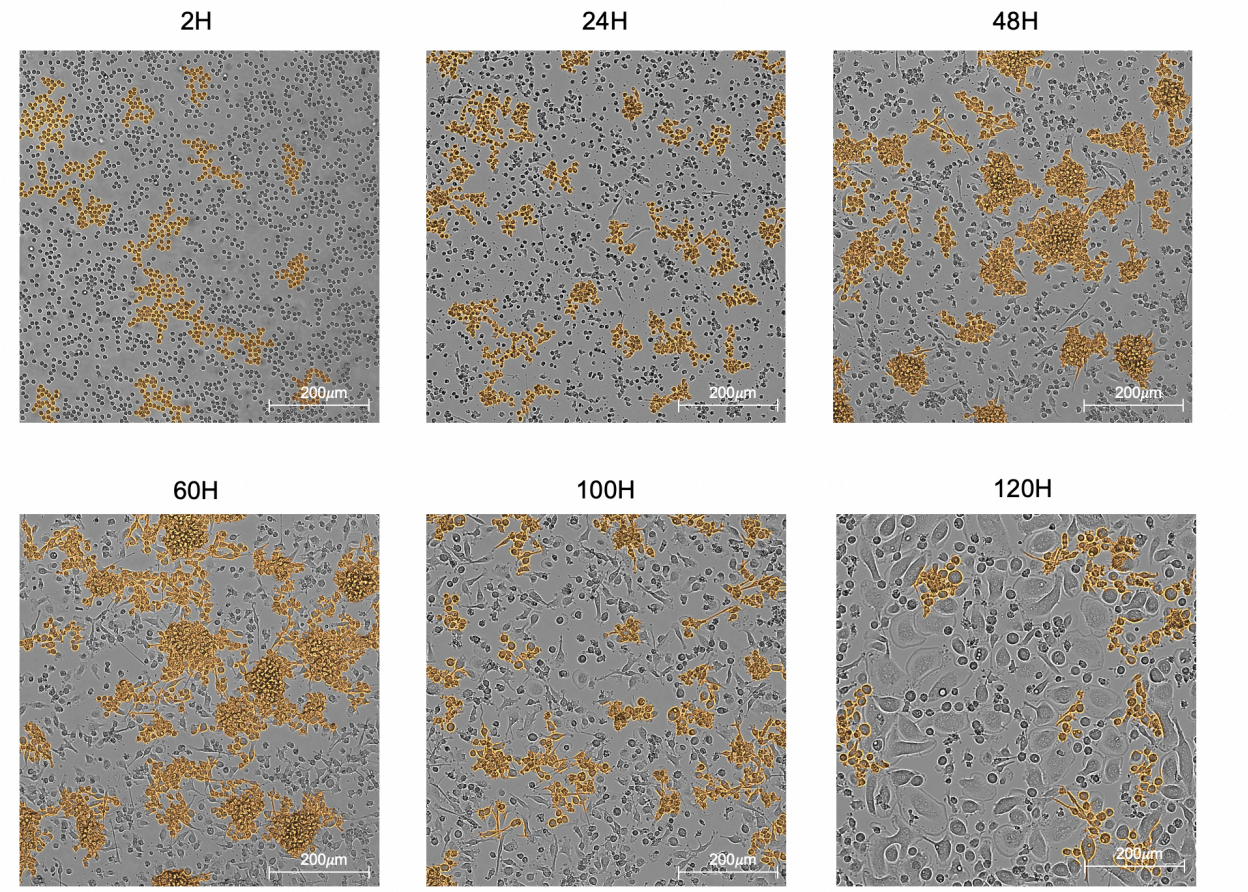

Figure 4.14 Label-free monitoring of osteoclast differentiation using an xCELLigence RTCA eSight analyser.

Images tracking the progression of cell spreading and aggregation showing the formation of clusters over time. Images from 2, 24, 48-, 60-, 100-, and 120-hour time-points highlight the initiation of cluster formation at early time points; displaying with a higher intensity and larger surface area of masking (displayed in orange) after 48 and 60 hours of seeding. Clustering of monocytes (which is a characteristic of differentiation) becomes more robust. At later time points, monocyte clusters contain less of the orange masking, but display an increase in CI and cytoplasm elongation and appear to be progressing into mature osteoclasts. Finally, after 120 hours of seeding, the masking of aggregates slowly disappears with the emergence of multinucleated cells.

To gain more insight into the proliferation of osteoclasts, the clustering confluence percentage function was used for the first time here in the presence of IMiDs. This function allowed the examination of the effects of 10 μM of IMiDs on the attachment of monocytes before they merge to become multi-nucleated giant cells, which gives insight into cell-cell interactions.

DMSO-treated monocytes had more clusters form (displayed as object count), in comparison to IMiD-treated cells, as a decrease in the object number was seen with each IMiD (Figure 4.15 A). When combining the graph from the CI signal with the clustering objects counts (Figure 4.15 B), it highlights IMiDs impedance readouts in comparison to IMiDs cluster objects count readouts. Measurements of cellular clusters formed using Cluster Differentiation Function on the RTCA eSight Software (Figure 4.15 A) revealed that IMiD treatment reduced the number of pre-osteoclastic clusters. This reduction in cluster formation becomes evident after the first media change recorded at 55 hours. Juxtaposing the two different readouts within the same plot (Figure 4.15 B) highlights the increased clustered objects in the DMSO (VC) treated cells compared to the IMiDs. In contrast, the opposite was observed with the impedance readouts.

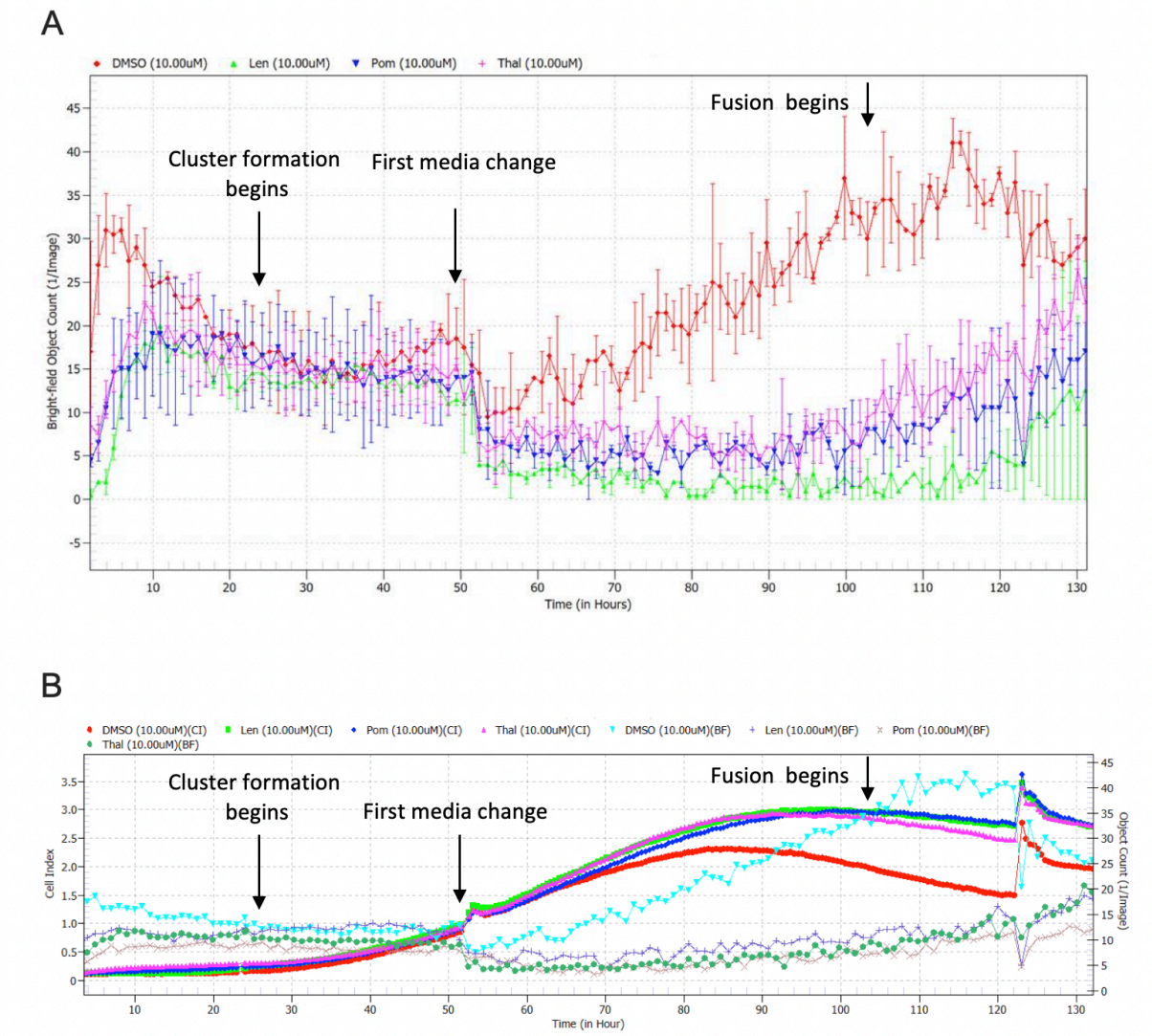

Figure 4.15 An example of pre-osteoclastic cluster formation in the presence of IMiDs. *A time point of 60-hour post-seeding showing the effects of IMiDs on the formation of osteoclastic clusters (A). A graph combining the CI signal and the object count (number of clusters) observed at the early stages of differentiation. CI signal and object counts shown in this graph were obtained from 1 donor in triplicates on the E-plate.*

While showing the effects on one donor gives an insight into the impact of IMiDs, it was important to determine whether the data obtained were reproducible. The experiment was repeated three times, and similar results were observed when combining the object count and the CI signal at a 60-hour time-point post-seeding. Figure 4.16 A illustrates the raw data obtained from measuring the CI and the object count from a single experiment. Figure 4.16 B demonstrates the CI signal and the object count of three repeated experiments. Lenalidomide slightly reduced the object count; this was not statistically significant. Pomalidomide and thalidomide significantly reduced the object count, which correlates to the clusters forming in pre-osteoclasts (p = 0.0129 and p = 0.0165, respectively).

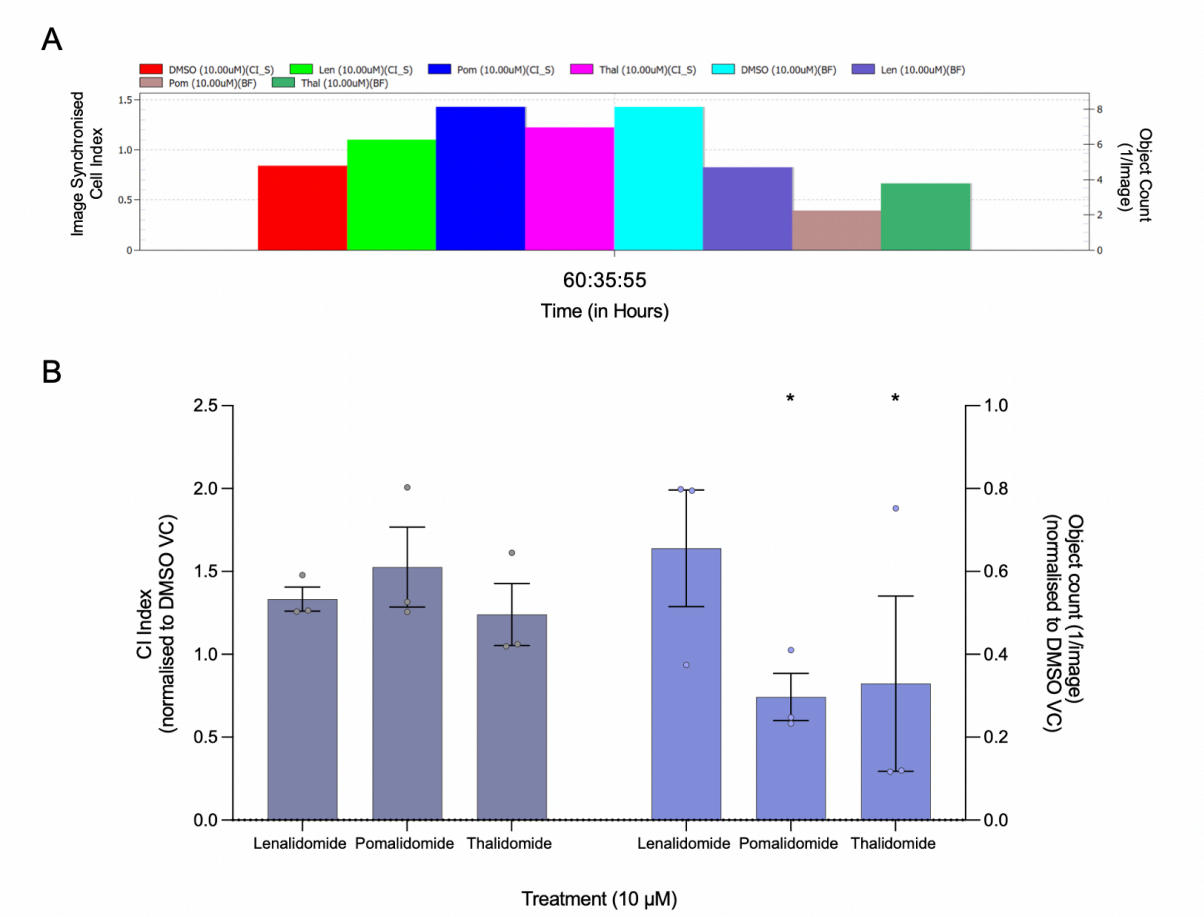

Figure 4.16 IMiDs reduce the formation of pre-osteoclast clusters.

*Measurements of cellular clusters formed by osteoclasts using Confluency Masking Function on the RTCA eSight (A) revealed that IMiD treatment reduced the number of pre-osteoclastic clusters. The CI signal of osteoclasts and the object count normalised to the DMSO (VC) at ~ 60 hours of repeated experiments (B). Data of three independent experiments expressed as the mean ± SEM; * $p \leq 0.05$.*
CI_S = Cell Index (Image Synchronised); BF = Bright Field (Object count).

4.3.8 Gelatine pre-coating influenced osteoclast proteolytic activity in the presence of IMiDs

To test the effect of the gelatine coating on the impedance in the presence of IMiDs, two concentrations of IMiDs were administered to the cells from the day of seeding (1 µM and 10 µM). Increasing the dosage of IMiDs has increased the CI signal when comparing the 1 µM (Figure 4.17 E) to the 10 µM (Figure 4.17 F). For both doses, pomalidomide showed the most increase in the CI signal, followed by lenalidomide and then thalidomide showing the least increase in CI.

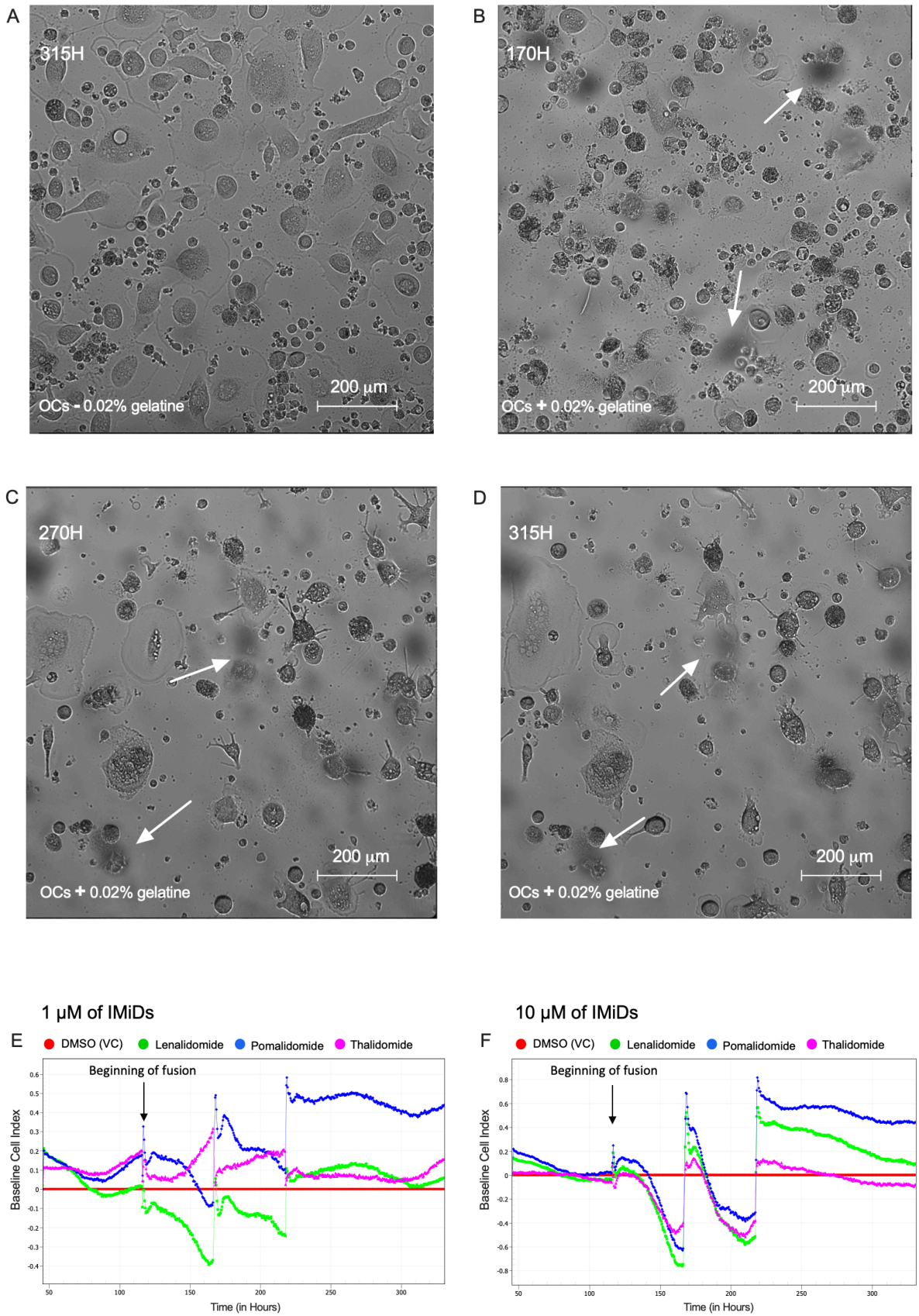

Figure 4.17 The analysis of the impedance of osteoclasts on gelatine upon treatment with IMiDs

Monocytes were seeded on an E-plate coated with 0.02 % gelatine. M-CSF and RANKL were used to differentiate monocytes into osteoclasts. Images were captured in the absence (A) and presence of gelatine (B-D) at different time-point of, showing the areas of digestion. A dosage of 1 and 10 μM (lenalidomide, pomalidomide and thalidomide) or DMSO (VC) was added to the media either on the day of seeding and when the media was changed every 2 – 3 days to monocytes seeded on an E-plate coated with 0.02 %. The impedance of osteoclasts in the presence of IMiDs shows the CI signal at 1 μM (E); the CI signal at 10 μM (F). The results are representative of n=3.

OCs= osteoclasts; H= hour; white arrows pointing towards the areas of digested gelatine.

4.3.9 The expression of integrins by monocyte-derived osteoclasts in the presence of IMiDs

The XCELLigence RTCA impedance is a direct measurement of the attachment and, therefore, the adhesion of cells to the plate. The expression of adhesion proteins such as integrins was examined using immunoblotting to further investigate the increase of impedance in osteoclasts upon IMiD treatment. The higher the impedance measured by the RTCA, the stronger the cells' adherence to the plate. Osteoclasts bind to the bone matrix by binding its surface integrins to a bone protein known as vitronectin[430,431]. To examine the role of integrins in changes to the osteoclastic impedance signal *in vitro,* the expression of $\alpha V\beta 3$ integrin was examined, since osteoclasts highly express this integrin complex, which binds to a variety of extracellular matrix proteins[432]. The cell lysates were harvested at the end of the differentiation period. At this time point, the expression of $\alpha V\beta 3$ has increased when treated with 10 μM of pomalidomide and lenalidomide in comparison to the DMSO vehicle control. However, the expression remains unchanged when treated with thalidomide. Densitometry results revealed the enhanced expression of $\alpha V\beta 3$ integrin, but this was not significant. Following the initial investigation of adhesion molecules, the expression of other integrin subunits was also tested using immunoblotting. This included $\alpha 5$, $\beta 1$, $\beta 5$, and $\alpha 4$[433,434]. These integrins were chosen as osteoclasts also express them; they induce the direct interaction of osteoclasts with different proteins. No significant changes were observed with these other integrin subunits. IMiDs have modified the expression of $\alpha V\beta 3$ integrin subunit. However, this was not significant. IMiDs did not modify the expression of the other integrin subunits studied (Figure 4.18).

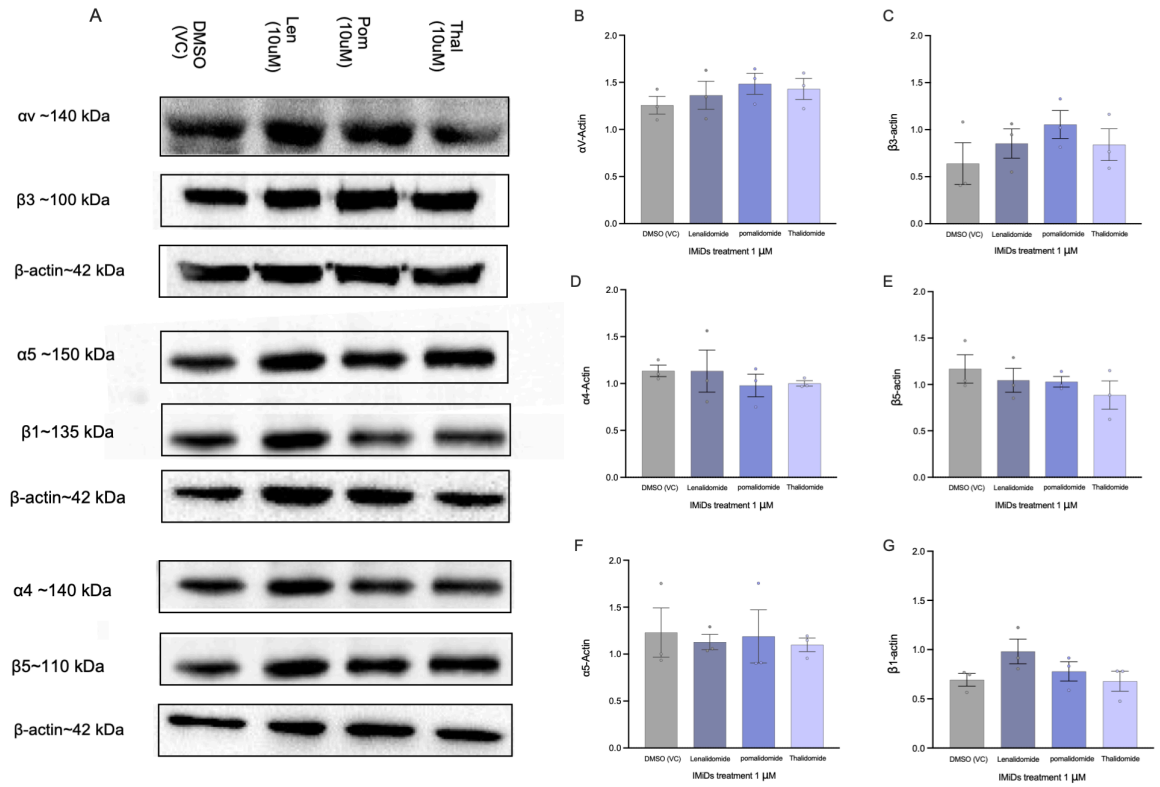

Figure 4.18 The effects of IMiDs on integrin expression of monocyte-derived osteoclasts.

M-CSF and RANKL were utilised to in vitro monocyte-derived osteoclasts. IMiDs (lenalidomide, pomalidomide and thalidomide) were added to the media on the day of seeding. Cell lysates were harvested on day 10, and total protein was estimated using a DC assay. Protein immunoblots representative of n=3 donors; β-actin was used to demonstrate equal protein loading (Figure 4. 10 A) and densitometry showing αV (B), β3 (C), α4 (D), β5 (E), α5 (F), β1 (G). Densitometry data normalised to β-actin. Statistics were performed with a one-way ANOVA and Dunnett's multiple comparisons test; means ± SEM.

4.4 Discussion

In the past several years, there has been a dramatic improvement in the treatment of patients with multiple myeloma (MM). A better understanding of the biology of the disease and its associated complications will further improve the quality of life and, potentially, the overall survival rate. Thalidomide was the first immunomodulatory imide drug (IMiD) to show activity in MM[435]. Favourable clinical results promoted the development of the thalidomide analogues lenalidomide and pomalidomide, collectively known as IMiDs. These analogues were designed to have better efficacy than thalidomide and reduce toxicity[436].

IMiDs exert their anti-cancer properties through several mechanisms, including immunomodulation, inhibition of angiogenesis, anti-inflammatory effects, direct anti-proliferative effects, reducing cytokine production and altering interactions with the bone marrow and tumour microenvironment[437]. Therefore, IMiDs can act directly on myeloma cells and indirectly by altering the interactions between myeloma cells and non-myeloma cells within the bone marrow microenvironment (BMM), including bone marrow stromal cells, immune cells and osteoclasts[436,438–440]. These treatments are often combined with other anti-myeloma therapies, such as steroids and proteasome inhibitors[441]. Interactions between myeloma cells and osteoclasts enhance osteoclastogenesis; osteoclasts, in turn, enhance myeloma cell growth and drug resistance[440]. Osteolytic bone disease in MM is caused by enhanced osteoclast activity accompanied by inhibition of osteoblast function[442]. Osteolytic bone lesions in myeloma patients arise with dysregulation of the normal bone remodelling process, with decreased osteoblast function and increased activity of osteoclast[443]. Adhesion of myeloma cells to the bone marrow stromal cells promotes the secretion of several osteolytic cytokines, such as IL-6, TNFα, IL-1β and RANKL[444,445].

From quantifying the confocal images, lenalidomide and pomalidomide significantly decrease osteoclast formation and multinucleation compared to the DMSO control. Their effects are evident by day 7 and persist through day 10, indicating their potent role in reducing osteoclast differentiation. Thalidomide shows a delayed and less pronounced effect on osteoclast differentiation, with more osteoclasts and more multinucleation compared to lenalidomide and pomalidomide. Overall, the data indicate that lenalidomide and pomalidomide are more effective than thalidomide in reducing osteoclast differentiation and maturation, as evidenced by the decreased number of osteoclasts and lower multinucleation rates.

MMP-9 and MMP-2 have been shown to be produced by myeloma cells, and the accumulation of MMPs in the BMM has significant roles in the pathogenesis of the disease[446]. Osteolytic bone degradation is caused by overly active osteoclasts and extracellular matrix remodelling

by bone marrow stromal cells, which in turn promotes the growth and invasion of myeloma cells[447]. Focal degradation of the extracellular matrix, mediated by MMPs, is the first step in the invasion of cancer cells[448,449]. It has been reported that IMiDs reduce the production of MMPs, therefore, preventing the degradation of the extracellular matrix[450]. Thalidomide was thought to be effective in reducing the expression of MMP-2 and MMP-9, as it was found to reduce melanoma tumour growth and blood supply in C57 mice[451], which is thought to enhance anti-tumour activities of thalidomide for the treatment of melanoma[452]. MMPs can degrade the extracellular matrix, which facilitates angiogenesis and tumorigenesis. The overexpression of MMPs has been correlated with the progression of several cancers, including breast cancer, ovarian cancer, and colorectal cancer[453].

As previously discussed in chapter 3, MMPs (MMP-9 and MMP-2) expression by osteoclasts was found to be correlated with osteoclast differentiation. The MMP-9 released by osteoclasts was found to be activated when subjected to *in gel* zymography. The activated MMP-9 was also found to be positively correlated with the stage of differentiation. This study demonstrates for the first time the direct comparison of the effects of IMiDs on osteoclast differentiation and activation in the same *in vitro* model. All three IMiDs tested (pomalidomide, lenalidomide and thalidomide) are used in the treatment of MM at different stages of the disease: thalidomide is now less commonly prescribed, lenalidomide is widely used in the treatment of newly diagnosed and relapsed/refractory MM, while pomalidomide is currently used in the relapsed/refractory disease state[454]. The effects of IMiDs on osteoclastogenesis have been of interest to many studies. The anti-osteoclastogenesis activity of lenalidomide specifically has been well documented. Lenalidomide was found to decrease TRAP-positive and multinucleated cells in a dose-dependent manner (0-10 μM range)[455]. Lenalidomide has also been found to reduce bone-remodelling markers, such as RANKL and OPG, in the serum of myeloma patients[456]. In another study, the combination of thalidomide with dexamethasone improved abnormal bone remodelling through the reduction of the RANKL/OPG ratio in refractory/relapsed myeloma patients[457]. However, a direct comparison of the effect of all IMiDs on osteoclastogenesis in the same osteoclast model is yet to be studied. Here, the addition of IMiDs on the day of seeding reduced osteoclastogenesis and MMP expression, but this was IMiD type-dependent. The use of eSight and RTCA also provided unique insights into osteoclastogenesis defects induced by IMiDs.

MMP-9 secretion was found to be significantly reduced in the presence of pomalidomide, and lenalidomide and pomalidomide were both found to decrease MMP-2 expression if IMiDs were added on the day of seeding and initiation of differentiation. When IMiDs were also added at different time points after differentiation had been initiated, they had minimal effect on MMP

production. The activity of MMP-9 seemed unaffected by the IMiDs when added three days post-seeding and for 24 hours after seven days of seeding. Therefore, IMiDs seem more effective when added to monocytes on the day of seeding to effectively reduce MMP-9 expression and activity. Stimulation with LPS did not alter MMP production in day 7 differentiated osteoclasts and IMiDs did not have any effect on this. A similar lack of effect was seen for IL-6 and TNFα production by osteoclasts. This was interesting to observe as IMiDs have been found to reduce TNFα and IL-6 production in monocytes after being triggered by LPS and other agonists in culture[458] (also see Chapter six). Since osteoclasts are derived from the monocytic lineage, it was hypothesised that the levels of such cytokines would be reduced upon IMiD treatment, but this was not the case. However, monocytes undergo many morphological and molecular changes through monocyte-to-osteoclast transition[459,460], which could explain the lack of efficacy of the IMiDs here. Similar effects were observed with MMP-9 secreted by osteoclasts. For this analysis, gelatine, a protein derived from hydrolysed collagen[461,462] was used as the substrate. Collagen is one of the most prominent components of the extracellular matrix and presents a substrate for osteoclast digestive activity[463,464,465], so this analysis provides insight into the effects of IMiDs on the maturation of osteoclast on gelatin.

Other ways of measuring the areas of the number of resorption pits produced by osteoclasts in response to stimuli with bone resorbing agents have also been considered[466]. Previous reports have demonstrated that pomalidomide is the most potent IMiD: 100 times the strength of thalidomide and 10 times that of lenalidomide[467,468]. All the data mentioned above support the notion that pomalidomide is the most efficient drug among IMiDs. It is important to note that pomalidomide is generally used in patients with advanced MM after pre-treatment with several drugs, including lenalidomide[469,470].

The real-time monitoring of osteoclastogenesis method established in chapter 3 was successfully used here to provide greater insight into the effects of IMiDs on osteoclastogenesis. From the results obtained in chapter three, we found that increased seeding density increases the impedance of osteoclasts in vitro; these results were highly reproducible and correlated with classic endpoint assays. IMiDs were predicted to decrease the impedance of osteoclasts as end-point assays illustrated in this study supported the hypothesis of IMiDs reducing osteoclastogenesis with the third generation IMiD, pomalidomide, being the most potent IMiD for down-regulation of osteoclast differentiation and activation. This included confocal microscopy and real-time imaging showing pomalidomide to marginally prevent the elongation of osteoclasts at the earlier stages of differentiation and multi-nucleation at the later stages of the differentiation. However, IMiDs were found to actually increase the impedance of osteoclasts, with pomalidomide the most potent IMiD in increasing

the impedance in a dose-dependent manner. This might suggest that IMiDs may have an impact on cell adhesion and migration. As previously discussed, the formation of clusters of pre-osteoclasts prior to fusion is a characteristic of osteoclastogenesis[471,472]. It is also something observed in chapter three throughout the characterisation of osteoclast morphology. Therefore, the effects of all IMiDs on the formation of clusters were studied alongside the impedance of osteoclasts in vitro. Pomalidomide was the only IMiD to significantly reduce the number of pre-osteoclastic clusters at 1 μM concentration. Interestingly, pomalidomide and thalidomide were found to have a significant increase in osteoclast impedance at 10 μM; this could be due to the IMiDs increasing the adhesion of osteoclasts to the E-plate by increasing the expression of certain proteins that enhance their adhesion, therefore, enhancing the CI signal. As previously discussed, it is already recognised that IMiDs exert a direct inhibitory effect on osteoclastogenesis, and the data generated using RTCA here adds new insights to this. Multinucleated osteoclasts are formed by cell-cell of pre-osteoclasts. Osteoclast fusion is considered to include four main steps: attraction/migration, recognition, cell-cell adhesion, and, finally, membrane fusion[473]. The initial contact of pre-osteoclasts with each other and other cells present in the bone marrow microenvironment is thought to be essential for osteoclast differentiation[474–476]; this process is mediated by the dendritic cell-specific transmembrane protein (DC-STAMP)[477–479]. It is this process that IMiDs seem to prohibit.

One of the key factors of thalidomide inhibitory activity in osteoclastogenesis is decreasing αVβ3 integrin complex[480–483]. This inhibition is thought to be mediated by a reduction in Cathepsin K, a protease involved in the degradation of the bony matrix and αVβ3 integrin[484]. The vitronectin receptor αVβ3 is predominantly expressed in osteoclasts and was found to be necessary for the contact of osteoclasts with the extracellular matrix[485]. Additionally, inhibition of αVβ3 integrins inhibits bone resorption in animal models[486]. Therefore, it was important to test the effects of IMiDs on integrins expressed by osteoclasts in the *in vitro* model being used herein. Pomalidomide was found to slightly increase αVβ3, although this was not significant. It also contrasts with previous reports of a decrease in αVβ3 upon IMiD treatments[487,788]. The lack of effects of IMiDs could be due to osteoclasts being derived from monocytes and not primary osteoclasts isolated from, for example, mouse bone marrow. Another reason could be that this experiment is conducted *in vitro,* and the absence of the extracellular matrix could alter the effects of IMiDs on integrin complexes.

The role of the vitronectin receptor αVβ3 in biology has been studied extensively, and it has become clear that mammalian osteoclasts utilise this receptor to adhere to a wide range of

extracellular matrix proteins that are mainly expressed in bone and the bone marrow[486,489,490]. Another receptor of interest to study here is the $\alpha 5\beta 1$, which is widely expressed by avian osteoclasts and is used as a fibronectin-binding receptor[490]. The functional aspects of $\alpha V\beta 1$ in osteoclasts have not been studied yet. This receptor is far less abundant than $\alpha V\beta 3$ in osteoclasts and is likely to be a receptor for collagen or possibly fibronectin in osteoclasts491 . A slight increase was observed with $\alpha V\beta 3$ upon treatment with the IMiDs, which supports the hypothesis that IMiDs predominantly affect $\alpha V\beta 3$ in osteoclasts. However, the effect was opposite to that observed in previous studies[480–482].

This study confirms the significant inhibitory effects of pomalidomide and lenalidomide on osteoclastogenic differentiation of monocytes *in vitro* at drug concentrations that have been shown to be clinically relevant[492–494]. This effect is also observed when testing the activity of MMP-9, as lenalidomide and pomalidomide reduced the activity of MMP-9 to digest the zymogen gel when the supernatants were subjected to *in gel* zymography. This pattern of activity of the IMiDs has been reported previously, with pomalidomide the most effective IMiD in previous *in vitro* and *in vivo* studies[495,496]. The relative absence of an effect of thalidomide could suggest that concentrations were not sufficient to exert an effect on MMPs in vitro. Future studies could include higher concentrations of thalidomide to test the efficacy at higher concentrations within the same osteoclast model. This has been observed in previous studies where 100-200 mg/day of thalidomide was required to have an effect on patients, whereas 25 mg/day of lenalidomide was required to see the same effects, and only 2-5 mg/day of pomalidomide was generally effective and well tolerated in patients[497–499]. However, it is important to notice that the dosage of IMiDs used in clinical settings can be lowered when used in combination with other treatments, such as dexamethasone[497,500–502]. Although the chemical structures of IMiDs are quite similar, they differ with respect to several pharmacological properties, including metabolism, half-time, absorption and clearanceClick or tap here to enter text.. Furthermore, pomalidomide has more neo-substrates targeted for degradation in comparison to lenalidomide and thalidomide[502], which could explain the higher potency observed with pomalidomide in reducing osteoclast differentiation and activation. Neo-substrates refer to the potential cellular proteins of CRBN targeted by the IMiDs[503].

4.5 Conclusion

IMiDs have become an essential part of MM therapy and have contributed vastly to the understanding of the pathophysiology of the disease. They have the ability to pair with other key therapies in a synergistic rather than additive way, which makes them ideal for combined regimes with manageable toxicities. There is clearly further work to be done in order to fully

understand the mechanisms by which IMiDs act in myeloma bone disease, to better guide treatment decisions, to understand resistance patterns, and to allow for further drug development targeting these pathways. The results obtained here give an insight into the possible mechanisms of action by which IMiDs affect the cells present in the tumour microenvironment, such as osteoclasts. The osteoclast model established here alongside the endpoint and the real-time assays illustrated here provides a powerful approach to testing potential treatments for myeloma bone disease. Using these techniques, pomalidomide has shown impressive results in reducing osteoclast differentiation and activity. The xCELLigence RTCA also allows the testing of the combination of different therapies with IMiDs for the treatment of myeloma bone disease and provides a powerful platform for testing the efficacy of potential new therapies for myeloma bone disease treatment. These data provide a basis for considering pomalidomide for use in the treatment of bone disease in MM and potentially other bone-related diseases.

Chapter Five

Measuring the Effects of Anti-inflammatory Cytokines on the Differentiation and Activation of Osteoclasts

5.1 Introduction

5.1.1 The biological effects of anti-inflammatory cytokines in osteoclasts

Interleukin (IL)-4 and IL-13 belong to the T helper 2 family of cytokines[504,505]. This group also includes other cytokines, such as IL-5, and IL-9[506–508]. They are considered pleiotropic cytokines produced by immune cells, with lymphocytes being one of the major sources of cytokines production; they play an essential role in inflammatory and immune responses[509]. IL-4 and IL-13 share 25% similarity at the amino acid level and have overlapping biological activities such as regulating antibody production and inflammation[510]. IL-4 and IL-13 share a joint receptor complex, and similar signals are activated within the cell by these cytokines[511,512] (Figure 5.1). Both cytokines can upregulate the expression of two IL-8 receptors, CXCR1 and CXCR2, in human monocytes[513;] IL-8 can increase the expression of RANKL expression in osteoblasts, which alters RANKL/OPG ratio to favour osteoclast formation. IL-4 suppresses RANKL-induced osteoclast differentiation through direct action on pre-osteoclastic cells[514]. In addition, IL-4 and IL-13 both increase the expression of osteoprotegerin (OPG)[515], a decoy receptor for RANKL produced by osteoblasts. OPG interrupts the interaction between RANKL and its receptor, RANK, whilst simultaneously decreasing RANK and RANKL expression in osteoclasts[515]. Both cytokines reduce OPG levels in an osteoclast coculture of mouse bone marrow-derived macrophages with UAMS-32 (an osteoblastic cell line) in the presence of 1α, 25-dihydroxy vitamin D_3 ($(OH)_2D_3$) an inducer of RANKL expression at a concentration of 10 ng/mL[511]. Both are involved in the downregulation of pro-inflammatory cytokines such as IL-1, IL-6, and TNFα[505] while inducing the upregulation of IL-1 receptor antagonist (IL-1Ra) and IL-1 receptor type II (IL-1RII) that are involved in the suppression of inflammation[516–518]. This underpins their well-documented anti-inflammatory properties in the pathogenesis of psoriasis, type I diabetes and multiple sclerosis[505].

IL-4 receptor-α (IL-4Rα) is shared by IL-4 and IL-13 for intracellular signalling. IL-4 but not IL-13 binds to a heterodimeric type I receptor comprised of IL-4Rα and the common γ chain (γc), whereas both cytokines can bind to a heterodimeric type II receptor comprised of IL-4Rα and IL-13 receptor-α1 (IL-13Rα1)[519, 520]. These receptors are expressed in human monocytes, B cells, basophils, eosinophils, mast cells, and endothelial cells[519, 521]. The interaction with IL-4 or IL-13 with these receptors causes the activation of Janus Kinase-1 (JAK1), JAK2 and/or JAK 3 and tyrosine kinase-2 (TYK2), leading to the phosphorylation of signal transducer and activator of transcription-6 (STAT6), that translocates to the nucleus. IL-13 can also bind to another receptor, IL-13Rα2, which is considered a decoy receptor[520] (Figure 5. 1). The activation of IL-4 and IL-13 signalling pathways inhibits cytokine production – such as TNFα, INFγ, IL-6 and IL-1 – upon lipopolysaccharide (LPS)- stimulation[505]. IL-13 inhibits TNFα production by MNCs from the peripheral blood of patients diagnosed with chronic inflammatory

arthritis[505]. IL-13 also has an inhibitory effect on IL-1 and TNFα in MNCs derived from rheumatoid arthritis (RA) patients[505].

The receptor subunits of IL-4/IL-13 are expressed at low levels under homeostatic settings; their expression is influenced by various factors, such as hormones, cellular stress, infection and inflammation[522, 523]. In solid tumours such as breast cancer and renal cell carcinoma, the attenuation of IL-4Rα expression is associated with reduced tumour survival[524–527]. This agrees with findings that phospho-STAT-6, a downstream of IL-4/IL-13 receptor recruitment, regulates pro-metastatic behaviours such as migration and tissue invasion as shown in human breast cancer cells and mouse models[527,528]. IL-4 has been shown to induce with high efficacy the phosphorylation of signalling adaptor molecule insulin receptor substrate-2 (IRS-2) in human monocytic cell lines and primary murine macrophages[529]. This was dependent on the expression of the γC receptor subunit. Interestingly IL-13 can also stimulate the phosphorylation of IRAS2; however, this was less significant than that induced by IL-4[529]. Therefore, even though they share a similar receptor complex, they can have different effects on cells, mainly monocytes and macrophages. These differences account for the subtle difference in cellular responses they exert during inflammation.

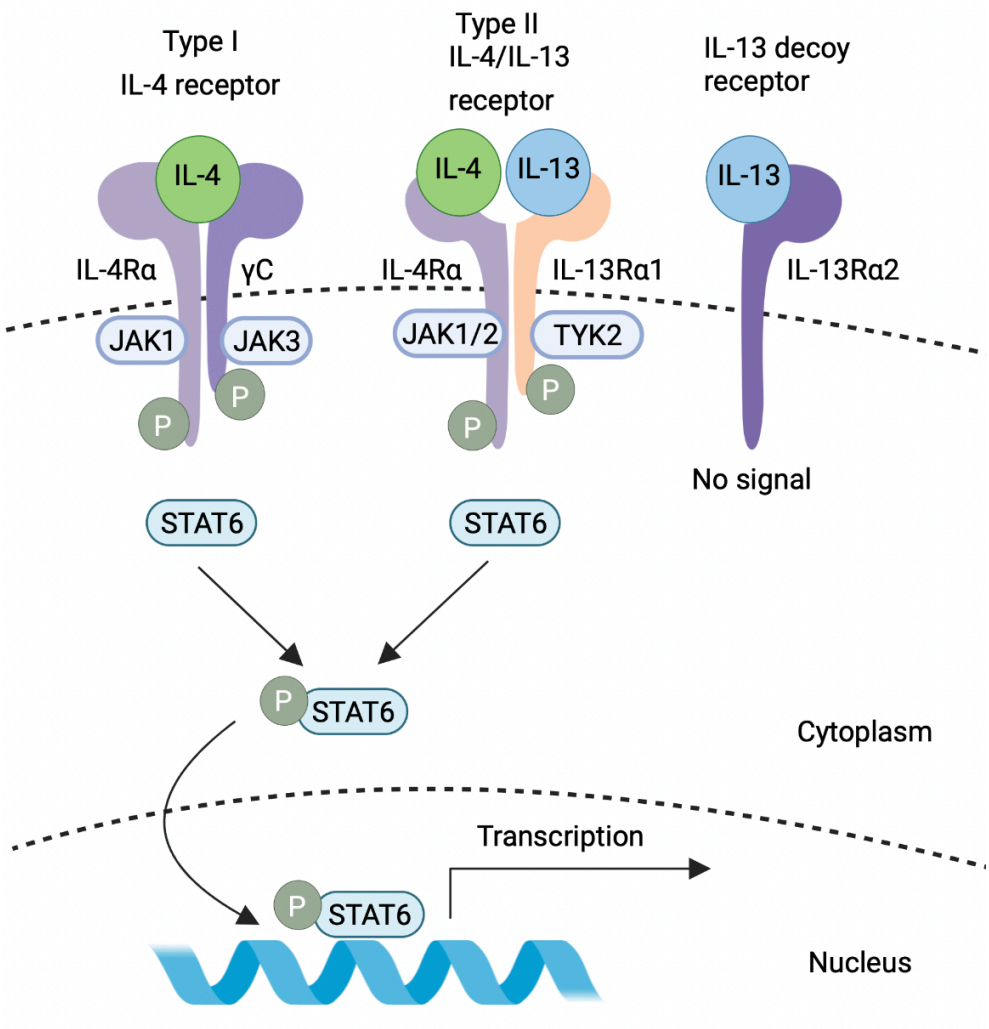

Figure 5.1 Receptor signalling for IL-4 and IL-13.

In haematopoietic cells, the binding of IL4 signals to two possible receptor complexes composed of a heterodimer of IL-4Rα (140 kDa) and γC chain (60 kDa) (type I receptor) or the IL-4Rα and IL-13Rα1 (65-70 kDa) chain (type II receptor). IL-4 binds to IL-4Rα with high affinity, initiating the heterodimerisation with the secondary signalling chain, leading to the activation of the JAK kinases and then the phosphorylation of STAT6. Similarly, in non-haematopoietic cells, such as epithelial cells, STAT6 is phosphorylated by the induction of the heterodimerisation of type IL-4Rα and IL-13Rα1 after the binding of IL-4 or IL-13 to their respective receptors. IL-13 also binds with high affinity to IL-13Rα2; however, this receptor lacks a signalling motif and acts as a decoy receptor. IL-13 binds IL-13Rα1, which complexes with the IL-4Rα, forming the type II receptor. Signalling through type II receptors predominantly activates STAT6. Figure made using BioRender.

IL-10 is a pleiotropic cytokine that is essential in immunoregulation and inflammation[530]. It is produced by B cells, mast cells, eosinophils, monocytic cells, and dendritic cells amongst others[531]. IL-10 is also produced by T helper 2 cells and downregulates the expression of cytokines, such as IL-1, IL-6 and TNFα, in T helper 1 cells [532]. Thus, like IL-4 and IL-13, IL-10 is considered an anti-inflammatory cytokine[533,534]. IL-10 has been described to inhibit osteoclast formation and bone resorption in osteoclast precursors through the inhibition of pro-inflammatory cytokines[535,536]. However, IL-10 is elevated in certain spinal cord injury cases alongside other circulating cytokines that have been detected that induce bone loss in spinal cord injury, including TNFα, IL-6, RANKL, and IL-17. The presence of such cytokines leads to both bone formation and bone loss. Due to these factors, it is still unclear which role IL-10 plays in spinal cord injury and bone loss[537]. Moreover, osteocytes in spinal cord injury were found to be positive for IL-10. Immunohistochemical staining of the distal femur revealed that cancellous osteocytes positive for TNFα, IL-6, IL-1, and IL-10 were elevated in the animal model[538].

IL-10 is recognised by a specific receptor[539]. The IL-10R1 subunit of the receptor is expressed at low levels by most hematopoietic cells and is part of the class II cytokine receptor family; receptor expression can be elevated due to stimuli[540,541]. All interferons (IFN) also signal through class II cytokine receptors[542] and are expressed predominately in immune cells. IL-10 receptor is comprised of two subunits, a ligand-binding subunit, IL-10R1, and an accessory subunit required for signal transduction, IL-10R2 (Figure 5.2). This means that IL-10R1 is essential for the binding of IL-10, whereas IL-10R2 is not critical but is important in activating the signalling pathway[543,544]. The receptor complex interacts with members of the JAK family, JAK1 and TYK2. The binding of IL-10 triggers TYK2 phosphorylation, leading to the activation of the transcription factor STAT3[545,546]. The activation of STAT3 promotes the expression of several genes responsible for the activity of IL-10 on the target cells[547,548]. IL-10 also inhibits the translocation of the transcriptional factor NF-kB and therefore inhibits the synthesis of pro-inflammatory cytokines[549]. Since IL-10 is a pleiotropic cytokine, it exerts anti-inflammatory and immunostimulatory functions[550]. In cancer, IL-10 may exert pro or anti-inflammatory effects[551]. IL-10 is considered a potent anti-inflammatory factor in bacterial endotoxemia, which is induced by LPS. LPS binds to Toll-like receptor 4 (TLR4), a pattern recognition receptor PRR) expressed on many myeloid and other cells[552]. PRRs have a central role in alerting the innate immune system of foreign molecules such as bacterial cell wall components or DNA and damaged cells within the body[553]. The stimulation of PRRs leads to an inflammatory reaction driven by the innate immune system. LPS also induces the release of inflammatory cytokines IL-12/IL-23, which stimulate inflammatory T-cells[554.] the activation of STAT3 induces transcriptional repressor nuclear factor, IL-3 regulated (NFIL3), which inhibits the transcription

of the shared p40 subunit of IL-12 and IL23, thereby inhibiting production of these critical inflammatory cytokines [555,556]. This activation also induces the suppressor of cytokine signalling 3 (SOCS3), which binds and inhibits the signalling of IL-6 and IL-12/IL23 receptors. IL-10 thereby intercepts the inflammatory responses to LPS and PRR signalling[557,558].

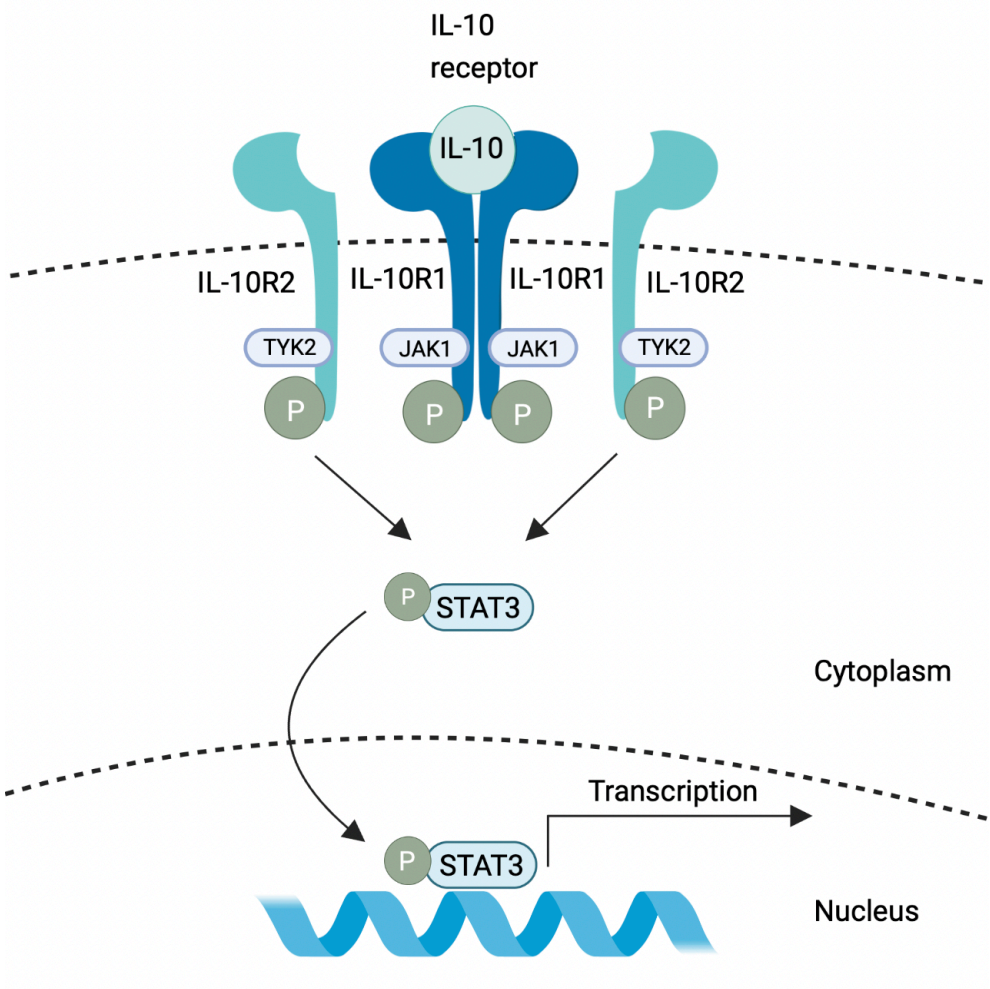

Figure 5.2 IL-10-induced signalling pathways.

IL-10 signals through a receptor consisting of two IL-10 receptor-1 (IL10R1) and two IL-10 receptor-2 (IL-10R2) chains. IL-10R1 is expressed on hematopoietic cells such as T cells, B cells and NK cells, whilst the IL-10R2 is expressed ubiquitously. The binding of the receptor chains forms a heterotetramer, permitting the assembly of the signalling complex. The associated kinases, JAK1 and TYK2, activate and phosphorylate the IL-10R1 chain. STAT3 becomes activated by phosphorylation. Active STAT3 molecules dimerise and undergo nuclear translocation, where binding to STAT3-binding elements of IL-10-responsive genes occurs to drive the expression of various anti-inflammatory mediators. Figure made using BioRender.

5.1.2 Rationale

IL-4, IL-10, and IL-13 display anti-inflammatory properties in osteoclasts[559,560]. The previously established *in vitro* model in Chapter three provides a useful tool for studying the effects of anti-inflammatory cytokines on the development and activation of osteoclasts. This would provide insights into their potential use for treating myeloma-related bone disease in myeloma patients. The techniques also could be used to test the efficacy and side effects of combining current anti-myeloma treatments with IL-4, IL-10, and IL-13. Determining the optimal capacity of current myeloma treatments and IL-4, IL-10, and IL-13 requires readily available *in vitro models*. The osteoclast model established in chapter 3 has shown great potential in solving this problem. Therefore, the primary purpose of this chapter is (i) to use the osteoclast in vitro model to study the effects of IL-4, IL-10, and IL-13 on the progression and activation of osteoclasts using various end-point methods; (ii) to demonstrate the usage of real-time live cell imaging and impedance for studying osteoclast differentiation and function in the presence of IL-4, IL-10, and IL-13 at different time points. The new technique will (iii) help to understand and control bone disease progression and identify new treatment targets in MM. This study (iv) can provide comprehensive results that will compare tests from endpoint results and real-time analysis that could potentially reveal novel targets for treating myeloma-related bone disease.

5.1.3 Hypothesis

xCELLigence real-time cell analysis (RTCA) is a valuable tool for studying the effects of IL-4, IL-10, and IL-13 on osteoclast differentiation and activation.

5.2 Experimental procedures

5.2.1 Samples

As per section 3.2.1, human peripheral blood was collected from healthy, non-fasted individuals aged over 18 years old into heparinised Vacuettes™ (Greiner Bio-one, Frickenhausen, Germany). All samples were collected with informed written consent as detailed in *Chapter 2.4 Sample collection and preparation.*

5.2.2 Monocyte isolation

Monocytes were isolated by positive selection on magnetic microbeads as described in Chapter *2.4.1 Blood* separation and *2.4.2 Mononuclear cell isolation*. Briefly, the pellet containing the monocytes was resuspended in differentiation or complete cell culture media (see per section 3.2.3). Cell density was determined using the Countess® automated cell counter (Life Technologies). To check monocyte purity, an anti-CD14 antibody (Clone 61D3; fluorophore eFluor®450; isotype mIgG1) was added to 100,000 monocytes. The cells were incubated with the antibody for 30 minutes. The cells were washed twice with FACS buffer (0.2% (w/v) bovine serum albumin (BSA), 0.05% (w/v) sodium azide (Sigma-Aldrich) in PBS) and centrifuged at 515 *x g* at 4 ºC for 7 minutes; the pellet was resuspended in the FACS buffer and checked for purity and acquired using the NovoCyte Flow Cytometer (BD Biosciences). Data analysis post-acquisition was using FlowJo Version 1.3 (Tree Star, Oregon, USA). Purity $\geq$ 92% was accepted for downstream experiments.

5.2.3 Differentiation of monocytes into osteoclasts using M-CSF and RANKL differentiation media

Monocyte differentiation into osteoclast as detailed in *3.2.3 Differentiation of monocytes into osteoclasts using M-CSF and RANKL differentiation media.* Fresh media was added to replace the media removed. Interleukin (IL)-4, IL-10, and IL-13 (Miltenyi Biotec; Cologne; Germany) were added every 2-3 days at either 10 ng/mL or 30 ng/mL concentration.

To assess the response to the inflammatory stimulus lipopolysaccharide (LPS), cells were cultured in RPMI 1640 GlutaMAX™ (ThermoFisher Scientific; Massachusetts, USA) supplemented with 10% fetal bovine serum (FBS, HyClone, Cytiva) and 0.5 µM 2-mercaptoethanol (2-ME) (ThermoFisher Scientific; Massachusetts, USA), +/- 10 ng/mL LPS (Ultrapure, InvivoGen (San Diego, USA)). The supernatants were collected after 24 hours and cultures were centrifuged at *515 x g* for 7 minutes, and cell-free supernatants were removed and stored immediately at - 20 °C until analysis of cytokines using specific ELISAs.

5.2.4 Confocal Microscopy

Isolated monocytes were seeded on Millicell EZ 8-well chamber slides (Merck Millipore, Massachusetts, USA) and cultured in differentiation media. The day of harvest was chosen to be on day 9/10. This is due to the results in Chapter 3 showing the mature osteoclast differentiation observed on day 10, and a plateau of MMP-9 production was observed after day 9/10. Sample preparation and confocal microscopy were performed as detailed in Chapter *2.13 Confocal microscopy.*

5.2.5 The differentiation of monocytes into osteoclasts on the RTCA E-plates

Monocyte differentiation into osteoclasts on the E-plates was performed as detailed in Chapter *2.16 The differentiation of monocytes into osteoclasts on the RTCA E-plates*. Every 2-3 days, the experiment was paused for approximately 15 minutes to allow media change and then resumed. IL-4, IL-10 and IL-13 were added to the cell cultures on the day of seeding and every 2-3 days at either 10ng/mL or 30 ng/mL. These concentrations were chosen based on the literature review [561-564].

The RTCA eSight Software (Research Use Only (RUO); Agilent, California; USA) was used in these experiments.

5.2.6 Enzyme-linked immunosorbent assay (ELISA)

Analysis of cytokines using ELISA was as per the manufacturer's instructions (DuoSet; Biotechne). See Chapter *2.6 Enzyme-Linked Immunosorbent assay (ELISA).* The ELISA kits used in this chapter were to detect the levels of matrix metalloprotease 9 (MMP-9) and MMP-2 secreted by osteoclasts into the supernatants during differentiation. ELISA kits specific to IL-6 and TNFα were used to demonstrate the effects of IL-4, IL-10, and IL-13 on the production of pro-inflammatory cytokines by osteoclasts upon LPS stimulation.

5.2.7 *In-gel* Zymography

Gelatine zymography is a method used to detect the activity of gelatinase enzymes, such as the matrix metalloproteases (MMPs) MMP-2 and MMP-9. *In gel* zymography was performed as detailed in Chapter 2.15 *In gel zymography*.

5.2.8 Immunoblot

Protein estimation was performed using a detergent-compatible (DC) protein assay (Bio-Rad, Hemel Hempstead, UK) as per Chapter *2.7 Protein estimation.* Freshly isolated osteoclast cell lysates were quantified using a microplate reader (POLARstar, BMG) and Excel (Microsoft, USA). Western blotting technique was performed as per Chapter *2.8 Sodium dodecyl sulphate-polyacrylamide gel electrophoresis (SDS-PAGE), 2.9 Semi-dry membrane transfer, and 2.10 Immunoblotting.* Membranes were probed with different integrin subunits antibodies targeting integrin αV polyclonal antibody (Cell Signalling; 4711), integrin β3 antibody (Cell Signalling; (D7X3P) XP® Rabbit IgG mAb 13166), α5 integrin polyclonal antibody (Cell Signalling; 4705), integrin β1 (Cell Signalling (D2E5) Rabbit IgG mAb 9699), integrin β5 (Cell Signalling (D24A5) Rabbit IgG mAb 13629) and integrin α4 (Cell Signalling; (D2E1) XP® Rabbit IgG mAb 8440). The protein loading was evaluated and normalised using monoclonal mouse β-actin Abcam (8226; isotype IgG1). All primary antibodies were previously optimised and used at 1:1000 dilutions in 5% (w/c) BSA, TBS, 0.1 Tween 20 (pH 7.6; MilliporeSigma; Burlington; USA) overnight at 4 C with gentle agitation. Analysis of the band size was determined using ImageJ Software. Densitometry was performed as per Chapter *2.11 Densitometry.*

5.2.9 Statistics

Statistical analysis was performed using GraphPad Prism version 9.4.1 (USA). Data are presented as the mean +/- standard error of the mean (SEM). Two-way ANOVA was used to compare the production of MMP-9 and MMP-2 in the presence of IL-4, IL-10, and IL-13 over the differentiation period. A two-way ANOVA was used to compare the means of MMP-9 and MMP-2 production by osteoclasts on day 7; +/- LPS upon IL-4, IL-10, and IL-13 treatment. A one-way ANOVA was used to compare MMP-9 proteolytic activity *in gel* zymography upon Il-4, IL-10 and IL-13 treatment. All experiments have replicated sample sizes of at least n=3 as indicated, and significant values were taken as $p < 0.05$ graphically denoted as * $p \leq 0.05$, ** $p \leq 0.01$, *** $p \leq 0.001$ and **** $p \leq 0.0001$.

The xCELLigence graphs shown in this chapter are representative of several repeated experiments. The Cell Index (CI) data for IL-4, IL-10, IL-13 and IMiDs were averaged and presented as a ratio of DMSO (VC) $n \geq 4$. Two-way ANOVA was used to compare the effects of the different treatments; significant values were taken as $p < 0.05$ graphically denoted as * $p \leq 0.05$ and ** $p \leq 0.01$.

5.3 Results

5.3.1 Effects of IL-4, IL10, and IL-13 on osteoclast proteolytic activity examined using ELISA and *in gel* zymography

The same differentiation method used in chapter three was used here to demonstrate the effects of IL-4, IL-10 and IL-13 on the proteolytic activity of MMP-2 and MMP-9. Monocytes were seeded in the presence of M-CSF and RANKL to drive the differentiation into osteoclasts. 10ng/mL of IL-4, IL-10 and IL-13 was added to the media on the day of seeding. Supernatants were harvested throughout the differentiation process. MMP-2 and MMP-9 production was tested using specific ELISAs, as described in *5.2.7 Enzyme-linked immunosorbent assay (ELISA).* As illustrated in Figure 5.3 A, IL-4, IL13 at 10 ng/mL reduced the secretion of MMP-2 by osteoclasts; however, the change was not significant. In contrast, IL-10 at 10 ng/mL did not affect the expression of MMP-2 by osteoclasts. A similar effect was observed for MMP-9. IL-4 and IL-13 reduced the expression of MMP-9; however, this change was not significant, and IL-10 did not affect MMP-9 expression by osteoclasts, Figure 5.3 B.

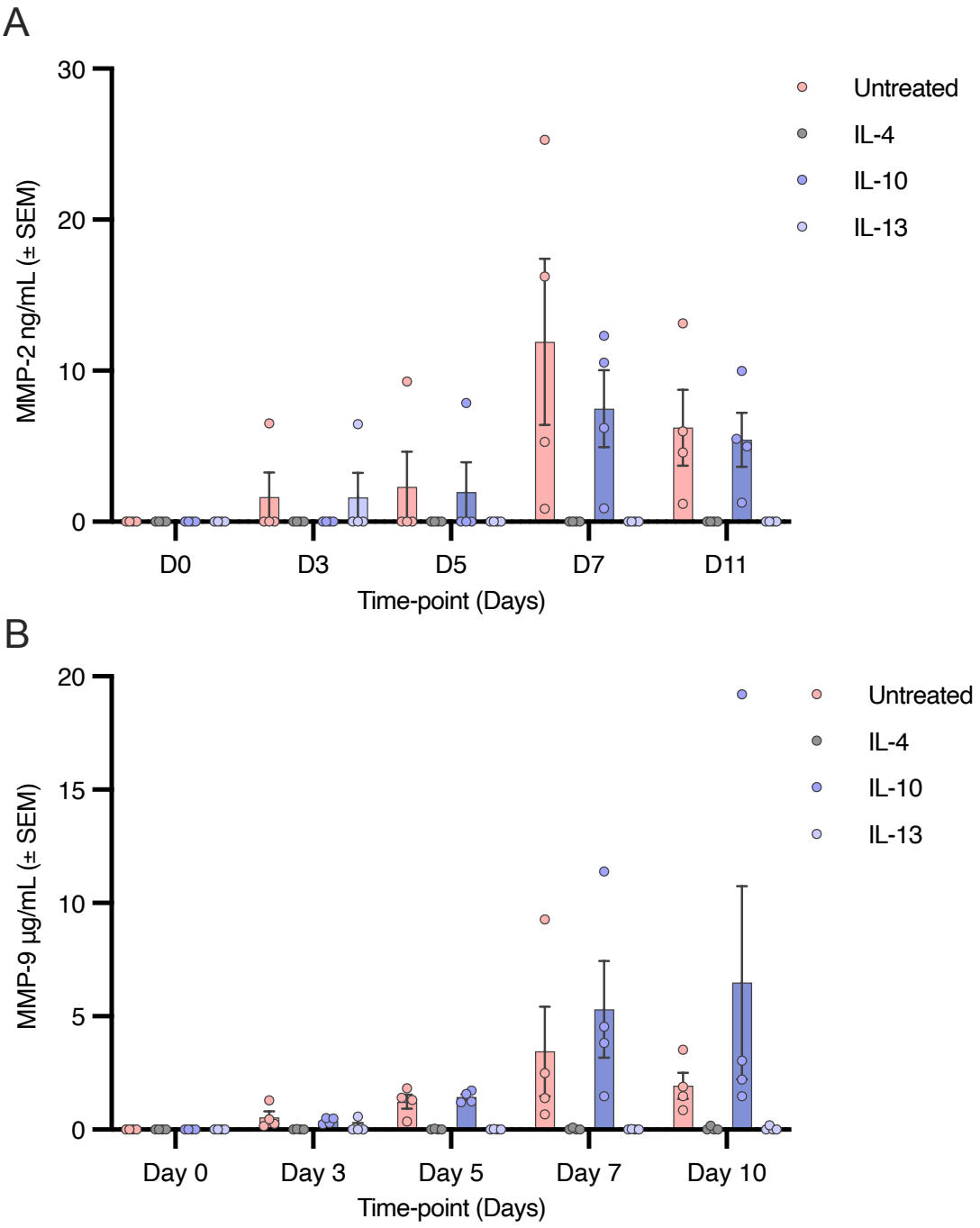

Figure 5.3 Quantifying the effects of IL-4, IL-10, and IL-13 on MMP-2 and MMP-9 production.

M-CSF and RANKL were used to differentiate monocytes into osteoclasts. Supernatants from monocyte-derived osteoclast treated with 10ng/mL IL-4, IL-10 and IL-13, in comparison to untreated samples, were used for MMP-2 (A) and MMP-9 (B) analysis using specific ELISAs. Statistics were performed with a two-way ANOVA and Dunnett's multiple comparisons test. Data are from n ≥ 4 independent experiments expressed as the mean ± SEM.

The effect of IL-4, IL-10 and IL-13 on MMP-9 proteolytic activity was then investigated using *in gel* zymography. The previous gelatine zymography experiments in chapter three demonstrated increased MMP-9 activity as monocytes differentiate into osteoclasts. A protein concentration of 30 µg in previous experiments in chapter three allowed the clear detection of molecular weight bands. Therefore, this concentration was used for all further zymography experiments. Monocytes were seeded in the presence of M-CSF and RANKL to drive the differentiation into osteoclasts. 10ng/mL of IL-4, IL-10 and IL-13 was added to the media on the day of seeding. Supernatants were harvested on the seventh day of differentiation. *In gel* zymography method was used to detect the activity of MMP-9, as per *5.2.8 in gel zymography*. Analysis of the intensity of the bands showed a reduction when treated with IL-4 and IL-13 compared to the non-treated samples. However, IL-10 did not affect MMP-9 activity, Figure 5.4 A-D. In addition, the effect of IL-4, IL-10 and IL-13 on osteoclasts when treated for only 24 hours with 10 ng/mL of IL-4, IL-10 and IL-13 seven days after differentiation. Those were then compared to the supernatants harvested on the seventh day of differentiation from the same donor. IL-4 and IL-13 have significantly reduced the levels of MMP-9 on day seven of differentiation ($p = 0.0006$ and $p = 0.0005$, respectively). In contrast, only IL-4 reduced the levels of MMP-9 when added for 24 hours on the seventh day of differentiation ($p = 0.0322$), Figure E-F.

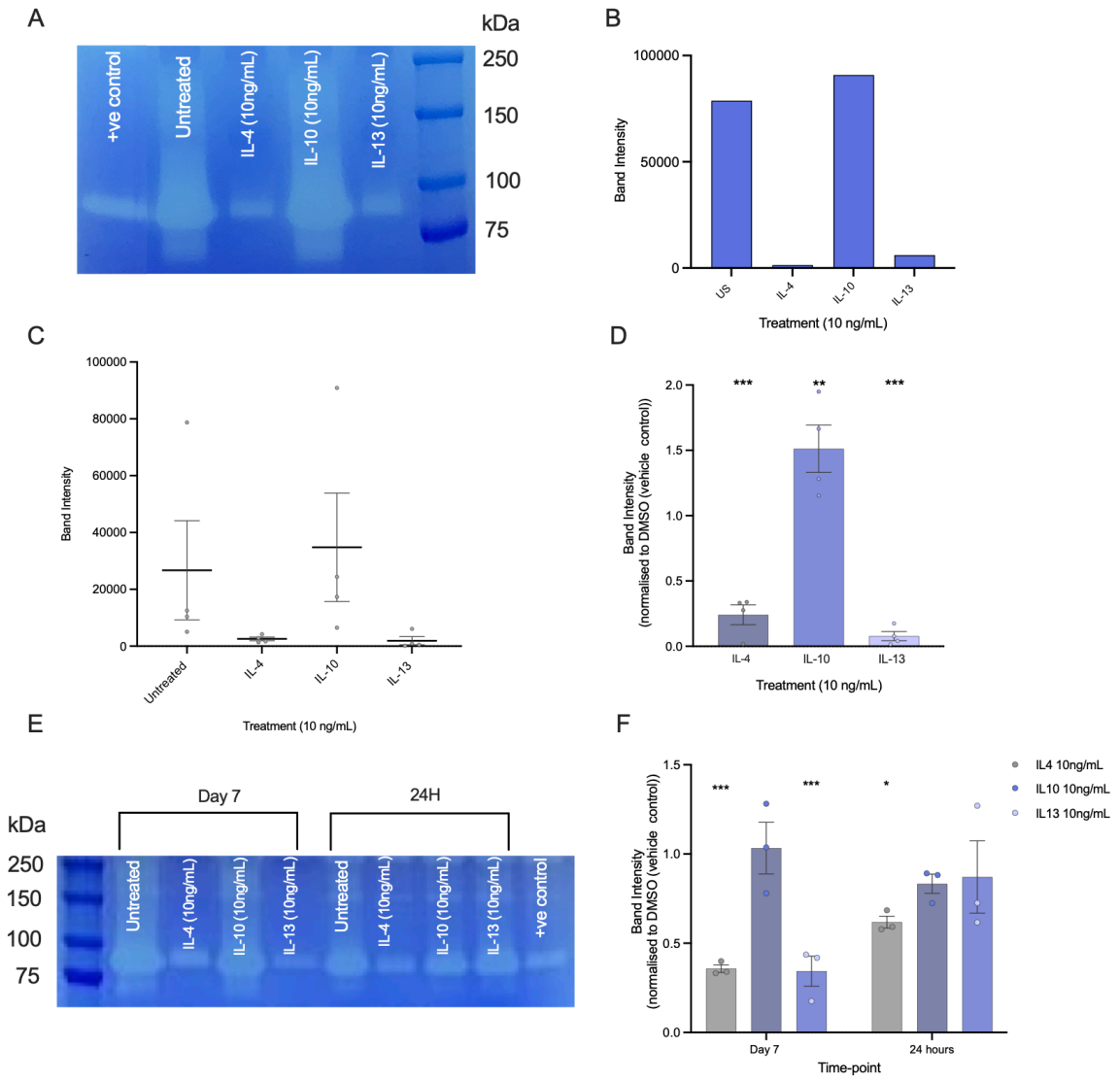

Figure 5.4 Gelatinase activity of IL-4, IL-10 and IL-13 treated monocyte-derived osteoclasts.

*Supernatants from monocyte-derived osteoclasts treated with 10 ng/mL IL-4, IL-10 and IL-13 (all 10ng/ml) were harvested on day seven of differentiation and were prepared for in gel zymography. A representative example of a gel (A) alongside the densitometry values of proteolytic bands corresponding to this representative gel (B) are shown. Summary data from three donors (C) and normalised to DMSO vehicle control (D) is then shown. The proteolytic activity of MMP-9 at day seven of differentiation in comparison to 24-hour incubation with IL-4, IL-10 and IL-13 from one representative gel (E); the band intensity calculated normalised to the DMSO (VC) (F). Statistics were performed with a two-way ANOVA and Dunnett's multiple comparisons test. Bar graphs represent means +/- SEM, n≥3 and significant values were taken as $p < 0.05$ graphically denoted as * $p \leq 0.05$, ** $p \leq 0.01$ and *** $p \leq 0.001$.*

5.3.2 Effects of IL-4, IL10, and IL-13 on LPS-stimulated mediator production by monocyte-derived osteoclasts

Under physiological conditions, the human immune system comprises multiple redundant pathways and immunoregulatory controls that act together to coordinate the immune response initiated by an external signal[565,566]. One of these complicated immune system components is the anti-inflammatory cytokine component, such as IL-4, IL-10 and IL-13[566]. Previous studies have reported that under chronic inflammatory conditions such as systemic autoimmune disease (e.g., rheumatoid arthritis), an increase in inflammatory cytokine levels within the joints induces pathological osteoclast differentiation, causing excessive bone resorption[567, 568, 569]. Upon LPS stimulation, pro-inflammatory mediators are produced, such as TNFα and IL-6, which have been shown to stimulate osteoclast differentiation; however, most of these studies have been conducted in mouse models[569–574]. Anti-inflammatory cytokines are involved in suppressing the activity of pro-inflammatory cytokines hence downregulating the inflammatory response[575,576]. Due to the lack of effects of IL-4, 10 and 13 observed in the 24-hour incubation, the effects of IL-4, IL-10, and IL-13 in conjunction with LPS stimulation of osteoclasts was tested next. LPS was added as well as IL-4, IL-10, and IL-13 on day seven of differentiation, and after 24 hours, supernatants were harvested and analysed for MMP-2, MMP-9, TNFα and IL-6 release by osteoclasts. The production of MMP-9 and MMP-2, Figure 5.5 A-B, respectively, was unaffected by LPS stimulation in the presence of IL-4, IL-10 and IL-13. The production of pro-inflammatory cytokines, such as TNFα and IL-6, under LPS stimulation, was also examined in the presence of IL-4, IL-10 and IL-13 in osteoclasts. The levels of TNFα were unaffected by IL-4, IL-10, and IL-13 treatment, Figure 5.5 C, whereas IL-6 production was significantly decreased in the presence of IL-4 and IL-13 ($p= 0.0010$ and $p= 0.0021$, respectively) Figure 5.5 D; IL-10 had a minor effect on the levels of IL-6; however, this was not significant, Figure 5.5 D.

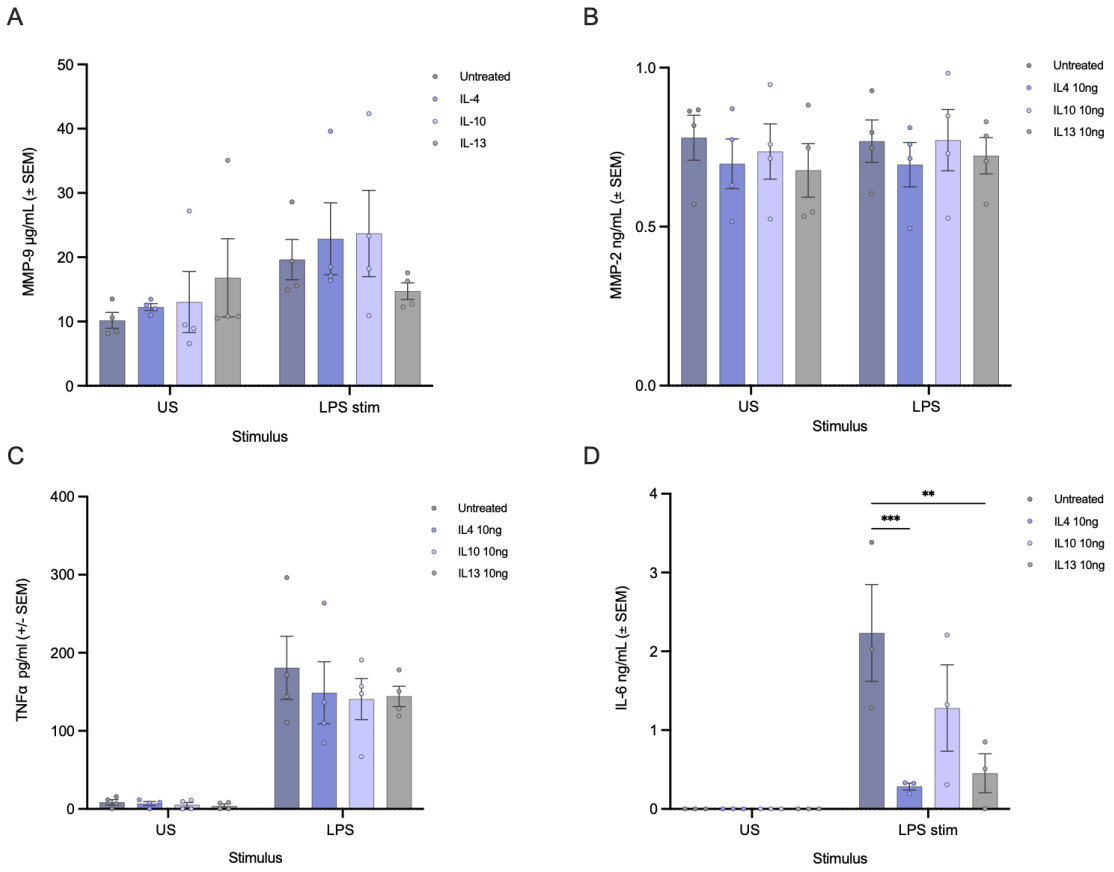

Figure 5.5 Effect of IL-4, IL-10 and IL-13 on the production of MMP-2, MMP-9, TNFα and IL-6 by osteoclasts.

*Supernatants from monocyte-derived osteoclasts treated with (LPS stim) or without (US) LPS (10ng/mL) plus/minus 10ng/mL of IL-4, IL-10 and IL-13 were used for MMP-9 (A), MMP-2 (B), TNFα (C) , and IL-6 (D) analysis using specific ELISAs. Statistics were performed with a two-way ANOVA and Dunnett's multiple comparisons test. Bar graphs represent means +/- SEM, n≥3 and significant values were taken as $p < 0.05$ graphically denoted as ** $p \leq 0.01$ and *** $p \leq 0.001$.*

5.3.3 Qualitative approach to the inhibition of the early and late stages of osteoclast differentiation by IL-4, IL10, and IL-13 in an in vitro model

As demonstrated in chapters three and four, confocal microscopy provided a valuable method to visualise the effects of various treatments on osteoclast differentiation and overall morphology. Therefore, confocal microscopy was used here to investigate the effects of IL-4, IL-10, and IL-13 on the morphology of osteoclasts in the *in vitro* model established within this

study comparing outcomes to those in the absence of the anti-inflammatory cytokines (untreated). At the early stages of differentiation, the addition of IL-4 and IL-13 at a concentration of 10 ng/mL to the osteogenic media prevented specific pre-osteoclast characteristics. These include elongation and migration of osteoclasts[577,578,] as fewer cells were observed in clusters within these wells in comparison to the untreated, whereas IL-10 did not have an effect on the elongation and migration as cell clusters and some multi-nucleated cells were observed (Figure 5.6 A, B). At later stages of differentiation, IL-4 and IL-13 seem to reduce the number of cells in comparison to the images of untreated cells.

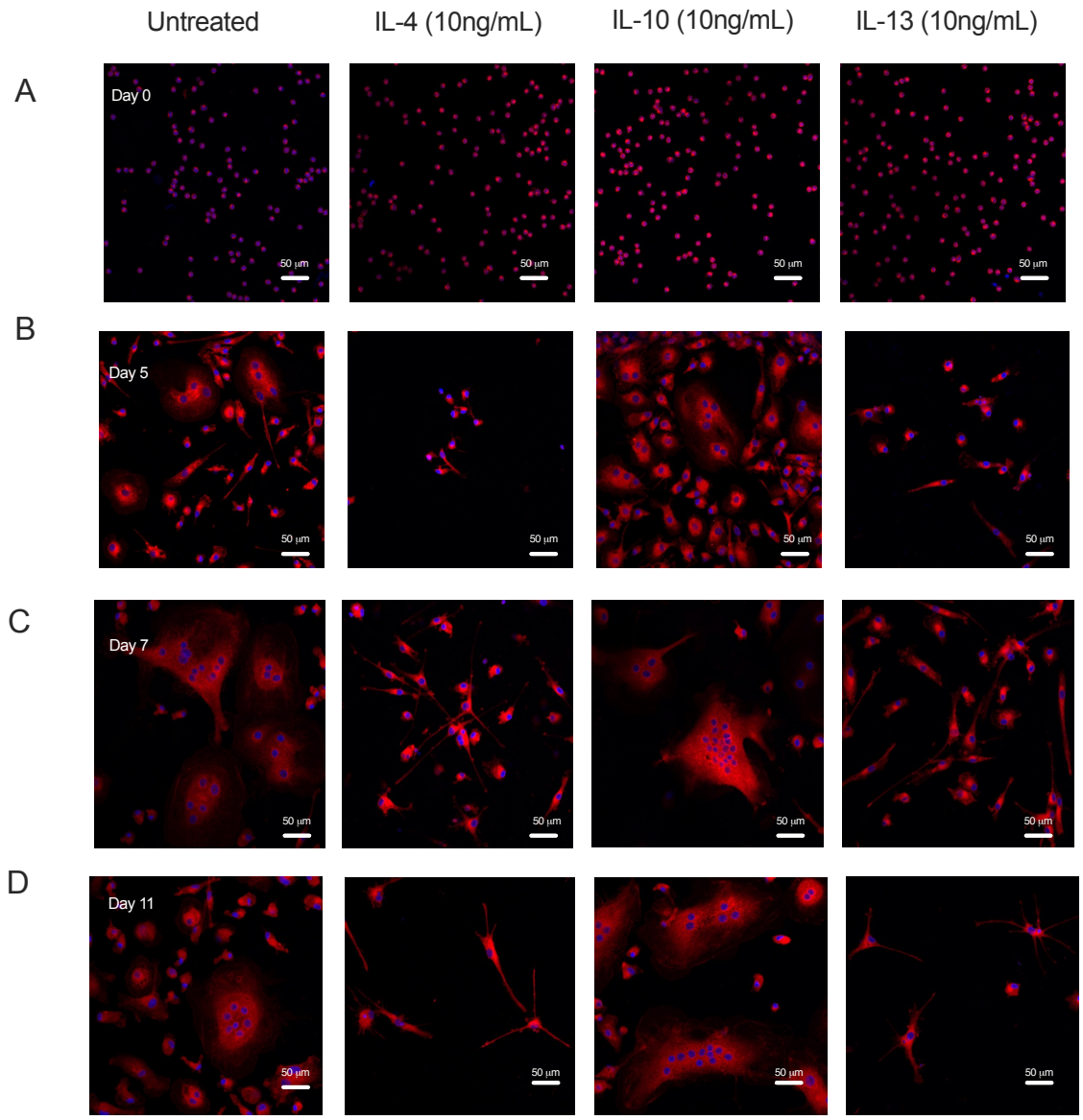

Figure 5.6 Effects of IL-4, IL-10, and IL-13 on monocyte-derived osteoclast differentiation in an in vitro model.

M-CSF and RANKL were used to differentiate monocytes into osteoclasts. A dosage of 10 ng/mL of IL-4, IL-10, and IL-13 was added to the media on the day of seeding and when the media was changed every 2 – 3 days. Nuclei were stained with Hoechst 33342 Solution, and the plasma membrane was stained with CellMask™ Orange on day 0 (A), day 5 (B), day 7 (C) and day 11 (D). Images were taken at 20X magnification, and a 50 µm scale bar was included. Representative images from n=6 experiments.

To quantify these images, confocal microscopy was used at 20X magnification, the number of osteoclasts per image view and the number of nuclei per osteoclast were calculated using manual scoring and presented in figure 5.8A and B, respectfully. Counting the number of osteoclasts revealed that osteoclasts have significantly decreased in the presence of IL-4 and IL-13 on day 7 ($p < 0.0001$ for both cytokines) *and day 11 (*$p < 0.0001$ for both cytokines) *The number of nuclei per osteoclast have decreased significantly in the presence of IL-4 and IL-13 on day 7 (*$p < 0.0001$ for both cytokines) *and on day 11 (*$p < 0.0001$ for both cytokines) *Whereas it was significantly higher in the presence of IL-10 on day 7 (p= 0.0012) and day 11 (p=0.0285).*

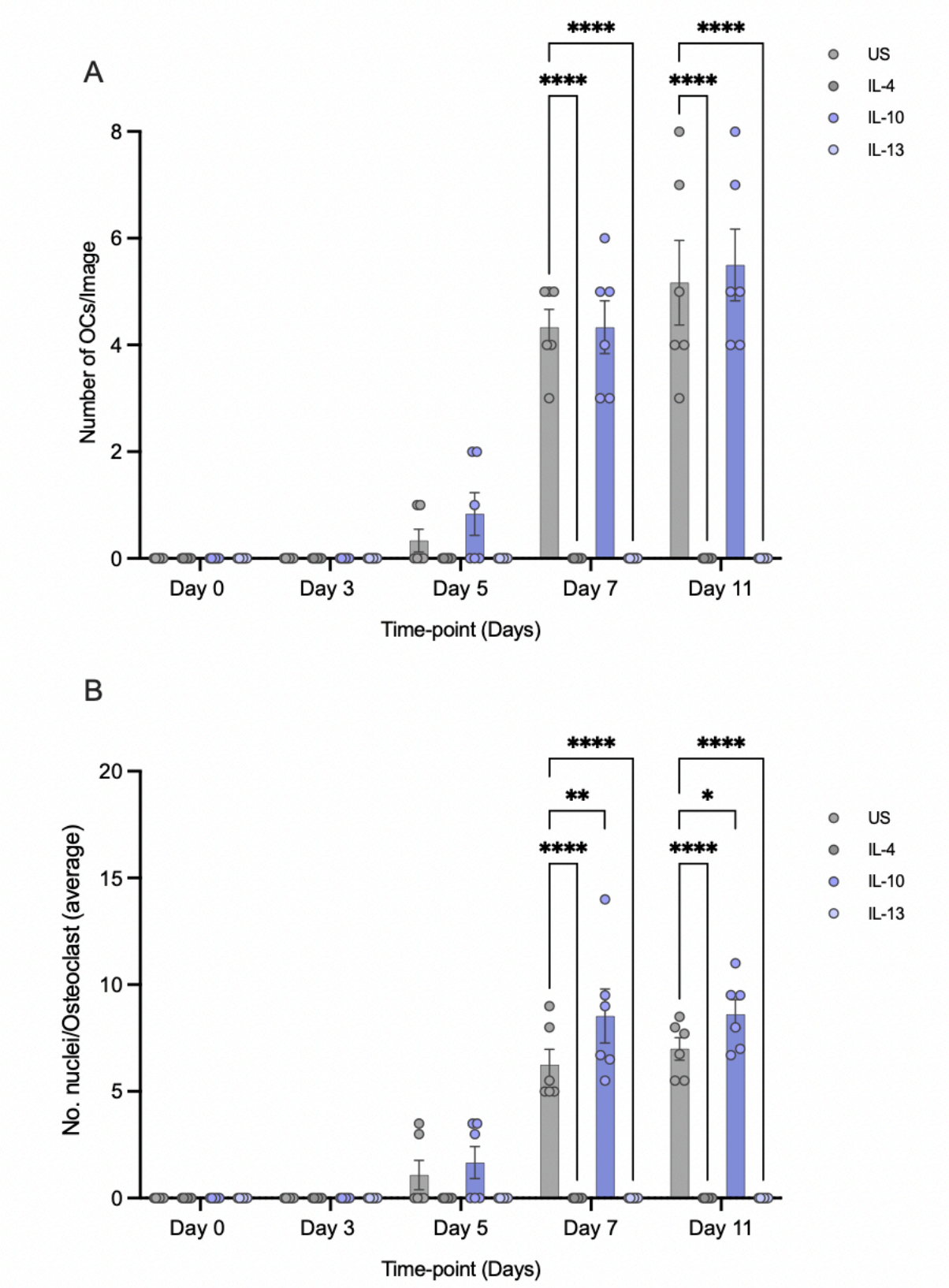

Figure 5.7 Quantification of the effects of IL-4, IL-10, and IL-13 on monocyte-derived osteoclast differentiation in an in vitro model.

*M-CSF and RANKL were used to differentiate monocytes into osteoclasts. A dosage of 10 ng/mL of IL-4, IL-10, and IL-13 was added to the media on the day of seeding and when the media was changed every 2 – 3 days. The number of osteoclasts per image and the number of nuclei per osteoclast were scored manually on day 0 (A), day 5 (B), day 7 (C) and day 11 (D). Statistics were performed with a two-way ANOVA and Dunnett's multiple comparisons test. Bar graphs represent means +/- SEM, n=6 and significant values were taken as $p < 0.05$ graphically denoted as * $p \leq 0.05$ and **** $p \leq 0.0001$. Representative images from n=6 experiments.*

5.3.4 Effects of IL-4/IL-10/IL-13 on osteoclast development using impedance-based techniques

As demonstrated in chapters 3 and 4, the xCELLigence RTCA was used to further investigate the role of IL-4, IL-10 and IL-13 on osteoclast differentiation, as this tool provides further insight into the effects of treatment on osteoclasts without the need to fix and stain the cells. A concentration of 10 ng/mL or 30 ng/mL of each cytokine was added on the day of seeding the cells on the E-plate and with each culture media change as previously. Two doses were chosen here (10 and 30 ng/mL) as this is an exciting new technique where the effect on the impedance will be tested; and it is something that has not been demonstrated in previous reports. The cells were allowed to differentiate for 14 days. Three images were taken every hour of the differentiation. Typical differentiation of osteoclasts was observed with the untreated cultures; after 24h (Figure 5.8 A), the clustering of monocytes begins (which is a characteristic of differentiation[577–579]) and becomes more robust at later time points at 120 hours (day 5) and later at 170 hours (day 7) (Figure 5.8 B-C). Untreated osteoclasts have differentiated more progressively than IL-4 and IL-13-treated cells, as a higher number of clusters are observed 24 hours post-treatment; this was accompanied by a more significant number of multinucleated cells with ruffled edges observed at 315 hours post-seeding with the untreated in comparison to the IL-4 and IL-13-treated cells. In contrast, IL-10 have enhanced the differentiation of osteoclasts; more multi-nucleated cells were observed when compared to the untreated at the later stages of differentiation (Figure 5.8 C).

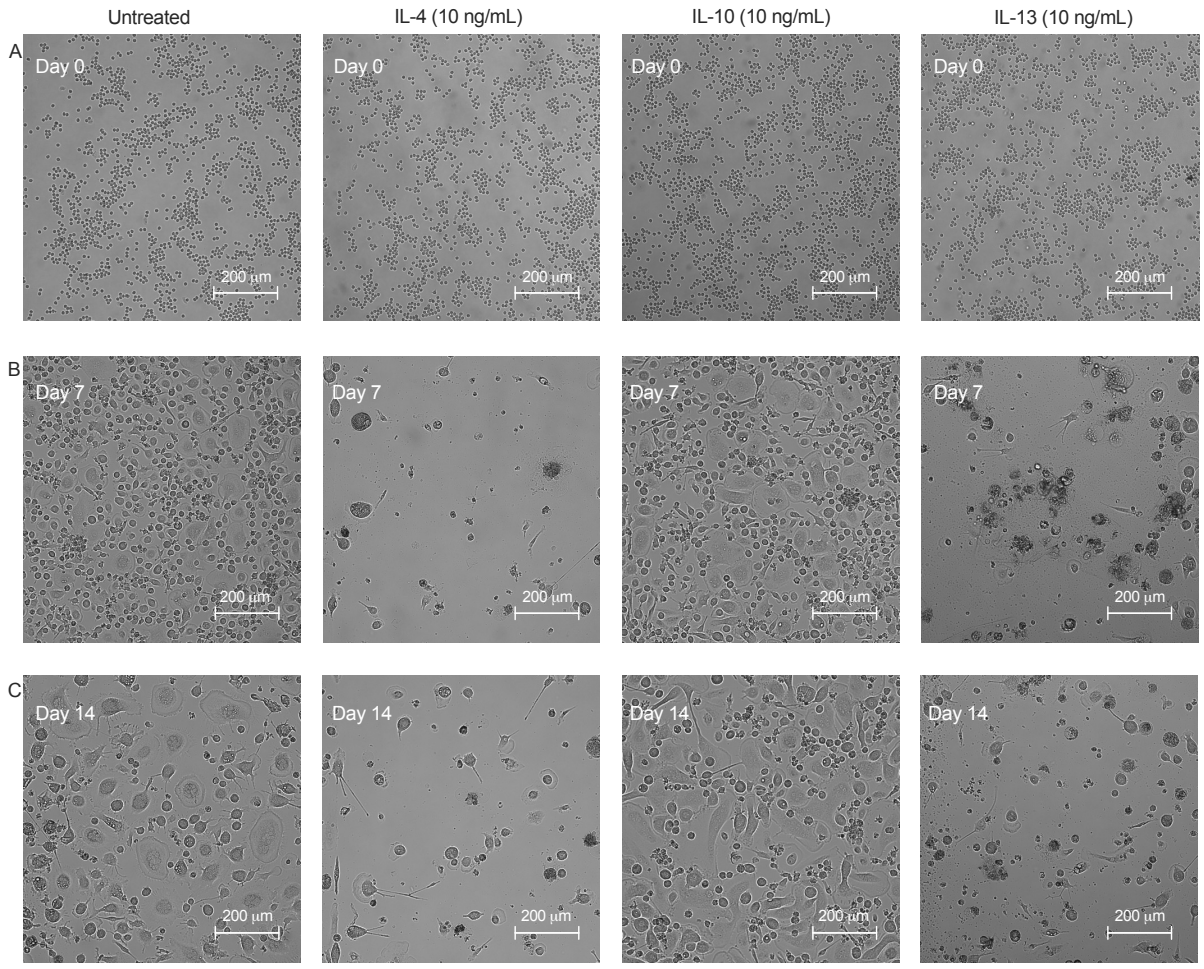

Figure 5.8 Real-time monitoring of the effects of IL-4, IL-10 and IL-13 on the differentiation of monocyte-derived osteoclasts.

Osteoclast differentiation was initiated with the addition of M-CSF and RANKL to monocytes. A dose of either 10 or 30 ng/mL of IL-4, IL-10 and IL-13 was added on the day of seeding. Images of day zero (A), day seven (B), and day fourteen (C). Images show the progression of osteoclast differentiation in the presence of IMiDs. Images shown here) were obtained from one experiment. Similar results were observed with four independent experiments.

The graphs shown in Figure 5.9 depict the bright-field confluence percentage over time (in hours) for cells treated with different IL-4, IL-10, and IL-13 at two different concentrations (10 ng/mL (A) and 30 ng/mL (B)). Both concentrations show similar trends in terms of the relative effects of each interleukin on cell confluence. The untreated cells consistently show the highest confluence percentages, indicating healthy and confluent cell growth. IL-10 treatment maintains relatively high confluence levels after an initial drop, slightly lower than untreated.

IL-4 treatment shows consistently lower confluency than IL-10 and untreated. IL-13 treatment shows the most significant decrease in confluence, indicating a strong inhibitory effect on cell growth or maintenance of confluence.

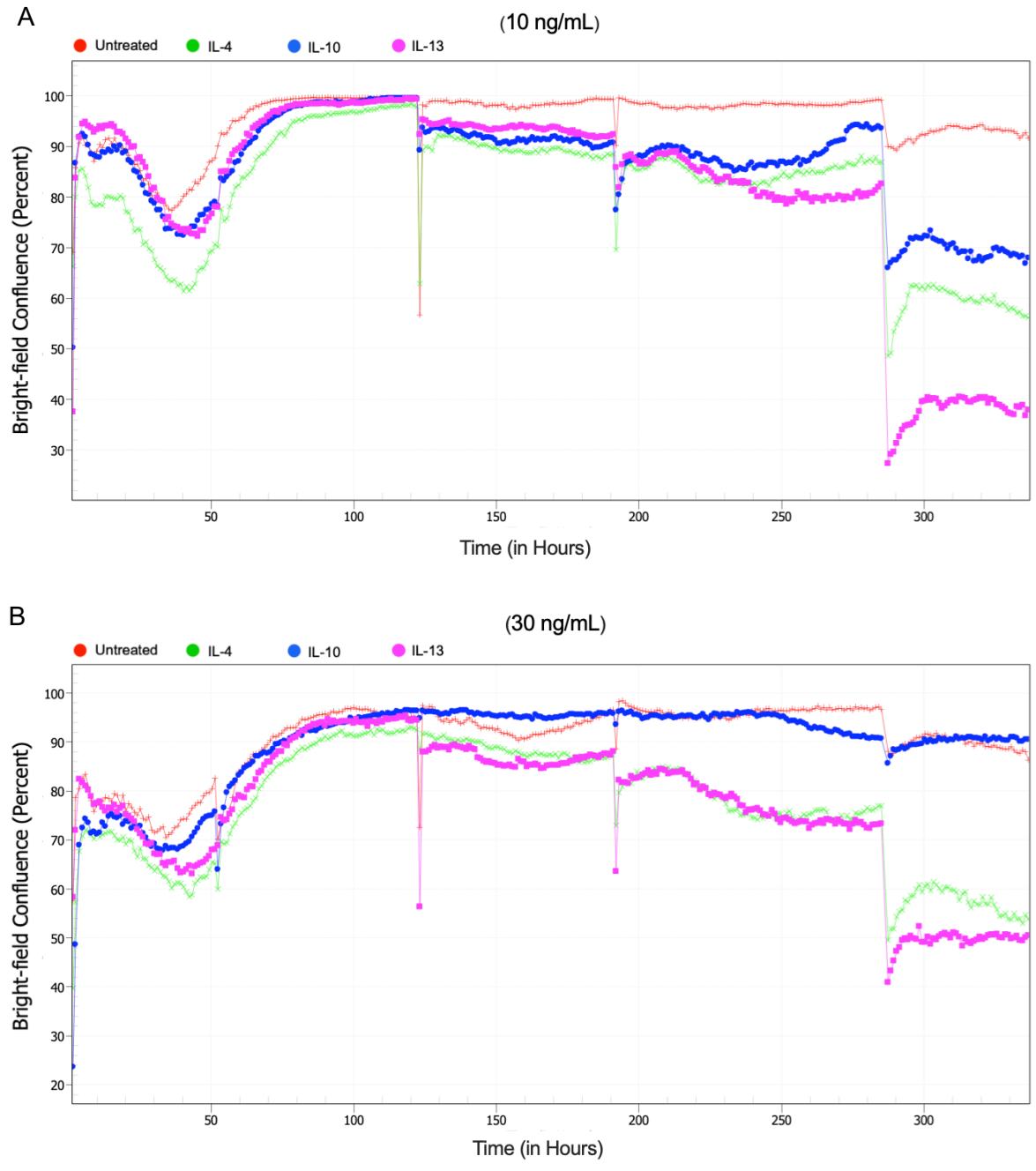

Figure 5.9 Percentage confluency profiles of monocyte differentiation in vitro in the presence of IL-4, IL-10, IL-13. *The cells were incubated in M-CSF and RANKL to differentiate into osteoclasts. A dosage of 10 (A) and 30 ng/mL (B) (IL-4, IL-10 and IL-13) was added to the media on the day of seeding and when the media was changed every 2 – 3 days. Untreated cells were used as a negative control for comparison. The data shown are representative of 1*

experiment, similar to that observed with repeated experiments obtained from n=4 independent repeats.

5.3.5 Quantifying the effects of IL-4, IL-10, and IL-13 on osteoclast differentiation using real-time impedance measurements

Next, the effects of IL-4, IL-10 and IL-13 on the impedance of osteoclasts were shown for the first time using the xCELLigence RTCA. Continuing to use 100,000 monocytes/well on the E-plate seeded in osteogenic media, two different doses of IL-4, IL-10 and IL-13 (10 and 30 ng/mL) were added. The CI signal, dependent upon osteoclasts being adhered to the E-plate, increases steadily for the untreated cells and IL-10 treated cells over the first ~ 70 hours, after which it briefly plateaus ~ 70-120 hours. The presence of IL-4 and IL-13 significantly decreases osteoclast impedance throughout the differentiation process at 10 ng/mL (Figure 5.10 A, B) and 30 ng/mL (Figure 5.10 C, D). Due to the impedance being so sensitive to changes in cell size and cell adhesion strength, the very early stages of differentiation can be detected. Impedance and live cell imaging results were obtained, yielding similar quantitative assessments of IL-4 and IL-13 efficacy in decreasing the impedance of osteoclasts. Interestingly, IL-10 was observed to increase the impedance of osteoclasts in a dose-dependent manner, exerting greater effects on the impedance at later stages of differentiation (Figure 5.10 A-D).

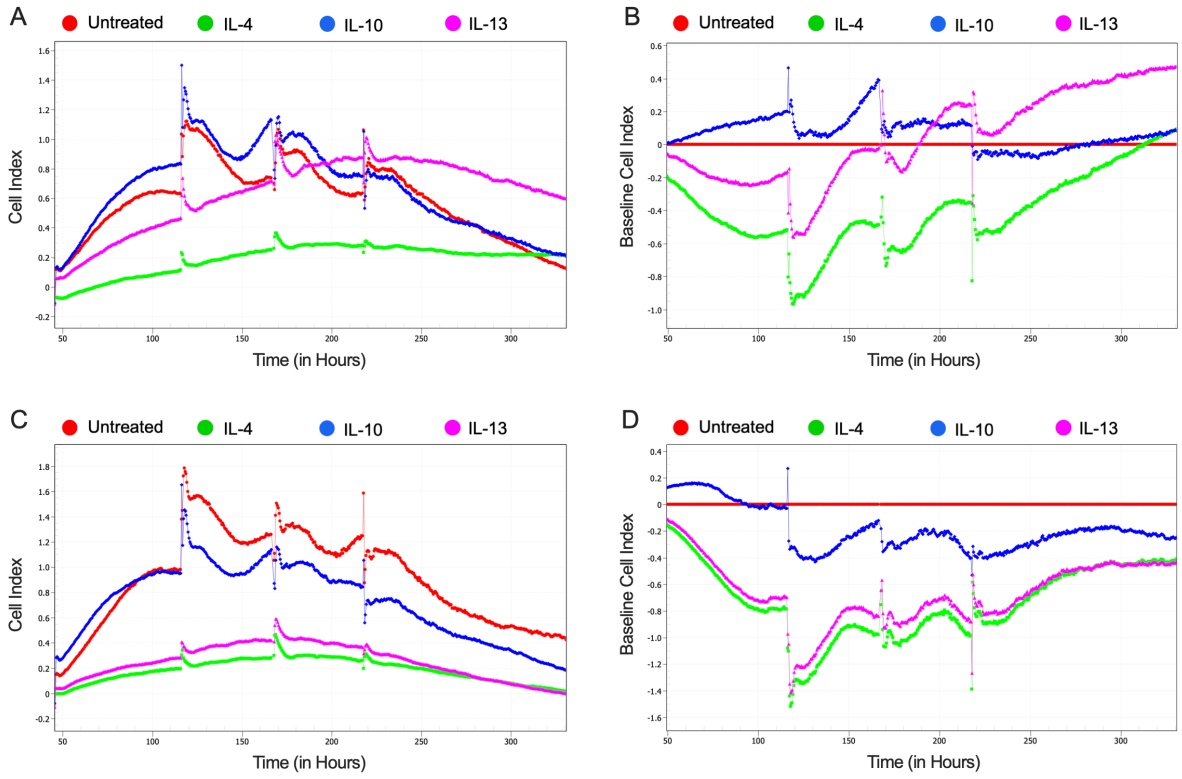

Figure 5.10 CI signal displaying the impedance of osteoclasts in the presence of IL-4, IL-10, and IL-13.

M-CSF and RANKL were used to differentiate monocytes into osteoclasts. The impedance of osteoclasts in the presence of anti-inflammatory cytokines showing the CI signal at 10 ng/mL of each cytokine (A), untreated (negative control) as CI baseline at 10 ng/mL of each cytokine (B), the CI signal at 30 ng/mL of each cytokine (C), and untreated (negative control) as CI baseline 30 ng/mL of each cytokine (D). The data shown are representative of one experiment, similar to that observed with repeated experiments obtained from n=4 independent repeats.

The ability to quantify the effects of the anti-inflammatory cytokines on the impedance of osteoclasts in multiple repeats from real-time live imaging without any additional staining is a unique property of the xCELLigence RTCA. The impedance data shown in Figure 5.11 illustrates the effects on the CI data reproduced in four independent experiments. IL-4 and IL-13 have reduced the impedance of osteoclasts to the E-plate at 10 ng/mL (Figure 5.11 A), whereas IL-10 has significantly increased the impedance when compared to the untreated sample 9 ($p = 0.0194$). A significant decrease was observed with IL-4 and IL-13 at 30 ng/mL concentration with the overall period of differentiation. IL-4 significantly reduced the impedance at 300 hours $p = 0.0445$. IL-13 significantly reduced the impedance from 200 hours

onwards (200 hours p = 0.0141; 250 hours p = 0.0173; 300 hours p = 0.0056, and 350 hours p = 0.0459). IL-10 has marginally increased the impedance. However, this was not statically significant (Figure 5.11 B).

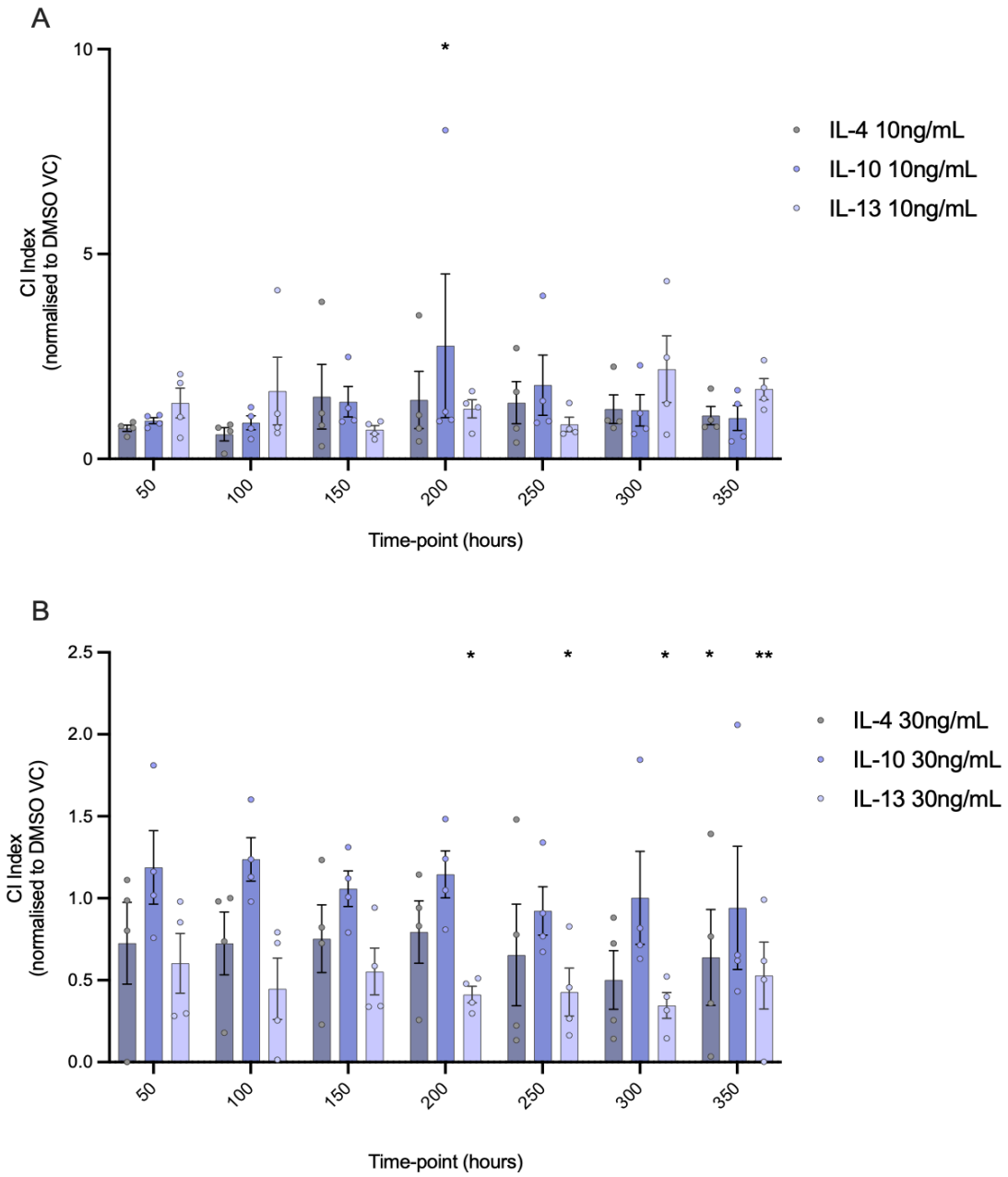

Figure 5.11 Effect of IL-4, IL-10, and IL-13 on CI signal of monocyte-derived osteoclasts as a measure of impedance.

Monocytes were seeded on E-plates and differentiate into osteoclasts using M-CSF and RANKL in the presence of 10 ng/mL or 30 ng/mL IL-4, IL-10, or IL-13. The impedance was monitored continuously for the 14 days of osteoclast differentiation. Quantitative measures of the impedance displayed as a CI signal in the presence of anti-inflammatory cytokines at 10

*ng/mL (A) and 30 ng/mL (B). Statistics were performed with a two-way ANOVA and Dunnett's multiple comparisons test. Bar graphs represent means +/- SEM, n=4 and significant values were taken as $p < 0.05$ graphically denoted as * $p \leq 0.05$ and ** $p \leq 0.01$.*

Only one-time point was chosen to demonstrate the differentiation of pre-osteoclasts and the effect of the object count. This time-point of 60:35 hours was chosen as pre-osteoclast clusters were shown to be starting to form around this time-point. The masking parameters used in chapter 4 are used again here, using the untreated sample to define them, and then the same masking parameters were applied to all the wells in the presence and absence of IL-4, IL-10 and IL-13 (Figure 5.12).

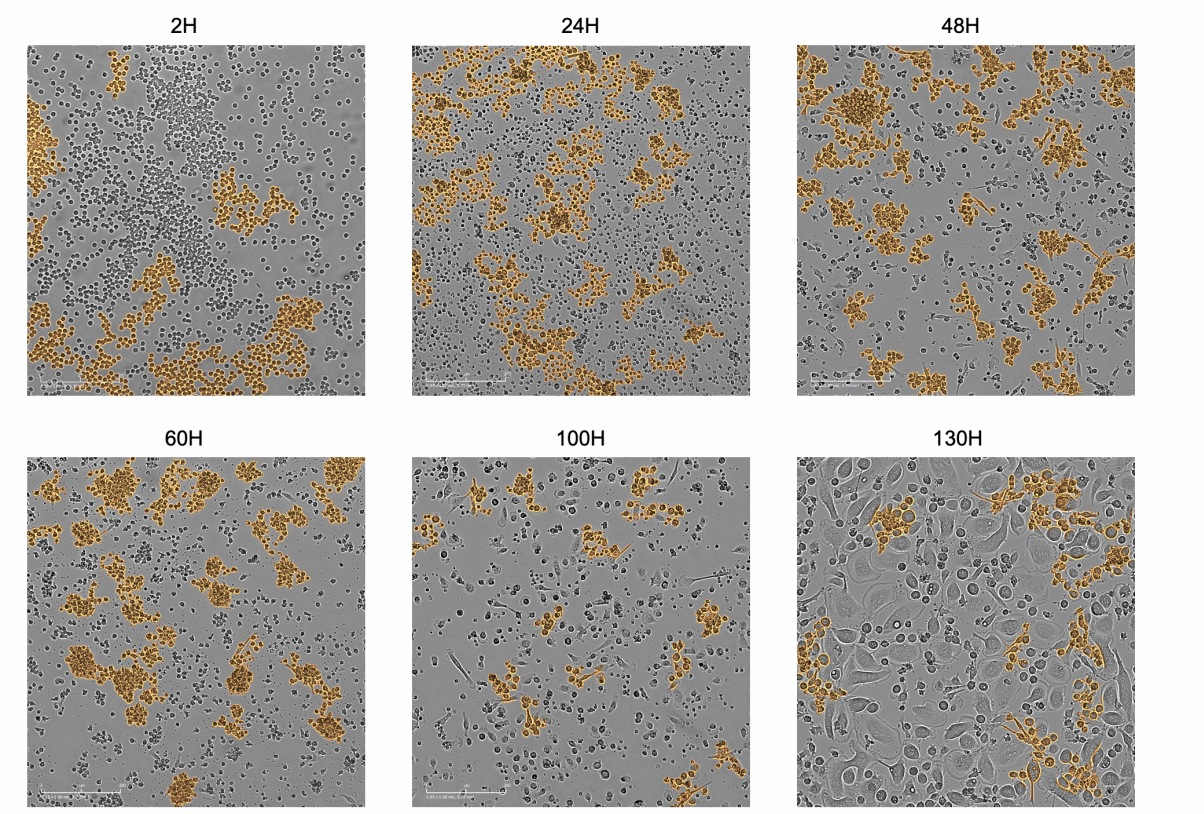

Figure 5.12 Label-free monitoring of osteoclast differentiation using an xCELLigence RTCA eSight analyser.

Images tracking the progression of cell spreading and the aggregation displaying clusters forming over time. Images from 2-, 24-, 48-, 60-, 100-, and 130-hour time points highlight the formation of clusters at early time points, displaying the higher intensity and larger surface area of masking (displayed in orange) after 48 and 60 hours of seeding. Clustering of monocytes (which is a characteristic of differentiation) becomes more robust. At later time

points, these osteoclasts clusters contain less of the orange masking, which displays an increase in CI and cytoplasm elongation and appears to be progressing into mature osteoclasts. Finally, after 120 hours of seeding, the masking of aggregates slowly disappears with the emergence of multinucleated cells. An outline of the masking was selected using bright field microscopy images. H=Hour

An example of a single experiment, where the clusters formed throughout the duration of the differentiation process with the addition of 30 ng/mL IL-4 and IL-10, and IL-13 were measured, is shown in Figure 5.11. As shown in Figure 5.13, using the untreated cells to determine the time-point in which the cells display the highest numbers of clustering through differentiation, a 60-hour post-seeding time point was chosen to test the efficacy of the anti-inflammatory cytokines on the rate of cluster formation. This is displayed in Figure 5.13 A, where the clustering for ~130 hours is displayed (at 60 hours is highlighted by the arrow). In addition, the cluster formation measurement is shown in comparison to the CI measured at that time point (Figure 5.13 B). Combining the CI signal at the early stages of differentiation displays a similar pattern to that observed with the object count (clusters formed) by osteoclasts in the presence of IL-4, IL-10 and IL-13.

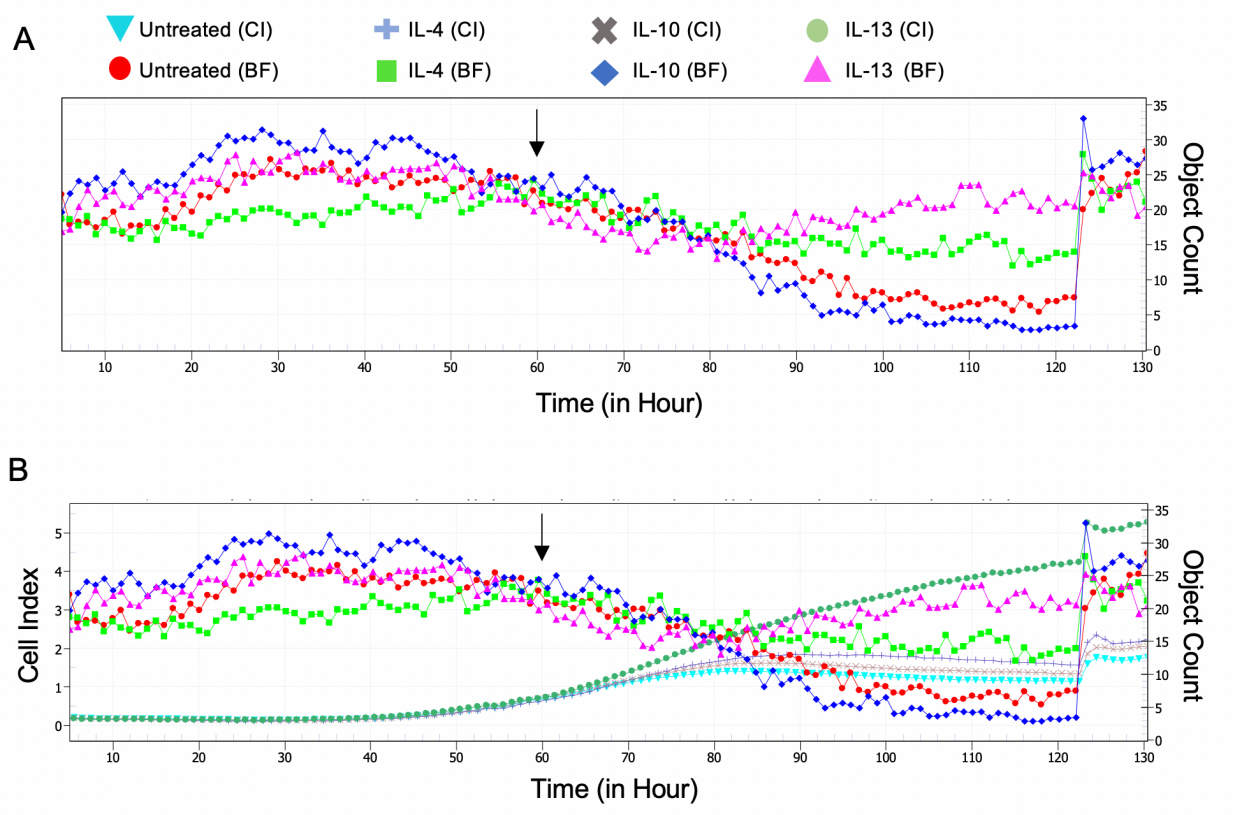

Figure 5.13 An example of pre-osteoclastic cluster formation in the presence of IL-4, IL-10 and IL-13.

Time points between 0-130 hours post-seeding showing the effects of IL-4, IL10, and IL-13 on the formation of osteoclastic clusters (A). A graph combing the CI signal and the object count (number of clusters) observed at the early stages of differentiation. CI signal and object counts shown in this graph were obtained from one donor in triplicates on the E-plate. The arrow pointing at 60-hour time point.

While showing the effects on one donor gives an insight into the impact of IL-4, IL-10 and IL-13, it was important to determine whether the data obtained were reproducible. The experiment was repeated three times, and similar results were observed when combining the number of object counts and the CI signal at a 60-hour time-point post-seeding. A single experiment displaying the raw data obtained when measuring the CI and the object count is shown (Figure 5.14 A). When normalised to the untreated samples, IL-4 and IL-13 have reduced the CI signal, with IL-13 displaying a significant reduction in the CI signal ($p = 0.0130$). Similar results were obtained when measuring the number of clusters formed by monocytes by 60:35 hours, as IL-4 and IL-13 both caused reductions that were significant for IL-13 ($p = 0.0020$); no effect was observed with IL-10 treatment (Figure 5.14 B).

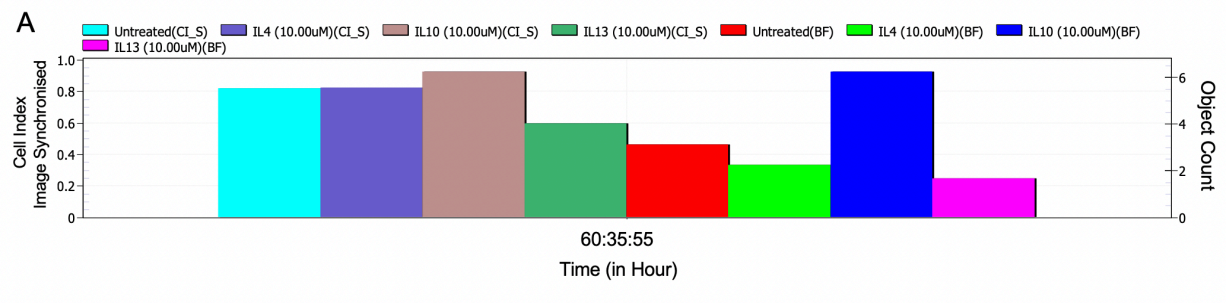

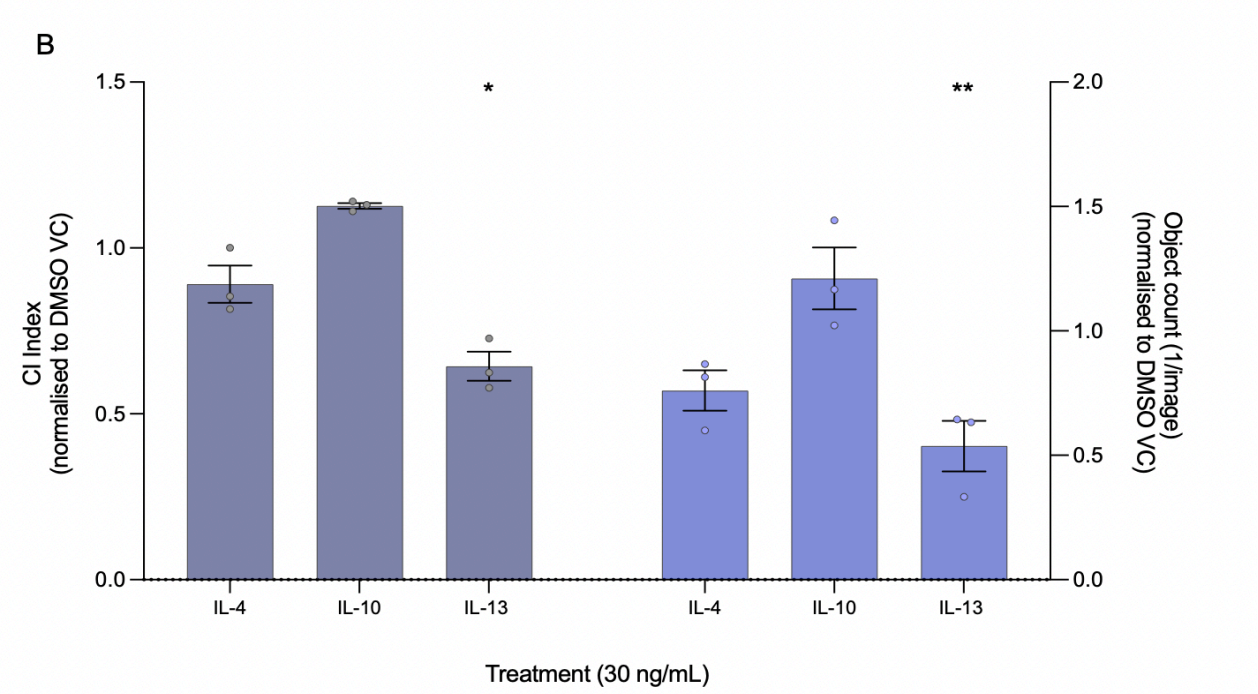

Figure 5.14 CI signal and object count per image of pre-osteoclasts in the presence of IL-4, IL-10, and IL-13.

*M-CSF and RANKL were used to differentiate monocytes into osteoclasts. A dose of 10 ng/mL and 30 ng/mL IL-4, IL-10 or IL-1) was added to the media on the day of seeding and when the media was changed every 2 – 3 days; an untreated was always included. The object count for pre-osteoclasts of one individual experiment (A); a bar graph obtained from the same experiment (B). Statistics were performed with a two-way ANOVA and Šidák multiple comparisons test. Bar graphs represent means +/- SEM, n=3 and significant values were taken as $p < 0.05$ graphically denoted as * $p \leq 0.05$.*

5.3.6 The expression of integrins in the presence of anti-inflammatory cytokines in an *in vitro* osteoclast differentiation model

The expression of integrins in the presence of IL-4, IL-10 and IL-13 was investigated next. Since a significant effect was observed with 10 ng/mL of IL-4, IL, 10, and IL-13 in the end-point methods presented above, this concentration was used to investigate the expression of integrins on day 10/11 osteoclasts. IL-4 and IL-13 exerted a significant effect on the expression of all integrins used here, whereby the expression was reduced significantly in the presence of IL-4 and IL-13. The presence of IL-10 did not have an effect on the expression of integrins (Figure 5.15 A-G). The most significant increase was observed on $\alpha5\beta1$ integrin complex; $p \leq 0.0001$, whereas the least effect of IL-4 and IL-13 was observed with the $\alpha v\beta3$ integrin complex. This is followed by $\alpha4\beta5$ expression (P> 0.01).

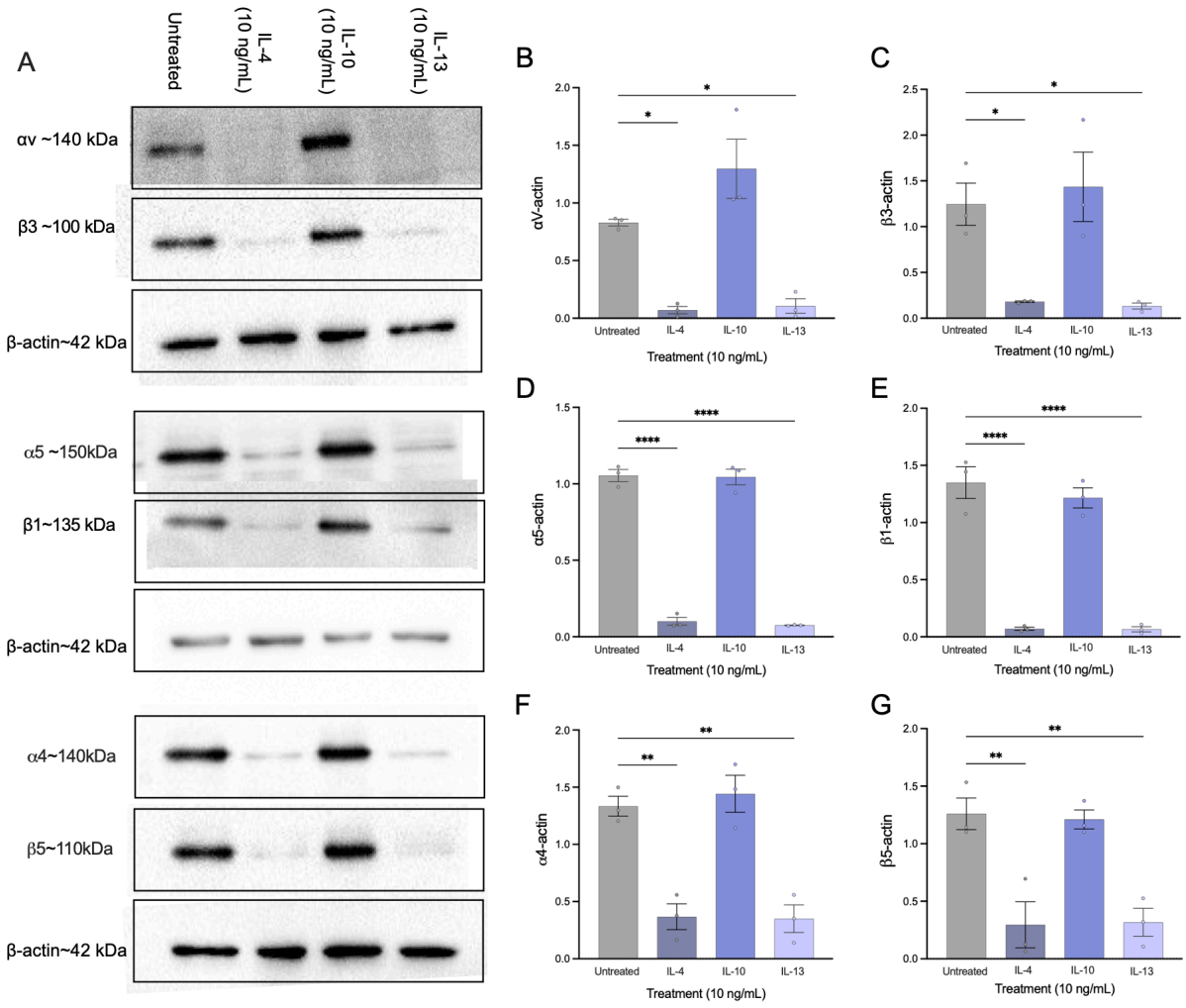

Figure 5.15 Effect of IL-4, IL-10 and IL-13 on expression of integrins by monocyte-derived osteoclasts.

*M-CSF and RANKL were used to differentiate monocytes into osteoclasts in the presence or absence of 10 ng/mL IL-4, IL-10 or IL-13. IL-4 and IL-13 at a significantly reduced the expression of $\alpha v\beta 3$, $\alpha 5$, $\beta 1$, $\alpha 4$ and $\beta 5$. β actin was used as a loading control. A representative immunoblot of three is shown (A) and then relative densitometry of (B) αv, (C) $\beta 3$, (D) $\alpha 5$, (E) $\beta 1$, (F) $\alpha 4$, and (G) $\beta 5$ for n = 3 as mean +/- SEM. All targets were normalised to β actin. Statistics were performed with a one-way ANOVA and Dunnett's multiple comparisons test, statistical significance is shown as * $p \leq 0.05$, ** $p \leq 0.01$, *** $p \leq 0.001$ and **** $p \leq 0.0001$.*

5.4 Discussion

The results in this chapter demonstrate that (i) IL-4 and IL-13 downregulate the activity of osteoclasts and their differentiation by preventing the adhesion of monocytes/pre-osteoclasts in vitro, whereas (ii) the opposite effect was observed with IL-10 on the differentiation and the activation of osteoclasts, and finally, (iii) a new method has been here to measure the effects of such cytokines on osteoclastogenesis in real-time *in vitro*.

It is well known that bone loss diseases, such as RA, psoriasis, and multiple sclerosis, are affected by inflammation[570–582]. Much emphasis has been guided towards the effects of cytokines in the pathogenesis of bone resorption. Cytokines produced at the site of bone resorption are thought to play a pivotal part in perpetuating the bone lesions formed, leading to bone destruction and loss[583]. However, many of these cytokines that exist in the bone tissue and influence bone formation and resorption are still not thoroughly understood. IL-4, IL-10 and IL-13 are all classed as potent immunoregulatory cytokines that play a key role in bone metabolism with protective properties against bone resorption[583–585]. IL-4 is a multifaceted anti-inflammatory cytokine with known anti-angiogenic properties[586]. IL-4 shares a receptor and many cellular functions with IL-13. IL-4 and IL-13 are critical components of Th2-mediated immunity, and they play a crucial role in the pathogenesis of allergic inflammation and parasite infection[587,588] by activating signal transducer and activator of transcription 6 (STAT6)589. Both cytokines exert an effect on a wide range of cells, such as B cells, monocytes, fibroblasts and basophils[590–592]. Interestingly, both cytokines have been reported to have different mechanisms in certain inflammatory conditions despite both cytokines sharing a receptor. For example, IL-4 and IL-13 play an important role in the pathogenesis of allergic asthma. IL-4 plays a pivotal role in Th2 cell proliferation, cytokine production, and IgE synthesis, while IL-13 plays a role in asthma's pathological features, such as mucus production[593]. Results from animal and *ex vivo* studies suggest that the anti-inflammatory properties of IL-4 and IL-13 might be beneficial in the context of inflammatory arthritis treatment[587,594]. Activation of the IL-4/IL-13 signalling pathway might constitute a novel and powerful approach in the therapy of inflammatory arthritis, and therefore, it was important to study those effects in an osteoclast model; further studies are crucial to uncover and understand the mechanism of IL-4/IL-13 action and its exact role in MM. Furthermore, the production of the two cytokines is not identical; IL-4 production is calcineurin-dependent, whilst IL-13 production is only partially dependent on calcineurin[595]. Both cytokines play a key role in bone metabolism and inhibition of bone resorption[587,596,597]. *In vitro,* both cytokines have already been shown to inhibit osteoclastogenesis by decreasing RANK and RANKL expression[598]. Consistently, the data shown herein also demonstrate that IL-4 and IL-13 prevented osteoclastogenesis by reducing the multinucleation of osteoclast precursors; these data also showed a downregulation of MMP-2 and MMP-9 production from osteoclasts upon IL-4 and IL-13 treatment.

In contrast, IL-10 did not have the same effect as IL-4 and IL-13; in fact, IL-10 marginally increased MMP-9 expression and had no effect on or slightly enhanced osteoclastogenesis. This functional discordance has been seen throughout all the data presented in this chapter. This is inconsistent with previous reports as IL-10 has also been described as a potent inhibitor of osteoclast differentiation and function in many studies conducted in the murine monocyte/macrophage-like cell line, RAW 264.7 and mice/rat-derived bone marrow precursor culture systems[554,599–603]. This suggests that human monocytes and osteoclasts have a different response to IL-10 compared to their murine counterparts. However, in a previous study, the effects of IL-10 on human osteoclasts were found to be similar to those observed in mouse[604]. This suggest that the effect observed here could be due to the fact that IL-10 cannot act directly on osteoclast and requires the present of other bone cells, such as osteoblasts, to exert its inhibitory effects[605].

In this study, a significant effect of IL-10 was seen on the activity of MMP-9 released by osteoclasts as supernatants from IL-10 treated cells significantly increased the digestion of the zymography gel, creating augmented digested surface area, indicating IL-10 increased the activity of osteoclasts *in vitro*. This effect has not been documented in previous reports, and the direct comparison of all three cytokines on the same zymography gel has been illustrated here for the first time in an *in vitro* osteoclast model.

Increased osteoclast differentiation and increased production of MMP-2 and MMP-9 by IL-10 but a significant decrease of both MMP-9 activity and osteoclastogenesis with IL-4 and IL-13 could also be due to IL-4 and IL-13 sharing a common receptor on osteoclasts, activating similar signalling pathways that are different to those activated by IL-10. This requires further investigation that could include downstream processes and cellular functions stimulated by these cytokines. A previous study had demonstrated the lack of IL-10-mediated suppression of bone resorption in bone marrow cultures and in cocultures of bone marrow stromal cells with murine hematopoietic spleen cells[606]. However, osteoclast differentiation was substantially reduced by IL-10 in both systems. One study has reported the direct anti-osteoclastic effect of IL-10; this was reported in bone marrow precursors isolated from mice and RAW 264.7 cells[602]. Not only were these non-human models, the dose of IL-10 used was ten times higher than that used in the studies described herein[602].

The measurement of osteoclasts activity osteoclasts in the presence of IL-4 and IL-13 using *in gel* zymography has not been studied in previous reports. This was done for the first time in this chapter. The activity of osteoclasts was significantly reduced upon IL-4 and IL-13 treatment in the supernatants harvested on day 10/11. This effect of IL-4 and IL-13 was greatly reduced when treatment was added seven days post monocyte seeding. The results obtained indicate the importance of the period of incubation with IL-4 and IL-13, as the cytokines had

little effect on the activity of mature osteoclasts suggesting that IL-4 and IL-13 downregulate the earlier stages of differentiation. Both cytokines were found to exert more potent inhibitory effects on osteoclast activity when present at the initial stages of osteoclastogenesis. This is consistent with previous studies highlighting the inhibitory properties of both cytokines on osteoclast precursors[607,608]. This analysis included consideration of the effects of IL-4, IL-10 and IL-13 on the production of pro-inflammatory cytokines such as IL-6 and TNFα. These cytokines were selected to be tested due to their elevated presence and their effects on the progression of MM, as discussed in *1.9.2 Pathogenesis of myeloma bone disease.* IL-4 and IL-13 reduced the LPS-stimulated secretion of IL-6 by osteoclasts. These results suggest that the anti-inflammatory activity of IL-4 is more potent than IL-13, which is consistent with previous findings[609–611]. Neither IL-4, IL-10, nor IL-13 had an effect on LP-stimulated TNFα production; this was also observed with LPS-stimulated MMP-2 and MMP-9 production by osteoclasts.

IL-10 did not have any effect on LPS-stimulated IL-6 or any of the other measures made for this part of the work. Inconsistent with these findings, the activity of IL-4 and IL-10 has been reported to have shared effects on cartilage, subchondral bone, and joint[612,613] tissues. Both cytokines directly inhibit MMP production by monocytes; this includes MMP-1, MMP-2, and MMP-3[614]. However, not all effects of IL-4 and IL-10 are shared. For example, IL-10 induces the expression of tissue inhibitor of metalloproteinases 1 (TIMP-1) by monocytes, which is an effect have not been reported with IL-4[615,616]. IL-10 was also found to inhibit LPS-mediated TNFα and IL-6 production in T cells[617,618]. Interestingly, TNFα has been found to stimulate osteoclastogenesis in the absence of RANKL[619–621]. However, this area of research remains controversial due to the inability to successfully isolate and select human osteoclast progenitors exclusively[622]. Therefore, new methods are needed for a highly specific selection of osteoclast progenitors to study RANKL-dependent versus RANKL-independent osteoclastogenesis. The work here provides an *in vitro* model that would allow future studies to compare the effects of the different osteoclastogenesis stimulants.

The inhibition of RANKL-mediated osteoclastogenesis by IL-4 is thought to be stronger than that observed with IL-13; this inhibition is shown to be irreversible[559]. Similar to this, the potency of IL-4 is observed here to be greater than IL-13 in reducing the activity and the cytokines released by osteoclasts in many endpoint methods used throughout this chapter. However, IL-13 seems to exert a more significant effect on reducing the impedance of osteoclasts than IL-4. As previously mentioned, IL-4 and IL-13 share many biological and immunoregulatory functions; however, their precise mechanisms of regulations give rise to distinct effects and functions.

There are many options for endpoints to measure in the phenotypic assay. These measurements include cell cytotoxicology, proliferation, intracellular signalling, cell surface or secreted proteins, metabolites and gene expression[623,624]. Some of these endpoint assays were utilised here to measure the effects of IL-4, IL-10, and IL-13 on osteoclast differentiation and function. Here for the first time, the effects of IL-4, IL-10 and IL-13 on the differentiation of osteoclasts and the cytokine secreted by them are illustrated in an *in vitro* osteoclast model system to measure the effects on osteoclast precursors (monocytes) and mature osteoclasts in real-time. This is particularly effective for assessing the impact of treatment, where inhibitory effects on differentiation are easily noticeable but might be missed using endpoint-based methods[625]. The xCELLigence uses electrical impedance to measure both cellular adhesion strength and surface area coverage as a combined proxy of cellular proliferation. Cellular impedance assays have an essential role in understanding the pathophysiology of bone resorption and help in understanding the effects of IL-4, IL-10 and IL-13 in lesion development in MM. Real-time data collection is particularly advantageous in studying osteoclast development due to its ability to monitor changes in morphology, such as cell elongation, fusion and migration, which are known characteristics of osteoclast differentiation and development, thus offering a great tool to study the effects of treatment agents on such characteristics, which gives an indication of their efficacy in the overall osteoclast development.

The effects of IL-4, IL-10 and IL-13 were measured, in real-time, which provided qualitative and quantitative measures of cell proliferation, and differentiation *in vitro*. IL-4 and IL-13 significantly reduced the cellular impedance of differentiating monocytes in a dose-dependent manner. In contrast, IL-10 was found to increase cellular impedance. It was also interesting to measure the effects of IL-4, IL-10 and IL-13 on the formation of cellular aggregations by pre-osteoclasts. IL-4 and IL-13 reduced the formation of cellular aggregations; however, only IL-13 caused a statistically significant decrease. This new method for measuring the efficacy of anti-inflammatory cytokines can be utilised for further testing of such cytokines in combination with other mediators and would be especially valuable in drug testing for the early exclusion of compounds from further expensive clinical trial testing.

However, it is crucial to consider maintaining the balance between pro- and anti-inflammatory signals provided by different cell populations, as it allows the maintenance of normal physiology and the suppression of cancer development and progression. Overexpression of anti-inflammatory cytokines can lead to complications such as depression of the immune system, which increases the risk of systemic infection[626,627].

To explore how IL-4 and IL-13 might be exerting their anti-osteoclastogenic effects, there effect on integrin expression was considered. Integrins are transmembrane heterodimers consisting of individual α and β subunits. Many of these recognise and anchor cells to

extracellular matrices, which is highly associated with the transmission of signals across the plasma membrane. In terms of osteoclasts, integrin αVβ3 has been shown to be vital to its matrix recognition and degrative activity of bone[628,629]. Cytokines can also enhance osteoclastogenesis, for example, IL-1, IL-6, and TNFα, which are all suppressed by IL-4 and IL-13. In a previous study, IL-4 was found to be the most potent cytokine to increase β3 mRNA steady-state levels in mice bone marrow, which enhanced the appearance of the plasma membrane αvβ3, which binds with high affinity to vitronectin. In the osteoclast model used here, IL-4, alongside IL-13, significantly reduced α5β1, αVβ3, and α4β5 integrin complexes. This integrin inhibition by IL-4 and IL-13 could prevent the fusion and multinucleation of osteoclast precursors, leading to their dissociation and, ultimately, cell death *in vitro.* Interestingly, a previous study has demonstrated that IL-4 enhanced mRNA levels of β3 by transactivating the β3 gene in mouse bone marrow macrophages, which are known to differentiate into osteoclasts[630]. In contrast, IL-10 did not have the same effect on the integrin complexes tested in this study. In fact, IL-10 seemed to increase the two integrin subunits that make the integrin complex, αVβ3, which, as previously discussed, is the most expressed integrin complex on the plasma membrane of osteoclasts, and it is essential for their resorptive function.

5.5 Conclusion

There appears to be a significant difference in the efficacy of IL-4/IL-13 and IL10 on osteoclast differentiation and activation. Taking these differences in activity into consideration would enable the emergence of more targeted approaches aimed at blocking inflammation. These effects were demonstrated using endpoint methods and, for the first time, in regard to cellular impedance. This technique allowed the effects of IL-4/IL-13 and IL-10 to be observed in real-time without fixing or labelling the cells. We found that IL-4 and IL-13 reduced the impedance of osteoclasts and the object count of pre-osteoclast; in contrast, IL-10 was found to increase the impedance of osteoclasts and increase the object count of pre-osteoclasts. Integrins expressed in osteoclasts were also affected, as IL-4 and IL-13 reduced their expression. These findings should inform the further development and testing of reagents designed to modulate IL-4/IL-13 or their downstream signalling molecules for the treatment of myeloma bone disease. By better understanding their immune-regulatory signalling pathways, new therapeutic strategies for MM and myeloma bone disease can be envisioned that aim to balance and resolve, rather than suppress, bone resorption. Therefore, this project looks for the potential therapeutic agents that would reduce and even block the production of pro-inflammatory cytokines and, moreover, their action on the targets related to bone destruction.

Chapter Six

The Effects of IMiDs and Anti-inflammatory Cytokines on Mononuclear Cells and Myeloma Cell Lines

6.1 Introduction

6.1.1 Bone marrow microenvironment in MM

Bone marrow (BM) is the spongy liquid tissue in the centre of some bones. It accommodates hematopoietic and non-hemopoietic cells and non-cellular components, such as the extracellular matrix and soluble factors, which work together to maintain the haematopoietic stem cell pool and its descendants[631, 632]. It is rich in stem cells, and its main job is making the cells that circulate in the blood[633]. There are two main types of stem cells: mesenchymal and hematopoietic[634,635]. Yellow bone marrow contains mesenchymal stem cells or marrow stromal cells; these produce fat, cartilage and bone. Hematopoietic stem cells (HSCs) in the BM give rise to two main types of cells: myeloid and lymphoid lineage. Cells of the myeloid lineage are monocytes, macrophages, neutrophils, basophils, eosinophils, erythrocytes, dendritic cells and megakaryocytes, or platelets-they form the primary component of the innate immune system and act as the first line of defence against infections[636]. Cells of the lymphoid lineage are T cells, B cells, and NK cells; these cells perform diverse roles in the immune response-cytotoxic T cells kill infected or malignant cells, T helper cells influence the functions of other cells during an immune response, B cells are antibody-producing cells, NK cells kill infected and malignant cells[637,638]. In multiple myeloma, many abnormal plasma cells (myeloma cells), which are a subset of B cells, accumulate in the BM. Normally plasma cells make up less than 2% of the cells in the BM; however, in individuals with MM, abnormal plasma cells make up at least 10% of the cells in the BM[639,640]. They crowd out other blood cells, such as red blood cells, platelets, and white blood cells. As a result, the individual with MM becomes anaemic due to the lack of blood cells, bleeds easily due to lack of platelets, and has more frequent infections due to the lack of white blood cells.

The BM microenvironment (BMM) comprises various cellular elements that play a vital role in the survival, growth and differentiation of normal stem and progenitor cells. It provides the niche that regulates HSCs. Haematopoiesis occurs hierarchically, with more immature multipotent stem and progenitor cells progressively committing into lineage-restricted progenitors before giving rise to mature blood cells. These hematopoietic progenitors also depend on the signals from the BMM for maintenance and differentiation. In addition, the BM is also known to be home to many immune cells. B cells develop from HSCs in the BM and migrate to peripheral lymphoid organs for further maturation[641,642]. Plasma cells present the terminal stage of B cell differentiation. Upon antigen activation, antigen-producing plasma cells return to and reside in the BM until their re-activation to support a humoral response. This process is highly regulated by the expression of chemokine receptors and adhesion molecules (such as integrins and lectins) on plasma cell precursors[643,644]. As terminally differentiated

cells, long-lived plasma cells remain quiescent in the BM, unable to proliferate[645]. Furthermore, they receive signals from multiple cellular niches for their retention and survival.

The BMM is incredibly complex, with multiple cells cooperating to integrate signals and provide input to regulate HSCs, hematopoietic progenitors and blood cell input. Therefore, understanding how the BMM functions is essential for understanding how haematopoiesis is regulated and might lead to the development of therapies that target a specific aspect of the BMM to modulate blood cell production if needed. Most cancers affecting BM are either leukaemias, lymphomas, or MM[646]. The tumour microenvironment is ever-evolving in response to changes in molecular biochemistry, genetic profiling, and cell population types and numbers[647]. The BMM in multiple myeloma is a focal area of research[648]. The BMM is a primary modulator of myeloma disease progression and malignant transformation. This is due to the many properties of BMM, which allow the infiltration, proliferation, growth, adhesion and migration of myeloma cells[648,649]. As well as providing an optimal substrate for myeloma disease initiation and progression, the BM also provides activated inflammatory agents, including cytokines, chemokines and growth factors such as IL-6, TNFα, VEGF, IGF-1, that are secreted by various types of cells present in the BMM[650, 651]. These factors then support the growth, drug resistance and cytotoxicity of various cell types within this microenvironment. The myeloma tumour microenvironment contains several cellular mediators and cell subtypes, including mesenchymal stromal cells, bone cells (such as osteoblasts and osteoclasts), and a variety of other immunomodulatory cell types (such as macrophages, NK cells, regulatory T cells, etc). In addition, immunomodulatory mediators in the BMM, such as osteal macrophages (OsteoMacs) and other immune cells, are also present in the BMM[652]. OsteoMacs (BM resident macrophages; CD68+ in humans)[652] regulate HSCs in the BM niche by directing their homing and colonisation and their transition between active and dormant stem cells[653]. The relapse of MM disease is believed to stem from dormant myeloma cells that are in specific niches. These cells exhibit resistance to treatment and have the capability to repopulate the tumour. Intravital imaging was utilized to track individual myeloma cells as they colonized the endosteal niche, entered a dormant state, and subsequently reactivated to form colonies. The reversibility of myeloma cell dormancy was observed to be instigated by interactions with bone-lining cells or osteoblasts and terminated by the remodeling of the endosteal niche by osteoclasts[653]. Dormant myeloma cells were found to be impervious to chemotherapy targeting dividing cells. The critical role of the endosteal niche in controlling myeloma cell dormancy was demonstrated, emphasizing the potential of targeting extracellular mechanisms to overcome drug resistance and prevent disease relapse. The findings indicated that myeloma cells infiltrated the bone marrow, exited the vasculature, and migrated directly

towards endosteal surfaces, where they arrested in locations containing type-I collagen-expressing osteoblasts or bone-lining cells[653].

Additionally, intravital imaging has provided evidence that RANKL-stimulated osteoclasts exhibit an alternative cell fate by giving rise to daughter cells termed osteomorphs through a process known as fission. Inhibition of RANKL interrupts this cellular recycling mechanism, leading to the accumulation of osteomorphs. Single-cell RNA sequencing analysis has demonstrated that osteomorphs possess a distinct transcriptional profile compared to osteoclasts and macrophages, expressing a unique set of non-canonical osteoclast genes[654]. Deletion of these genes in mice has been associated with structural and functional bone phenotypes. Moreover, genetic variations in human orthologs of osteomorph genes are linked to monogenic skeletal disorders and are correlated with bone mineral density, supporting the notion that osteomorphs play a crucial role in bone resorption regulation and may represent a viable target for therapeutic intervention in skeletal diseases[654].

Other immune cells in the BMM include additional macrophage populations, neutrophils, and myeloid-derived suppressor cells, all of which respond to stress and affect tumour growth, bone turnover, and other BM cells. Regulatory T cells in the BMM create an immune-privileged or immunosuppressive environment that can be corrupted by colonising entities, including some cancer cell types, especially MM[655].

The tumour can re-program immune cells in the BMM to provide optimal conditions for myeloma tumour growth. Myeloid-lineage progenitors have been shown to support myeloma cells both *in vitro* and *in vivo*[656]. Moreover, Gr+CD11b+, also known as myeloid suppressor cells, are composed of immature myeloid cells at the early stages of differentiation[657]. They represent one mechanism of how tumours escape immune system control; they are overproduced in tumour hosts, including cancer patients, infiltrate the tumour microenvironment, and promote tumour angiogenesis by producing angiogenic factors and high levels of MMP-9; the deletion of MMP-9 in these cells eliminates their tumour-supporting ability[658, 659]. Immune cells are often distorted by myeloma cells. Increasing regulatory T cells bring their immune inhibiting capabilities and decrease the number and activity of effector T cells, so down-regulating the tumour-killing cells present in the BMM[660]. Upon tumour invasion, mononuclear cells (MNCs) produce and secrete factors such as IL-6, TNFα, and VEGF, which stimulate the overall mobilisation of endothelial cells and subsequent tumour vascularisation[661]. The interaction between malignant cells and immune cells is critical in determining disease outcomes in cancer patients[662,663]. In multiple myeloma, the functionality of immune cells, such as T cells and natural killer cells, is compromised, resulting in defective antigen-presenting and poor NK cell capacity to kill transformed cells[664].

In advanced cases of MM, myeloma cells can extravasate from the BM leading to extramedullary plasmacytomas and elevated circulating plasma cells in the blood[665,666]. Therefore, detecting the levels of plasma cells in MM is essential for the prognosis of the disease. BM tests (such as using BM aspirate and/or biopsy) are performed routinely to diagnose multiple myeloma and for monitoring during the course of treatment. The importance of evaluating plasma cell infiltrates in BM aspirates, and BM biopsy slides in diagnosing and monitoring the course of MM and their effect on patient survival has been demonstrated in many studies[667, 668, 669, 670]. The BM aspirate/biopsy provides information about the amount of the disease, the aggressiveness of the disease, and the molecular and genetic abnormalities that help predict the disease course[671]. Additionally, BM tests, in the form of aspirates and biopsies, are performed routinely to monitor the course of treatment[672]. BM aspirate, and BM core biopsy are methods to collect liquid and solid parts of the BM. In aspiration, a syringe draws out the liquid part of the marrow (a BM aspirate)[673]. For biopsy collection, a 1-2 cm core of BM tissue is removed in one piece (a BM trephine biopsy). The BM samples are usually taken from the pelvic bone. A needle is inserted through the skin into the bone, and a sample is drawn up through a syringe. The procedure is performed under local anaesthetic with or without sedation (see Figure 6.1). The necessary tests provide samples for the direct means of examining the myeloma cells under the microscope[674]. Other markers can be used in other tests to allow the identification of myeloma progression. Furthermore, abnormal plasma cells in the BM secrete large amounts of a single type of antibody, known as M-protein (also known as paraprotein), which has no useful function. As mentioned in *1.2.2 Myeloma-defining events,* these M-proteins can be measured in blood and urine for diagnosis, prognosis, treatment response, and to detect relapsed cases. BM tests are also essential to determine the presence and amount of myeloma cells in the BM in proportion to the other blood cells [675].

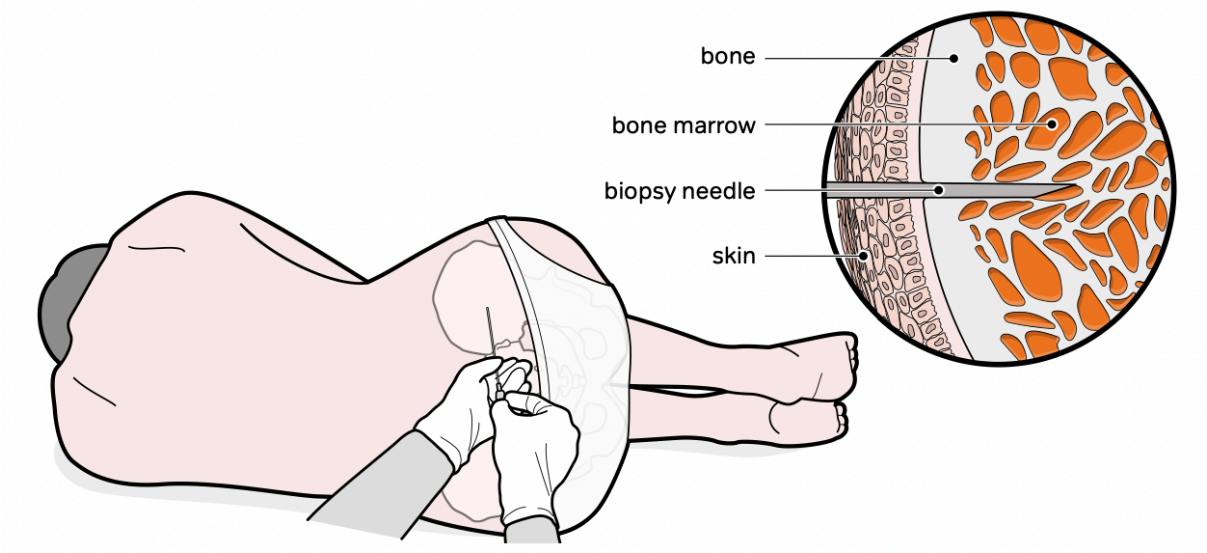

Figure 6.1 Bone marrow aspirate sample being taken from the pelvic bone.
A bone marrow needle is inserted into the patient's hip bone. Samples of blood (bone marrow aspiration) and bone marrow (biopsy) are removed for examination. Image adapted from myeloma.org.uk.

Chemokine receptors are named based on the type of chemokine they bind. In multiple myeloma, levels of a number of chemokines are found to be elevated in bone marrow infiltrating macrophages, and the levels of these chemokines are positively correlated with the percentage of BM-infiltrating macrophages[676]. These include CCL-3 (macrophage inflammatory protein-1 α, MIP-1α, is a direct stimulator of osteoclastogenesis.), CCL2 and CCL14 (promoting chemotaxis of monocytes into the bone marrow) [677–680]. Bone-homing tumour cells tend to overexpress several chemokine receptors. Here, the expression of three chemokine receptors is determined using the monocyte panel described in Chapter 6.2.13. CCR2, as it appears to be important in the mobilisation of monocytes from the bone marrow to the blood in normal conditions and in response to inflammation[64]; CCR10, as its expression is elevated in peripheral blood of patients with inflammatory conditions, such as RA[681,682]; and, CX3CR1, as it is essential for monocyte homeostasis and cell survival under normal conditions, and is associated with immune cell infiltration and interact with the tumour microenvironment in cancer by regulating monocyte polymerisation[683,684].

CD71 (transferase receptor 1) was another receptor that was of interest to study. It is an integral membrane glycoprotein that plays a major role in the cellular uptake of iron. It was chosen as it is known to be a marker for cell proliferation and activation. It has been used as a successful marker to diagnose acute erythroid leukaemia (AEL) by flow cytometry. In a study

investigating CD71 expression, it was found to be an indicator of cell proliferation activity in haematological malignancies generally and MM specifically[685].

6.1.2 Rationale

1) Total human mononuclear cells (MNCs) derived from the peripheral blood and the BM aspirates of individuals with multiple myeloma were chosen as the study material. Reasons for this were: (i) MNCs provide a cell model to quickly reveal the effects of IMiDs on the cells in the tumour microenvironment to provide an understanding of interactions of cells with plasma cells and understanding of the effects of IMiDs on cells directly in the tumour microenvironment, this effect will be compared to the results obtained from myeloma-related cell lines; (ii) clonal plasma cells detected in the peripheral blood of newly diagnosed multiple myeloma patients have been associated with adverse prognostic features and poor overall survival[686]; they reflect tumour burden in newly diagnosed multiple myeloma. A new study shows that CCPC quantification at diagnosis provides a powerful prognosis factor for newly diagnosed myeloma patients[687] and is associated with a worse prognosis in myeloma patients[688]; (iii) the interactions between malignant plasma cells and their microenvironment are essential for MM pathogenesis. The binding of MM cells to the BM stromal cells triggers the expression of adhesion molecules, cytokines, and chemokine, promoting growth, drug resistance and migration of cancer[689]. BM mononuclear cells (BM-MNCs) are a rich source of haematopoietic stem cells and have been used widely in experimental therapies for patients with ischemic disease. BM-MNCs activate angiogenesis, and this is believed to be one major BM-MNC mode of action[690]. Therefore, BM-MNCs and CCPC will provide a model for studying the effects of current anti-myeloma treatments (IMiDs) to further understand their mechanism of action to optimise their therapeutic potential.

6.1.3 Hypothesis

i) IMiDs are effective in reducing inflammatory cytokines in MNCs derived from early-diagnosed patients.

ii) The anti-inflammatory cytokines IL-4, IL-10 and IL-13 are effective in reducing inflammatory cytokines in MNCs derived from early-diagnosed patients.

6.2 Experimental procedures

6.2.1 Samples

Fresh human peripheral blood and BM biopsy aspirates from newly diagnosed myeloma patients were collected into heparinised Vacuettes™ (Greiner Bio-one, Frickenhausen, Germany). Peripheral blood from healthy donors was used as well. All samples were prepared as detailed in *2.4 Sample collection and preparation.* Ethical approval for all groups was provided by a Health Research Authority (HRA) Research Ethics Committee (13/WA/0190 – healthy volunteers; 20/WM/0037 –myeloma patients). Informed written consent was obtained from all donors.

6.2.2 Mononuclear cell isolation

Mononuclear cells (MNCs) were isolated as described as per sections 2.4.1 and 2.4.2. Cell density was determined using the Countess® automated cell counter (Life Technologies) and MNCs were then cultured in cell culture media (RPMI Glutamax/10% FBS HyClone/0.2% 2-ME) +/- LPS (Ultrapure, 10ng/mL; InvivoGen, San Diego, USA) at 37 °C in 5% CO2-in-air for 24 hours. Additional treatments were added for the duration of the 24-hour incubation. After 24 hours, cultures were centrifuged at 515 *x g* for 7 minutes and cell-free supernatants were removed and stored at -20 °C until analysis of cytokines by ELISAs.

6.2.3 Monocyte isolation and purity check using flow cytometry

Monocytes were isolated, as in *2.4.3 Monocyte isolation*, prior to seeding on chamber slides for visualisation. An anti-CD14 antibody (Clone 61D3; fluorophore eFluor®450; isotype mIgG1) was added to 100,000 monocytes to check monocyte purity as detailed in *2.6 monocyte purity*. Data analysis post-acquisition was interpreted using FlowJo Version 1.3 (Tree Star, Oregon, USA). Purity ≥ 92% was accepted for downstream experiments.

6.2.4 Adhesion to the chamber slides

To ensure the adherence of monocytes to the chamber slides prior to staining, Cell-Tak was used, as detailed in *2.12 Adhesion of cells using Cell-Tak*.

6.2.5 Confocal Microscopy

Primary cells were adhered on Millicell EZ 8-well chamber slides (Merck Millipore, Massachusetts, USA) in cell culture media. Samples were prepared for confocal microscopy as per *2.13 Confocal microscopy*. Cells were visualised at 20 X magnification using a laser

scanning confocal microscope (Zeiss LSM720, Oberkochen, Germany). Image analysis was performed using ImageJ Software.

6.2.6 Enzyme-linked immunosorbent assay (ELISA)

Analysis of cytokines using ELISA was carried out as in *2.6 Enzyme-Linked Immunosorbent Assay (ELISA)*. The ELISA kits used in this chapter were to detect levels of IL-6, TNFα, and MMP-9 secreted by MNCs +/- LPS (DuoSet; R&D systems; Biotechne).

6.2.7 Gating strategy for selection of monocytes

Monocytes within MNC preparations isolated from peripheral blood and bone marrow of early-diagnosed myeloma patients were analysed using flow cytometry (Figure 6.2). Forward scatter (FSC) and (SSC) plots allowed for the rough selection of monocytes according to their size and granularity profile. Single cells were selected next, and then CD14 expression was used to confirm that monocytes were selected from the MNC population. The CD14 and CD16 expression of the monocytes was then used to determine the individual subsets: CD14++CD16++ (classical monocytes), CD14++CD16+ (intermediate monocytes) and CD14+CD16++ (non-classical). Median fluorescence intensity (MFI) or percentage of positive cells was then used to analyse phenotypic markers. A more detailed analysis of the monocytes was made using the antibodies in the monocyte phenotypic panel shown in Table 6.1.

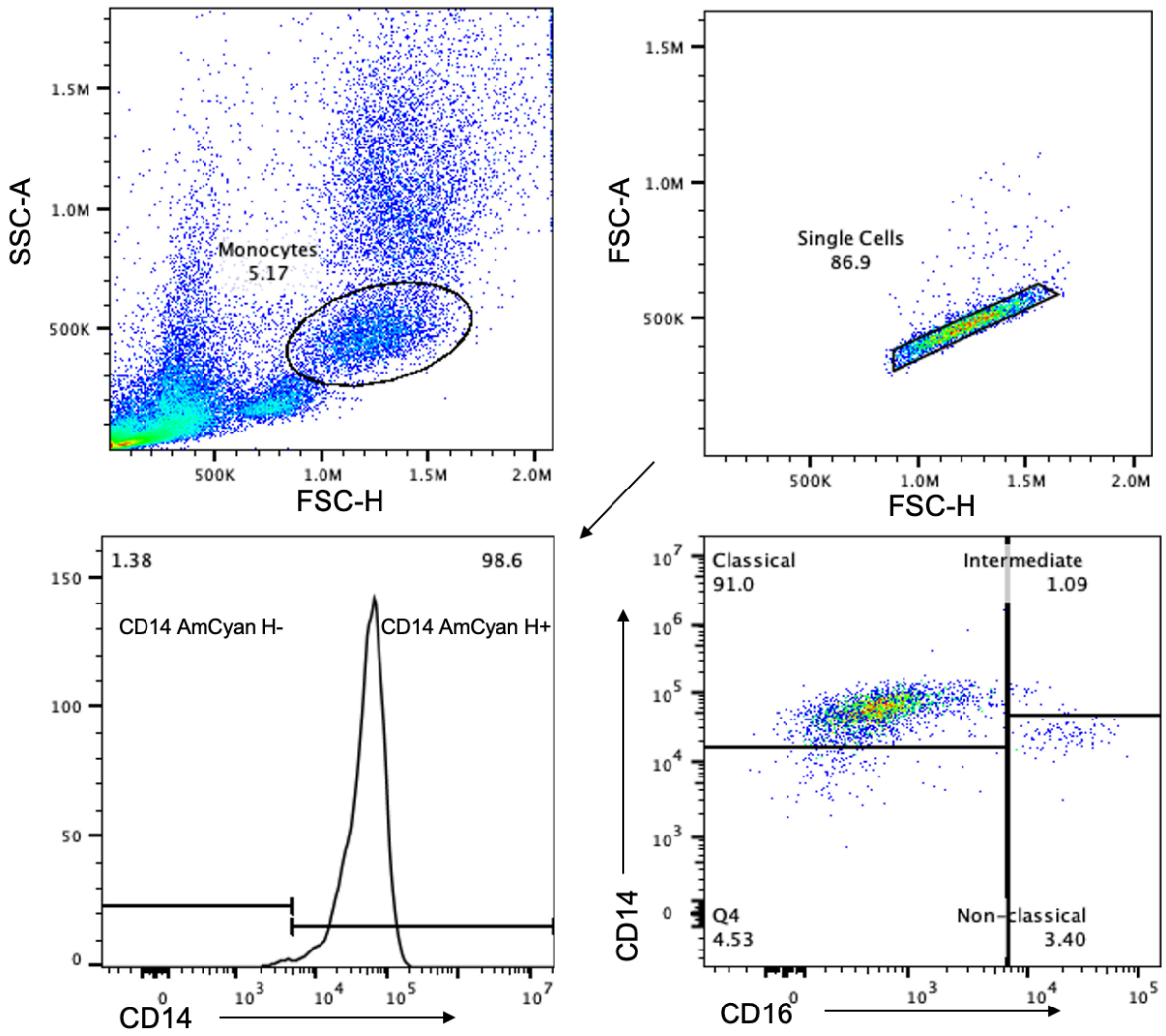

Figure 6.2 Gating strategy for the selection of monocytes and their subsets in MNCs. *Monocytes were identified using an FSC-H vs SSC-H dot plot according to their size and granularity. Singlets were selected using FSC-H vs FSC-A dot plot. A histogram visualising the CD14 expression enables the gating on the CD14-positive peak. Monocyte subsets were then identified according to their CD14/CD16 profile.*

Antibody	Fluorochrome	Isotype	Clone	Company
CD14	Brilliant Violet 510	Mouse IgG2a, k	M5E2	Biolegened
CD16	Brilliant violet 771	Mouse IgG1, k	3G8	Biolegened
CD3	FITC	Mouse igG2a, k	BW264/56	Miltenyi Biotec
CD4	FITC	Human IgG1	REA623	Miltenyi Biotec
CD8	FITC	Human IgG1	REA734	Miltenyi Biotec
CD15	FITC	Mouse IgM	VIMC6	Miltenyi Biotec
CD19	FITC	Mouse IgG1, k	LT19	Miltenyi Biotec
CD20	FITC	Human IgG1	REA780	Miltenyi Biotec
CD34	FITC	Mouse IgG2a, k	AC136	Miltenyi Biotec
CD56	FITC	Human IgG1	REA196	Miltenyi Biotec
FceR1	FITC	Mouse IgG2b, k	CRA1	Miltenyi Biotec
CD36	Brilliant Violet 421	Mouse IgG2a, k	5-271	Biolegened
CD71	Brilliant Violet 650	Mouse IgG2a, k	Cy1G4	Biolegened
CD98	APC	Human IgG1	REA387	Miltenyi Biotec
CD220	PE	Human IgG1	REA260	Miltenyi Biotec

Table 6.1 Antibodies were used for the phenotypic analysis of monocytes.

The list includes their fluorochrome, isotype, clone and manufacturer.

6.2.8 Gating strategy for selection of B cells

B cells within MNCs isolated from peripheral blood and bone marrow of early-diagnosed myeloma patients were analysed using flow cytometry (Figure 6. X). Forward scatter (FSC) and (SSC) plots allowed for the rough selection of lymphocytes according to their size and granularity profile. Single cells were selected next. A dump channel allowed the combined exclusion of T cells, NK cells, and monocytes; CD19-positive expression allowed the selection of B cells from the lymphocyte population. Identification of specific subsets was performed by further sequential gating upon surface expression of various markers. CD27 and IgD expression was used to determine the individual subsets: naïve, class-switched and non-class-switched memory. Finally, plasmablasts were identified as CD38-positive and CD20-negative, making up bout 0.1 % of all B cells. Median fluorescence intensity (MFI) or percentage of positive cells was then used to analyse phenotypic markers. The antibodies used in the B cell phenotypic panel are shown in Table 6.2.

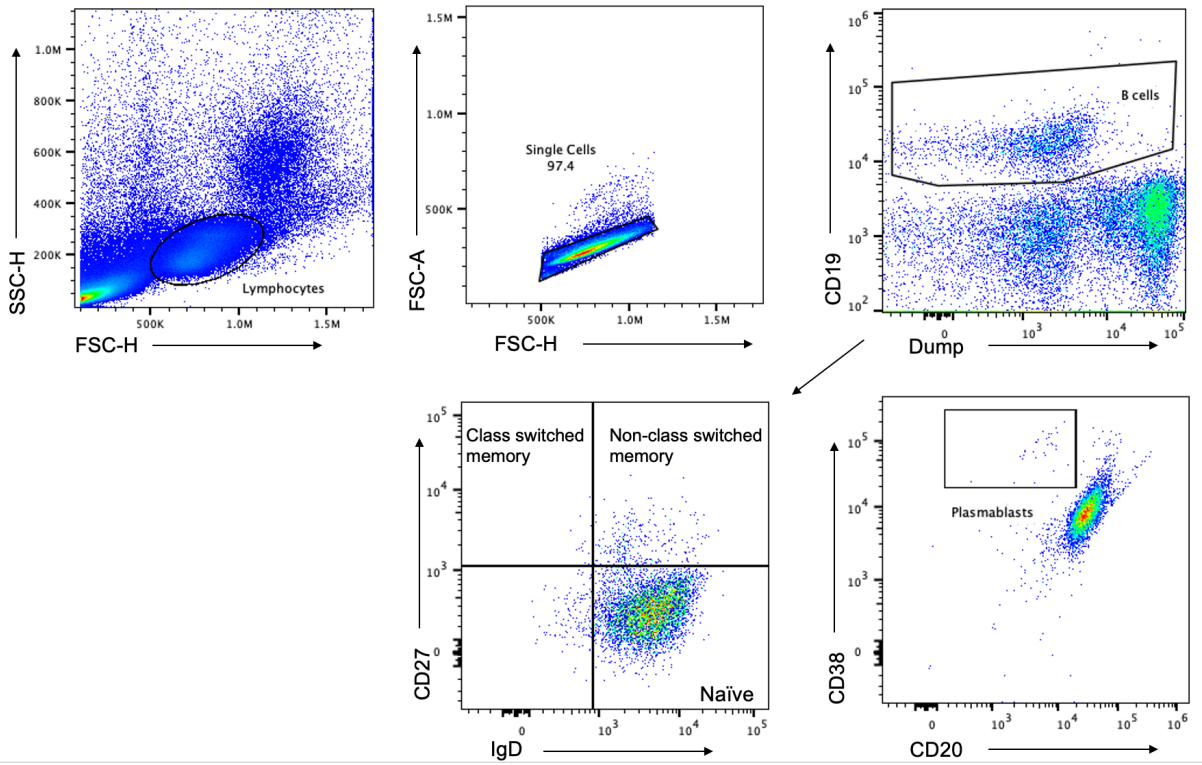

Figure 6.3 Gating strategy for selecting B cells and their subsets in MNCs.

Lymphocytes were identified using an FSC-H vs SSC-H dot plot according to their size and granularity. Singlets were selected using FSC-H vs FSC-A dot plot. B cells were identified as CD19-positive and CD3, CD14 and CD56-negative (FITC Dump). CD27 and IgD allowed the identification of class switched and non-class switched memory and naïve B cells. CD20 and CD38 allowed the identification of plasmablasts (plasma cells).

Antibody	Fluorochrome	Isotype	Clone	Company
CD19	Pacific blue	Mouse IgG1, k	HIB19	Biolegened
CD3	FITC	Mouse igG2a, k	BW264/56	Miltenyi Biotec
CD14	FITC	Mouse IgG1, k	HCD14	Biolegened
CD56	FITC	Human IgG1	REA196	Miltenyi Biotec
CD27	PE-Vio 770	Mouse IgG1, k	M-T271	Miltenyi Biotec
IgD	Brilliant Violet 785	Mouse IgG2a, k	IA6-2	Biolegened
CD38	APC	Mouse IgG1, k	HB-7	Miltenyi Biotec
CD20	APC-Cy7	Human IgG2b, k	2H7	Biolegened
CD36	PE	Mouse IgG2a, k	5-271	Biolegened
CD98	PE	Human IgG1	REA387	Miltenyi Biotec

Table 6.2 Antibodies used for the phenotypic analysis of B cells.

The list includes their fluorochrome, isotype, clone and manufacturer.

6.2.14 Statistics

Statistical analysis was performed using GraphPad Prism version 9.4.1 (USA). Data are presented as the mean +/- standard error of the mean (SEM). A one-way ANOVA was used to compare the production of TNFα, IL-6 and MMP-9 by PB and BM MNCs. Statistical analysis for the monocyte and the B cell panel data was determined using a Mann-Whitney test.

All experiments have replicated sample sizes of at least n=3 (except for LPS-activated PB and BM monocytes n=1; confocal images of BM monocytes n=2), and significant values were taken as $p < 0.05$ graphically denoted as * $p \leq 0.05$, ** $p \leq 0.01$, *** $p \leq 0.001$ and **** $p \leq 0.0001$.

6.3 Results

6.3.1 The effect of IMiDs on primary cells derived from healthy donors and newly diagnosed myeloma patients

The LPS-stimulated cytokine output by MNCs isolated from healthy individuals and PB and BM MNCs derived from early diagnosed myeloma patients in the presence of IMiDs (1 and 10 μM) was analysed using ELISA. All the IMiDs reduced the production of TNFα in all three-study groups – peripheral blood from healthy and MM patient, and bone marrow for MM patient. Pomalidomide caused a dose-dependent, statistically significant decrease in TNFα production in peripheral blood MNCs isolated from healthy individuals ($p = 0.0294$) (Figure 6.4 A). No significant decrease was observed with lenalidomide- and thalidomide-treated MNCs. Both lenalidomide and pomalidomide were statistically significant in reducing TNFα produced by peripheral blood MNCs isolated from myeloma patients (lenalidomide $p = 0.0167$; $p = 0.0138$ and pomalidomide $p = 0.0061$; $p = 0.0042$) (Figure 6.4 B); pomalidomide displayed a more significant decrease than lenalidomide at both doses used. Pomalidomide was the only IMiD to significantly decrease TNFα production in MNCs isolated from the BM aspirates (Figure 6.4 C) at both doses ($p = 0.0268$; $p = 0.0223$).

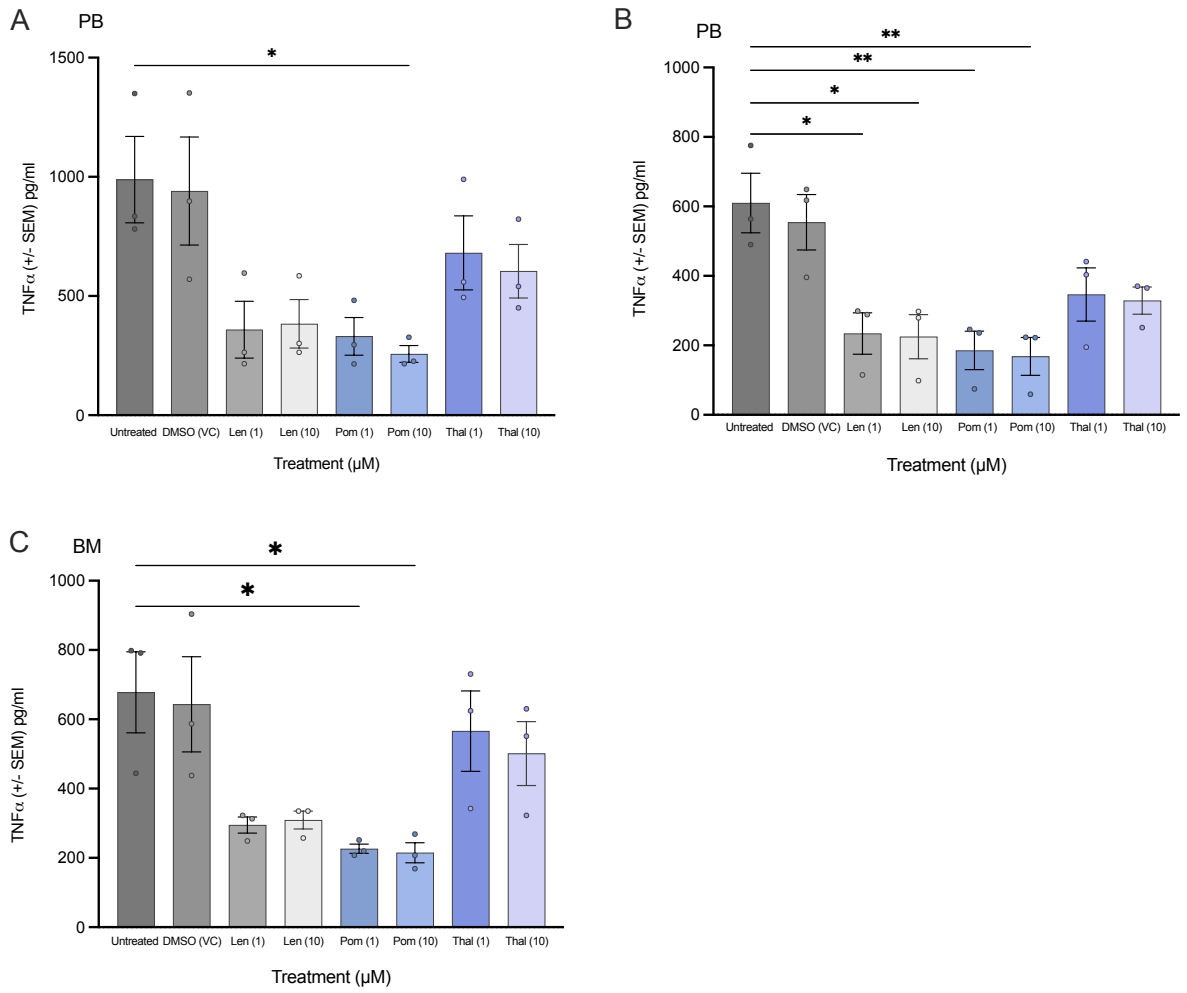

Figure 6.4 TNFα production is reduced in a dose-dependent manner upon IMiD treatment.

*MNCs from peripheral blood of (A) healthy individuals and (B) myeloma patients and MNCs derived from (C) bone marrow of individuals with multiple myeloma were stimulated with LPS (10 ng/ml) in the presence of 1 or 10 μM of each IMiD: lenalidomide (Len), pomalidomide (Pom) or thalidomide (Thal). TNFα (mean pg/ml ± SEM) was measured using a specific ELISA in cell free supernatants harvested after 24 hours. PB= peripheral blood, BM= bone marrow. Statistics were performed with a one-way ANOVA and Dunnett's multiple comparisons test. Data are from n=3 independent experiments: * $p \leq 0.05$, ** $p \leq 0.01$.*

We next examined the effects of these treatments on the levels of IL-6 in MNCs derived from healthy individuals and peripheral blood and bone marrow of early-diagnosed myeloma patients. Levels of LPS-stimulated IL-6 were decreased upon treatment of MNCs isolated from peripheral blood of healthy individuals with lenalidomide and pomalidomide at both doses (1 and 10 μM) (lenalidomide p = 0.002; 0.0016 and pomalidomide p = 0.0004; 0.0004, respectively) (Figure 6.4 A) but no significant effect was observed for thalidomide (Figure 6.5

A). In contrast, no statistically significant decrease was observed in the levels of LPS-stimulated IL-6 in MNCs isolated from the peripheral blood (Figure 6.5 B) and BM aspirates (Figure 6.5 C) from early diagnosed myeloma patients was observed in the presence of any of the IMiDs.

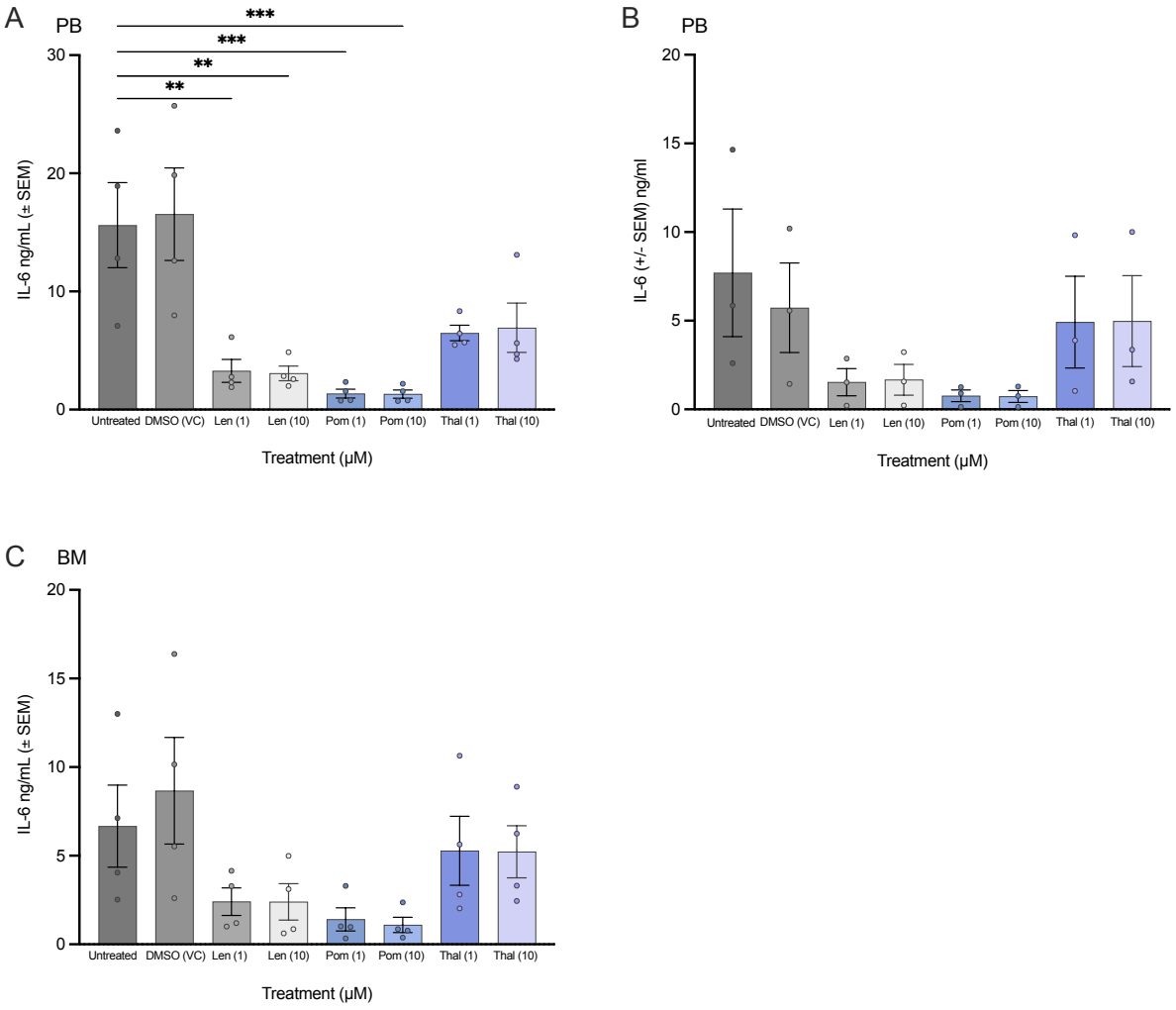

Figure 6.5 IL-6 production is reduced in a dose-dependent manner upon IMiD treatment. *MNCs from peripheral blood of (A) healthy individuals and (B) myeloma patients and MNCs derived from the (C) bone marrow of individuals with multiple myeloma were stimulated with LPS (10 ng/ml) in the presence of 1 or 10 μM of each IMiD: lenalidomide (Len), pomalidomide (Pom) or thalidomide (Thal). IL-6 (mean ng/ml ± SEM) was measured using a specific ELISA in cell free supernatants harvested after 24 hours. PB= peripheral blood, BM= bone marrow. Statistics were performed with a one-way ANOVA and Dunnett's multiple comparisons test. Data are from n≥3 independent experiments expressed as the mean ± SEM: ** $p \leq 0.01$, *** $p \leq 0.001$.*

6.3.2 The effect of IL-4, IL-10, and IL-13 on primary cells derived from healthy donors and newly diagnosed myeloma patients

The inhibitory activities of IL-4, IL-10 and IL-13 in the presence of LPS were compared using MNCs derived from the peripheral blood of healthy individuals and the peripheral blood and bone marrow of early-diagnosed patients. In general, TNFα levels were lower by cells isolated from MM patients in comparison to healthy volunteers. As shown in Figure 6.6 A, IL-4 and IL-13 at 30 ng/mL significantly reduced the levels of LPS-stimulated TNFα from healthy MNCs ($p = 0.0329$ and $p = 0.0239$). For MNCs from peripheral blood of early diagnosed myeloma patients, it was IL-4 and IL-10 at 30 ng/mL that significantly reduced TNFα production ($p = 0.0470$ and $p = 0.0380$, respectively) (Figure 6.6 B), with IL-13 not having a significant effect. In the case of bone marrow treated with the anti-inflammatory cytokines at similar concentrations (10 and 30 ng/mL), a statistically significant effect of IL-10 and IL-13 in the reduction of TNFα was noticed at 30 ng/mL ($p = 0.0264$ and $p = 0.0219$) (Figure 6.6 C); in contrast, the effect of IL-4 was not statistically significant.

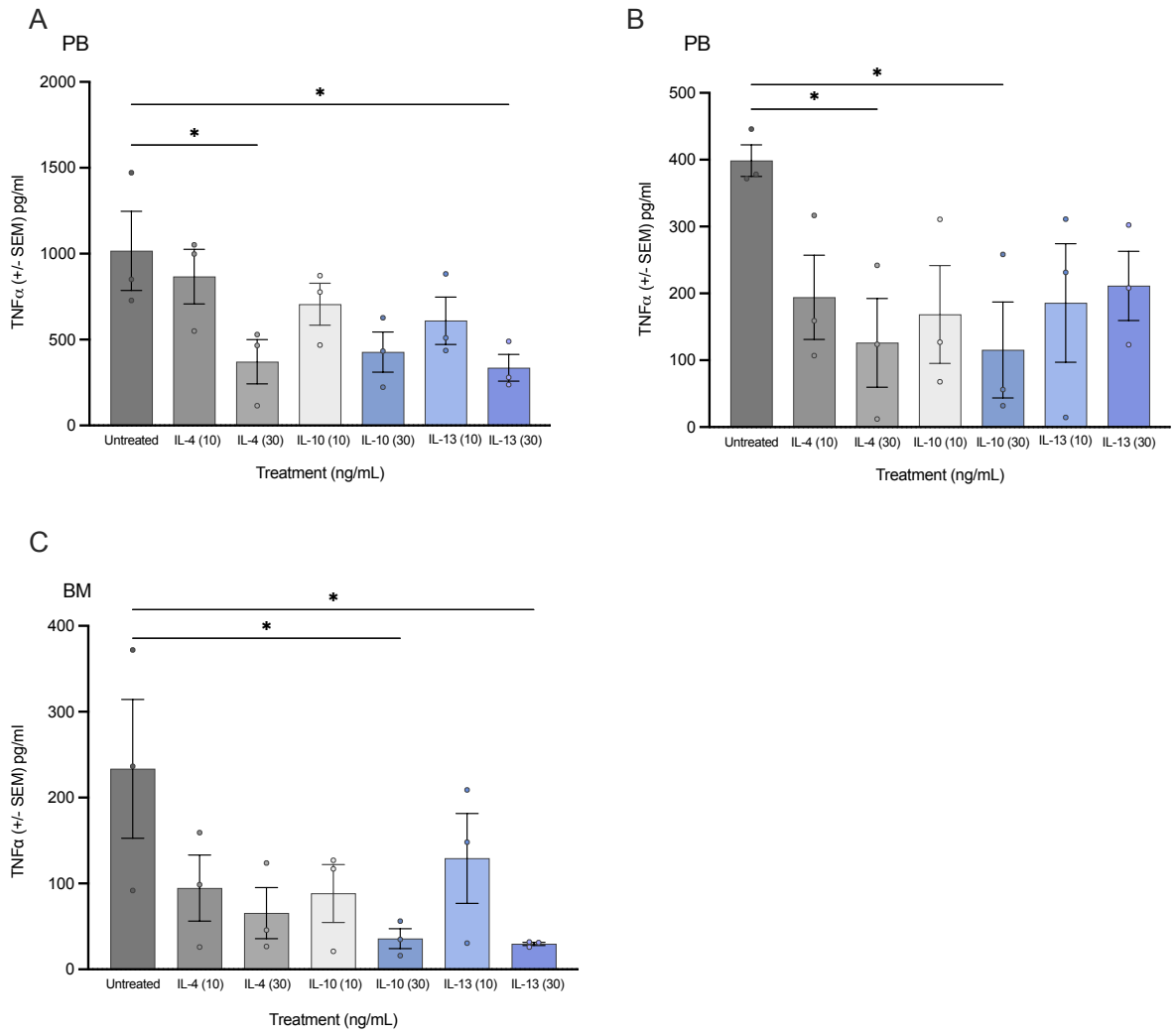

Figure 6.6 LPS-stimulated TNFα upon treatment with IL-4, IL-10 and IL-13 on MNCs derived from the peripheral blood and bone marrow aspirates of early-diagnosed myeloma patients.

*MNCs from peripheral blood of (A) healthy individuals and (B) myeloma patients; MNCs derived from the (C) bone marrow of individuals with multiple myeloma were stimulated with LPS (10 ng/ml) in the presence of 1 or 10 μM of each IMiD: lenalidomide (Len), pomalidomide (Pom) or thalidomide (Thal). TNFα (mean pg/ml ± SEM) was measured using a specific ELISA in cell free supernatants harvested after 24 hours. PB= peripheral blood, BM= bone marrow. Statistics were performed with a one-way ANOVA and Dunnett's multiple comparisons test. Data are from n=3 independent experiments: * $p \leq 0.05$, ** $p \leq 0.01$. Data are from n=3 independent experiments expressed as the mean ± SEM: * $p \leq 0.05$.*

Next, the effects of these treatments on the levels of IL-6 in MNCs derived from healthy individuals and peripheral blood and bone marrow of early-diagnosed myeloma patients was determined. Figure 6.7 A shows that IL-4 (at 30 ng/mL), IL-10 (at 30 ng/mL), and IL-13 (at 10 and 30 ng/mL) effectively reduced IL-6 levels in MNCs derived from PB of healthy donors (IL-4 p = 0.0420, IL-10 p = 0.0207, and IL-13 p = 0.0126; p = 0.0014). For MNCs from PB of MM donors, IL-4 and IL-13 at 30 ng/mL effectively reduced IL-6 levels (IL-4 p = 0.0051 and IL-13 p = 0.0312; p = 0.0153), whereas IL-10 did not have a significant effect at a similar concentration. IL-13 was the only anti-inflammatory cytokine to significantly reduce LPS-stimulated IL-6 production at both 10 ng/mL and 30 ng/mL (Figure 6.7 B). The anti-inflammatory cytokines were ineffective in reducing IL-6 production in MNCs from the bone marrow of early-diagnosed myeloma patients (Figure 6.7 C).

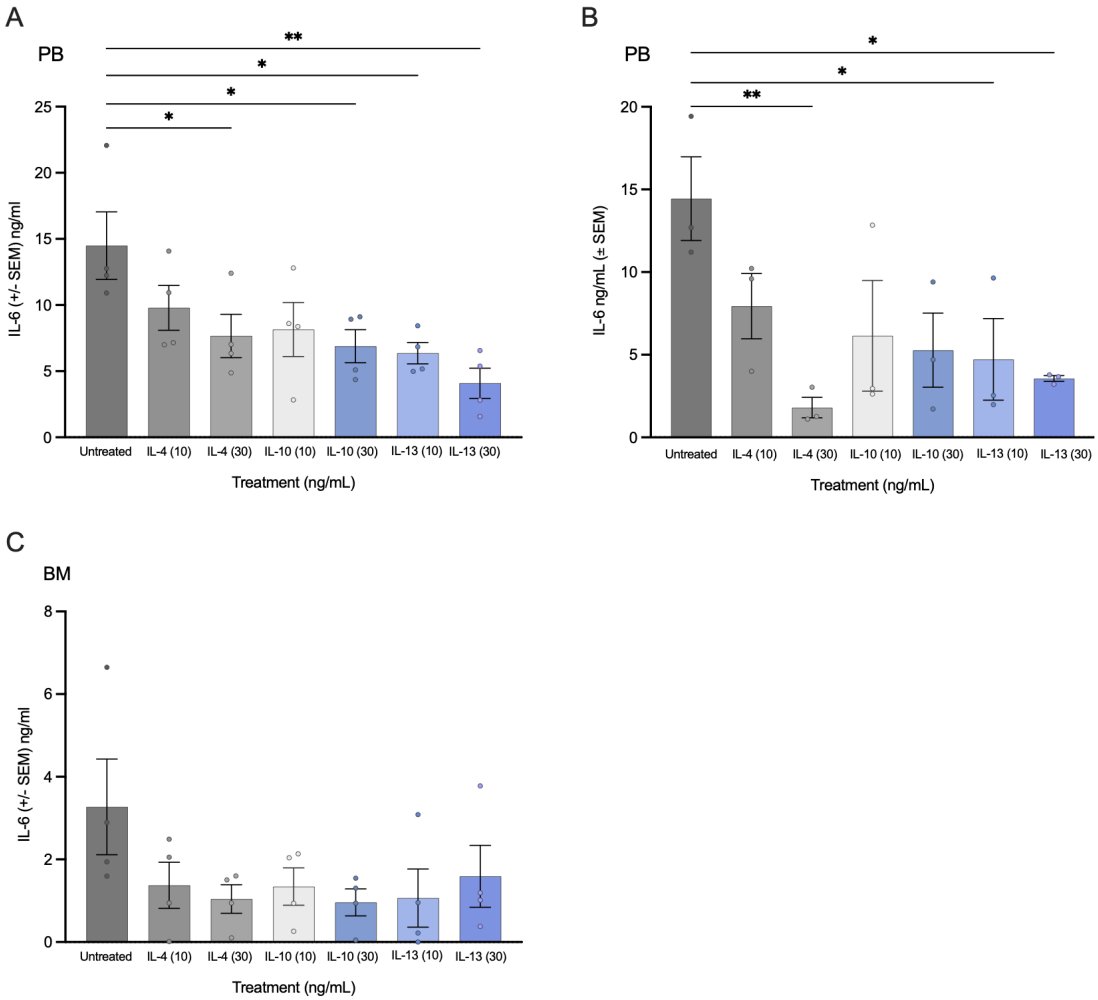

Figure 6.7 LPS-stimulated IL-6 upon treatment with IL-4, IL-10 and IL-13 on MNCs derived from the peripheral blood and bone marrow aspirates of early-diagnosed myeloma patients.

*MNCs from peripheral blood of (A) healthy individuals and (B) myeloma patients; MNCs derived from the (C) bone marrow of individuals with multiple myeloma were stimulated with LPS (10 ng/ml) in the presence of 10 or 30 ng/mL of each anti-inflammatory cytokine: IL-4, IL-10 or IL-13. IL-6 (mean ng/ml ± SEM) was measured using a specific ELISA in cell free supernatants harvested after 24 hours. PB= peripheral blood, BM= bone marrow. Statistics were performed with a one-way ANOVA and Dunnett's multiple comparisons test. Data are from n=3 independent experiments: * $p \leq 0.05$, ** $p \leq 0.01$.*

6.3.3 IMiDs and IL-4, IL-10, and IL-13 do not affect MMP-9 expression by MNCs derived from the bone marrow of newly diagnosed myeloma patients

Finally, the levels of MMP-9 were measured upon LPS stimulation of bone marrow MNCs from early-diagnosed myeloma patients in the presence of either the IMiDs at 1 and 10 μM or IL-4,

IL-10 and IL-13 at 10 and 30 ng/mL for 24 hours. Cell free supernatants were harvested after 24 hours and analysed using a specific ELISA. There was no statistically significant decrease when treated with the IMiDs although pomalidomide at 10 μM displays a reduction in MMP-9 production (Figure 6.8 A). There were no inhibitory effects of IL-4, IL-10, and IL-13 on MNCs derived from BM aspirates. In fact, an increase is observed with IL-10; however, this increase was not significant (Figure 6.8 B).

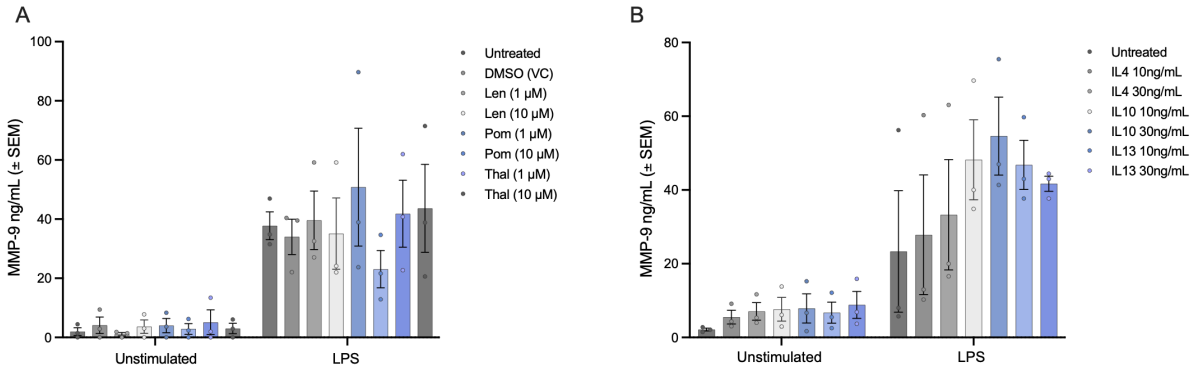

Figure 6.8 MMP-9 levels of bone marrow-derived MNCs are unaffected by IMiDs and IL-4, IL-10 and IL-13.

MNCs derived from the bone marrow of individuals with multiple myeloma were stimulated with LPS (10 ng/ml) in the presence of either 1 or 10 μM of each IMiD: lenalidomide (Len), pomalidomide (Pom) or thalidomide (Thal) (A); 10 or 30 ng/mL of each anti-inflammatory cytokine: IL-4, IL-10 or IL-13 (B). MMP-9 (mean ng/ml ± SEM) was measured using a specific ELISA in cell free supernatants harvested after 24 hours. PB= peripheral blood, BM= bone marrow. Statistics were performed with a two-way ANOVA and Dunnett's multiple comparisons test. Data represented n=3 independent experiments expressed as the mean ± SEM.

6.3.4 Immunophenotyping of monocytes from peripheral blood and bone marrow by flow cytometry

As discussed in *1.4 monocytes in multiple myeloma*, monocytes are heterogenous and vary with the inflammation status of the donor. As MM and its associated side effects indicate a state of heightened inflammation[688], the levels of the different subunits of monocytes in the PB and the BM needed to be considered. Figure 6.9 illustrates the expression of CD14 and CD16 in MNCs derived from the PB and BM of individuals with MM. A similar expression of CD16 was observed in PB and the BM, whereas a decrease was observed in the expression of

CD14 monocytes derived from the BM in comparison to PB. However, this was not statistically significant. Using the monocyte subset panel detailed in 6.2.13, the identification of monocyte subsets was first determined using CD14 and CD16 and expression, followed by further markers and sequential gating.

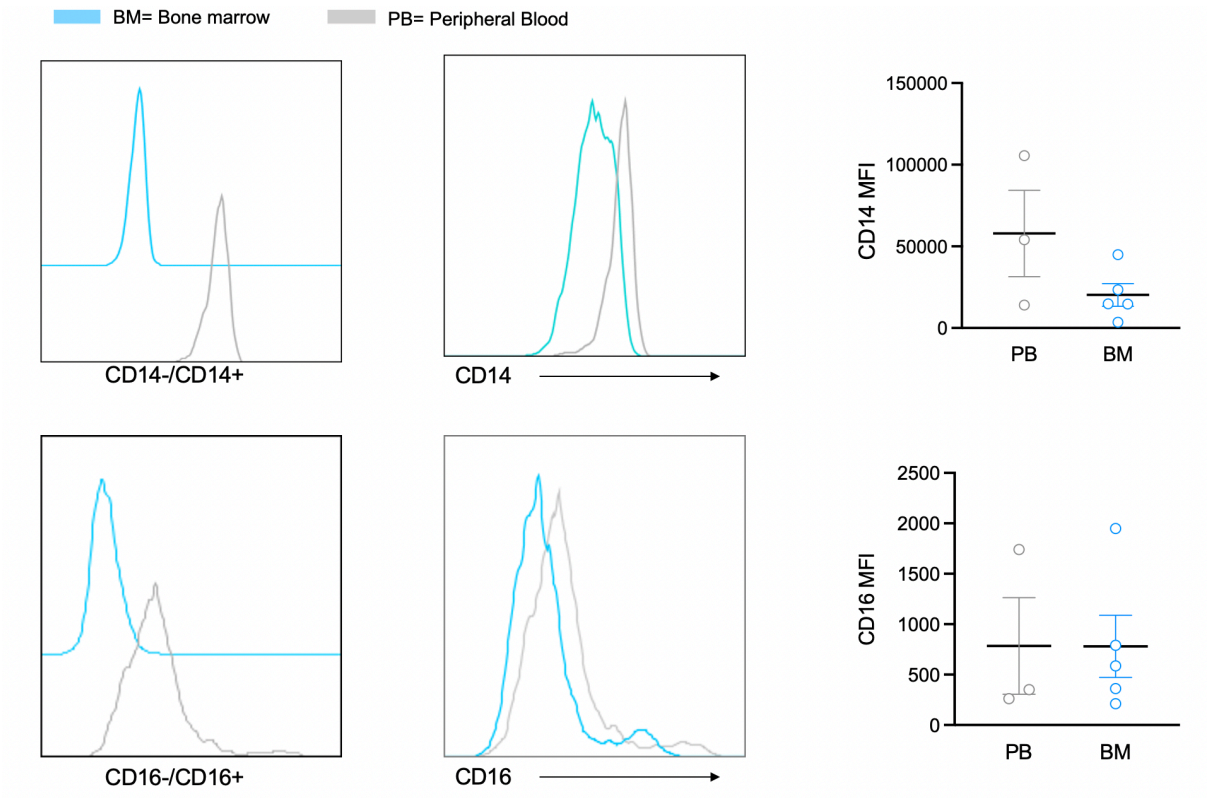

Figure 6.9 The expression of CD14 and CD16 monocytes in MNCs derived from PB and BM of people newly diagnosed with multiple myeloma.

MNCs derived from PB (grey), and BM (blue) were isolated, and monocytes were identified as per 6.2.13. Example histograms are shown of the stained and unstained samples of CD14 and CD16. An example histogram for each group is shown next and the summary data are shown on the right as scatter plots. Data represented PB n=3; BM n=5 independent experiments expressed as the mean ± SEM. Statistical analysis was determined using a Mann-Whitney test.

To investigate if there is a change in monocyte subsets, the percentage of classical (CD14++CD16-), intermediate (CD14++CD16+), and non-classical (CD14CD16++) monocytes in PB and BM MNCs was compared next. The percentage of classical monocytes appears to be increased in PB in comparison to BM. However, this was not a statistically

significant increase (Figure 6.10 A). The percentage of intermediate and non-classical monocytes appear to be similar in PB and BM (Figure 6.10 B and 6.10 C, respectively).

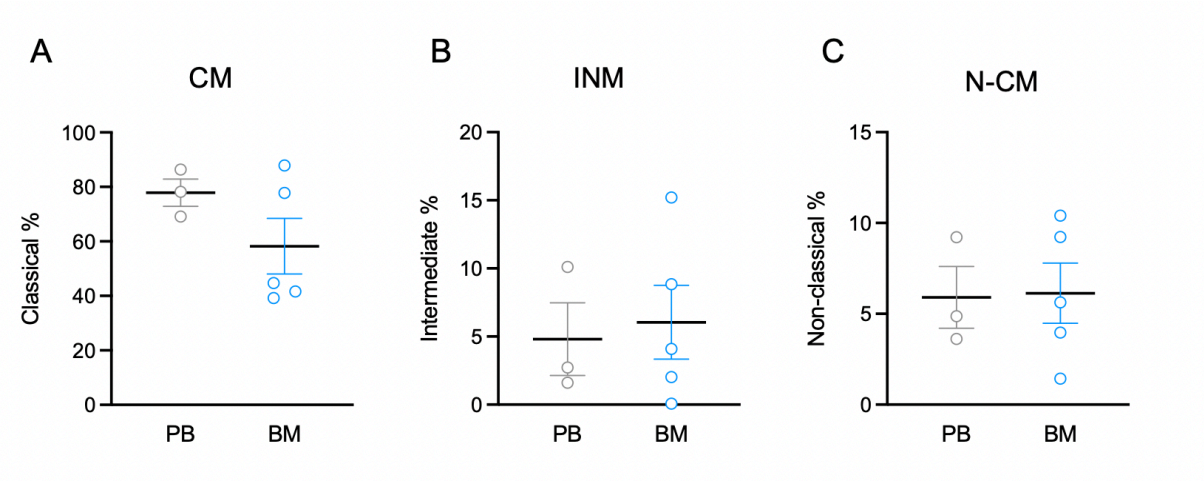

Figure 6.10 The percentage expression of monocyte subsets in PB and BM of early-diagnosis myeloma patients. *The percentage of the different monocyte subsets ((A) classical = C; (B) intermediate = INM; (C) non-classical = N-CM) was determined by flow cytometry of the MNCs as described in 6.2.13. Data represented n=3-5 independent experiments expressed as the mean ± SEM. Statistical analysis was determined using a Mann-Whitney test.*

Monocytes express chemokine receptors of every known chemokine receptor family. However, receptor expression differs between the subsets, thus making them receptive to various chemokines resulting in differential functional consequences[692]. Chemokines can be split into four subfamilies with two major subfamilies consisting of CC with two cysteines next to each other and CXC with two cysteines separated by one amino acid: CC, CXC. The minor subfamilies consist of CX_3C; two cysteines separated by three amino acids, and XC, with the first cysteine, lacking. In humans, there are 27 CC chemokines, 17 CXC chemokines, 2 XC chemokines and 1 CX3C chemokine[693].

A decrease was observed with the expression of BM CCR10 (Figure 6.11 A), CCR2 (Figure 6.11 B), and CX3CR1 (Figure 6.11 C) when compared to the PB, with the most noticeable decrease observed with BM CX3CR1. However, this difference was insignificant. No difference was observed with CD71 expression (Figure 6.11 D).

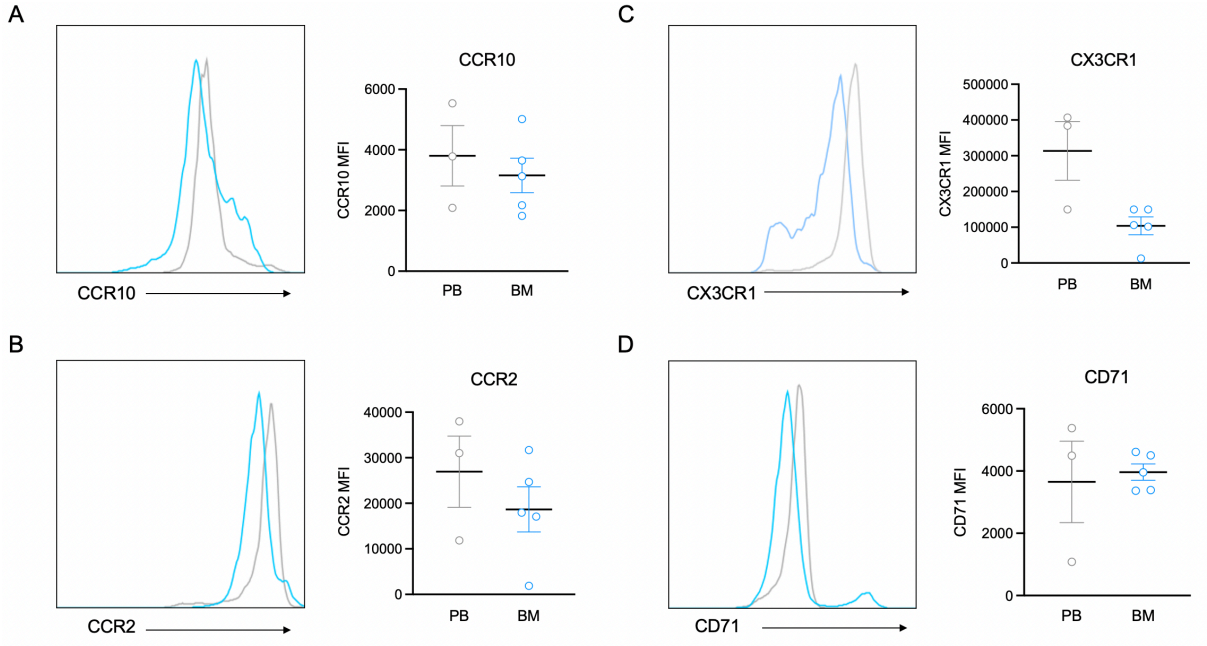

Figure 6.11 Chemokine receptor expression on PB and BM MNCs derived from early-diagnosed myeloma patients.

The median fluorescence intensity (MFI) of (A) CCR10, (B) CCR2, (C) CX3CR1 and (D) CD71on total CD14+ monocytes was determined using flow cytometry of MNCs as described in 6.2.13. PB samples are illustrated in grey and BM in blue. An example histogram of each group is shown first, and summary data are shown as scatter plots. Data represented n=3-5 independent experiments expressed as the mean ± SEM. Statistical analysis was determined using a Mann-Whitney test.

6.3.5 Immunophenotyping of B cells isolated from PB and BM by flow cytometry

As discussed in *1.3 B cells in MM*, one of the distinguishing features of MM is the proliferation of a clonal plasma cell population in the BM. Therefore, the relative abundance of different B cells subsets in PB and BM of newly diagnosed MM patients was determined.

Overall, no statistical differences (P>0.05, Mann-Whitney test) were observed in the distribution of B cells (CD19+) between PB and BM MNCs. This was the case for total B cells (Figure 6.12 A), class switched memory (Figure 6.12 B), non-class switched memory (Figure 6.12 C), as well as naïve B cells (Figure 6.12 D) using the gating strategy summarised in Figure 6.3. No statistical differences were observed in CD27 (Figure 6.12 E) and IgD (Figure 6.12 F) within B cell subsets.

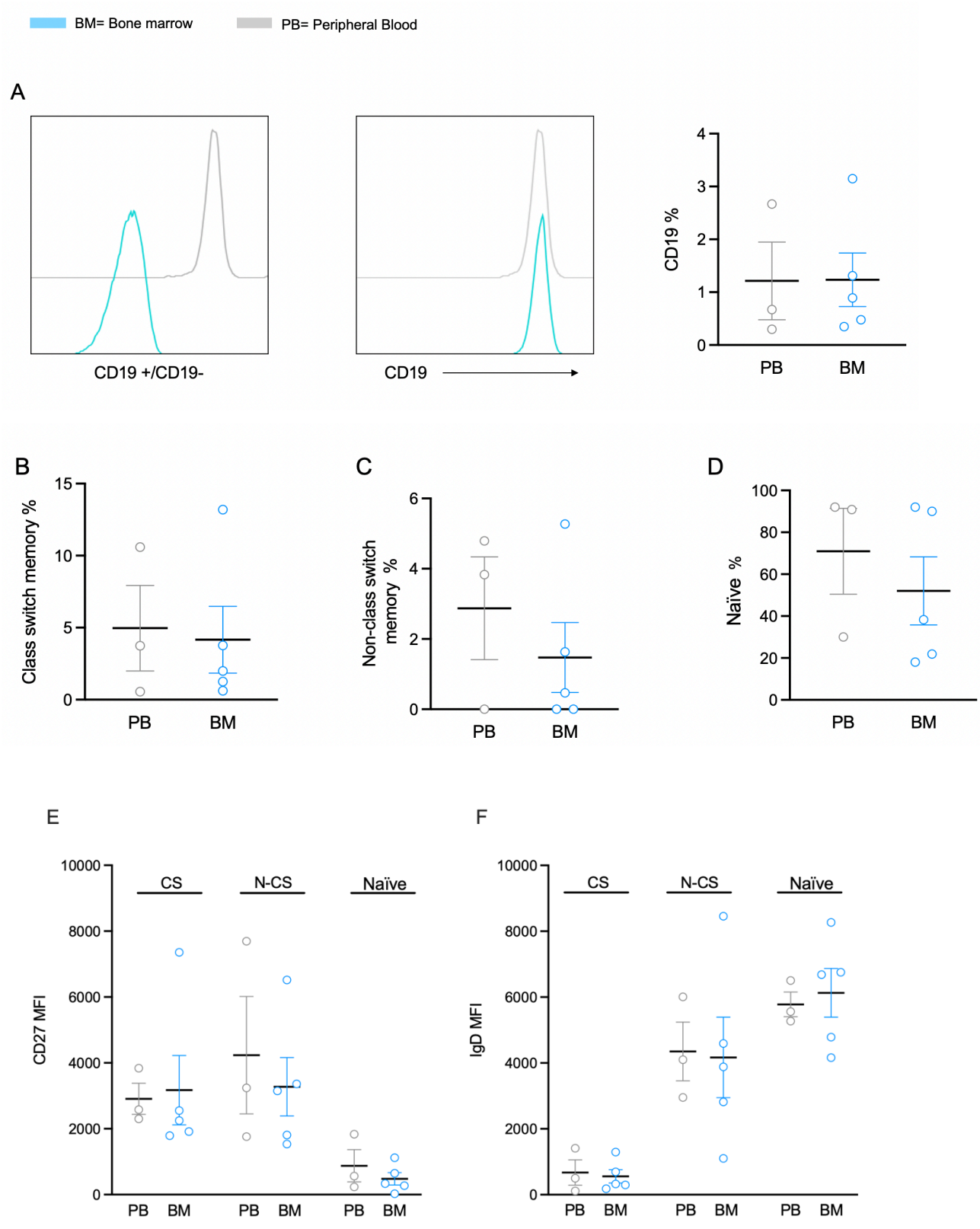

Figure 6.12 Distribution of total B cells and subsets in peripheral blood and bone marrow of MNCs from early-diagnosed myeloma patients.

PB samples are illustrated in grey and BM in blue. (A) An example histogram of CD19-/CD19+, percentage of CD19 of total peripheral blood (PB) and bone marrow (BM); and summary data are shown as scatter plots. B cell subsets are shown as a percentage of the total B cell population determined using the gating strategy shown in Figure 6.3 as scatter plots: class switched memory (B), non-class switched memory (C), and naïve (D). The expression of CD27 (E) and IgD (F) within the different B cell subsets. Data represented n=3-5 independent experiments expressed as the mean ± SEM. Statistical analysis was determined using a Mann-Whitney test for figures A-D and two-way ANOVA with Šidák multiple comparisons test for E-F.

CS = Class switch, N-CS = Non-class switch memory

The expression of plasma cells in PB and BM in B cells was determined using flow cytometry and the gating strategy summarised in Figure 6.3. The expression of plasma cells (expressed as a percentage of total B cells) in the BM was significantly higher than that in the PB of newly-diagnosed myeloma patients (Figure 6.14).

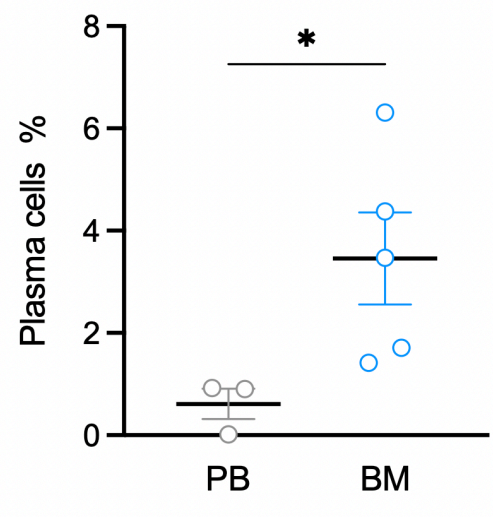

Figure 6.13 The percentage expression of plasma cells in B cells of peripheral blood and bone marrow in MNCs of newly-diagnosed myeloma patients.

MNCs derived from peripheral blood (PB; illustrated in grey) and bone marrow (BM; illustrated in blue) were isolated, and B cells were identified. Plasma cells are expressed as a percentage of total B cells. Data represented n=3-5 independent experiments expressed as the mean ± SEM. Statistical analysis was determined using a Mann-Whitney test.

MM cells are dependent on glucose via glycolysis as well as on glutamine for energy equivalents through a process known as glutaminolysis[694,695]. Glutaminolysis is elevated in chemotherapy-resistant myeloma cells[696]. Glutamine is crucial for the survival of certain cancer cells, and glutamine starvation induces cancer cell death[696,697]. Glutamine transporters such as SNAT, ASCT2 and CD98/L-type amino acid transporter-1 (LAT1) are expressed at high levels in MM and are associated with poor prognosis in patients with newly diagnosed MM[698,699]. Therefore, the expression of key metabolic transporters was considered by flow cytometry. CD98 is a transmembrane glycoprotein amino acid transporter that was chosen to investigate not only for its role in amino acid metabolism but as it has a function in integrin signalling[700], which appear to be important in tumour growth and metastasis, as previously discussed.

CD36 is another interesting transporter that was considered for investigation here. It is a class B scavenger receptor expressed on the surface of a wide range of innate and adaptative immune cells[701]. CD36 binds to a variety of extracellular signals, including long-chain fatty acids and danger-associated and pathogen-associated molecular patterns (DAMPs and PAMPs)[701,702]. Upon binding, CD36 assembles and interacts with other membrane signalling complexes, such as $\alpha V\beta 3$ integrin, which relay the signals to various downstream effectors[703–706]. The expression of CD98 and CD36 within MNCs derived from the PB and the BM of early diagnosed myeloma patients was determined using flow cytometry as described in *6.2.14 Gating strategy for selection of B cells*. The expression of both CD98 (Figure 6.13 A) and CD36 (Figure 6.13 B) in PB and BM monocytes was found to be similar.

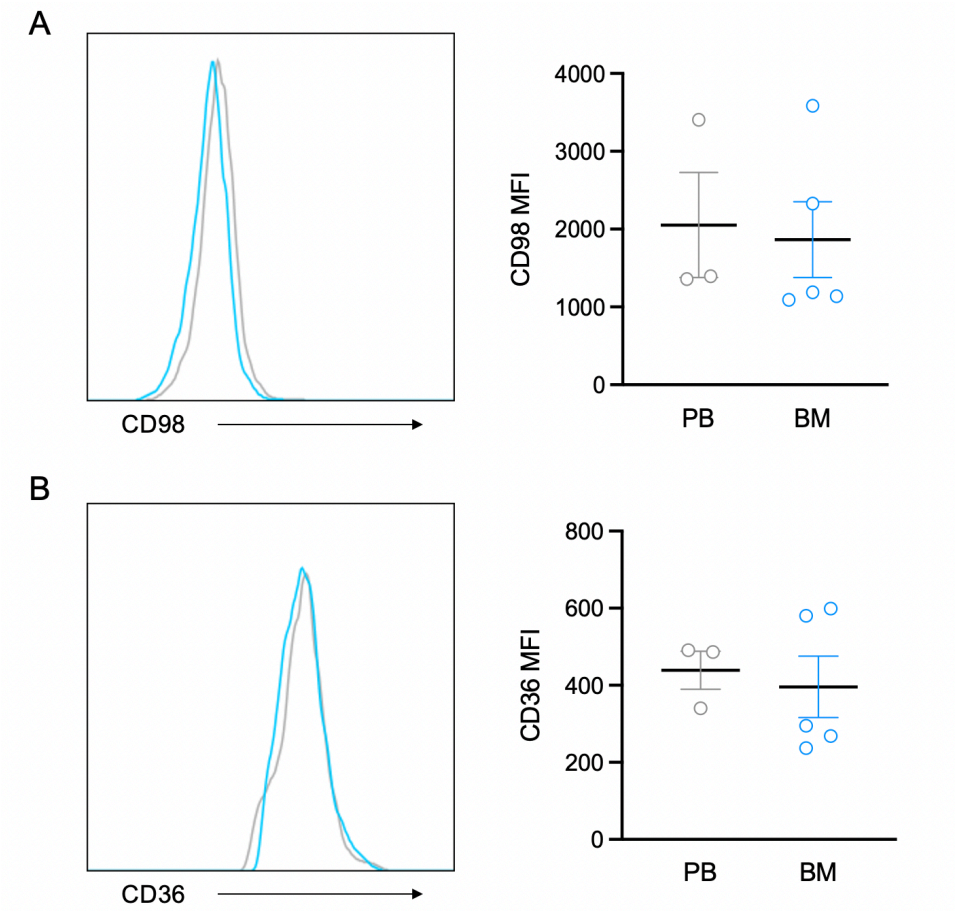

Figure 6.14 Expression of metabolic transporters in peripheral blood and bone marrow in B cells of newly-diagnosed myeloma patients.

Peripheral blood (PB; illustrated in grey) and bone marrow (BM; illustrated in blue) were analysed for key metabolic transporters expression with flow cytometry as described in 6.2.15. Data represented n=3 independent experiments expressed as the mean ± SEM. Statistical analysis was determined using a Mann-Whitney test.

6.3.6 Monocyte morphology and response to LPS in myeloma patients

The morphology of monocytes isolated from peripheral blood and BM from newly diagnosed myeloma patients was determined using confocal microscopy. Confocal images show monocytes isolated from PB (Figure 6.15 A), and the BM (Figure 6.15 B) displayed the common morphology of monocytes.

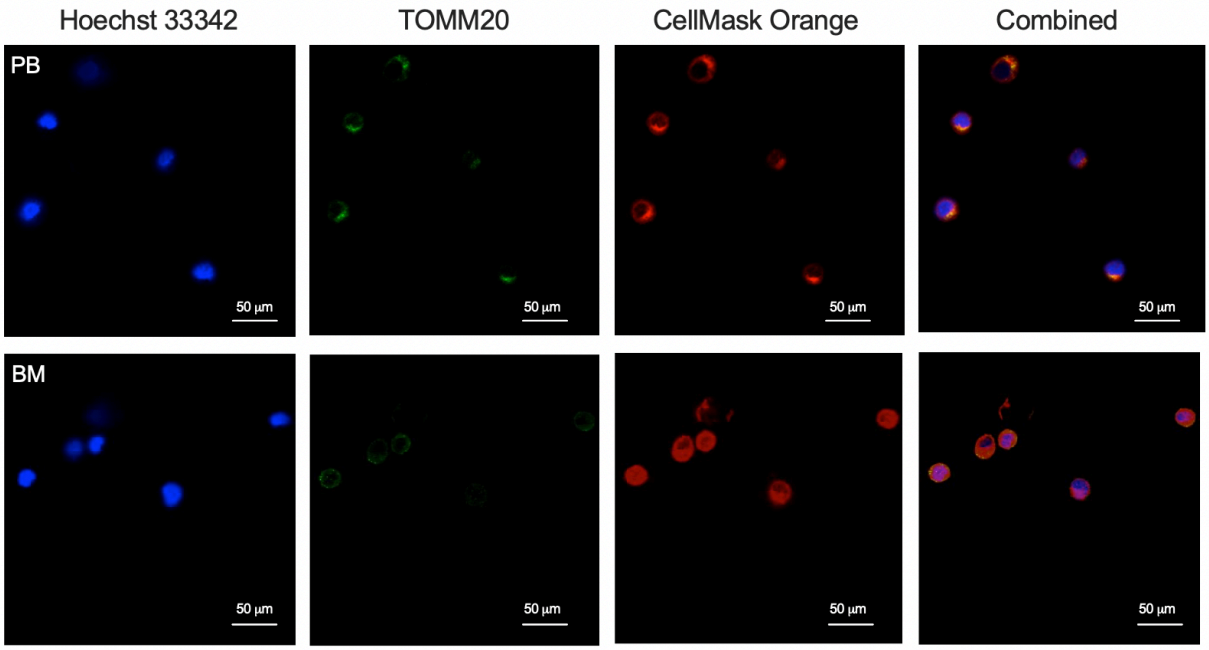

Figure 6.15 Confocal images of monocytes derived from bone marrow and peripheral blood of newly diagnosed myeloma patient

Peripheral blood (PB)-derived CD14+ monocytes shown in top row; bone marrow (BM)-derived CD14+ monocytes/macrophages are shown in bottom row. The monocytes were stained with the nuclei stain, Hoechst 33342 Solution (blue) and CellMask™ Orange (red) for plasma membrane stain (ThermoFisher Scientific; Massachusetts, USA). The mitochondrial antibody TOMM20 (green). Images were taken at 20 X magnification, and a 50 µm scale bar was included. Examples shown are representative of data from PB=3; BM=2).

Monocytes isolated from PB of healthy volunteers and newly-diagnosed myeloma patients and BM of newly-diagnosed myeloma patients were also tested for their ability to respond to LPS stimulation *in vitro*. All three cytokines tested (TNFα, IL-6 and MMP-9) responded to LPS as all were elevated 24 hours after treatment (Figure 6.16). There was a slightly higher response to LPS in monocytes isolated from healthy volunteers for TNFα (Figure 6.16 A) and MMP-9 (Figure 6.16 C). The levels of IL-6 appear to be similar in all three categories (Figure (6.16 B).

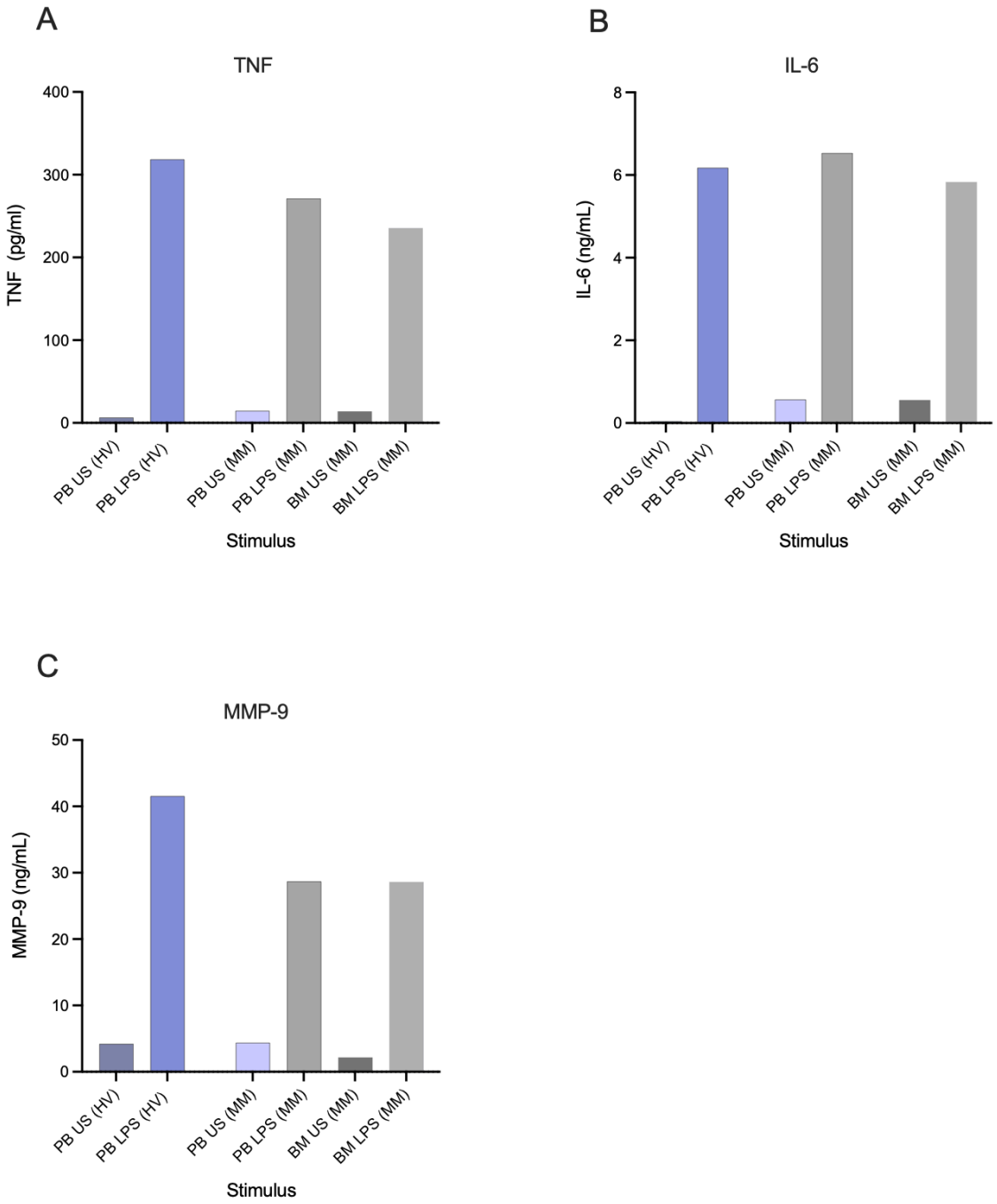

Figure 6.16 LPS-stimulated TNFα, IL-6 and MMP-9 production in positively selected CD14+ cells from the peripheral blood of healthy volunteers and early diagnosed myeloma patients and bone marrow aspirates of early-diagnosed myeloma patients.

CD14+ cells isolated from the peripheral blood (PB) of healthy volunteers (HV) and individuals with multiple myeloma (MM) and bone marrow (BM) of individuals with multiple myeloma using CD14 magnetic microbeads were stimulated with LPS (10 ng/ml). TNFα (A), IL-6 (B), and MMP-9 (C) levels were measured after 24 hours using ELISA. Data obtained from one donor.

6.4 Discussion

This chapter demonstrates (ii) the effects of IMiDs and IL-4, IL-10, and IL-13 on pro-inflammatory cytokine release in PB and BM MNCs of newly-diagnosed myeloma patients. This chapter investigated (ii) the immunophenotypic profile of monocytes and B cells in the peripheral blood (PB) and the bone marrow (BM) of newly diagnosed patients. In this chapter, we found that (ii) pomalidomide showed the highest potency in primary cells.

The original, pre-COVID-19 goal of this chapter was to use primary cells from people newly diagnosed with MM to determine how IMiDs modify cellular metabolism and thereby cell function. Therefore, the original strategy was to consider key functional outputs before progressing to experiments that looked specifically at immunometabolism. The foundational work for this was to confirm that IMiDs modulated cytokine expression. Cytokines, as well as chemokines, are potent signalling molecules important to life as hormones and neurotransmitters. Each cytokine binds to a specific surface receptor to generate a cell signalling cascade that affects cell function. This can provide negative or positive regulation of many genes and their transcription factors[707],[708]. Cytokines and chemokines in the BMM influence MM cells directly and indirectly. Well-known cytokines, including IL-6 and TNFα, are produced by bone marrow stromal cells and MM cells, and directly affect the growth and the overall survival of myeloma cells[709–711]. This study demonstrated the effects of IMiDs on the production of TNFα and IL-6.

TNFα is a pro-inflammatory cytokine that mediates the inflammatory response and regulates immune functions[712]. Inappropriate production of TNFα or sustained activity has been implicated in the pathogenesis of several diseases[713,714]. As previously discussed in *6.1 Introduction,* TNFα is associated with multiple processes that promote MM progression and survival, such as cell growth, death and differentiation. In the aspirates of patients with MM, increased TNFα levels are associated with poor prognosis[715,716]. In a previous study, the production of TNFα by BM cells from patients with MM was greater than in the control group[717]. TNFα is also a potent inducer of IL-6 gene expression and, therefore, production by stromal cells and osteoblasts; accumulated IL-6 promotes myeloma cell growth[718,719]. IL-6 plays a pivotal role in inflammation and immunity and has been studied extensively for its role in plasma cells[720]. IL-6 is a proliferative factor in MM that while suppressing immune cell proliferation and response to MM cells, affects the progression and treatment responsiveness; it is associated with poor prognosis[721–723]. It acts directly via the IL-6 receptor/JAK/STAT3 signalling pathway and has a role in drug resistance in MM[724, 725]. IL-6 is mainly secreted by myeloid lineage cells when these cells were isolated from MM-infiltrated BM[726],[727]. IL-6 and

TNFα are elevated in MM patients, and it is believed their primary function is to act directly on myeloma cells to promote their survival and growth and to increase angiogenesis[728]. Serum levels of IL-6 and TNFα in MM differ at different stages of the disease and indicate disease activity[729]. Studies also suggest that the overexpression of TNFα and IL-6 by myeloma cells allows them to overcome the anti-myeloma effects of thalidomide[730]. Consequently, it was essential to study the production of TNFα and IL-6 by MNCs derived from PB and BM as a key functional readout. LPS, a potent pro-inflammatory activator of *in vivo* and *in vitro*, was used to stimulate cytokine production in MNCs of healthy PB and early diagnosed myeloma PB and BM. Pomalidomide was found to be the most effective IMiD in reducing TNF levels in LPS-treated MNCs in all three groups. This is consistent with a previous report demonstrating that pomalidomide (out of the three IMiDs) was the most potent inhibitor of TNFα production in a human monocytic cell line[731]. In an earlier study, thalidomide was found to inhibit TNFα release in LPS-stimulated MNCs derived from human PB and the thalidomide analogue lenalidomide was also found to be a more potent inhibitor[732]. Interestingly, in this chapter, lenalidomide was found to be effective in reducing TNFα levels in LPS-treated PB from early-diagnosed myeloma patients but not in MNCs derived from healthy PB and MNCs derived from BM of myeloma patients.

Downregulation of IL-6 production in pomalidomide and lenalidomide-treated cells was observed in MNCs derived from healthy PB; this effect was absent in the MNCs derived from PB and BM of early-diagnosed myeloma patients. This is in contrast with a previous report illustrating the inhibitory effects of pomalidomide and lenalidomide on IL-6 production in MNCs derived from the PB and the BM of myeloma patients[733]. Results in this chapter identified TNFα and IL-6 production by MNCs isolated from PB and BM of early diagnosed myeloma patients in short-term (24 hours) cell culture assay. The results obtained in this chapter also demonstrated that IMiDs play a critical role in reducing pro-inflammatory cytokine release and also that pomalidomide is more effective than lenalidomide, and lenalidomide is more effective than thalidomide. Thus, this highlights the importance of these IMiDs in myeloma treatment and the importance of choosing the right thalidomide analogue depending on the stage of disease and identifying high-risk patients. Because MM demonstrates such genetic heterogeneity and high levels of refractory disease, targeting the cells in the BMM and tumour cells directly is an ideal plan for targeting MM.

Cells were then treated with IL-4/IL-10/IL-13, and the levels of TNFα and IL-6 were detected by ELISA. Down-regulation of TNFα production in early-diagnosed myeloma PB under treatment with IL-4 and IL-10 was observed at 30ng/mL; for the secretion of IL-6, IL-4 at

30ng/mL and IL-13 at both doses. However, similar effects of the cytokines were observed in the healthy control groups, suggesting the immunosuppressive activity of IL-4, IL10, and IL-13 does not seem to be a disease-specific phenomenon. This is also seen in other diseases involving the activation of immune cells, such as inflammatory bowel disease. The data obtained in this chapter demonstrate that the anti-inflammatory cytokines show different inhibition patterns of inflammatory mediators in PB and BM MNCs. The down-regulation role of IL-4 and IL-13 on PB in other inflammatory diseases has been shown in previous studies[734–737]. The comparable effects of IL-4 and IL-13 on IL-6 production by PB MNCs suggest the existence of a common IL-4/IL-13 receptor subunit or a common intracellular pathway[738,739]. The data agree with the findings of distinct receptors for IL-4 and IL-13 with a common subunit discussed in chapter *5.1 introduction*.

In addition to TNFα and IL-6 as two key cytokines in the BMM, MMP-9 has been recognised as a contributor to the processes related to cancer tissue formation, growth and metastasis[740–743]. Increased levels of MMP-9 have been associated with many types of cancer and are directly correlated with negative clinical outcomes[744]. The proteolytic ability of MM-9 allows the degradation of structural proteins, and remodelling of the ECM allows the passage of cancer cells through the BM and, therefore, the invasion of healthy tissues[745,746]. This makes MMP-9 an attractive target for cancer therapies. However, this has been hard to develop due to a highly conservative active site and the accumulation of side effects[747]. Further understanding of the mechanisms by which MMP-9 contributes to the growth, progression and survival of cancer will help develop the next generation of therapeutics for targeting MMP-9 with better accuracy and potency. LPS has been shown to enhance MMP-9 expression and cell migration via TLR4 activation[748]. The results presented in this chapter demonstrate that pomalidomide was the only IMiD to show an effect on LPS-stimulated MMP-9 production by MNCs derived from the BM of newly diagnosed myeloma patients; however, this was not significant. Interestingly, a lack of efficacy was observed with IL-4, IL-10 and IL-13 treatment. In fact, IL-10 slightly upregulated MMP-9 levels in a dose-dependent manner compared to the untreated; however, this was not significant. This is in contrast with previous studies showing the efficacy of IL-4 in reducing MMP-9 levels in human and mouse macrophages; IL-10 was also shown to negatively influence MMP-9 production[749–751]. However, MMP-9 downregulation by IL-4 and IL-10 has been demonstrated in different model systems than in this study[752–754]. The lack of MMP-9 modulation by IL-13 as shown here has yet to be demonstrated in other publications. In fact, IL-13 has been shown to increase active MMP-9 production in keratinocytes[755].

Given the effects of IMiDs on cytokines, as summarised above, the next step was to consider the immunometabolic contribution to this. As discussed in *1.4 Monocytes in MM*, monocytes

play a vital role in the progression of MM cells and in the development of myeloma bone disease through their release of several soluble mediators that stimulate osteoclastogenesis and the presence of non-classical monocytes could be a potential marker for increased osteoclast precursors[756]. Therefore, the levels of circulating (PB) and BM total monocytes and monocyte subsets in newly diagnosed myeloma patients were determined to ascertain these cells as a key cell type for further study. Unfortunately, due to COVID-19, far fewer primary samples were available than anticipated at the outset of this study.

The expression of the chemokine receptors CCR2 and CCR10 seems to be similar in PB and BM. At the same time, a slight increase was observed in CX3CR1 expression in PB compared to BM. Each chemokine and its receptor form an axis that promotes cancer cell progression via enhancing cell survival and angiogenesis. The expression of CX3CR1 was confirmed in myeloma cell lines which may indicate their importance regarding survival and progression [757]. The progression of multiple myeloma requires the adherence of cells to the extracellular matrix components such as VCAM-1 and fibronectin in the bone marrow. This activates several signalling pathways that enhance anti-apoptotic proteins and upregulates proliferation signalling pathways. In the same study, treatment with CX3CL-1 (fractalkine-ligand to CX3CR1) induced myeloma cell adhesion to the extracellular matrix and induced osteoclast differentiation[757]. It is important to note that osteoclast precursors selectively express CX3CR1 and that osteoblasts express CX3CL1. Thus, it is important to determine the expression of such chemokines and their receptors in multiple myeloma. Future studies should be aimed at investigating the relationship between the expression of such cytokines and their receptors in the different cells in the PB and BM on the progression of the disease as it could present with potential therapeutic targets; blocking of this axis would inhibit not only myeloma progression but also could potentially suppress myeloma bone disease in MM patients. Flow cytometry was used to determine the expression of the different markers on the surface of PB and BM-derived from newly diagnosed MM patients; the same panel could be utilised to monitor the expression of the different markers throughout the disease course and could help to monitor the effects of treatment on the chemokine expression, which could give an indication on treatment response and efficacy in patients with MM.

Increased numbers of circulating naïve B cells in PB. Collectively, these could drive the shift towards increased numbers in newly generated B cells in PB findings would support the hypothesis that the regeneration of B cell precursors in the PB, which could eventually lead to the increase of plasma cells in the BM. A detailed analyse of PB and BM CD19 cells in newly diagnosed patients. Our analysis of blood CD19 cells in untreated patients has yielded several new insights. Plasma cells do circulate in the PB of myeloma patients but appear to be present

at very low levels when compared to BM[758]. These observations may be associated with the stage of the disease. Importantly, initial PB CD19 levels significantly correlate with survival and treatment response.

MM is diagnosed by observing clonal bone marrow plasma cells >10 %[759]. Previous studies have analysed PB lymphocytes in myeloma patients and have found circulating PB CD19+ cells that exhibit typical features of so-called early plasma cells that might already be committed to entering the BM [760]. This might explain the increase in plasma cells in the BM observed here, as it might be due to some of these patients' PB plasma cells already committed to entering the BM. One report has observed that CD19+ B cells in MM patients are consistently above the control group values and that the PB monoclonal CD19+ B cells share clonotypic Ig heavy with the BM plasma cells[761]. The same report suggests that the malignant clone in myeloma is heterogenous, involving multiple differentiation stages with different B-lineage subsets at different times and stages of the disease. The results obtained in this chapter add confirmatory evidence that there are small numbers of plasma cells in the PB of early-diagnosed myeloma patients. Particularly, more information was added as this study compares that to BM plasma cells. The relatively low level of clonal cells was not associated with the levels of CD19+ in the PB detected in myeloma patients. The precise quantification of PB, BM monocytes, and B cells can give valuable information about the host immune system. Deficiencies of total monocytes and B cells would suggest immune system alternation and inability to fight infectious agents and overall immune system impairment.

To initiate the immunometabolic aspects of the proposed work, expression of various nutrient substrate transporters was considered. As previously discussed, CD98 and CD36 expression has been associated with the progression of MM[698,762]; therefore, monitoring their expression can be a potential biomarker that can be of use to predict myeloma patient outcomes. CD98 (SLC3A2) and LAT1 (SLC7A5) form a heterodimeric transmembrane protein complex that mediates amino acid transport; this complex is overexpressed in aggressive human cancers[763,764]. CD98 expression levels are correlated with LAT1 expression levels[764]. Increased expression of LAT1/CD98 heterodimer was found to be associated with poor prognosis in newly diagnosed myeloma patients[698,765]. We found that CD98 expression is similar in PB and BM-derived MNCs. LAT1 and CD98 expression could present a promising pathological marker for identifying high-risk MM[698]. The overexpression of CD98 in MM and its ability to transport substrates allows exploiting this protein in diagnostics and clinics. Radiolabelled molecules, specifically in cancer foci. The used molecules are tyrosine, phenylalanine and methionine derivatives, which are delivered to cells via CD98. Targeting fatty acid and amino acid uptake might be an effective strategy for treating MM cancer. Thus,

targeting CD98/LAT1 can appear to be an attractive therapeutic target. Additionally, this can be used to predict and monitor IMID sensitivity in MM patients.

CD36 expression was found to be similar in PB and BM-derived MNCs. Ferroptosis is a type of regulated cell death by lipid peroxide accumulation. This process is shown to be mediated by CD36[766]. Targeting CD36 and ferroptosis may be an attractive target to improve the anti-tumour efficacy of T cell-based immunotherapy. The results obtained here confirm the expression of CD36 in PB and BM cells. Monitoring CD36 and CD98 throughout the disease could give an indication of disease prognosis and high-risk myeloma patients[767]. Additionally, this provides important insights to utilise this technique to target and manipulate lipid and glutamine metabolism in MM to improve the clinical effectiveness of cancer immunotherapies. One clear limitation of this study is the sample size and the need for sample size calculation. This was a result of the ethical approval for studying cells isolated from early-diagnosed patients in detail was received shortly before the COVID-19 pandemic.

6.5 Conclusion

MM develops in the BM, indicating the substantial requirement of this tumour for the peculiar BMM, rich in cytokines and hematopoietic precursor cells. The clinical use of IMiDs in MM has significantly improved long-term survival and quality of life. This chapter demonstrates the efficacy of the three most readily available IMiDs, with novel potential targets illustrated in primary cell mode and cell lines. IMiDs are effective in reducing pro-inflammatory cytokines, with pomalidomide being the most effective IMiD. This efficacy differs between the IMiDs and between PB and BM-derived MNCs. Overall, pomalidomide was found to be the most effective IMiD.

In summary, these results contribute to the characterisation of the immunomodulatory effects exerted by IMiDs in MM and should be taken into consideration for the implementation of new therapeutic strategies targeting the cell cycle checkpoints to be combined with drugs already used or novel treatments (such as anti-inflammatory cytokines) in MM treatment, especially in newly-diagnosed disease stages. The study describes the anti-inflammatory properties of IL-4, IL-10 and IL-13; similar to other immunoinhibitory mediators, all cytokines decrease IL-6 and TNFα. The difference in the downregulation of cytokines by IL-4, IL-10 and IL-13 suggests an evaluation in further studies in vitro and in vivo of the potential effects of the anti-inflammatory cytokines in combination with other anti-inflammatory mediators. To further analyse the differences between MNCs derived from PB and BM, flow cytometry was used to analyse subsets of immune cells as well as relevant inflammatory mediators in PB and BM of early-diagnosed myeloma patients. This data shows similar immunophenotypes of B cells and

monocytes between PB and BM, which might be an indication of cells escaping the BM into the circulatory system.

Future studies could be looking into new combinations of pomalidomide and lenalidomide with anti-inflammatory cytokines, monoclonal antibodies, and cell cycle checkpoint blockers. Further research understanding the role of different cytokines in various stages of MM is needed.

Chapter Seven

General Discussion

7.1 Overview

This thesis has presented novel findings on how IMiDs and IL-4, IL-10 and IL-13 affect the differentiation and activation of osteoclasts *in vitro*. Key findings have included: an optimised method for an efficient production of human active osteoclasts after only a 10/11-day culture period; the novel technique of measuring impedance and performing cluster analysis to monitor osteoclast differentiation and pre-osteoclast formation; and the effect of IMiDs on metabolic parameters in MM cell lines. IMiDs, IL-4 and IL-13 were found to reduce impedance and pre-osteoclast formation monitored in real-time over the course of differentiation *in vitro* whereas, IL-10 increased the impedance and pre-osteoclastic cluster formation. IMiDs, IL-4, IL-10 and IL-13 were also effective in reducing pro-inflammatory cytokine release by MNCs isolated from peripheral blood and bone marrow aspirate of patients with MM. The results show that IMiDs also regulate two major MM cell lines (RPMI 8226 and JJN-3) with different effects.

7.2 Active osteoclasts were successfully generated from peripheral blood monocytes

A hallmark of MM is chronic bone pain characterised by uncontrolled differentiation and activation of osteoclasts[768]. Persistent bone resorption leads to cartilage and bone destruction; therefore, controlling such cells with local systemic treatment protects bones from destruction. Radiography and x-rays have indicated that the first signs of bone loss in MM are the presence of bone lesions in the vertebral bodies. Thus, controlling the production of the factors involved in the perpetuation of bone resorption and bone lesion formation is one of the major treatment goals in MM.

Osteoclasts play a central role in bone homeostasis by regulating osteoclastic bone resorption. When hyperactivated, osteoclasts can cause dramatic and destructive bone loss in diseases such as myeloma bone disease[769]. As our understanding of these cellular and molecular mechanisms increases, potential therapeutic targets could be identified which can be effective in the treatment of myeloma bone disease. Initially, osteoclasts were differentiated over a 14-day period; however, in our culture conditions, we observed many osteoclasts generated only after a 10/11-day culture. These osteoclasts were active as the supernatants harvested during the differentiation process had enzymatic activity that would correlate to the resorptive activity of the cells *in vivo.* This was determined using *in gel* zymography, another optimised method used in this study to detect the activity of the osteoclast model. By examining the area of gelatine digestion in the gel, it was observed that osteoclasts were able to digest the gel with this detectable after only three days of culture. Osteoclasts were at their peak of activity on day seven of differentiation as they were able to significantly digest the gel. Therefore, a method for the efficient production of active human osteoclasts, displaying the main

characteristics and parameters of osteoclasts and retaining their resorptive activities has been optimised. This method paves the way to investigate the basic mechanisms underlying the proliferation and activation of monocyte-derived osteoclasts from peripheral blood obtained from patients with bone diseases such as myeloma bone disease and rheumatoid arthritis.

MM is a disorder primarily affecting people older than 60 years of age, in particular males[770]. It would therefore be interesting to test osteoclast differentiation in monocytes isolated from older individuals and men versus women. At the present time, there is no *in vitro* model to study myeloma bone disease. Therefore, the osteoclast *in vitro* model is excellently suited to study the biology behind age and sex-specific bone remodelling and to test the efficiency of current and potentially novel therapeutics. In conclusion, the model described in the present study provides unique and novel insight into the cell interactions taking place during osteoclastogenesis. This makes monocyte-derived osteoclasts described in this study an efficient and valuable *in vitro* model for future drug testing to identify anti-resorptive and bone anabolic compounds.

7.3 Osteoclast differentiation and activation is affected by all the IMiDs

The emergence of new anti-myeloma drugs has led to improved therapeutic outcomes with prolonged survival in patients with MM. Henceforward, it will be important to address the therapeutic efficacy against bone lesions in MM, as this will improve and maintain the patient's quality of life. A potent and effective treatment to restore bone in MM lesions with bone loss has yet to be developed. Therefore, the development of novel therapies that suppress tumours and efficiently restore bone formation in bone lesions is urgently needed and is an important clinical challenge for the future. Improved understanding of biological development, molecular abnormalities and the BM microenvironment of MM would enable effective treatment and management for patients. To date, the survival of MM patients has improved as many therapeutic agents have emerged[771]. Next-generation IMiDs and other novel agents are favourable advancements, and autologous stem cell transplant (ASCT) is still essential during management. When designing treatment strategies, personalised situations, tolerability and molecular information should be considered. Patients with high-risk features need to be identified early, and the application of biomarkers can help to select the subgroups for appropriate treatment. Studies are underway to figure out potential combination strategies, mechanisms of drug resistance, new targets and new drug classes. Combining therapies with multiple targeting strategies man immunotherapies is a promising path for the new-generation treatment for MM.

In research, the focus has been placed mainly on the efficacy of IMiDs on osteoclasts isolated from an animal model to test their inhibition of osteoclast resorption and survival. Much less attention has been paid to understanding the effects of IMiDs on early osteoclast differentiation, maturation and activation in humans. Our *in vitro* observations suggest these early differentiation stages deserve further investigation, especially in the context of therapeutic use. Confocal microscopy is useful in understanding the characterisation of osteoclasts emerging as monocytes differentiate and merge in an *in vitro* context. Interestingly we found that this merging process has slowed down in the presence of IMiDs. This suggests that IMiDs would affect the efficiency of bone resorption in the BM microenvironment by disrupting osteoclast signalling and osteoclast distribution. Notably, the IMiD treatment was more effective when added on the day of seeding than when the cells had already transitioned into pre-osteoclasts. Further studies are needed to show if a similar effect also persists in the presence of bone matrix and whether this activity is altered as well as the effect on maturation in lesion sites. It will be interesting to test in detail in future experiments whether this IMiD treatment effect on osteoclast maturation is also present in osteoclasts isolated from newly diagnosed myeloma patients, as these cells are hyperactive in MM patients[772]. Whether this reflects the efficacy *in vivo* is to be elucidated in future experiments.

Physical interactions between MM cells and other cells in the BM microenvironment, including stromal cells, osteoclasts and immune cells, are important for tumour proliferation and survival[773]. Results here suggest that IMiDs alone can reduce the overall differentiation and activation of osteoclasts as well as being important in the reduction of pro-inflammatory cytokines in cells in the BM microenvironment, which predicts the anti-myeloma properties and the anti-inflammatory efficacy of IMiDs. However, it remains unclear whether this effect is also achievable upon osteoclast precursors' interactions with the mineralised matrix. Prevention of osteoclast differentiation and activation of osteoclasts is a novel therapeutic strategy of IMiDs. By inhibiting osteoclast recruitment as well as improving bone fragility and bone lesion formation in MM, IMiDs can improve the overall patients' quality of life supporting the development of therapeutic approaches that block specific osteoclast development markers.

7.4 Osteoclast differentiation and activation is affected by IL-4, IL-10 and IL-13

The role of cytokines in the pathogenesis and progression of neoplastic diseases is undeniable. Consequently, cytokines could be employed as therapeutics with numerous benefits. Cytokines influence numerous processes in parallel, which can be a disadvantage in

some cases. Nevertheless, anti-inflammatory therapies might theoretically reduce protective antitumour immunity. As previously mentioned, proinflammatory cytokines can have both pro- and anti-cancer activities, while cytokines with potent anti-inflammatory activity might strongly favour the growth of tumours. Approaches to fighting cancer should be promoting rather than reducing the immune response against tumours. Therefore, it is essential to better comprehend the relationship between immune cells, inflammation, and cancer. A desynchronised cytokine system typically exemplifies MM with an increase in pro-inflammatory cytokines[774]. New perspectives concerning intervention seem possible, and the use of nanotechnology could be a powerful approach to the use of cytokines in the prevention and treatment of cancer. Nanoparticles can be used as vehicles for these immunotherapeutic agents to fight cancer[775]. A better understanding of the relationship between inflammation and MM will ensure more effective therapeutic interventions. In our studies, inhibition of osteoclast differentiation and activation was observed in the presence of IL-4 and IL-13. IL-4 and IL-13 are known to suppress RANKL-induced osteoclast differentiation through direct actions on osteoclast precursors. Previous reports have demonstrated that IL-4 prevented the differentiation of osteoclast precursors into mature osteoclasts in a mouse model[776]. Herein, we show in the *in vitro* model, the inhibitory effects of IL-4 and IL-13 on the differentiation and resorptive activity by directly acting on osteoclasts. We found that IL-4 and IL-13 inhibited the expression of integrins in osteoclasts, thereby preventing their adhesion to each other and to the plate.

Surprisingly, accelerated osteoclast differentiation was found with IL-10 treatment, which would suggest a catabolic effect of IL-10 on this osteoclast model. This contrasts with the effects observed with IL-10 when tested in osteoclasts derived from the monocytic cell line RAW264.7 when stimulated with RANKL and in animal models, as previously discussed in *5.4 Discussion*, and at present, this effect of IL-10 on osteoclast differentiation rate and activation can't be explained. This effect was greatly reduced when the treatment was applied at a later stage of the differentiation. Future studies using similar techniques to test the underlying effects of IL-10 on osteoclasts *in vivo* under different mineralisation conditions to uncover the mechanisms underlying the catabolic effects of IL-10 are needed. IL-10 has a role in the tumour microenvironment as it is present in tumour-associated macrophages (TAMs) and CD8+ T cells[777]. IL-10 is considered an immunosuppressive cytokine, enhancing cancer escape from immune surveillance. However, the immunosuppressive effects of IL-10 are not consistent, and they have been proposed to have some immunostimulant properties which allow the anti-cancer response[778]. It is controversial what the role and the effects of IL-10 are in the tumour microenvironment. A previous study has shown that IL-10 can increase the growth of B cells, and it has been shown to promote their differentiation into plasma cells and

induces the production of immunoglobulin in plasma cells[779]. It is shown to function as a proliferation factor for MM cells[780], and increased serum levels of IL-10 have been higher in MM patients compared to controls[781,782] and have been shown to correlate with advanced MM stages[783]. IL-10 has pleiotropic effects on the immune system. It acts as a cytotoxic T cells differentiation factor[784].

The attempt to merge therapeutic targets with cytokines should be careful not to ignore the possibility of generating a cytokine storm that might manipulate immune responses against myeloma cells and/or the tumour-associated microenvironment. The disadvantages of cytokines being used as treatments come from the fact that they influence a number of processes in parallel, pleiotropic cytokines. Alterations in the cytokine system can lead to altered immune balance and, therefore, a dramatic effect on the immune response.

Subsets of osteoclasts with various immune functions

Recent studies have expanded the understanding of osteoclasts beyond their traditional role in bone resorption, revealing several subsets with distinct immune functions. Inflammatory osteoclasts emerge under pathological conditions, such as rheumatoid arthritis and osteoporosis. These osteoclasts not only enhance bone resorption but also produce pro-inflammatory cytokines, contributing to the inflammatory milieu. This dual role exacerbates bone loss and inflammation, linking osteoclast activity to autoimmune and inflammatory diseases. This was highlighted in a study that investigated the shared mechanisms between the immune system and bone, underscoring the osteoclasts' participation in immune responses[785]. Regulatory osteoclasts, on the other hand, are characterized by their ability to produce anti-inflammatory cytokines. These osteoclasts help resolve inflammation and maintain immune homeostasis, offering a counterbalance to the destructive activities of inflammatory osteoclasts. Research by a study demonstrated that regulatory osteoclasts can prime TNFα-producing CD4+ T cells while expressing CX3CR1, which is crucial for their anti-inflammatory functions[786]. Another subset, immune-suppressive osteoclasts, plays a role in immune tolerance by suppressing T-cell proliferation and activation. This function is particularly important in preventing excessive immune responses and maintaining tissue integrity[787]. Osteomacs, or osteal tissue macrophages, are a macrophage-like cell population associated with bone surfaces. These cells support osteoblast function, aiding in bone formation and repair, and participate in immune responses. A study revealed that osteomacs are intercalated throughout bone lining tissues, where they regulate osteoblast activity and contribute to the local immune environment[652]. These findings collectively underscore the diverse roles of osteoclasts in immune modulation and inflammatory responses. The

identification of these osteoclast subsets opens new avenues for therapeutic interventions targeting both bone and immune disorders, offering hope for more comprehensive treatment strategies.

7.5 Measuring impedance by the eSight Real-time cell analyser (RTCA) technique enabled further investigation of osteoclastogenesis

This study shows for the first time the usage of real-time cell analysis using the impedance and object count to quantify the changes in osteoclast formation upon treatment in real-time. The use of this technique in this study enabled a comprehensive insight into the health, cell behaviour, function and biological processes of osteoclasts using live, simultaneous, impedance-based and image-based measurements. The distinguishing feature of the eSight RTCA is its continuous nature. Unlike endpoint methods, real-time assay systems allow the tracking of differentiation over the entire course of osteoclast differentiation. This is particularly effective for assessing the impact of treatment, where differentiation inhibitory effects are easily noticeable but may be missed using endpoint-based methods[625]. Real-time assays are typically performed using equipment capable of capturing images at regular time intervals and quantifying cellular impedance and object count as a measure of proliferation. Such methods also facilitate the visualisation of drug/treatment-induced cell morphology changes. The major advantage of this technique is real-time data collection in a label-free manner; therefore, studies can be extended over the period necessary to investigate the effects of treatment for as long as required. The application of cellular impedance in osteoclasts in the presence of current myeloma treatments offers the opportunity to advance the study and understanding of their effects in bone disease, which facilitate novel targets for treatment and, ultimately, drug development.

Tracking osteoclastogenesis in real time made it possible to focus analyses on the most appropriate time region for the application of the IMiDs. For example, Figure 4.11 indicates that the IMiDs had less of an impact on osteoclast impedance which further highlighted the decrease in IMiD activity when added at a later stage of the differentiation. The ability to generate videos of the differentiation process (Appendix 10.7-10.11) enabled the visualisation of the effects of IMiDs on osteoclast migration *in vitro*. This is in stark contrast to traditional end-point methods, which provide only a snapshot of the differentiation process that is devoid of contextual information. The fact that the eSight is retained in a standard incubator means that osteoclastogenesis assays in the absence and the presence of treatment can be run

under steadily, physiologically relevant conditions without having to shuttle the samples between an incubator, a hood, and an analytical instrument. Once the experiment was terminated, its intuitive software was used to quickly extract meaningful and actionable quantitative information on the impedance of osteoclasts in the presence of IMiDs and IL-4, IL-10, and IL-13. Analysing the image count was possible by measuring the surface area and adjusting the parameters to detect the presence of pre-osteoclastic clusters in the presence of the various treatments used in this study as well as determining the optimal cell count for such analysis. This method is amendable for both drug discovery/development as well as basic research/mechanistic studies.

7.6 IMiDs and IL-4, Il-10 and IL-13 reduced cytokine production by MNCs of myeloma patients

As discussed in *6.1 introduction*, inflammation plays a crucial part in the survival and progression of MM and is associated with poor prognosis. In recent years, it has become evident that the microenvironment is very important not only in the oncogenesis of myeloma but also in the clinical presentation and treatment response. Pro and anti-inflammatory cytokines are present in MM and their main function is to regulate the cells of the immune system, such as Th17, Th22, CD4 and CD8 cells[788]. Interestingly, these cells can have both pro- and anti-cancer actions and strong anti-inflammatory cytokines might support cancer proliferation and progression as the disruption of such balance could lead to the progression of MGUS to MM. Monocytes, macrophages and dendritic cells are essential components of the myeloma environment. These cells can be stimulated by myeloma-derived products, and mitochondrial DNA released from dying myeloma cells could support the overall growth of MM[789]. Additionally, there is an interaction between osteoclasts and other immune cells that has been reported in clinical settings of increased bone resorption in typical inflammatory bone diseases, such as RA and periodontal disease[790]. The cross-talk between immune and bone cells via cytokines, chemokines, growth factors, signalling molecules and transcription factors has begun to be intensively researched under the concept of osteoimmunology. This study has provided important data on the effects of IMiDs and anti-inflammatory cytokines on the generation of pro-inflammatory cytokines released by MNCs isolated from myeloma patients in response to LPS.

Pro-inflammatory cytokines were measured in the presence of three IMiDs, pomalidomide, lenalidomide and thalidomide, in a dose-dependent manner. Many MM therapies influence cytokine balance. Lenalidomide and pomalidomide have been shown previously to have cytotoxic actions on MM cells and, anti-inflammation effects, alongside immunomodulatory

and antiangiogenic actions on BM cells. They influence subsets of T cells to secret Th1 cytokines such as IL-2 and IFNγ. Meanwhile, they can suppress the production of other cytokines, such as IL-6 and TNFα[791,792]. Agreeing with previous studies, lenalidomide and pomalidomide have decreased the production of IL-6 and TNFα more potently than thalidomide in LPS-stimulated PB and BM MNCs. All three IMiDs reduced the expression of IL-6, with pomalidomide exerting the highest efficacy. This is consistent with previous studies that illustrated that thalidomide analogues (including lenalidomide and pomalidomide) are more effective than thalidomide itself in reducing the overall cytokine production in MM. However, what is provided here is the direct comparison of the effects of IMiDs in PB and BM-derived MNCs in newly-diagnosed patients. These results also demonstrate that lenalidomide and pomalidomide alone, not in combination with another treatment, were able to reduce the secretion of IL-6 and TNFα.

Along with investigating the effects of IMiDs on pro-inflammatory mediators in MM, anti-inflammatory cytokines were tested for their efficacy. The addition of the immunoregulatory IL-4, IL-10 and IL-13 at two different doses resulted in strong down-regulation of cytokine response in PB and BM MNCs of myeloma patients. As previously discussed, the cytokines tested in this study are increased in the different stages of MM[793–796]. The increased production of these cytokines in MM supports the hypothesis that these cytokines play an essential part in disease progression. Immune cells in MM are known to produce a variety of cytokines upon activation, which may induce a cascade of immunological mechanisms. Therefore, it was of interest to test the capacity of immunoregulatory cytokines to suppress the cytokines secreted by activated cells within the MNCs population. Th2 cytokines such as IL-4, IL-10 and IL-13 have been reported to exert potent anti-inflammatory effects on several cell types, especially monocytes. The results obtained here demonstrate that all three anti-inflammatory cytokines were able to down-regulate the cytokine response by LPS-activated MNCs derived from PB and BM. The suppressive capacity of each cytokine was observed to be greatly dependent on the dose applied.

7.7 Future work

This study has established an efficient osteoclast model which does not rely on an animal model to study the differentiation and activation of osteoclasts. In the future, this method would help with the reduction and refinement of research so such a model complies with the 3Rs. This method would also enable the identification of future promising drug candidates with the use of RTCA to study their efficacy for the treatment of bone disorders such as myeloma bone

disease. Using similar end point and real-time techniques, future studies could investigate developing a model to study osteoblastogenesis in the presence of IMiDs and IL-4, IL-10 and IL-13, where targeting osteoclastic and enhancing osteoblastic differentiation and activity could provide the ultimate therapy in the treatment of myeloma bone disease. This could also reveal synergistic or additive effects when testing different drug combinations. Currently, more potent next-generation IMiDs are in clinical development, with an expanding number of active agents, therapeutic modalities and more combinational possibilities. The osteoclast model optimised here, and the real-time monitoring method could help establish and understand drug mechanisms in bone disease and their applications in combination settings.

In addition, the treatment journey from newly diagnosed myeloma patients to early and late MM relapses is connected to genomic and immune changes associated with disease progression and the acquisition of resistant mechanisms. Therefore, future studies could look into the immunophenotyping of monocytes and B cells as well as investigate the metabolic changes using methods such as the Seahorse XF technology to measure mitochondrial respiration and glycolysis of cells isolated from patients in the presence of various treatments to better understand the treatment journey.

While most newly diagnosed MM patients respond to IMiD therapy, most eventually develop resistance. The underlying mechanisms defining this non-responsiveness are still incompletely understood. Future studies could investigate developing tests to potentially predict high-risk patients and target their treatment accordingly. The idea of detecting circulating tumour DNA or ct DNA in the blood, for example, could act as a liquid biopsy which could be detected with flow cytometry.

Chapter Eight

Bibliography

1. Taylor BJ, Kriangkum J, Pittman JA, et al. Analysis of clonotypic switch junctions reveals multiple myeloma originates from a single class switch event with ongoing mutation in the isotype-switched progeny. *Blood*. 2008;112(5):1894-1903. doi:10.1182/BLOOD-2008-01-129221
2. Hallek M, Bergsagel PL, Anderson KC. Multiple Myeloma: Increasing Evidence for a Multistep Transformation Process. *Blood*. 1998;91(1):3. doi:10.1182/blood.v91.1.3
3. Tiburzy B, Kulkarni U, Hauser AE, Abram M, Manz RA. Plasma cells in immunopathology: concepts and therapeutic strategies. *Semin Immunopathol*. 2014;36(3):277-288. doi:10.1007/S00281-014-0426-8
4. Healy CF, Murray JG, Eustace SJ, Madewell J, O'Gorman PJ, O'Sullivan P. Multiple Myeloma: A Review of Imaging Features and Radiological Techniques. *Bone Marrow Res*. 2011;2011:1-9. doi:10.1155/2011/583439
5. Zamagni E, Cavo M, Fakhri B, Vij R, Roodman D. Bones in Multiple Myeloma: Imaging and Therapy. *American Society of Clinical Oncology Educational Book*. 2018;(38):638-646. doi:10.1200/edbk_205583
6. PET scan | Tests and scans | Cancer Research UK. Accessed March 29, 2023. https://www.cancerresearchuk.org/about-cancer/tests-and-scans/pet-scan
7. Positron Emission Tomography and Computed Tomography (PET-CT) Scans | Cancer.Net. Accessed March 29, 2023. https://www.cancer.net/navigating-cancer-care/diagnosing-cancer/tests-and-procedures/positron-emission-tomography-and-computed-tomography-pet-ct-scans
8. Shakoori AR. Fluorescence In Situ Hybridization (FISH) and Its Applications. *Chromosome Structure and Aberrations*. Published online January 1, 2017:343. doi:10.1007/978-81-322-3673-3_16
9. Zingone A, Kuehl WM. Pathogenesis of Monoclonal Gammopathy of Undetermined Significance (MGUS) and Progression to Multiple Myeloma. *Semin Hematol*. 2011;48(1):4. doi:10.1053/J.SEMINHEMATOL.2010.11.003
10. Kristinsson SY, Björkholm M, Andersson TML, et al. Patterns of survival and causes of death following a diagnosis of monoclonal gammopathy of undetermined significance: A population-based study. *Haematologica*. 2009;94(12):1714-1720. doi:10.3324/HAEMATOL.2009.010066
11. Landgren O, Graubard BI, Katzmann JA, et al. Racial disparities in the prevalence of monoclonal gammopathies: A population-based study of 12 482 persons from the national

health and nutritional examination survey. *Leukemia*. 2014;28(7):1537-1542. doi:10.1038/LEU.2014.34

12. Kleinstern G, Larson DR, Allmer C, et al. Body mass index associated with monoclonal gammopathy of undetermined significance (MGUS) progression in Olmsted County, Minnesota. *Blood Cancer J*. 2022;12(4). doi:10.1038/S41408-022-00659-9
13. Landgren O, Kristinsson SY, Goldin LR, et al. Risk of plasma cell and lymphoproliferative disorders among 14621 first-degree relatives of 4458 patients with monoclonal gammopathy of undetermined significance in Sweden. *Blood*. 2009;114(4):791. doi:10.1182/BLOOD-2008-12-191676
14. Thordardottir M, Lindqvist EK, Lund SH, et al. Obesity and risk of monoclonal gammopathy of undetermined significance and progression to multiple myeloma: A population-based study. *Blood Adv*. 2017;1(24):2186-2192. doi:10.1182/BLOODADVANCES.2017007609
15. Clay-Gilmour AI, Kumar S, Rajkumar SV, et al. Risk of MGUS in relatives of multiple myeloma cases by clinical and tumor characteristics. *Leukemia*. 2019;33(2):499-507. doi:10.1038/S41375-018-0246-2
16. Dhodapkar M v., Sexton R, Waheed S, et al. Clinical, genomic, and imaging predictors of myeloma progression from asymptomatic monoclonal gammopathies (swog s0120). *Blood*. 2014;123(1):78-85. doi:10.1182/BLOOD-2013-07-515239
17. Manasanch EE, Han G, Mathur R, et al. A pilot study of pembrolizumab in smoldering myeloma: report of the clinical, immune, and genomic analysis. *Blood Adv*. 2019;3(15):2400. doi:10.1182/BLOODADVANCES.2019000300
18. Rajkumar SV, Landgren O, Mateos MV. Smoldering multiple myeloma. *Blood*. 2015;125(20):3069. doi:10.1182/BLOOD-2014-09-568899
19. Slowing the Progression of Smoldering Myeloma - NCI. Accessed March 29, 2023. https://www.cancer.gov/news-events/cancer-currents-blog/2019/lenalidomide-slows-progression-smoldering-myeloma
20. Kuehl WM, Bergsagel PL. Molecular pathogenesis of multiple myeloma and its premalignant precursor. *Journal of Clinical Investigation*. 2012;122(10):3456-3463. doi:10.1172/JCI61188
21. Bida JP, Kyle RA, Therneau TM, et al. Disease Associations With Monoclonal Gammopathy of Undetermined Significance: A Population-Based Study of 17,398 Patients. *Mayo Clin Proc*. 2009;84(8):685-693. Accessed September 19, 2022. www.mayoclinicproceedings.com
22. Blum A, Bazou D, O'Gorman P. Smoldering multiple myeloma: prevalence and current evidence guiding treatment decisions. *Blood Lymphat Cancer*. 2018;8:21. doi:10.2147/BLCTT.S136447
23. Rajkumar SV, Dimopoulos MA, Palumbo A, et al. International Myeloma Working Group updated criteria for the diagnosis of multiple myeloma. *Lancet Oncol*. 2014;15(12):e538-e548. doi:10.1016/S1470-2045(14)70442-5

24. Cesana C, Klersy C, Barbarano L, et al. Prognostic factors for malignant transformation in monoclonal gammopathy of undetermined significance and smoldering multiple myeloma. *J Clin Oncol*. 2002;20(6):1625-1634. doi:10.1200/JCO.2002.20.6.1625
25. DeWeerdt S. Burning questions about smouldering myeloma. *Nature*. 2020;587(7835):S58-S59. doi:10.1038/D41586-020-03225-0
26. Kyle RA, Remstein ED, Therneau TM, et al. Clinical Course and Prognosis of Smoldering (Asymptomatic) Multiple Myeloma A bs t r ac t. Published online 2007. Accessed September 19, 2022. www.nejm.org
27. Cenci S, Daniel P, Boise LH, Barwick BG, Gupta VA, Vertino PM. Cell of Origin and Genetic Alterations in the Pathogenesis of Multiple Myeloma A BRIEF HISTORY OF PLASMA CELLS AND MALIGNANCY. *Frontiers in Immunology | www.frontiersin.org*. 2019;1:1121. doi:10.3389/fimmu.2019.01121
28. Radtke D, Bannard O. Expression of the plasma cell transcriptional regulator Blimp-1 by dark zone germinal center B cells during periods of proliferation. *Front Immunol*. 2019;10(JAN):3106. doi:10.3389/FIMMU.2018.03106/BIBTEX
29. Low MSY, Brodie EJ, Fedele PL, et al. IRF4 Activity Is Required in Established Plasma Cells to Regulate Gene Transcription and Mitochondrial Homeostasis. *Cell Rep*. 2019;29(9):2634-2645.e5. doi:10.1016/J.CELREP.2019.10.097
30. Ellebedy AH, Jackson KJL, Kissick HT, et al. Defining antigen-specific plasmablast and memory B cell subsets in blood following viral infection and vaccination of humans. *Nat Immunol*. 2016;17(10):1226. doi:10.1038/NI.3533
31. Roth K, Oehme L, Zehentmeier S, Zhang Y, Niesner R, Hauser AE. Tracking plasma cell differentiation and survival. *Cytometry Part A*. 2014;85(1):15-24. doi:10.1002/CYTO.A.22355
32. Pelletier N, McHeyzer-Williams LJ, Wong KA, Urich E, Fazilleau N, McHeyzer-Williams MG. Plasma cells negatively regulate the follicular helper T cell program. *Nature Immunology 2010 11:12*. 2010;11(12):1110-1118. doi:10.1038/ni.1954
33. Jang E, Cho WS, Oh YK, et al. Splenic Long-Lived Plasma Cells Promote the Development of Follicular Helper T Cells during Autoimmune Responses. *The Journal of Immunology*. 2016;196(3):1026-1035. doi:10.4049/JIMMUNOL.1401059/-/DCSUPPLEMENTAL
34. Akkaya M, Kwak K, Pierce SK. B cell memory: building two walls of protection against pathogens. *Nature Reviews Immunology 2019 20:4*. 2019;20(4):229-238. doi:10.1038/s41577-019-0244-2
35. Bhattacharya M, Bhattacharya M. Understanding B Lymphocyte Development: A Long Way to Go. *Lymphocytes*. Published online November 5, 2018. doi:10.5772/INTECHOPEN.79663
36. Kraal G, Mebius R. New Insights into the Cell Biology of the Marginal Zone of the Spleen. *Int Rev Cytol*. 2006;250:175. doi:10.1016/S0074-7696(06)50005-1

37. Tangye SG. Staying alive: Regulation of plasma cell survival. *Trends Immunol*. 2011;32(12):595-602. doi:10.1016/j.it.2011.09.001
38. Akkaya M, Kwak K, Pierce SK. B cell memory: building two walls of protection against pathogens. *Nature Reviews Immunology 2019 20:4*. 2019;20(4):229-238. doi:10.1038/s41577-019-0244-2
39. Tripathy S. The Role of Serum Protein Electrophoresis in the Detection of Multiple Myeloma: An Experience of a Corporate Hospital. *J Clin Diagn Res*. 2012;6(9):1458.
40. Annunziata CM, Davis RE, Demchenko Y, et al. Frequent engagement of the classical and alternative NF-kappaB pathways by diverse genetic abnormalities in multiple myeloma. *Cancer Cell*. 2007;12(2):115-130. doi:10.1016/J.CCR.2007.07.004
41. Keats JJ, Fonseca R, Chesi M, et al. Promiscuous mutations activate the noncanonical NF-kappaB pathway in multiple myeloma. *Cancer Cell*. 2007;12(2):131-144. doi:10.1016/J.CCR.2007.07.003
42. Sewify EM, Afifi OA, Mosad E, Zaki AH, El Gammal SA. Cyclin D1 amplification in multiple myeloma is associated with multidrug resistance expression. *Clin Lymphoma Myeloma Leuk*. 2014;14(3):215-222. doi:10.1016/j.clml.2013.07.008
43. Chesi M, Nardini E, Brents LA, et al. Frequent translocation t(4;14)(p16.3;q32.3) in multiple myeloma is associated with increased expression and activating mutations of fibroblast growth factor receptor 3. *Nat Genet*. 1997;16(3):260-264. doi:10.1038/NG0797-260
44. Caprio C, Sacco A, Giustini V, Roccaro AM. Epigenetic Aberrations in Multiple Myeloma. *Cancers (Basel)*. 2020;12(10):1-16. doi:10.3390/CANCERS12102996
45. Leif Bergsagel P, Michael Kuehl W. Chromosome translocations in multiple myeloma. *Oncogene 2001 20:40*. 2001;20(40):5611-5622. doi:10.1038/sj.onc.1204641
46. Lionetti M, Barbieri M, Manzoni M, et al. Molecular spectrum of TP53 mutations in plasma cell dyscrasias by next generation sequencing: an Italian cohort study and overview of the literature. *Oncotarget*. 2016;7(16):21353. doi:10.18632/ONCOTARGET.7241
47. Jones JR, Weinhold N, Ashby C, et al. Clonal evolution in myeloma: the impact of maintenance lenalidomide and depth of response on the genetics and sub-clonal structure of relapsed disease in uniformly treated newly diagnosed patients. *Haematologica*. 2019;104(7):1440. doi:10.3324/HAEMATOL.2018.202200
48. Bolli N, Avet-Loiseau H, Wedge DC, et al. ARTICLE Heterogeneity of genomic evolution and mutational profiles in multiple myeloma. Published online 2014. doi:10.1038/ncomms3997
49. Palumbo A, Anderson K. Multiple Myeloma. *New England Journal of Medicine*. 2011;364(11):1046-1060. doi:10.1056/NEJMRA1011442
50. Ding L, Saunders TL, Enikolopov G, Morrison SJ. Endothelial and perivascular cells maintain haematopoietic stem cells. *Nature*. 2012;481(7382):457-462. doi:10.1038/NATURE10783

51. Velten L, Haas SF, Raffel S, et al. Human haematopoietic stem cell lineage commitment is a continuous process. *Nat Cell Biol*. 2017;19(4):271. doi:10.1038/NCB3493
52. Choi K, Kennedy M, Kazarov A, Papadimitriou JC, Keller G. A common precursor for hematopoietic and endothelial cells. *Development*. 1998;125(4):725-732. doi:10.1242/DEV.125.4.725
53. Schofield R. The relationship between the spleen colony-forming cell and the haemopoietic stem cell. A hypothesis. *Blood Cells*. 1978;4(1-2):7-25.
54. Fliedner MC. Research within the field of blood and marrow transplantation nursing: how can it contribute to higher quality of care? *Int J Hematol*. 2002;76 Suppl 2:289-291. doi:10.1007/BF03165135
55. Pang WW, Price EA, Sahoo D, et al. Human bone marrow hematopoietic stem cells are increased in frequency and myeloid-biased with age. *Proc Natl Acad Sci U S A*. 2011;108(50):20012-20017. doi:10.1073/PNAS.1116110108/-/DCSUPPLEMENTAL
56. de Kleer I, Willems F, Lambrecht B, Goriely S. Ontogeny of myeloid cells. *Front Immunol*. 2014;5(AUG):423. doi:10.3389/FIMMU.2014.00423/BIBTEX
57. Kondo M, Wagers AJ, Manz MG, et al. Biology of hematopoietic stem cells and progenitors: implications for clinical application. *Annu Rev Immunol*. 2003;21:759-806. doi:10.1146/ANNUREV.IMMUNOL.21.120601.141007
58. Szade K, Gulati GS, Chan CKF, et al. Where Hematopoietic Stem Cells Live: The Bone Marrow Niche. *Antioxid Redox Signal*. 2018;29(2):191-204. doi:10.1089/ARS.2017.7419
59. Granick JL, Simon SI, Borjesson DL. Hematopoietic Stem and Progenitor Cells as Effectors in Innate Immunity. *Bone Marrow Res*. 2012;2012:1-8. doi:10.1155/2012/165107
60. Mitalipov S, Wolf D. Totipotency, Pluripotency and Nuclear Reprogramming. *Adv Biochem Eng Biotechnol*. 2009;114:185. doi:10.1007/10_2008_45
61. What is the difference between totipotent, pluripotent, and multipotent? | NYSTEM. Accessed September 19, 2022. https://stemcell.ny.gov/faqs/what-difference-between-totipotent-pluripotent-and-multipotent
62. Bishop AE, Buttery LDK, Polak JM. Haematopoietic stem cells. *Journal of Pathology*. 2002;197(4):430-440. doi:10.1002/PATH.1153
63. Challen GA, Boles N, Lin KKY, Goodell MA. Mouse Hematopoietic Stem Cell Identification And Analysis. *Cytometry A*. 2009;75(1):14. doi:10.1002/CYTO.A.20674
64. Zhang P, Zhang C, Li J, Han J, Liu X, Yang H. The physical microenvironment of hematopoietic stem cells and its emerging roles in engineering applications. *Stem Cell Research & Therapy 2019 10:1*. 2019;10(1):1-13. doi:10.1186/S13287-019-1422-7
65. Trowbridge JJ. Intrinsic and Extrinsic Factors Driving Hematopoietic Stem Cell Aging and Bone Marrow Failure. *Blood*. 2019;134(Supplement_1):SCI-35. doi:10.1182/BLOOD-2019-121044

66. Irvin DK, Dhaka A, Hicks C, Weinmaster G, Kornblum HI. Extrinsic and intrinsic factors governing cell fate in cortical progenitor cultures. *Dev Neurosci*. 2003;25(2-4):162-172. doi:10.1159/000072265
67. Teif VB, Rippe K. Predicting nucleosome positions on the DNA: combining intrinsic sequence preferences and remodeler activities. *Nucleic Acids Res*. 2009;37(17):5641. doi:10.1093/NAR/GKP610
68. Rizo A, Vellenga E, de Haan G, Schuringa JJ. Signaling pathways in self-renewing hematopoietic and leukemic stem cells: do all stem cells need a niche? *Hum Mol Genet*. 2006;15(suppl_2):R210-R219. doi:10.1093/HMG/DDL175
69. Mevel R, Draper JE, Lie-A-Ling M, Kouskoff V, Lacaud G. RUNX transcription factors: Orchestrators of development. *Development (Cambridge)*. 2019;146(17). doi:10.1242/DEV.148296/222975
70. Bresnick EH, Katsumura KR, Lee HY, Johnson KD, Perkins AS. Master regulatory GATA transcription factors: mechanistic principles and emerging links to hematologic malignancies. *Nucleic Acids Res*. 2012;40(13):5819. doi:10.1093/NAR/GKS281
71. Bee T, Liddiard K, Swiers G, et al. Alternative Runx1 promoter usage in mouse developmental hematopoiesis. *Blood Cells Mol Dis*. 2009;43(1):35-42. doi:10.1016/J.BCMD.2009.03.011
72. Bresciani E, Carrington B, Wincovitch S, et al. CBFβ and RUNX1 are required at 2 different steps during the development of hematopoietic stem cells in zebrafish. *Blood*. 2014;124(1):70-78. doi:10.1182/BLOOD-2013-10-531988
73. Rodrigues NP, Tipping AJ, Wang Z, Enver T. GATA-2 mediated regulation of normal hematopoietic stem/progenitor cell function, myelodysplasia and myeloid leukemia. *Int J Biochem Cell Biol*. 2012;44(3):457. doi:10.1016/J.BIOCEL.2011.12.004
74. Wanet A, Bassal MA, Patel SB, et al. E-cadherin is regulated by GATA-2 and marks the early commitment of mouse hematopoietic progenitors to the basophil and mast cell fates. *Sci Immunol*. 2021;6(56). doi:10.1126/SCIIMMUNOL.ABA0178
75. Castaño J, Aranda S, Bueno C, et al. GATA2 Promotes Hematopoietic Development and Represses Cardiac Differentiation of Human Mesoderm. *Stem Cell Reports*. 2019;13(3):515. doi:10.1016/J.STEMCR.2019.07.009
76. Buisman SC, de Haan G. Epigenetic Changes as a Target in Aging Haematopoietic Stem Cells and Age-Related Malignancies. *Cells*. 2019;8(8):868. doi:10.3390/CELLS8080868
77. Jiang P, Wang H, Zheng J, Han Y, Huang H, Qian P. Epigenetic regulation of hematopoietic stem cell homeostasis. *Blood Science*. 2019;1(1):19. doi:10.1097/BS9.0000000000000018
78. Spencer JA, Ferraro F, Roussakis E, et al. Direct measurement of local oxygen concentration in the bone marrow of live animals. *Nature*. 2014;508(7495):269. doi:10.1038/NATURE13034

79. Hira VVV, Wormer JR, Kakar H, et al. Periarteriolar Glioblastoma Stem Cell Niches Express Bone Marrow Hematopoietic Stem Cell Niche Proteins. *Journal of Histochemistry and Cytochemistry*. 2018;66(3):155-173. doi:10.1369/0022155417749174
80. Zhang CC, Sadek HA. Hypoxia and Metabolic Properties of Hematopoietic Stem Cells. *Antioxid Redox Signal*. 2014;20(12):1891. doi:10.1089/ARS.2012.5019
81. Eliasson P, Rehn M, Hammar P, et al. Hypoxia mediates low cell-cycle activity and increases the proportion of long-term-reconstituting hematopoietic stem cells during in vitro culture. *Exp Hematol*. 2010;38(4):301-310.e2. doi:10.1016/J.EXPHEM.2010.01.005
82. Tabarowski Z, Gibson-Berry K, Felten SY. Noradrenergic and peptidergic innervation of the mouse femur bone marrow. *Acta Histochem*. 1996;98(4):453-457. doi:10.1016/S0065-1281(96)80013-4
83. Hanoun M, Maryanovich M, Arnal-Estapé A, Frenette PS. Neural regulation of hematopoiesis, inflammation and cancer. *Neuron*. 2015;86(2):360. doi:10.1016/J.NEURON.2015.01.026
84. Arranz L, Sánchez-Aguilera A, Martín-Pérez D, et al. Neuropathy of haematopoietic stem cell niche is essential for myeloproliferative neoplasms. *Nature 2014 512:7512*. 2014;512(7512):78-81. doi:10.1038/nature13383
85. Yamazaki S, Ema H, Karlsson G, et al. Nonmyelinating schwann cells maintain hematopoietic stem cell hibernation in the bone marrow niche. *Cell*. 2011;147(5):1146-1158. doi:10.1016/J.CELL.2011.09.053/ATTACHMENT/31E1E500-3884-4644-A972-A6A89A119AC9/MMC1.AVI
86. Russo S, Scotto di Carlo F, Gianfrancesco F. The Osteoclast Traces the Route to Bone Tumors and Metastases. *Front Cell Dev Biol*. 2022;10:788. doi:10.3389/FCELL.2022.886305/BIBTEX
87. Teitelbaum SL. Bone resorption by osteoclasts. *Science (1979)*. 2000;289(5484):1504-1508. doi:10.1126/SCIENCE.289.5484.1504/ASSET/7F1E58BF-C087-4C6F-9C06-C190FE05FFD3/ASSETS/GRAPHIC/SE3408789003.JPEG
88. Ikeda K, Takeshita S. The role of osteoclast differentiation and function in skeletal homeostasis. *The Journal of Biochemistry*. 2016;159(1):1-8. doi:10.1093/JB/MVV112
89. Kenkre JS, Bassett JHD. The bone remodelling cycle. *Ann Clin Biochem*. 2018;55(3):308-327. doi:10.1177/0004563218759371
90. Zaidi M. Skeletal remodeling in health and disease. *Nat Med*. 2007;13(7):791-801. doi:10.1038/NM1593
91. Peruzzi B, Teti A. The Physiology and Pathophysiology of the Osteoclast. *Clinical Reviews in Bone and Mineral Metabolism 2011 10:2*. 2011;10(2):71-97. doi:10.1007/S12018-011-9086-6

92. Kollet O, Dar A, Shivtiel S, et al. Osteoclasts degrade endosteal components and promote mobilization of hematopoietic progenitor cells. *Nature Medicine 2006 12:6*. 2006;12(6):657-664. doi:10.1038/nm1417
93. Jiang Y, Bonig H, Ulyanova T, Chang KH, Papayannopoulou T. On the adaptation of endosteal stem cell niche function in response to stress. *Blood*. 2009;114(18):3773-3782. doi:10.1182/BLOOD-2009-05-219840
94. Rao M, Supakorndej T, Schmidt AP, Link DC. Osteoclasts are dispensable for hematopoietic progenitor mobilization by granulocyte colony-stimulating factor in mice. *Exp Hematol*. 2015;43(2):110-114.e2. doi:10.1016/J.EXPHEM.2014.10.012
95. Miyamoto K, Yoshida S, Kawasumi M, et al. Osteoclasts are dispensable for hematopoietic stem cell maintenance and mobilization. *J Exp Med*. 2011;208(11):2175-2181. doi:10.1084/JEM.20101890
96. Rademakers T, Goedhart M, Hoogenboezem M, et al. Hematopoietic stem and progenitor cells use podosomes to transcellularly cross the bone marrow endothelium. *Haematologica*. 2020;105(12):2746. doi:10.3324/HAEMATOL.2018.196329
97. Xu C, Gao X, Wei Q, et al. Stem cell factor is selectively secreted by arterial endothelial cells in bone marrow. *Nat Commun*. 2018;9(1). doi:10.1038/S41467-018-04726-3
98. Ley K, Allietta M, Bullard DC, Morgan S. Importance of E-Selectin for Firm Leukocyte Adhesion In Vivo. *Circ Res*. 1998;83(3):287-294. doi:10.1161/01.RES.83.3.287
99. Karin N. The multiple faces of CXCL12 (SDF-1α) in the regulation of immunity during health and disease. *J Leukoc Biol*. 2010;88(3):463-473. doi:10.1189/JLB.0909602
100. Li B, Bai W, Sun P, Zhou B, Hu B, Ying J. The effect of CXCL12 on endothelial progenitor cells: potential target for angiogenesis in intracerebral hemorrhage. *J Interferon Cytokine Res*. 2015;35(1):23-31. doi:10.1089/JIR.2014.0004
101. Winkler IG, Barbier V, Nowlan B, et al. Vascular niche E-selectin regulates hematopoietic stem cell dormancy, self renewal and chemoresistance. *Nat Med*. 2012;18(11):1651-1657. doi:10.1038/NM.2969
102. Barbier V, Erbani J, Fiveash C, et al. Endothelial E-selectin inhibition improves acute myeloid leukaemia therapy by disrupting vascular niche-mediated chemoresistance. *Nat Commun*. 2020;11(1). doi:10.1038/S41467-020-15817-5
103. Himburg HA, Muramoto GG, Daher P, et al. Pleiotrophin regulates the expansion and regeneration of hematopoietic stem cells. *Nat Med*. 2010;16(4):475. doi:10.1038/NM.2119
104. Hirayama D, Iida T, Nakase H. The Phagocytic Function of Macrophage-Enforcing Innate Immunity and Tissue Homeostasis. *Int J Mol Sci*. 2018;19(1). doi:10.3390/IJMS19010092
105. Chambers M, Rees A, Cronin JG, Nair M, Jones N, Thornton CA. Macrophage Plasticity in Reproduction and Environmental Influences on Their Function. *Front Immunol*. 2021;11. doi:10.3389/FIMMU.2020.607328

106. Winkler IG, Sims NA, Pettit AR, et al. Bone marrow macrophages maintain hematopoietic stem cell (HSC) niches and their depletion mobilizes HSCs. *Blood*. 2010;116(23):4815-4828. doi:10.1182/BLOOD-2009-11-253534
107. Chow A, Lucas D, Hidalgo A, et al. Bone marrow CD169+ macrophages promote the retention of hematopoietic stem and progenitor cells in the mesenchymal stem cell niche. *J Exp Med*. 2011;208(2):261. doi:10.1084/JEM.20101688
108. Wang J, Xie J, Wang D, et al. CXCR4high megakaryocytes regulate host-defense immunity against bacterial pathogens. *Elife*. 2022;11. doi:10.7554/ELIFE.78662
109. Malara A, Abbonante V, Zingariello M, Migliaccio A, Balduini A. Megakaryocyte Contribution to Bone Marrow Fibrosis: many Arrows in the Quiver. *Mediterr J Hematol Infect Dis*. 2018;10(1):2018068. doi:10.4084/MJHID.2018.068
110. Coppinger JA, Cagney G, Toomey S, et al. Characterization of the proteins released from activated platelets leads to localization of novel platelet proteins in human atherosclerotic lesions. *Blood*. 2004;103(6):2096-2104. doi:10.1182/BLOOD-2003-08-2804
111. Yoshihara H, Arai F, Hosokawa K, et al. Thrombopoietin/MPL Signaling Regulates Hematopoietic Stem Cell Quiescence and Interaction with the Osteoblastic Niche. *Cell Stem Cell*. 2007;1(6):685-697. doi:10.1016/J.STEM.2007.10.020/ATTACHMENT/3327ED9C-D29A-44D4-B0E3-9A471097DD5F/MMC1.PDF
112. Kaushansky K. Thrombopoietin: the primary regulator of megakaryocyte and platelet production. *Thromb Haemost*. 1995;74:521-525.
113. Rudensky AY. Regulatory T Cells and Foxp3. *Immunol Rev*. 2011;241(1):260. doi:10.1111/J.1600-065X.2011.01018.X
114. Wheaton JD, Ciofani M. JunB controls intestinal effector programs in regulatory T cells. *bioRxiv*. Published online November 13, 2019:772194. doi:10.1101/772194
115. Hirata Y, Kakiuchi M, Robson SC, Fujisaki J. CD150high CD4 T cells and CD150high regulatory T cells regulate hematopoietic stem cell quiescence via CD73. *Haematologica*. 2019;104(6):1136. doi:10.3324/HAEMATOL.2018.198283
116. Glatman Zaretsky A, Konradt C, Dépis F, et al. T Regulatory Cells Support Plasma Cell Populations in the Bone Marrow. *Cell Rep*. 2017;18(8):1906-1916. doi:10.1016/J.CELREP.2017.01.067
117. Horwitz EM, Andreef M, Frassoni F. Mesenchymal Stromal Cells. *Curr Opin Hematol*. 2006;13(6):419. doi:10.1097/01.MOH.0000245697.54887.6F
118. Brennen WN, Chen S, Denmeade SR, Isaacs JT. Quantification of Mesenchymal Stem Cells (MSCs) at Sites of Human Prostate Cancer. *Oncotarget*. 2013;4(1):106. doi:10.18632/ONCOTARGET.805

119. Dominici M, le Blanc K, Mueller I, et al. Minimal criteria for defining multipotent mesenchymal stromal cells. The International Society for Cellular Therapy position statement. *Cytotherapy*. 2006;8(4):315-317. doi:10.1080/14653240600855905
120. Mayack SR, Wagers AJ. Osteolineage niche cells initiate hematopoietic stem cell mobilization. *Blood*. 2008;112(3):519. doi:10.1182/BLOOD-2008-01-133710
121. Ryan JM, Barry FP, Murphy JM, Mahon BP. Mesenchymal stem cells avoid allogeneic rejection. *J Inflamm (Lond)*. 2005;2:8. doi:10.1186/1476-9255-2-8
122. Mackay AM, Beck SC, Murphy JM, Barry FP, Chichester CO, Pittenger MF. Chondrogenic differentiation of cultured human mesenchymal stem cells from marrow. *Tissue Eng*. 1998;4(4):415-428. doi:10.1089/TEN.1998.4.415
123. Asada N, Katayama Y. Regulation of hematopoiesis in endosteal microenvironments. *Int J Hematol*. 2014;99(6):679-684. doi:10.1007/S12185-014-1583-1/FIGURES/3
124. Xie Z, Tang S, Ye G, et al. Interleukin-6/interleukin-6 receptor complex promotes osteogenic differentiation of bone marrow-derived mesenchymal stem cells. *Stem Cell Res Ther*. 2018;9(1). doi:10.1186/S13287-017-0766-0
125. Grano M, Galimi F, Zambonin G, et al. Hepatocyte growth factor is a coupling factor for osteoclasts and osteoblasts in vitro. *Proc Natl Acad Sci U S A*. 1996;93(15):7644-7648. doi:10.1073/PNAS.93.15.7644
126. lo Celso C, Fleming HE, Wu JW, et al. Live-animal tracking of individual haematopoietic stem/progenitor cells in their niche. *Nature*. 2009;457(7225):92. doi:10.1038/NATURE07434
127. Dallas SL, Bonewald LF. Dynamics of the Transition from Osteoblast to Osteocyte. *Ann N Y Acad Sci*. 2010;1192:437. doi:10.1111/J.1749-6632.2009.05246.X
128. Olivares-Navarrete R, Raines AL, Hyzy SL, et al. Osteoblast Maturation and New Bone Formation in Response to Titanium Implant Surface Features are Reduced with Age. *J Bone Miner Res*. 2012;27(8):1773-1783. doi:10.1002/JBMR.1628
129. Aisha MD, Nor-Ashikin MNK, Sharaniza AB, Nawawi HM, Kapitonova MY, Froemming GRA. Short-term moderate hypothermia stimulates alkaline phosphatase activity and osteocalcin expression in osteoblasts by upregulating Runx2 and osterix in vitro. *Exp Cell Res*. 2014;326(1):46-56. doi:10.1016/J.YEXCR.2014.06.003
130. Mansour A, Abou-Ezzi G, Sitnicka E, Jacobsen SEW, Wakkach A, Blin-Wakkach C. Osteoclasts promote the formation of hematopoietic stem cell niches in the bone marrow. *J Exp Med*. 2012;209(3):537. doi:10.1084/JEM.20110994
131. Blaber EA, Dvorochkin N, Torres ML, et al. Mechanical unloading of bone in microgravity reduces mesenchymal and hematopoietic stem cell-mediated tissue regeneration. *Stem Cell Res*. 2014;13(2):181-201. doi:10.1016/J.SCR.2014.05.005
132. Shi S, Gronthos S. Perivascular Niche of Postnatal Mesenchymal Stem Cells in Human Bone Marrow and Dental Pulp. Published online 2003.

133. Yu VWC, Scadden DT. Hematopoietic Stem Cell and Its Bone Marrow Niche. *Curr Top Dev Biol*. 2016;118:21. doi:10.1016/BS.CTDB.2016.01.009
134. Sugiyama T, Kohara H, Noda M, Nagasawa T. Maintenance of the Hematopoietic Stem Cell Pool by CXCL12-CXCR4 Chemokine Signaling in Bone Marrow Stromal Cell Niches. *Immunity*. 2006;25(6):977-988. doi:10.1016/J.IMMUNI.2006.10.016
135. Asada N, Kunisaki Y, Pierce H, et al. Differential cytokine contributions of perivascular haematopoietic stem cell niches. *Nat Cell Biol*. 2017;19(3):214. doi:10.1038/NCB3475
136. Mendelson A, Frenette PS. Hematopoietic stem cell niche maintenance during homeostasis and regeneration. *Nat Med*. 2014;20(8):833-846. doi:10.1038/NM.3647
137. Naveiras O, Nardi V, Wenzel PL, Hauschka P v., Fahey F, Daley GQ. Bone marrow adipocytes as negative regulators of the hematopoietic microenvironment. *Nature*. 2009;460(7252):259. doi:10.1038/NATURE08099
138. Zhou BO, Yu H, Yue R, et al. Bone marrow adipocytes promote the regeneration of stem cells and hematopoiesis by secreting SCF. *Nat Cell Biol*. 2017;19(8):891. doi:10.1038/NCB3570
139. Omatsu Y, Sugiyama T, Kohara H, et al. The essential functions of adipo-osteogenic progenitors as the hematopoietic stem and progenitor cell niche. *Immunity*. 2010;33(3):387-399. doi:10.1016/J.IMMUNI.2010.08.017
140. Diaz-Delcastillo M, Andrews RE, Mandal A, Andersen TL, Chantry AD, Heegaard AM. Bone pain in multiple myeloma (Bpmm)—a protocol for a prospective, longitudinal, observational study. *Cancers (Basel)*. 2021;13(7). doi:10.3390/CANCERS13071596/S1
142. Edwards CM, Zhuang J, Mundy GR. The pathogenesis of the bone disease of multiple myeloma. *Bone*. Published online 2008. doi:10.1016/j.bone.2008.01.027
143. Xu F, Teitelbaum SL. Osteoclasts: New Insights. *Bone Res*. Published online 2013. doi:10.4248/BR201301003
144. Papadopoulou EC, Batzios SP, Dimitriadou M, Perifanis V, Garipidou V. Multiple myeloma and bone disease: Pathogenesis and current therapeutic approaches. *Hippokratia*. Published online 2010.
145. Liu XH, Kirschenbaum A, Yao S, Levine AC. Interactive effect of interleukin-6 and prostaglandin E2 on osteoclastogenesis via the OPG/RANKL/RANK system. In: *Annals of the New York Academy of Sciences*. ; 2006. doi:10.1196/annals.1346.047
146. Chauhan D, Kharbanda S, Ogata A, et al. Interleukin-6 inhibits Fas-induced apoptosis and stress-activated protein kinase activation in multiple myeloma cells. *Blood*. Published online 1997. doi:10.1182/blood.v89.1.227.227_227_234
147. Liu XH, Kirschenbaum A, Yao S, Levine AC. Cross-talk between the interleukin-6 and prostaglandin E2 signaling systems results in enhancement of osteoclastogenesis through

effects on the osteoprotegerin/receptor activator of nuclear factor-κB (RANK) ligand/RANK system. *Endocrinology*. Published online 2005. doi:10.1210/en.2004-1167

148. Adebanjo OA, Moonga BS, Yamate T, et al. Mode of action of interleukin-6 on mature osteoclasts. Novel interactions with extracellular Ca2+ sensing in the regulation of osteoclastic bone resorption. *Journal of Cell Biology*. Published online 1998. doi:10.1083/jcb.142.5.1347
149. Wu Q, Zhou X, Huang D, Ji Y, Kang F. IL-6 enhances osteocyte-mediated osteoclastogenesis by promoting JAK2 and RANKL activity in vitro. *Cellular Physiology and Biochemistry*. Published online 2017. doi:10.1159/000465455
150. Rozen N, Ish-Shalom S, Rachmiel A, Stein H, Lewinson D. Interleukin-6 modulates trabecular and endochondral bone turnover in the nude mouse by stimulating osteoclast differentiation. *Bone*. Published online 2000. doi:10.1016/S8756-3282(00)00263-5
151. Dinarello CA. Interleukin-1 in the pathogenesis and treatment of inflammatory diseases. *Blood*. Published online 2011. doi:10.1182/blood-2010-07-273417
152. Trebec-Reynolds DP, Voronov I, Heersche JNM, Manolson MF. IL-1α and IL-1β have different effects on formation and activity of large osteoclasts. *J Cell Biochem*. Published online 2010. doi:10.1002/jcb.22476
153. Shiratori T, Kyumoto-Nakamura Y, Kukita A, et al. IL-1β Induces Pathologically Activated Osteoclasts Bearing Extremely High Levels of Resorbing Activity: A Possible Pathological Subpopulation of Osteoclasts, Accompanied by Suppressed Expression of Kindlin-3 and Talin-1. *The Journal of Immunology*. Published online 2018. doi:10.4049/jimmunol.1602035
154. Kim JH, Jin HM, Kim K, et al. The Mechanism of Osteoclast Differentiation Induced by IL-1. *The Journal of Immunology*. Published online 2009. doi:10.4049/jimmunol.0803007
155. Malik A, Kanneganti TD. Function and regulation of IL-1α in inflammatory diseases and cancer. *Immunol Rev*. 2018;281(1):124. doi:10.1111/IMR.12615
156. Kono H, Karmarkar D, Iwakura Y, Rock KL. Identification of the cellular sensor that stimulates the inflammatory response to sterile cell death. *J Immunol*. 2010;184(8):4470. doi:10.4049/JIMMUNOL.0902485
157. Pietras EM, Mirantes-Barbeito C, Fong S, et al. Chronic interleukin-1 exposure drives haematopoietic stem cells towards precocious myeloid differentiation at the expense of self-renewal. *Nat Cell Biol*. Published online 2016. doi:10.1038/ncb3346
158. Pietras EM, Mirantes-Barbeito C, Fong S, et al. Interleukin-1 Drives Precocious Myeloid Differentiation of Hematopoietic Stem Cells at the Expense of Self-Renewal. *Blood*. Published online 2015. doi:10.1182/blood.v126.23.778.778
159. Lacy MQ, Donovan KA, Heimbach JK, Ahmann GJ, Lust JA. Comparison of interleukin-1β expression by in situ hybridization in monoclonal gammopathy of undetermined significance

and multiple myeloma. *Blood*. Published online 1999. doi:10.1182/blood.v93.1.300.401k36_300_305

160. Costes V, Portier M, Lu ZY, Rossi JF, Bataille R, Klein B. Interleukin-1 in multiple myeloma: Producer cells and their role in the control of IL-6 production. *Br J Haematol*. Published online 1998. doi:10.1046/j.1365-2141.1998.01101.x
161. Glier H, Heijnen I, Hauwel M, et al. Standardization of 8-color flow cytometry across different flow cytometer instruments: A feasibility study in clinical laboratories in Switzerland. *J Immunol Methods*. Published online July 29, 2017. doi:10.1016/j.jim.2017.07.013
162. Lee JW, Chung HY, Ehrlich LA, et al. IL-3 expression by myeloma cells increases both osteoclast formation and growth of myeloma cells. *Blood*. Published online 2004. doi:10.1182/blood-2003-06-1992
163. MERICO F, BERGUI L, GREGORETTI MG, et al. Cytokines involved in the progression of multiple myeloma. *Clin Exp Immunol*. Published online 2008. doi:10.1111/j.1365-2249.1993.tb05943.x
164. Zhang YH, Heulsmann A, Tondravi MM, Mukherjee A, Abu-Amer Y. Tumor necrosis factor-α (TNF) stimulates RANKL-induced osteoclastogenesis via coupling of TNF type 1 receptor and RANK signaling pathways. *Journal of Biological Chemistry*. Published online 2001. doi:10.1074/jbc.M008198200
165. Calip GS, Lee WJ, Lee TA, Schumock GT, Chiu BCH. Tumor Necrosis Factor-Alpha Inhibitor Medications for Inflammatory Conditions and Incidence of Multiple Myeloma. *Blood*. 2015;126(23).
166. Lu X, Gilbert L, He X, Rubin J, Nanes MS. Transcriptional regulation of the osterix (Osx, Sp7) promoter by tumor necrosis factor identifies disparate effects of mitogen-activated protein kinase and NFκB pathways. *Journal of Biological Chemistry*. Published online 2006. doi:10.1074/jbc.M507804200
167. Abe M, Hiura K, Wilde J, et al. Role for macrophage inflammatory protein (MIP)-1α and MIP-1β in the development of osteolytic lesions in multiple myeloma. *Blood*. Published online 2002. doi:10.1182/blood.v100.6.2195.h81802002195_2195_2202
168. Aggarwal R, Ghobrial IM, Roodman GD. Chemokines in multiple myeloma. *Exp Hematol*. Published online 2006. doi:10.1016/j.exphem.2006.06.017
169. Laurence JS, Blanpain C, Burgner JW, Parmentier M, LiWang PJ. CC chemokine MIP-1β can function as a monomer and depends on Phe13 for receptor binding. *Biochemistry*. Published online 2000. doi:10.1021/bi9923196
170. Barmania F, Pepper MS. C-C chemokine receptor type five (CCR5): An emerging target for the control of HIV infection. *Appl Transl Genom*. Published online 2013. doi:10.1016/j.atg.2013.05.004

171. Baniwal SK, Shah PK, Shi Y, et al. Runx2 promotes both osteoblastogenesis and novel osteoclastogenic signals in ST2 mesenchymal progenitor cells. *Osteoporosis International*. Published online 2012. doi:10.1007/s00198-011-1728-5
172. Fu R, Liu H, Zhao S, et al. Osteoblast inhibition by chemokine cytokine ligand3 in myeloma-induced bone disease. *Cancer Cell Int*. Published online 2014. doi:10.1186/s12935-014-0132-6
173. Hashimoto T, Abe M, Oshima T, et al. Ability of myeloma cells to secrete macrophage inflammatory protein (MIP)-1α and MIP-1β correlates with lytic bone lesions in patients with multiple myeloma. *Br J Haematol*. Published online 2004. doi:10.1111/j.1365-2141.2004.04864.x
174. Terpos E, Politou M, Szydlo R, Goldman JM, Apperley JF, Rahemtulla A. Serum levels of macrophage inflammatory protein-1 alpha (MIP-1α) correlate with the extent of bone disease and survival in patients with multiple myeloma. *Br J Haematol*. Published online 2003. doi:10.1046/j.1365-2141.2003.04561.x
175. Standal T, Abildgaard N, Fagerli UM, et al. rao inhibits BMP-induced osteoblastogenesis: Possible implications for the bone disease of multiple myeloma. *Blood*. Published online 2007. doi:10.1182/blood-2006-07-034884
176. Jain AP, Pundir S, Sharma A. Bone morphogenetic proteins: The anomalous molecules. *J Indian Soc Periodontol*. Published online 2013. doi:10.4103/0972-124X.119275
177. Hjertner Ø, Torgersen ML, Seidel C, et al. Hepatocyte growth factor (HGF) induces interleukin-11 secretion from osteoblasts: A possible role for HGF in myeloma-associated osteolytic bone disease. *Blood*. Published online 1999. doi:10.1182/blood.v94.11.3883.423k21_3883_3888
178. Jurczyszyn A, Czepiel J, Biesiada G, et al. HGF, sIL-6R and TGF-β1 play a significant role in the progression of multiple myeloma. *J Cancer*. Published online 2014. doi:10.7150/jca.9266
179. Rampa C, Tian E, Våtsveen TK, et al. Identification of the source of elevated hepatocyte growth factor levels in multiple myeloma patients. *Biomark Res*. Published online 2014. doi:10.1186/2050-7771-2-8
180. Duda DG, Kozin S V., Kirkpatrick ND, Xu L, Fukumura D, Jain RK. CXCL12 (SDF1α)-CXCR4/CXCR7 pathway inhibition: An emerging sensitizer for anticancer therapies? *Clinical Cancer Research*. Published online 2011. doi:10.1158/1078-0432.CCR-10-2636
181. Bouyssou JMC, Ghobrial IM, Roccaro AM. Targeting SDF-1 in multiple myeloma tumor microenvironment. *Cancer Lett*. Published online 2016. doi:10.1016/j.canlet.2015.11.028
182. Azab AK, Sahin I, Azab F, et al. CXCR7-dependent angiogenic mononuclear cell trafficking regulates tumor progression in multiple myeloma. *Blood*. Published online 2014. doi:10.1182/blood-2014-02-558742

183. Zhang H, Trivedi A, Lee JU, et al. Matrix metalloproteinase-9 and stromal cell-derived factor-1 act synergistically to support migration of blood-borne monocytes into the injured spinal cord. *Journal of Neuroscience*. Published online 2011. doi:10.1523/JNEUROSCI.3943-11.2011
184. D'Souza S, Kurihara N, Shiozawa Y, et al. Annexin II interactions with the annexin II receptor enhance multiple myeloma cell adhesion and growth in the bone marrow microenvironment. *Blood*. Published online 2012. doi:10.1182/blood-2011-11-393348
185. Niida S, Kaku M, Amano H, et al. Vascular endothelial growth factor can substitute for macrophage colony- stimulating factor in the support of osteoclastic bone resorption. *Journal of Experimental Medicine*. Published online 1999. doi:10.1084/jem.190.2.293
186. Terpos E, Heath DJ, Rahemtulla A, et al. Bortezomib reduces serum dickkopf-1 and receptor activator of nuclear factor-κB ligand concentrations and normalises indices of bone remodelling in patients with relapsed multiple myeloma. *Br J Haematol*. Published online 2006. doi:10.1111/j.1365-2141.2006.06356.x
187. Kohli SS, Kohli VS. Role of RANKL–RANK/osteoprotegerin molecular complex in bone remodeling and its immunopathologic implications. *Indian J Endocrinol Metab*. 2011;15(3):175. doi:10.4103/2230-8210.83401
188. Ben-awadh AN, Delgado-Calle J, Tu X, et al. Parathyroid Hormone Receptor Signaling Induces Bone Resorption in the Adult Skeleton by Directly Regulating the RANKL Gene in Osteocytes. *Endocrinology*. 2014;155(8):2797. doi:10.1210/EN.2014-1046
189. Mosheimer BA, Kaneider NC, Feistritzer C, et al. Syndecan-1 is involved in osteoprotegerin-induced chemotaxis in human peripheral blood monocytes. *J Clin Endocrinol Metab*. 2005;90(5):2964-2971. doi:10.1210/JC.2004-1895
190. Kong YY, Yoshida H, Sarosi I, et al. OPGL is a key regulator of osteoclastogenesis, lymphocyte development and lymph-node organogenesis. *Nature*. Published online 1999. doi:10.1038/16852
190. Nagae M, Hiraga T, Wakabayashi H, Wang L, Iwata K, Yoneda T. Osteoclasts play a part in pain due to the inflammation adjacent to bone. *Bone*. Published online 2006. doi:10.1016/j.bone.2006.04.033
191. Madel MB, Ibáñez L, Wakkach A, et al. Immune Function and Diversity of Osteoclasts in Normal and Pathological Conditions. *Front Immunol*. 2019;10(JUN):1408. doi:10.3389/FIMMU.2019.01408
192. Li B, Wang P, Jiao J, Wei H, Xu W, Zhou P. Roles of the RANKL–RANK Axis in Immunity—Implications for Pathogenesis and Treatment of Bone Metastasis. *Front Immunol*. 2022;13:1. doi:10.3389/FIMMU.2022.824117
193. Basbaum AI, Bautista DM, Scherrer G, Julius D. Cellular and Molecular Mechanisms of Pain. *Cell*. Published online 2009. doi:10.1016/j.cell.2009.09.028

194. Hiasa M, Okui T, Allette YM, et al. Bone pain induced by multiple myeloma is reduced by targeting V-ATPase and ASIC3. *Cancer Res*. Published online 2017. doi:10.1158/0008-5472.CAN-15-3545
195. Gu Q, Lee LY. Acid-Sensing ion channels and pain. *Pharmaceuticals*. Published online 2010. doi:10.3390/ph3051411
196. Teitelbaum SL. Bone resorption by osteoclasts. *Science (1979)*. Published online 2000. doi:10.1126/science.289.5484.1504
197. Mamet J, Baron A, Lazdunski M, Voilley N. Proinflammatory mediators, stimulators of sensory neuron excitability via the expression of acid-sensing ion channels. *Journal of Neuroscience*. Published online 2002. doi:10.1523/jneurosci.22-24-10662.2002
198. Riemann A, Wußling H, Loppnow H, Fu H, Reime S, Thews O. Acidosis differently modulates the inflammatory program in monocytes and macrophages. *Biochim Biophys Acta Mol Basis Dis*. Published online 2016. doi:10.1016/j.bbadis.2015.10.017
199. Abdelhamid RE, Sluka KA. ASICs mediate pain and inflammation in musculoskeletal diseases. *Physiology*. Published online 2015. doi:10.1152/physiol.00030.2015
200. De Jongh RF, Vissers KC, Meert TF, Booij LHDJ, De Deyne CS, Heylen RJ. The role of interleukin-6 in nociception and pain. *Anesth Analg*. Published online 2003. doi:10.1213/01.ANE.0000055362.56604.78
201. Schaible HG, Von Banchet GS, Boettger MK, et al. The role of proinflammatory cytokines in the generation and maintenance of joint pain. *Ann N Y Acad Sci*. Published online 2010. doi:10.1111/j.1749-6632.2009.05301.x
202. Renaghan AD, Rosner MH. Hypercalcemia: Etiology and management. *Nephrology Dialysis Transplantation*. Published online 2018. doi:10.1093/ndt/gfy054
203. Mirrakhimov AE. Hypercalcemia of malignancy: An update on pathogenesis and management. *N Am J Med Sci*. Published online 2015. doi:10.4103/1947-2714.170600
204. Tanaka M, Yamazaki S, Hayashino Y, et al. Hypercalcaemia is associated with poor mental health in haemodialysis patients: Results from Japan DOPPS. *Nephrology Dialysis Transplantation*. Published online 2007. doi:10.1093/ndt/gfm008
205. Iacovelli E, Gilio F, Mascia ML, et al. Acute and chronic effects of hypercalcaemia on cortical excitability as studied by 5 Hz repetitive transcranial magnetic stimulation. *Journal of Physiology*. Published online 2011. doi:10.1113/jphysiol.2010.201111
206. Hussain N, Khan M, Natarajan A, et al. A Case of Multiple Myeloma Coexisting with Primary Hyperparathyroidism and Review of the Literature. *Case Rep Oncol Med*. Published online 2013. doi:10.1155/2013/420565
207. Jilka RL, Weinstein RS, Bellido T, Parfitt AM, Manolagas SC. Osteoblast programmed cell death (apoptosis): Modulation by growth factors and cytokines. *Journal of Bone and Mineral Research*. Published online 1998. doi:10.1359/jbmr.1998.13.5.793

208. Hock JM, Krishnan V, Onyia JE, et al. Osteoblast apoptosis and bone turnover. *Journal of Bone and Mineral Research*. Published online 2001. doi:10.1359/jbmr.2001.16.6.975
209. Silvestris F, Cafforio P, Tucci M, Grinello D, Dammacco F. Upregulation of osteoblast apoptosis by malignant plasma cells: A role in myeloma bone disease. *Br J Haematol*. Published online 2003. doi:10.1046/j.1365-2141.2003.04374.x
210. Silvestris F, Cafforio P, Calvani N, Dammacco F. Impaired osteoblastogenesis in myeloma bone disease: Role of upregulated apoptosis by cytokines and malignant plasma cells. *Br J Haematol*. Published online 2004. doi:10.1111/j.1365-2141.2004.05084.x
211. Giuliani N, Rizzoli V, Roodman GD. Multiple myeloma bone disease: Pathophysiology of osteoblast inhibition. *Blood*. Published online 2006. doi:10.1182/blood-2006-05-026112
212. Rutkovskiy A, Stensløkken KO, Vaage IJ. Osteoblast Differentiation at a Glance. *Med Sci Monit Basic Res*. Published online 2016. doi:10.12659/msmbr.901142
213. Ottewell PD. The role of osteoblasts in bone metastasis. *J Bone Oncol*. Published online 2016. doi:10.1016/j.jbo.2016.03.007
214. Habibi H, Abroun S, Hajifathali A, et al. Osteogenic inhibition in multiple myeloma. *Cell J*. Published online 2013.
215. Qiang YW, Chen Y, Stephens O, et al. Myeloma-derived dickkopf-1 disrupts Wnt-regulated osteoprotegerin and RANKL production by osteoblasts: A potential mechanism underlying osteolytic bone lesions in multiple myeloma. *Blood*. Published online 2008. doi:10.1182/blood-2008-01-132134
216. Yavropoulou MP, Yovos JG. The role of the Wnt signaling pathway in osteoblast commitment and differentiation. *Hormones (Athens)*. Published online 2007. doi:10.14310/horm.2002.1111024
217. Kawano Y, Kypta R. Secreted antagonists of the Wnt signalling pathway. *J Cell Sci*. Published online 2003. doi:10.1242/jcs.00623
218. Jin L, Cao Y, Yu G, et al. SFRP2 enhances the osteogenic differentiation of apical papilla stem cells by antagonizing the canonical WNT pathway. *Cell Mol Biol Lett*. Published online 2017. doi:10.1186/s11658-017-0044-2
219. Oshima T, Abe M, Asano J, et al. Myeloma cells suppress bone formation by secreting a soluble Wnt inhibitor, sFRP-2. *Blood*. Published online 2005. doi:10.1182/blood-2004-12-4940
220. Barhanpurkar AP, Gupta N, Srivastava RK, et al. IL-3 promotes osteoblast differentiation and bone formation in human mesenchymal stem cells. *Biochem Biophys Res Commun*. Published online 2012. doi:10.1016/j.bbrc.2012.01.074
221. Zhou F, Meng S, Song H, Claret FX. Dickkopf-1 is a key regulator of myeloma bone disease: Opportunities and challenges for therapeutic intervention. *Blood Rev*. Published online 2013. doi:10.1016/j.blre.2013.08.002

222. Terpos E, Gavriatopoulou M. Multiple myeloma bone disease. *Encyclopedia of Endocrine Diseases*. 2018;4:329-340. doi:10.1016/B978-0-12-801238-3.65375-8
223. Pinzone JJ, Hall BM, Thudi NK, et al. The role of Dickkopf-1 in bone development, homeostasis, and disease. *Blood*. Published online 2009. doi:10.1182/blood-2008-03-145169
224. Li Y, Qiu SS, Shao Y, et al. Dickkopf-1 has an inhibitory effect on mesenchymal stem cells to fibroblast differentiation. *Chin Med J (Engl)*. Published online 2016. doi:10.4103/0366-6999.181974
225. Politou MC, Heath DJ, Rahemtulla A, et al. Serum concentrations of Dickkopf-1 protein are increased in patients with multiple myeloma and reduced after autologous stem cell transplantation. *Int J Cancer*. Published online 2006. doi:10.1002/ijc.22033
226. Giuliani N, Colla S, Morandi F, et al. Myeloma cells block RUNX2/CBFA1 activity in human bone marrow osteoblast progenitors and inhibit osteoblast formation and differentiation. *Blood*. Published online 2005. doi:10.1182/blood-2004-12-4986
227. Amarasekara DS, Yun H, Kim S, Lee N, Kim H, Rho J. Regulation of Osteoclast Differentiation by Cytokine Networks. *Immune Netw*. 2018;18(1). doi:10.4110/IN.2018.18.E8
228. Arboleya L, Castañeda S. Osteoimmunology: the study of the relationship between the immune system and bone tissue. *Reumatol Clin*. 2013;9(5):303-315. doi:10.1016/J.REUMA.2013.02.008
229. Gaudio A, Xourafa A, Rapisarda R, Zanoli L, Signorelli SS, Castellino P. Hematological diseases and osteoporosis. *Int J Mol Sci*. Published online 2020. doi:10.3390/ijms21103538
230. Brunetti G, Oranger A, Mori G, et al. Sclerostin is overexpressed by plasma cells from multiple myeloma patients. *Ann N Y Acad Sci*. Published online 2011. doi:10.1111/j.1749-6632.2011.06196.x
231. Wu M, Chen G, Li YP. TGF-β and BMP signaling in osteoblast, skeletal development, and bone formation, homeostasis and disease. *Bone Res*. Published online 2016. doi:10.1038/boneres.2016.9
232. Dong M, Blobe GC. Role of transforming growth factor-β in hematologic malignancies. *Blood*. Published online 2006. doi:10.1182/blood-2005-10-4169
233. Ehnert S, Baur J, Schmitt A, et al. TGF-β1 as possible link between loss of bone mineral density and chronic inflammation. *PLoS One*. Published online 2010. doi:10.1371/journal.pone.0014073
234. Talamo G, Dimaio C, Abbi KKS, et al. Current role of radiation therapy for multiple myeloma. *Front Oncol*. Published online 2015. doi:10.3389/fonc.2015.00040
235. Fervers P, Celik E, Bratke G, et al. Radiotherapy Response Assessment of Multiple Myeloma: A Dual-Energy CT Approach With Virtual Non-Calcium Images. *Front Oncol*. 2021;11. doi:10.3389/FONC.2021.734819/FULL

236. Matuschek C, Ochtrop TA, Bölke E, et al. Effects of Radiotherapy in the treatment of multiple myeloma: A retrospective analysis of a Single Institution. *Radiation Oncology*. Published online 2015. doi:10.1186/s13014-015-0374-z
237. McDonald RJ, Trout AT, Gray LA, Dispenzieri A, Thielen KR, Kallmes DF. Vertebroplasty in multiple myeloma: Outcomes in a large patient series. *American Journal of Neuroradiology*. Published online 2008. doi:10.3174/ajnr.A0918
238. Huber FX, McArthur N, Tanner M, et al. Kyphoplasty for patients with multiple myeloma is a safe surgical procedure: Results from a large patient cohort. *Clin Lymphoma Myeloma*. Published online 2009. doi:10.3816/CLM.2009.n.073
239. Omoigui S. The Interleukin-6 inflammation pathway from cholesterol to aging - Role of statins, bisphosphonates and plant polyphenols in aging and age-related diseases. *Immunity and Ageing*. Published online 2007. doi:10.1186/1742-4933-4-1
240. Colucci S, Minielli V, Zambonin G, et al. Alendronate reduces adhesion of human osteoclast-like cells to bone and bone protein-coated surfaces. *Calcif Tissue Int*. Published online 1998. doi:10.1007/s002239900519
241. Terpos E, Ntanasis-Stathopoulos I, Gavriatopoulou M, Dimopoulos MA. Pathogenesis of bone disease in multiple myeloma: From bench to bedside. *Blood Cancer J*. Published online 2018. doi:10.1038/s41408-017-0037-4
242. Reszka AA, Halasy-Nagy JM, Masarachia PJ, Rodan GA. Bisphosphonates act directly on the osteoclast to induce caspase cleavage of Mst1 kinase during apoptosis. A link between inhibition of the mevalonate pathway and regulation of an apoptosis-promoting kinase. *Journal of Biological Chemistry*. Published online 1999. doi:10.1074/jbc.274.49.34967
243. Terpos E, Dimopoulos MA, Sezer O. The effect of novel anti-myeloma agents on bone metabolism of patients with multiple myeloma. *Leukemia*. Published online 2007. doi:10.1038/sj.leu.2404843
244. Pharmacology of bisphosphonates - UpToDate. Accessed June 24, 2024. https://www.uptodate.com/contents/pharmacology-of-bisphosphonates#subscribeMessage
245. Zangari M, Suva LJ. The effects of proteasome inhibitors on bone remodeling in multiple myeloma. *Bone*. 2016;86:131. doi:10.1016/J.BONE.2016.02.019
246. Wagner EF, Matsuo K. Signalling in osteoclasts and the role of Fos/AP1 proteins. In: *Annals of the Rheumatic Diseases*. ; 2003. doi:10.1136/ard.62.1.83
247. Ring ES, Lawson MA, Snowden JA, Jolley I, Chantry AD. New agents in the Treatment of Myeloma Bone Disease. *Calcif Tissue Int*. Published online 2018. doi:10.1007/s00223-017-0351-7
248. Nooka AK, Lonial S. Mechanism of action and novel IMiD-Based compounds and combinations in multiple myeloma. *Cancer Journal (United States)*. Published online 2019. doi:10.1097/PPO.0000000000000354

249. Usmani SZ, Nooka AK. *Personalized Therapy for Multiple Myeloma*.; 2017. doi:10.1007/978-3-319-61872-2
250. Terpos E, Christoulas D, Kastritis E, et al. The combination of lenalidomide and dexamethasone reduces bone resorption in responding patients with relapsed/refractory multiple myeloma but has no effect on bone formation: Final results on 205 patients of the Greek myeloma study group. *Am J Hematol*. Published online 2014. doi:10.1002/ajh.23577
251. Tosi P, Zamagni E, Cellini C, et al. First-line therapy with thalidomide, dexamethasone and zoledronic acid decreases bone resorption markers in patients with multiple myeloma. *Eur J Haematol*. Published online 2006. doi:10.1111/j.0902-4441.2005.t01-1-EJH2520.
252. Raje NS, Bhatta S, Terpos E. Role of the RANK/RANKL pathway in multiple myeloma. *Clinical Cancer Research*. Published online 2019. doi:10.1158/1078-0432.CCR-18-1537
253. Roodman GD. Bone building with bortezomib. *Journal of Clinical Investigation*. Published online 2008. doi:10.1172/JCI34734
254. Bolzoni M, Storti P, Bonomini S, et al. Immunomodulatory drugs lenalidomide and pomalidomide inhibit multiple myeloma-induced osteoclast formation and the RANKL/OPG ratio in the myeloma microenvironment targeting the expression of adhesion molecules. *Exp Hematol*. Published online 2013. doi:10.1016/j.exphem.2012.11.005
255. Breitkreutz I, Raab MS, Vallet S, et al. Lenalidomide inhibits osteoclastogenesis, survival factors and bone-remodeling markers in multiple myeloma. *Leukemia*. Published online 2008. doi:10.1038/leu.2008.174
256. Richardson PG, Siegel DS, Vij R, et al. Pomalidomide alone or in combination with low-dose dexamethasone in relapsed and refractory multiple myeloma: A randomized phase 2 study. *Blood*. Published online 2014. doi:10.1182/blood-2013-11-538835
257. Rendo MJ, Joseph JJ, Phan LM, DeStefano CB. CAR T-Cell Therapy for Patients with Multiple Myeloma: Current Evidence and Challenges. *Blood Lymphat Cancer*. 2022;12:119. doi:10.2147/BLCTT.S327016
258. Zhang X, Zhang H, Lan H, Wu J, Xiao Y. CAR-T cell therapy in multiple myeloma: Current limitations and potential strategies. *Front Immunol*. 2023;14. doi:10.3389/FIMMU.2023.1101495
259. Kikuchi H, Amofa E, Mcenery M, et al. Inhibition of PI3K Class IA Kinases Using GDC-0941 Overcomes Cytoprotection of Multiple Myeloma Cells in the Osteoclastic Bone Marrow Microenvironment Enhancing the Efficacy of Current Clinical Therapeutics. *Cancers (Basel)*. 2023;15(2). doi:10.3390/CANCERS15020462/S1
260. Wu P, Morgan GJ. Targeting bone as a therapy for myeloma. *Cancer Microenvironment*. Published online 2011. doi:10.1007/s12307-011-0079-2
261. Morgan GJ, Child JA, Gregory WM, et al. Effects of zoledronic acid versus clodronic acid on skeletal morbidity in patients with newly diagnosed multiple myeloma (MRC Myeloma IX):

secondary outcomes from a randomised controlled trial. *Lancet Oncol*. Published online 2011. doi:10.1016/S1470-2045(11)70157-7

262. Nishida H. Bone-targeted agents in multiple myeloma. *Hematol Rep*. Published online 2018. doi:10.4081/hr.2018.7401
263. Boyette LB, MacEdo C, Hadi K, et al. Phenotype, function, and differentiation potential of human monocyte subsets. *PLoS One*. 2017;12(4). doi:10.1371/JOURNAL.PONE.0176460
264. Haziot A, Chen S, Ferrero E, Low MG, Silber R, Goyert SM. The monocyte differentiation antigen, CD14, is anchored to the cell membrane by a phosphatidylinositol linkage. *The Journal of Immunology*. 1988;141(2):547-552. doi:10.4049/JIMMUNOL.141.2.547
265. Penido MGMG, Alon US. Phosphate homeostasis and its role in bone health. *Pediatr Nephrol*. 2012;27(11):2039. doi:10.1007/S00467-012-2175-Z
266. Kearns AE, Khosla S, Kostenuik PJ. Receptor Activator of Nuclear Factor κB Ligand and Osteoprotegerin Regulation of Bone Remodeling in Health and Disease. *Endocr Rev*. 2008;29(2):155. doi:10.1210/ER.2007-0014
267. Kang H, Chang W, Hurley M, Vignery A, Wu D. Important roles of PI3Kγ in osteoclastogenesis and bone homeostasis. *Proc Natl Acad Sci U S A*. 2010;107(29):12901-12906. doi:10.1073/PNAS.1001499107/SUPPL_FILE/PNAS.201001499SI.PDF
268. Udagawa N, Takahashi N, Akatsu T, et al. Origin of osteoclasts: mature monocytes and macrophages are capable of differentiating into osteoclasts under a suitable microenvironment prepared by bone marrow-derived stromal cells. *Proc Natl Acad Sci U S A*. 1990;87(18):7260. doi:10.1073/PNAS.87.18.7260
269. Shalhoub V, Elliott G, Chiu L, et al. Characterization of osteoclast precursors in human blood. *Br J Haematol*. 2000;111(2):501-512. doi:10.1111/J.1365-2141.2000.02379.X
270. Kapellos TS, Bonaguro L, Gemünd I, et al. Human monocyte subsets and phenotypes in major chronic inflammatory diseases. *Front Immunol*. 2019;10(AUG):2035. doi:10.3389/FIMMU.2019.02035/BIBTEX
271. Ziegler-Heitbrock L, Ancuta P, Crowe S, et al. Nomenclature of monocytes and dendritic cells in blood. *Blood*. 2010;116(16):e74-e80. doi:10.1182/BLOOD-2010-02-258558
272. Sampath P, Moideen K, Ranganathan UD, Bethunaickan R. Monocyte Subsets: Phenotypes and Function in Tuberculosis Infection. *Front Immunol*. 2018;9:1726. doi:10.3389/FIMMU.2018.01726/BIBTEX
273. Komano Y, Nanki T, Hayashida K, Taniguchi K, Nobuyuki M. Identification of a human peripheral blood monocyte subset that differentiates into osteoclasts. *Arthritis Res Ther*. 2006;8(5):R152. doi:10.1186/AR2046
274. Boyle WJ, Simonet WS, Lacey DL. Osteoclast differentiation and activation. *Nature*. 2003;423(6937):337-342. doi:10.1038/NATURE01658

275. Zhu L, Tang Y, Li XY, et al. Osteoclast-mediated bone resorption is controlled by a compensatory network of secreted and membrane-tethered metalloproteinases. *Sci Transl Med*. 2020;12(529). doi:10.1126/SCITRANSLMED.AAW6143
276. Delaisse JM, Eeckhout Y, Vaes G. Inhibition of bone resorption in culture by inhibitors of thiol proteinases. *Biochemical Journal*. 1980;192(1):365. doi:10.1042/BJ1920365
277. Knowles HJ, Athanasou NA. Canonical and non-canonical pathways of osteoclast formation. *Histol Histopathol*. 2009;24(3):337-346. doi:10.14670/HH-24.337
278. Henriksen K, Bollerslev J, Everts V, Karsdal MA. Osteoclast Activity and Subtypes as a Function of Physiology and Pathology—Implications for Future Treatments of Osteoporosis. *Endocr Rev*. 2011;32(1):31-63. doi:10.1210/ER.2010-0006
279. Roodman GD. Cell biology of the osteoclast. *Exp Hematol*. 1999;27(8):1229-1241. doi:10.1016/S0301-472X(99)00061-2
280. CELL-MATRIX INTERACTIONS OF THE OSTEOCLAST.
281. Boyce BF, Xing L. Functions of RANKL/RANK/OPG in bone modeling and remodeling. *Arch Biochem Biophys*. 2008;473(2):139. doi:10.1016/J.ABB.2008.03.018
282. Teitelbaum SL, Ross FP. Genetic regulation of osteoclast development and function. *Nature Reviews Genetics 2003 4:8*. 2003;4(8):638-649. doi:10.1038/nrg1122
283. Takito J, Inoue S, Nakamura M. The Sealing Zone in Osteoclasts: A Self-Organized Structure on the Bone. *Int J Mol Sci*. 2018;19(4). doi:10.3390/IJMS19040984
284. Teitelbaum SL. Bone resorption by osteoclasts. *Science (1979)*. 2000;289(5484):1504-1508. doi:10.1126/SCIENCE.289.5484.1504/ASSET/7F1E58BF-C087-4C6F-9C06-C190FE05FFD3/ASSETS/GRAPHIC/SE3408789003.JPEG
285. Boyce B, Yao Z, Xing L. Osteoclasts have Multiple Roles in Bone in Addition to Bone Resorption. *Crit Rev Eukaryot Gene Expr*. 2009;19(3):171. doi:10.1615/CRITREVEUKARGENEEXPR.V19.I3.10
286. Costa AG, Cusano NE, Silva BC, Cremers S, Bilezikian JP. Cathepsin K: its skeletal actions and role as a therapeutic target in osteoporosis. *Nat Rev Rheumatol*. 2011;7(8):447-456. doi:10.1038/NRRHEUM.2011.77
287. Osteoclast-mediated bone resorption is controlled by a compensatory network of secreted and membrane-tethered metalloproteinases HHS Public Access. *J Sci Transl Med*. 2020;12(529). doi:10.1126/scitranslmed.aaw6143
288. Christensen J, Shastri VP. Matrix-metalloproteinase-9 is cleaved and activated by Cathepsin K. *BMC Res Notes*. 2015;8(1):322. doi:10.1186/S13104-015-1284-8
289. Christensen J, Shastri VP. Matrix-metalloproteinase-9 is cleaved and activated by Cathepsin K. *BMC Res Notes*. 2015;8(1):1-8. doi:10.1186/S13104-015-1284-8/FIGURES/3
290. Van Wart HE, Birkedal-Hansen H. The cysteine switch: A principle of regulation of metalloproteinase activity with potential applicability to the entire matrix metalloproteinase

gene family. *Proc Natl Acad Sci U S A*. 1990;87(14):5578-5582. doi:10.1073/PNAS.87.14.5578

291. Bonnans C, Chou J, Werb Z. Remodelling the extracellular matrix in development and disease. *Nat Rev Mol Cell Biol*. 2014;15(12):786. doi:10.1038/NRM3904
292. Martinho FC, Teixeira FFC, Cardoso FGR, et al. Clinical Investigation of Matrix Metalloproteinases, Tissue Inhibitors of Matrix Metalloproteinases, and Matrix Metalloproteinase/Tissue Inhibitors of Matrix Metalloproteinase Complexes and Their Networks in Apical Periodontitis. *J Endod*. 2016;42(7):1082-1088. doi:10.1016/J.JOEN.2016.04.001
293. Zhang H, Liu L, Jiang C, Pan K, Deng J, Wan C. MMP9 protects against LPS-induced inflammation in osteoblasts. *Innate Immun*. 2020;26(4):259-269. doi:10.1177/1753425919887236/ASSET/IMAGES/LARGE/10.1177_1753425919887236-FIG2.JPEG
294. Allan JA, Docherty AJP, Barker PJ, Huskisson NS, Reynolds JJ, Murphy G. Binding of gelatinases A and B to type-I collagen and other matrix components. *Biochem J*. 1995;309 (Pt 1)(Pt 1):299-306. doi:10.1042/BJ3090299
295. Faccio R, Takeshita S, Zallone A, Ross FP, Teitelbaum SL. c-Fms and the αvβ3 integrin collaborate during osteoclast differentiation. *Journal of Clinical Investigation*. 2003;111(5):749. doi:10.1172/JCI16924
296. Izawa T, Zou W, Chappel JC, Ashley JW, Feng X, Teitelbaum SL. c-Src Links a RANK/αvβ3 Integrin Complex to the Osteoclast Cytoskeleton. *Mol Cell Biol*. 2012;32(14):2943. doi:10.1128/MCB.00077-12
297. Teitelbaum SL, Acad Sci AN. Osteoclasts and Integrins. *Ann N Y Acad Sci*. 2006;1068(1):95-99. doi:10.1196/ANNALS.1346.017
298. Matsuo K, Galson DL, Zhao C, et al. Nuclear factor of activated T-cells (NFAT) rescues osteoclastogenesis in precursors lacking c-Fos. *Journal of Biological Chemistry*. 2004;279(25):26475-26480. doi:10.1074/jbc.M313973200
299. Udagawa N, Takahashi N, Yasuda H, et al. Osteoprotegerin Produced by Osteoblasts Is an Important Regulator in Osteoclast Development and Function. *Endocrinology*. 2000;141(9):3478-3484. doi:10.1210/ENDO.141.9.7634
300. Kung YY, Felge U, Sarosi I, et al. Activated T cells regulate bone loss and joint destruction in adjuvant arthritis through osteoprotegerin ligand. *Nature*. 1999;402(6759):304-309. doi:10.1038/46303
301. Xiong J, O'Brien CA. Osteocyte RANKL: new insights into the control of bone remodeling. *J Bone Miner Res*. 2012;27(3):499-505. doi:10.1002/JBMR.1547

302. Boyce BF, Xing L. Functions of RANKL/RANK/OPG in bone modeling and remodeling. *Arch Biochem Biophys*. 2008;473(2):139. doi:10.1016/J.ABB.2008.03.018
303. Armstrong AP, Tometsko ME, Glaccum M, Sutherland CL, Cosman D, Dougall WC. A RANK/TRAF6-dependent Signal Transduction Pathway Is Essential for Osteoclast Cytoskeletal Organization and Resorptive Function*. *J Biol Chem*. 2002;277(46):44347-44356. doi:10.1074/jbc.M202009200
304. Park JH, Lee NK, Lee SY. Current Understanding of RANK Signaling in Osteoclast Differentiation and Maturation. *Mol Cells*. 2017;40(10):706. doi:10.14348/MOLCELLS.2017.0225
305. Lee ZH, Kim HH. Signal transduction by receptor activator of nuclear factor kappa B in osteoclasts. *Biochem Biophys Res Commun*. 2003;305(2):211-214. doi:10.1016/S0006-291X(03)00695-8
306. Boyle WJ, Simonet WS, Lacey DL. Osteoclast differentiation and activation. *Nature*. 2003;423(6937):337-342. doi:10.1038/NATURE01658
307. Westhrin M, Kovcic V, Zhang Z, et al. Monoclonal immunoglobulins promote bone loss in multiple myeloma. *Blood*. 2020;136(23):2656-2666. doi:10.1182/BLOOD.2020006045
308. Hussein MA. Multiple myeloma: most common end-organ damage and management. *J Natl Compr Canc Netw*. 2007;5(2):170-178. doi:10.6004/JNCCN.2007.0017
309. Hameed A, Brady JJ, Dowling P, Clynes M, O'Gorman P. Bone Disease in Multiple Myeloma: Pathophysiology and Management. *Cancer Growth Metastasis*. 2014;7:CGM.S16817. doi:10.4137/CGM.S16817
310. Melton LJ, Kyle RA, Achenbach SJ, Oberg AL, Rajkumar SV. Fracture risk with multiple myeloma: A population-based study. *Journal of Bone and Mineral Research*. 2005;20(3):487-493. doi:10.1359/JBMR.041131
311. Dao A, McDonald MM, Savage PB, Little DG, Schindeler A. Preventing osteolytic lesions and osteomyelitis in multiple myeloma. *J Bone Oncol*. 2022;37. doi:10.1016/J.JBO.2022.100460
312. Saad F, Lipton A, Cook R, Chen YM, Smith M, Coleman R. Pathologic fractures correlate with reduced survival in patients with malignant bone disease. *Cancer*. 2007;110(8):1860-1867. doi:10.1002/CNCR.22991
313. Mwania M, Karim N, Wambui S, Mohammedali S, Njau A. Plasma cell myeloma lytic lesions mimicking vanishing bone syndrome in a young patient. *BJR|case reports*. 2019;5(4):20190025. doi:10.1259/BJRCR.20190025
314. Subramanian S, Viswanathan VK. Lytic Bone Lesions. *StatPearls*. Published online October 22, 2022. Accessed December 12, 2022. https://www.ncbi.nlm.nih.gov/books/NBK539837/

315. Rasche L, Angtuaco EJ, Alpe TL, et al. The presence of large focal lesions is a strong independent prognostic factor in multiple myeloma. *Blood*. 2018;132(1):59. doi:10.1182/BLOOD-2018-04-842880
316. Andrews RE, Brown JE, Lawson MA, Chantry AD. Myeloma Bone Disease: The Osteoblast in the Spotlight. *J Clin Med*. 2021;10(17). doi:10.3390/JCM10173973
317. Sezer O, Heider U, Jakob C, et al. Immunocytochemistry reveals RANKL expression of myeloma cells. *Blood*. 2002;99(12):4646-4647. doi:10.1182/BLOOD-2002-01-0148
318. Bi H, Chen X, Gao S, et al. Key Triggers of Osteoclast-Related Diseases and Available Strategies for Targeted Therapies: A Review. *Front Med (Lausanne)*. 2017;4(DEC):234. doi:10.3389/FMED.2017.00234
319. Giuliani N, Bataille R, Mancini C, Lazzaretti M, Barillé S. Myeloma cells induce imbalance in the osteoprotegerin/osteoprotegerin ligand system in the human bone marrow environment. *Blood*. 2001;98(13):3527-3533. doi:10.1182/BLOOD.V98.13.3527
320. Larocca A, Child JA, Cook G, et al. The impact of response on bone-directed therapy in patients with multiple myeloma. *Blood*. 2013;122(17):2974-2977. doi:10.1182/BLOOD-2013-04-498139
321. Tosi P. Diagnosis and Treatment of Bone Disease in Multiple Myeloma: Spotlight on Spinal Involvement. *Scientifica (Cairo)*. 2013;2013:1-12. doi:10.1155/2013/104546
322. Boyce B, Yao Z, Xing L. Osteoclasts have Multiple Roles in Bone in Addition to Bone Resorption. *Crit Rev Eukaryot Gene Expr*. 2009;19(3):171. doi:10.1615/CRITREVEUKARGENEEXPR.V19.I3.10
323. Boyce BF, Li J, Xing L, Yao Z. Bone Remodeling and the Role of TRAF3 in Osteoclastic Bone Resorption. *Front Immunol*. 2018;9:2263. doi:10.3389/FIMMU.2018.02263/BIBTEX
324. Amarasekara DS, Yun H, Kim S, Lee N, Kim H, Rho J. Regulation of Osteoclast Differentiation by Cytokine Networks. *Immune Netw*. 2018;18(1). doi:10.4110/IN.2018.18.E8
325. David Roodman G, Roodman D. Role of stromal-derived cytokines and growth factors in bone metastasis. *Cancer*. 2003;97(S3):733-738. doi:10.1002/CNCR.11148
326. Suva LJ, Washam C, Nicholas RW, Griffin RJ. Bone metastasis: mechanisms and therapeutic opportunities. *Nat Rev Endocrinol*. 2011;7(4):208. doi:10.1038/NRENDO.2010.227
327. Abildgaard N, Brixen K, Kristensen JE, Eriksen EF, Nielsen JL, Heickendorff L. Comparison of five biochemical markers of bone resorption in multiple myeloma: elevated pre-treatment levels of S-ICTP and U-Ntx are predictive for early progression of the bone disease during standard chemotherapy. *Br J Haematol*. 2003;120(2):235-242. doi:10.1046/J.1365-2141.2003.04050.X

328. Lipton A, Cook RJ, Coleman RE, et al. Clinical Utility of Biochemical Markers of Bone Metabolism for Improving the Management of Patients with Advanced Multiple Myeloma. *Clin Lymphoma Myeloma*. 2007;7(5):346-353. doi:10.3816/CLM.2007.N.011
329. Giannakoulas N, Ntanasis-Stathopoulos I, Terpos E. The Role of Marrow Microenvironment in the Growth and Development of Malignant Plasma Cells in Multiple Myeloma. *Int J Mol Sci*. 2021;22(9):4462. doi:10.3390/IJMS22094462
330. Bernardo L, Corallo L, Caterini J, Su J, Gisonni-Lex L, Gajewska B. Application of xCELLigence real-time cell analysis to the microplate assay for pertussis toxin induced clustering in CHO cells. *PLoS One*. 2021;16(3):e0248491. doi:10.1371/JOURNAL.PONE.0248491
331. Hamidi H, Lilja J, Ivaska J. Using xCELLigence RTCA Instrument to Measure Cell Adhesion. *Bio Protoc*. 2017;7(24). doi:10.21769/BIOPROTOC.2646
332. Teng Z, Kuang X, Wang J, Zhang X. Real-time cell analysis – A new method for dynamic, quantitative measurement of infectious viruses and antiserum neutralizing activity. *J Virol Methods*. 2013;193(2):364-370. doi:10.1016/J.JVIROMET.2013.06.034
333. Asphahani F, Thein M, Veiseh O, et al. Influence of cell adhesion and spreading on impedance characteristics of cell-based sensors. *Biosens Bioelectron*. 2008;23(8):1307. doi:10.1016/J.BIOS.2007.11.021
334. Hayman A. Tartrate-resistant acid phosphatase (TRAP) and the osteoclast/immune cell dichotomy. *Autoimmunity*. 2008;41(3):218-223. doi:10.1080/08916930701694667
335. Blumer MJF, Hausott B, Schwarzer C, Hayman AR, Stempel J, Fritsch H. Role of tartrate-resistant acid phosphatase (TRAP) in long bone development. *Mech Dev*. 2012;129(5-8):162-176. doi:10.1016/J.MOD.2012.04.003
336. Hollberg K, Nordahl J, Hultenby K, Mengarelli-Widholm S, Andersson G, Reinholt FP. Polarization and secretion of cathepsin K precede tartrate-resistant acid phosphatase secretion to the ruffled border area during the activation of matrix-resorbing clasts. *J Bone Miner Metab*. 2005;23(6):441-449. doi:10.1007/S00774-005-0626-3/METRICS
337. Ek-Rylander B, Flores M, Wendel M, Heinegard D, Andersson G. Dephosphorylation of osteopontin and bone sialoprotein by osteoclastic tartrate-resistant acid phosphatase. Modulation of osteoclast adhesion in vitro. *Journal of Biological Chemistry*. 1994;269(21):14853-14856. doi:10.1016/S0021-9258(17)36541-9
338. Indo Y, Takeshita S, Ishii KA, et al. Metabolic regulation of osteoclast differentiation and function. *Journal of Bone and Mineral Research*. 2013;28(11):2392-2399. doi:10.1002/JBMR.1976
339. Da W, Tao L, Zhu Y. The Role of Osteoclast Energy Metabolism in the Occurrence and Development of Osteoporosis. *Front Endocrinol (Lausanne)*. 2021;12:556. doi:10.3389/FENDO.2021.675385/BIBTEX

340. Kim JM, Jeong D, Kang HK, Jung SY, Kang SS, Min BM. Osteoclast precursors display dynamic metabolic shifts toward accelerated glucose metabolism at an early stage of RANKL-stimulated osteoclast differentiation. *Cell Physiol Biochem*. 2007;20(6):935-946. doi:10.1159/000110454
341. Karner CM, Long F. Glucose metabolism in bone. *Bone*. 2018;115:2. doi:10.1016/J.BONE.2017.08.008
342. Kho D, MacDonald C, Johnson R, et al. Application of xCELLigence RTCA Biosensor Technology for Revealing the Profile and Window of Drug Responsiveness in Real Time. *Biosensors (Basel)*. 2015;5(2):199. doi:10.3390/BIOS5020199
343. Bernardo L, Corallo L, Caterini J, Su J, Gisonni-Lex L, Gajewska B. Application of xCELLigence real-time cell analysis to the microplate assay for pertussis toxin induced clustering in CHO cells. *PLoS One*. 2021;16(3). doi:10.1371/JOURNAL.PONE.0248491
344. Şener LT, Albeniz G, Dinç B, Albeniz I. iCELLigence real-time cell analysis system for examining the cytotoxicity of drugs to cancer cell lines. *Exp Ther Med*. 2017;14(3):1866-1870. doi:10.3892/ETM.2017.4781
345. Jonsson MKB, Wang QD, Becker B. Impedance-Based Detection of Beating Rhythm and Proarrhythmic Effects of Compounds on Stem Cell-Derived Cardiomyocytes. *https://home.liebertpub.com/adt*. 2011;9(6):589-599. doi:10.1089/ADT.2011.0396
346. Robinson A, Han CZ, Glass CK, Pollard JW. Monocyte Regulation in Homeostasis and Malignancy. *Trends Immunol*. 2021;42(2):104-119. doi:10.1016/J.IT.2020.12.001
347. Italiani P, Boraschi D. From monocytes to M1/M2 macrophages: Phenotypical vs. functional differentiation. *Front Immunol*. 2014;5(OCT):514. doi:10.3389/FIMMU.2014.00514/BIBTEX
348. Guilliams M, Mildner A, Yona S. Developmental and Functional Heterogeneity of Monocytes. *Immunity*. 2018;49(4):595-613. doi:10.1016/J.IMMUNI.2018.10.005
349. Shapouri-Moghaddam A, Mohammadian S, Vazini H, et al. Macrophage plasticity, polarization, and function in health and disease. *J Cell Physiol*. 2018;233(9):6425-6440. doi:10.1002/JCP.26429
350. Arai F, Miyamoto T, Ohneda O, et al. Commitment and Differentiation of Osteoclast Precursor Cells by the Sequential Expression of C-Fms and Receptor Activator of Nuclear Factor κb (Rank) Receptors. *Journal of Experimental Medicine*. 1999;190(12):1741-1754. doi:10.1084/JEM.190.12.1741
351. Zhou Y, Deng HW, Shen H. Circulating monocytes: an appropriate model for bone-related study. *Osteoporosis International 2015 26:11*. 2015;26(11):2561-2572. doi:10.1007/S00198-015-3250-7
352. Atkins GJ, Kostakis P, Vincent C, et al. RANK Expression as a Cell Surface Marker of Human Osteoclast Precursors in Peripheral Blood, Bone Marrow, and Giant Cell Tumors of

Bone. *Journal of Bone and Mineral Research*. 2006;21(9):1339-1349. doi:10.1359/JBMR.060604

353. Roberts HC, Knott L, Avery NC, Cox TM, Evans MJ, Hayman AR. Altered collagen in tartrate-resistant acid phosphatase (TRAP)-deficient mice: a role for TRAP in bone collagen metabolism. *Calcif Tissue Int*. 2007;80(6):400-410. doi:10.1007/S00223-007-9032-2

354. Yu M, Moreno JL, Stains JP, Keegan AD. Complex Regulation of Tartrate-resistant Acid Phosphatase (TRAP) Expression by Interleukin 4 (IL-4): IL-4 INDIRECTLY SUPPRESSES RECEPTOR ACTIVATOR OF NF-κB LIGAND (RANKL)-MEDIATED TRAP EXPRESSION BUT MODESTLY INDUCES ITS EXPRESSION DIRECTLY*. *J Biol Chem*. 2009;284(47):32968. doi:10.1074/JBC.M109.001016

355. Yao Y, Cai X, Ren F, et al. The Macrophage-Osteoclast Axis in Osteoimmunity and Osteo-Related Diseases. *Front Immunol*. 2021;12:1066. doi:10.3389/FIMMU.2021.664871/BIBTEX

356. Baron R, Neff L, Phuc Tran Van, Nefussi JR, Vignery A. Kinetic and cytochemical identification of osteoclast precursors and their differentiation into multinucleated osteoclasts. *Am J Pathol*. 1986;122(2):363. Accessed March 19, 2023. /pmc/articles/PMC1888102/?report=abstract

357. Ballanti P, Minisola S, Pacitti MT, et al. Tartrate-Resistant Acid Phosphate Activity as Osteoclastic Marker: Sensitivity of Cytochemical Assessment and Serum Assay in Comparison with Standardized Osteoclast Histomorphometry. 1997;7:39-43.

358. de Vrieze E, Sharif F, Metz JR, Flik G, Richardson MK. Matrix metalloproteinases in osteoclasts of ontogenetic and regenerating zebrafish scales. *Bone*. 2011;48(4):704-712. doi:10.1016/J.BONE.2010.12.017

359. Inui T, Ishibashi O, Origane Y, Fujimori K, Kokubo T, Nakajima M. Matrix Metalloproteinases and Lysosomal Cysteine Proteases in Osteoclasts Contribute to Bone Resorption through Distinct Modes of Action. *Biochem Biophys Res Commun*. 1999;258(1):173-178. doi:10.1006/BBRC.1999.0473

361. REPONEN P, SAHLBERG C, MUNAUT C, THESLEFF I, TRYGGVASON K. High expression of 92-kDa type IV collagenase (gelatinase) in the osteoclast lineage during mouse development. *Ann N Y Acad Sci*. 1994;732(1):472-475. doi:10.1111/J.1749-6632.1994.TB24789.X

362. Alexander CM, Hansell EJ, Behrendtsen O, et al. Expression and function of matrix metalloproteinases and their inhibitors at the maternal-embryonic boundary during mouse embryo implantation. *Development*. 1996;122(6):1723-1736. doi:10.1242/DEV.122.6.1723

363. Po H, Liang H, Xu J, Xue M, Jackson CJ. Matrix metalloproteinases in bone development and pathology: current knowledge and potential clinical utility. *Metalloproteinases Med*. 2016;3:93-102. doi:10.2147/MNM.S92187
364. Tang Y, Rowe RG, Botvinick EL, et al. MT1-MMP-Dependent Control of Skeletal Stem Cell Commitment via a β1-Integrin/YAP/TAZ Signaling Axis. *Dev Cell*. 2013;25(4):402. doi:10.1016/J.DEVCEL.2013.04.011
365. Orgaz JL, Pandya P, Dalmeida R, et al. Diverse matrix metalloproteinase functions regulate cancer amoeboid migration. *Nat Commun*. 2014;5:4255. doi:10.1038/NCOMMS5255
366. Shimizu-Hirota R, Xiong W, Baxter BT, et al. MT1-MMP regulates the PI3Kδ·Mi-2/NuRD-dependent control of macrophage immune function. *Genes Dev*. 2012;26(4):395-413. doi:10.1101/GAD.178749.111
367. Lebourgeois S, Fraisse A, Hennechart-Collette C, Guillier L, Perelle S, Martin-Latil S. Development of a Real-Time Cell Analysis (RTCA) Method as a Fast and Accurate Method for Detecting Infectious Particles of the Adapted Strain of Hepatitis A Virus. *Front Cell Infect Microbiol*. 2018;8:335. doi:10.3389/FCIMB.2018.00335
368. Yan G, Du Q, Wei X, et al. Application of Real-Time Cell Electronic Analysis System in Modern Pharmaceutical Evaluation and Analysis. *Molecules*. 2018;23(12):3280. doi:10.3390/MOLECULES23123280
369. Saltel F, Chabadel A, Bonnelye E, Jurdic P. Actin cytoskeletal organisation in osteoclasts: A model to decipher transmigration and matrix degradation. *Eur J Cell Biol*. 2008;87(8-9):459-468. doi:10.1016/J.EJCB.2008.01.001
370. Zhao H, Liu X, Zou H, et al. Osteoprotegerin disrupts peripheral adhesive structures of osteoclasts by modulating Pyk2 and Src activities. *Cell Adh Migr*. 2016;10(3):299. doi:10.1080/19336918.2015.1129480
371. Georgess D, Machuca-Gayet I, Blangy A, Jurdic P. Podosome organization drives osteoclast-mediated bone resorption. *Cell Adh Migr*. 2014;8(3):192. doi:10.4161/CAM.27840
372. Novack D V., Faccio R. Osteoclast motility: putting the brakes on bone resorption. *Ageing Res Rev*. 2011;10(1):54. doi:10.1016/J.ARR.2009.09.005
373. Zhao H, Gu J, Dai N, et al. Osteoprotegerin exposure at different stages of osteoclastogenesis differentially affects osteoclast formation and function. *Cytotechnology*. 2016;68(4):1325. doi:10.1007/S10616-015-9892-7
374. Owen R, Reilly GC. In vitro models of bone remodelling and associated disorders. *Front Bioeng Biotechnol*. 2018;6(OCT):134. doi:10.3389/FBIOE.2018.00134/BIBTEX
375. Ohshiba T, Miyaura C, Inada M, Ito A. Role of RANKL-induced osteoclast formation and MMP-dependent matrix degradation in bone destruction by breast cancer metastasis. *British Journal of Cancer 2003 88:8*. 2003;88(8):1318-1326. doi:10.1038/sj.bjc.6600858

376. Alatalo SL, Halleen JM, Hentunen TA, Monkkonenh J, Vaananen HK. Rapid Screening Method for Osteoclast Differentiation in Vitro That Measures Tartrate-resistant Acid Phosphatase 5b Activity Secreted into the Culture Medium. *Clin Chem*. 2000;46(11):1751-1754. doi:10.1093/CLINCHEM/46.11.1751
377. Susa M, Luong-Nguyen NH, Cappellen D, Zamurovic N, Gamse R. Human primary osteoclasts: in vitro generation and applications as pharmacological and clinical assay. *J Transl Med*. 2004;2:6. doi:10.1186/1479-5876-2-6
378. Holstein SA, McCarthy PL. Immunomodulatory drugs in multiple myeloma: mechanisms of action and clinical experience. *Drugs*. 2017;77(5):505. doi:10.1007/S40265-017-0689-1
379. Kale V, List A. Immunomodulatory drugs (IMiDs): a new treatment option for myelodysplastic syndromes. *Curr Pharm Biotechnol*. 2006;7(5):339-342. doi:10.2174/138920106778521587
380. IMiDs® - Lenalidomide & Pomalidomide - Multiple Myeloma Treatment | Celgene Corp. Accessed December 24, 2022. https://www.celgene.com/research-development/medical-innovation/imids/
381. Quach H, Ritchie D, Stewart AK, et al. Mechanism of action of immunomodulatory drugs (IMiDS) in multiple myeloma. *Leukemia*. 2010;24(1):22. doi:10.1038/LEU.2009.236
382. Begna KH, Mesa RA, Pardanani A, et al. A phase-2 trial of low-dose pomalidomide in myelofibrosis. *Leukemia*. 2011;25(2):301-304. doi:10.1038/LEU.2010.254
383. Lacy MQ, Hayman SR, Gertz MA, et al. Pomalidomide (CC4047) plus low dose dexamethasone (Pom/dex) is active and well tolerated in lenalidomide refractory multiple myeloma (MM). *Leukemia : official journal of the Leukemia Society of America, Leukemia Research Fund, UK*. 2010;24(11):1934. doi:10.1038/LEU.2010.190
384. Tosi P, Zamagni E, Cellini C, et al. Thalidomide alone or in combination with dexamethasone in patients with advanced, relapsed or refractory multiple myeloma and renal failure. *Eur J Haematol*. 2004;73(2):98-103. doi:10.1111/j.1600-0609.2004.00272.x
385. Rajkumar SV, Hayman SR, Lacy MQ, et al. Combination therapy with lenalidomide plus dexamethasone (Rev/Dex) for newly diagnosed myeloma. *Blood*. 2005;106(13):4050. doi:10.1182/BLOOD-2005-07-2817
386. Lacy MQ, Hayman SR, Gertz MA, et al. Pomalidomide (CC4047) plus low-dose dexamethasone as therapy for relapsed multiple myeloma. *J Clin Oncol*. 2009;27(30):5008-5014. doi:10.1200/JCO.2009.23.6802
387. Ng YLD, Ramberger E, Bohl SR, et al. Proteomic profiling reveals CDK6 upregulation as a targetable resistance mechanism for lenalidomide in multiple myeloma. *Nature Communications 2022 13:1*. 2022;13(1):1-13. doi:10.1038/s41467-022-28515-1
388. Gooding S, Ansari-Pour N, Kazeroun M, et al. Loss of COP9 signalosome genes at 2q37 is associated with IMiD resistance in multiple myeloma. *Blood*. 2022;140(16):1816-1821. doi:10.1182/BLOOD.2022015909

389. Palumbo A, Dimopoulos M, Miguel JS, et al. Lenalidomide in combination with dexamethasone for the treatment of relapsed or refractory multiple myeloma. *Blood Rev*. 2009;23(2):87-93. doi:10.1016/J.BLRE.2008.07.003
390. Ito T, Handa H. Molecular mechanisms of thalidomide and its derivatives. *Proc Jpn Acad Ser B Phys Biol Sci*. 2020;96(6):189. doi:10.2183/PJAB.96.016
391. Ito T, Handa H. [Cereblon as a primary target of IMiDs]. *Rinsho Ketsueki*. 2019;60(9):1013-1019. doi:10.11406/RINKETSU.60.1013
392. Zhu YX, Shi CX, Bruins LA, et al. Identification of lenalidomide resistance pathways in myeloma and targeted resensitization using cereblon replacement, inhibition of STAT3 or targeting of IRF4. *Blood Cancer J*. 2019;9(2). doi:10.1038/S41408-019-0173-0
393. Shen C, Nayak A, Neitzel LR, et al. The E3 ubiquitin ligase component, Cereblon, is an evolutionarily conserved regulator of Wnt signaling. *Nat Commun*. 2021;12(1). doi:10.1038/S41467-021-25634-Z
394. Krönke J, Fink EC, Hollenbach PW, et al. Lenalidomide induces ubiquitination and degradation of CK1α in del(5q) MDS. *Nature*. 2015;523(7559):183. doi:10.1038/NATURE14610
395. Di Marzo L, Desantis V, Solimando AG, et al. Microenvironment drug resistance in multiple myeloma: emerging new players. *Oncotarget*. 2016;7(37):60698. doi:10.18632/ONCOTARGET.10849
396. Giannakoulas N, Ntanasis-Stathopoulos I, Terpos E. The Role of Marrow Microenvironment in the Growth and Development of Malignant Plasma Cells in Multiple Myeloma. *Int J Mol Sci*. 2021;22(9):4462. doi:10.3390/IJMS22094462
397. Azab AK, Quang P, Azab F, et al. P-selectin glycoprotein ligand regulates the interaction of multiple myeloma cells with the bone marrow microenvironment. *Blood*. 2012;119(6):1468-1478. doi:10.1182/BLOOD-2011-07-368050
398. Thomas X, Anglaret B, Magaud JP, Epstein J, Archimbaud E. Interdependence between cytokines and cell adhesion molecules to induce interleukin-6 production by stromal cells in myeloma. *Leuk Lymphoma*. 1998;32(1-2):107-119. doi:10.3109/10428199809059251
399. Li Y, Lu L, Xie Y, et al. Interleukin-6 Knockout Inhibits Senescence of Bone Mesenchymal Stem Cells in High-Fat Diet-Induced Bone Loss. *Front Endocrinol (Lausanne)*. 2020;11. doi:10.3389/FENDO.2020.622950
400. Choy E, Rose-John S. Interleukin-6 as a multifunctional regulator: Inflammation, immune response, and fibrosis. *J Scleroderma Relat Disord*. 2017;2:S1-S5. doi:10.5301/JSRD.5000265/ASSET/IMAGES/LARGE/10.5301_JSRD.5000265-FIG1.JPEG
401. Klein B, Zhang X, Jourdan M, et al. Paracrine Rather Than Autocrine Regulation of Myeloma-Cell Growth and Differentiation by Interleukin-6. *Blood*. 1989;73(2):517-526. doi:10.1182/BLOOD.V73.2.517.517

402. Klein B, Zhang XG, Lu ZY, Bataille R. Interleukin-6 in Human Multiple Myeloma. *Blood*. 1995;85(4):863-872. doi:10.1182/BLOOD.V85.4.863.BLOODJOURNAL854863
403. Liu XH, Kirschenbaum A, Yao S, Levine AC. Cross-talk between the interleukin-6 and prostaglandin E(2) signaling systems results in enhancement of osteoclastogenesis through effects on the osteoprotegerin/receptor activator of nuclear factor-{kappa}B (RANK) ligand/RANK system. *Endocrinology*. 2005;146(4):1991-1998. doi:10.1210/EN.2004-1167
404. Klein B, Wijdenes J, Zhang XG, et al. Murine Anti-Interleukin-6 Monoclonal Antibody Therapy for a Patient With Plasma Cell Leukemia. *Blood*. 1991;78(5):1198-1204. doi:10.1182/BLOOD.V78.5.1198.1198
405. Harmer D, Falank C, Reagan MR. Interleukin-6 Interweaves the Bone Marrow Microenvironment, Bone Loss, and Multiple Myeloma. *Front Endocrinol (Lausanne)*. 2018;9(JAN). doi:10.3389/FENDO.2018.00788
406. Dankbar B, Padró T, Leo R, et al. Vascular endothelial growth factor and interleukin-6 in paracrine tumor-stromal cell interactions in multiple myeloma. *Blood*. 2000;95(8):2630-2636. doi:10.1182/BLOOD.V95.8.2630
407. Dankbar B, Padró T, Leo R, et al. Vascular endothelial growth factor and interleukin-6 in paracrine tumor-stromal cell interactions in multiple myeloma. *Blood*. 2000;95(8):2630-2636. doi:10.1182/BLOOD.V95.8.2630
408. DeClerck YA. Interactions between tumour cells and stromal cells and proteolytic modification of the extracellular matrix by metalloproteinases in cancer. *Eur J Cancer*. 2000;36(10):1258-1268. doi:10.1016/S0959-8049(00)00094-0
409. Bergers G, Brekken R, McMahon G, et al. Matrix metalloproteinase-9 triggers the angiogenic switch during carcinogenesis. *Nat Cell Biol*. 2000;2(10):737. doi:10.1038/35036374
410. Dankbar B, Padró T, Leo R, et al. Vascular endothelial growth factor and interleukin-6 in paracrine tumor-stromal cell interactions in multiple myeloma. *Blood*. 2000;95(8):2630-2636. doi:10.1182/BLOOD.V95.8.2630
411. Sfiridaki A, Miyakis S, Tsirakis G, et al. Systemic levels of interleukin-6 and matrix metalloproteinase-9 in patients with multiple myeloma may be useful as prognostic indexes of bone disease. *Clin Chem Lab Med*. 2005;43(9):934-938. doi:10.1515/CCLM.2005.160/MACHINEREADABLECITATION/RIS
412. Jurišić V, Čolović M. Correlation of sera TNF-alpha with percentage of bone marrow plasma cells, LDH, beta2-microglobulin, and clinical stage in multiple myeloma. *Med Oncol*. 2002;19(3):133-139. doi:10.1385/MO:19:3:133
413. Lam J, Takeshita S, Barker JE, Kanagawa O, Ross FP, Teitelbaum SL. TNF-α induces osteoclastogenesis by direct stimulation of macrophages exposed to permissive levels of RANK ligand. *Journal of Clinical Investigation*. 2000;106(12):1481. doi:10.1172/JCI11176

414. Cabral-Pacheco GA, Garza-Veloz I, Rosa CCD La, et al. The Roles of Matrix Metalloproteinases and Their Inhibitors in Human Diseases. *Int J Mol Sci*. 2020;21(24):1-53. doi:10.3390/IJMS21249739

415. Liu J, Hideshima T, Xing L, et al. ERK signaling mediates resistance to immunomodulatory drugs in the bone marrow microenvironment. *Sci Adv*. 2021;7(23). doi:10.1126/SCIADV.ABG2697

416. Yamanaka S, Shoya Y, Matsuoka S, Nishida-Fukuda H, Shibata N, Sawasaki T. An IMiD-induced SALL4 degron system for selective degradation of target proteins. *Communications Biology 2020 3:1*. 2020;3(1):1-14. doi:10.1038/s42003-020-01240-5

417. Wang Y, Shimosaki S, Ikebe E, et al. IMiD/CELMoD-induced growth suppression of adult T-cell leukemia/lymphoma cells via cereblon through downregulation of target proteins and their downstream effectors. *Front Oncol*. 2023;13:1272528. doi:10.3389/FONC.2023.1272528/BIBTEX

418. Real-Time, Quantitative Cell Analysis, xCELLigence | Agilent. Accessed December 24, 2022. https://www.agilent.com/en/product/cell-analysis/real-time-cell-analysis

419. Hamidi H, Lilja J, Ivaska J. Using xCELLigence RTCA Instrument to Measure Cell Adhesion. *Bio Protoc*. 2017;7(24). doi:10.21769/BIOPROTOC.2646

420. Technologies A. Measure Cell Movement, Health, and Function With xCELLigence RTCA eSight Multiparametric real-time automated readouts using simultaneous cellular impedance and live cell imaging.

421. Teng Z, Kuang X, Wang J, Zhang X. Real-time cell analysis - A new method for dynamic, quantitative measurement of infectious viruses and antiserum neutralizing activity. *J Virol Methods*. 2013;193(2):364-370. doi:10.1016/J.JVIROMET.2013.06.034

422. Stefanowicz-Hajduk J, Ochocka JR. Real-time cell analysis system in cytotoxicity applications: Usefulness and comparison with tetrazolium salt assays. *Toxicol Rep*. 2020;7:335-344. doi:10.1016/J.TOXREP.2020.02.002

423. Stefanowicz-Hajduk J, Ochocka JR. Real-time cell analysis system in cytotoxicity applications: Usefulness and comparison with tetrazolium salt assays. *Toxicol Rep*. 2020;7:335-344. doi:10.1016/J.TOXREP.2020.02.002

424. Kustermann S, Boess F, Buness A, et al. A label-free, impedance-based real time assay to identify drug-induced toxicities and differentiate cytostatic from cytotoxic effects. *Toxicology in Vitro*. 2013;27(5):1589-1595. doi:10.1016/J.TIV.2012.08.019

425. Martinez-Serra J, Ggutierrez A, Muñoz-Ccapó S, et al. xCELLigence system for real-time label-free monitoring of growth and viability of cell lines from hematological malignancies. *Onco Targets Ther*. 2014;7:985. doi:10.2147/OTT.S62887

426. Bar-Shavit Z. The osteoclast: a multinucleated, hematopoietic-origin, bone-resorbing osteoimmune cell. *J Cell Biochem*. 2007;102(5):1130-1139. doi:10.1002/JCB.21553

427. Khan IA, Bordoni B. Histology, Osteoclasts. *StatPearls*. Published online April 28, 2022. Accessed February 18, 2023. https://www.ncbi.nlm.nih.gov/books/NBK554489/
428. Philip R, Fiorino C, Harrison RE. Terminally differentiated osteoclasts organize centrosomes into large clusters for microtubule nucleation and bone resorption. *Mol Biol Cell*. 2022;33(8). doi:10.1091/MBC.E22-03-0098
429. Leightner AC, Meyers CMG, Evans MD, Mansky KC, Gopalakrishnan R, Jensen ED. Regulation of Osteoclast Differentiation at Multiple Stages by Protein Kinase D Family Kinases. *Int J Mol Sci*. 2020;21(3). doi:10.3390/IJMS21031056
430. Lakkakorpi PT, Horton MA, Helfrich MH, Karhukorpi EK, Vaananen HK. Vitronectin receptor has a role in bone resorption but does not mediate tight sealing zone attachment of osteoclasts to the bone surface. *J Cell Biol*. 1991;115(4):1179-1186. doi:10.1083/JCB.115.4.1179
431. Teitelbaum SL. Osteoclasts: What do they do and how do they do it? *American Journal of Pathology*. 2007;170(2):427-435. doi:10.2353/AJPATH.2007.060834
432. Duong LT, Lakkakorpi P, Nakamura I, Rodan GA. Integrins and signaling in osteoclast function. *Matrix Biol*. 2000;19(2):97-105. doi:10.1016/S0945-053X(00)00051-2
433. Horton MA, Helfrich MH. Integrins and Development: Integrins in Skeletal Cell Function and Development. Published online 2013. Accessed March 23, 2023. https://www.ncbi.nlm.nih.gov/books/NBK6331/
434. Schmidt S, Nakchbandi I, Ruppert R, et al. Kindlin-3–mediated signaling from multiple integrin classes is required for osteoclast-mediated bone resorption. *J Cell Biol*. 2011;192(5):883. doi:10.1083/JCB.201007141
435. Holstein SA, McCarthy PL. Immunomodulatory drugs in multiple myeloma: mechanisms of action and clinical experience. *Drugs*. 2017;77(5):505. doi:10.1007/S40265-017-0689-1
436. Mccurdy AR, Lacy MQ. Pomalidomide and its clinical potential for relapsed or refractory multiple myeloma: an update for the hematologist. *Ther Adv Hematol*. 2013;4(3):211. doi:10.1177/2040620713480155
437. Zhu YX, Kortuem KM, Stewart AK. Molecular mechanism of action of immune-modulatory drugs thalidomide, lenalidomide and pomalidomide in multiple myeloma. *Leuk Lymphoma*. 2013;54(4):683. doi:10.3109/10428194.2012.728597
438. Giannakoulas N, Ntanasis-Stathopoulos I, Terpos E. The Role of Marrow Microenvironment in the Growth and Development of Malignant Plasma Cells in Multiple Myeloma. *International Journal of Molecular Sciences 2021, Vol 22, Page 4462*. 2021;22(9):4462. doi:10.3390/IJMS22094462
439. Yamamoto L, Amodio N, Gulla A, Anderson KC. Harnessing the Immune System Against Multiple Myeloma: Challenges and Opportunities. *Front Oncol*. 2021;10:3160. doi:10.3389/FONC.2020.606368/BIBTEX

440. Epstein J, Barlogie B, Johnson CL, Yaccoby S, Pearse RN, Choi Y. Myeloma interacts with the bone marrow microenvironment to induce osteoclastogenesis and is dependent on osteoclast activity. *Br J Haematol*. 2002;116(2):278-290. doi:10.1046/J.1365-2141.2002.03257.X
441. Gandolfi S, Prada CP, Richardson PG. How I treat the young patient with multiple myeloma. *Blood*. 2018;132(11):1114-1124. doi:10.1182/BLOOD-2017-05-693606
442. Hameed A, Brady JJ, Dowling P, Clynes M, O'Gorman P. Bone Disease in Multiple Myeloma: Pathophysiology and Management. *Cancer Growth Metastasis*. 2014;7:33. doi:10.4137/CGM.S16817
443. Yaccoby S. Advances in the understanding of myeloma bone disease and tumour growth. *Br J Haematol*. 2010;149(3):311. doi:10.1111/J.1365-2141.2010.08141.X
444. Kiss TL, Lipton JH, Bergsagel DE, et al. Determination of IL6, IL1, and IL4 in the Plasma of Patients with Multiple Myeloma. *https://doi.org/103109/10428199409049687*. 2009;14(3-4):335-340. doi:10.3109/10428199409049687
445. Lichtenstein A, Berenson J, Norman D, Chang M, Carlile A. Production of Cytokines by Bone Marrow Cells Obtained From Patients With Multiple Myeloma. *Blood*. 1989;74(4):1266-1273. doi:10.1182/BLOOD.V74.4.1266.1266
446. Kelly T, Børset M, Abe E, Gaddy-Kurten D, Sanderson RD. Matrix metalloproteinases in multiple myeloma. *Leuk Lymphoma*. 2000;37(3-4):273-281. doi:10.3109/10428190009089428
447. Kelly T, Børset M, Abe E, Gaddy-Kurten D, Sanderson RD. Matrix Metalloproteinases in Multiple Myeloma. *https://doi.org/103109/10428190009089428*. 2009;37(3-4):273-281. doi:10.3109/10428190009089428
448. Kessenbrock K, Plaks V, Werb Z. Matrix metalloproteinases: regulators of the tumor microenvironment. *Cell*. 2010;141(1):52-67. doi:10.1016/J.CELL.2010.03.015
449. Winkler J, Abisoye-Ogunniyan A, Metcalf KJ, Werb Z. Concepts of extracellular matrix remodelling in tumour progression and metastasis. *Nature Communications 2020 11:1*. 2020;11(1):1-19. doi:10.1038/s41467-020-18794-x
450. Chang X, Zhu Y, Shi C, Stewart AK. Mechanism of immunomodulatory drugs' action in the treatment of multiple myeloma. *Acta Biochim Biophys Sin (Shanghai)*. 2014;46(3):240. doi:10.1093/ABBS/GMT142
451. Zhang S, Li M, Gu Y, et al. Thalidomide influences growth and vasculogenic mimicry channel formation in melanoma. *J Exp Clin Cancer Res*. 2008;27(1):60. doi:10.1186/1756-9966-27-60
452. Heere-Ress E, Boehm J, Thallinger C, et al. Thalidomide enhances the anti-tumor activity of standard chemotherapy in a human melanoma xenotransplatation model. *J Invest Dermatol*. 2005;125(2):201-206. doi:10.1111/J.0022-202X.2005.23830.X

453. Roy R, Yang J, Moses MA. Matrix Metalloproteinases As Novel Biomarkers and Potential Therapeutic Targets in Human Cancer. *Journal of Clinical Oncology*. 2009;27(31):5287. doi:10.1200/JCO.2009.23.5556
454. Holstein SA, McCarthy PL. Immunomodulatory drugs in multiple myeloma: mechanisms of action and clinical experience. *Drugs*. 2017;77(5):505. doi:10.1007/S40265-017-0689-1
455. Breitkreutz I, Raab MS, Vallet S, et al. Lenalidomide inhibits osteoclastogenesis, survival factors and bone-remodeling markers in multiple myeloma. *Leukemia 2008 22:10*. 2008;22(10):1925-1932. doi:10.1038/leu.2008.174
456. Sezer O, Heider U, Zavrski I, Kühne CA, Hofbauer LC. RANK ligand and osteoprotegerin in myeloma bone disease. *Blood*. 2003;101(6):2094-2098. doi:10.1182/BLOOD-2002-09-2684
457. Terpos E, Mihou D, Szydlo R, et al. The combination of intermediate doses of thalidomide with dexamethasone is an effective treatment for patients with refractory/relapsed multiple myeloma and normalizes abnormal bone remodeling, through the reduction of sRANKL/osteoprotegerin ratio. *Leukemia 2005 19:11*. 2005;19(11):1969-1976. doi:10.1038/sj.leu.2403890
458. Sampaio EP, Sarno EN, Galilly R, Cohn ZA, Kaplan G. Thalidomide selectively inhibits tumor necrosis factor alpha production by stimulated human monocytes. *J Exp Med*. 1991;173(3):699. doi:10.1084/JEM.173.3.699
459. Iwamoto N, Kawakami A. The monocyte-to-osteoclast transition in rheumatoid arthritis: Recent findings. *Front Immunol*. 2022;13:5288. doi:10.3389/FIMMU.2022.998554/BIBTEX
460. Komano Y, Nanki T, Hayashida K, Taniguchi K, Nobuyuki M. Identification of a human peripheral blood monocyte subset that differentiates into osteoclasts. *Arthritis Res Ther*. 2006;8(5):1-14. doi:10.1186/AR2046/FIGURES/8
461. Liu D, Nikoo M, Boran G, Zhou P, Regenstein JM. Collagen and gelatin. *Annu Rev Food Sci Technol*. 2015;6:527-557. doi:10.1146/ANNUREV-FOOD-031414-111800
462. Moskowitz RW. Role of collagen hydrolysate in bone and joint disease. *Semin Arthritis Rheum*. 2000;30(2):87-99. doi:10.1053/SARH.2000.9622
463. Shu XZ, Liu Y, Palumbo F, Prestwich GD. Disulfide-crosslinked hyaluronan-gelatin hydrogel films: a covalent mimic of the extracellular matrix for in vitro cell growth. *Biomaterials*. 2003;24(21):3825-3834. doi:10.1016/S0142-9612(03)00267-9
464. Lu P, Takai K, Weaver VM, Werb Z. Extracellular Matrix Degradation and Remodeling in Development and Disease. *Cold Spring Harb Perspect Biol*. 2011;3(12). doi:10.1101/CSHPERSPECT.A005058
465. Lin X, Patil S, Gao YG, Qian A. The Bone Extracellular Matrix in Bone Formation and Regeneration. *Front Pharmacol*. 2020;11. doi:10.3389/FPHAR.2020.00757
466. Martin JT. Historically significant events in the discovery of RANK/RANKL/OPG. *World J Orthop*. 2013;4(4):186. doi:10.5312/WJO.V4.I4.186

467. Mccurdy AR, Lacy MQ. Pomalidomide and its clinical potential for relapsed or refractory multiple myeloma: an update for the hematologist. *Ther Adv Hematol*. 2013;4(3):211. doi:10.1177/2040620713480155
468. Gertz MA. Pomalidomide and myeloma meningitis. *Leuk Lymphoma*. 2013;54(4):681-682. doi:10.3109/10428194.2012.723708/SUPPL_FILE/DISCLOSURE.ZIP
469. Ríos-Tamayo R, Martín-García A, Alarcón-Payer C, et al. Pomalidomide in the treatment of multiple myeloma: design, development and place in therapy. *Drug Des Devel Ther*. 2017;11:2399. doi:10.2147/DDDT.S115456
470. Clark, PharmD SM, Steinbach, PharmD A, Clemmons, PharmD, BCOP AB. Pomalidomide for the Treatment of Multiple Myeloma. *J Adv Pract Oncol*. 2014;5(1):51. doi:10.6004/JADPRO.2014.5.1.7
471. Ng AYH, Tu C, Shen S, et al. Comparative Characterization of Osteoclasts Derived From Murine Bone Marrow Macrophages and RAW 264.7 Cells Using Quantitative Proteomics. *JBMR Plus*. 2018;2(6):328-340. doi:10.1002/JBM4.10058
472. Philip R, Fiorino C, Harrison RE. Terminally differentiated osteoclasts organize centrosomes into large clusters for microtubule nucleation and bone resorption. *Mol Biol Cell*. 2022;33(8). doi:10.1091/MBC.E22-03-0098
473. Søe K. Osteoclast Fusion: Physiological Regulation of Multinucleation through Heterogeneity—Potential Implications for Drug Sensitivity. *Int J Mol Sci*. 2020;21(20):1-17. doi:10.3390/IJMS21207717
474. Xu F, Teitelbaum SL. Osteoclasts: New Insights. *Bone Research 2013 1:1*. 2013;1(1):11-26. doi:10.4248/br201301003
475. Baron R, Neff L, Van T, Nefussi JR, Vignery A. Kinetic and Cytochemical Identfication of Osteoclast Precursors and Their Differentiation Into Mu ltinucleated Osteoclasts.
476. The preosteoclast and its cytodifferentiation into the osteoclast: ultrastructural and histochemical studies of rat fetal parietal bone - PubMed. Accessed March 15, 2023. https://pubmed.ncbi.nlm.nih.gov/6661003/
477. Leung R, Cuddy K, Wang Y, Rommens J, Glogauer M. Sbds is required for Rac2-mediated monocyte migration and signaling downstream of RANK during osteoclastogenesis. *Blood*. 2011;117(6):2044-2053. doi:10.1182/BLOOD-2010-05-282574
478. Zeng XZ, He LG, Wang S, et al. Aconine inhibits RANKL-induced osteoclast differentiation in RAW264.7 cells by suppressing NF-κB and NFATc1 activation and DC-STAMP expression. *Acta Pharmacologica Sinica 2016 37:2*. 2015;37(2):255-263. doi:10.1038/aps.2015.85
479. Chiu YH, Mensah KA, Schwarz EM, et al. Regulation of Human Osteoclast Development by Dendritic Cell-Specific Transmembrane Protein (DC-STAMP). *J Bone Miner Res*. 2012;27(1):79. doi:10.1002/JBMR.531

480. Neubert R, Hinz N, Thiel R, Neubert D. Down-regulation of adhesion receptors on cells of primate embryos as a probable mechanism of the teratogenic action of thalidomide. *Life Sci*. 1995;58(4):295-316. doi:10.1016/0024-3205(95)02290-2
481. Nogueira AC, Neubert R, Helge H, Neubert D. Thalidomide and the immune system. 3. Simultaneous up- and down-regulation of different integrin receptors on human white blood cells. *Life Sci*. 1994;55(2):77-92. doi:10.1016/0024-3205(94)90099-X
482. Chang X, Zhu Y, Shi C, Stewart AK. Mechanism of immunomodulatory drugs' action in the treatment of multiple myeloma. *Acta Biochim Biophys Sin (Shanghai)*. 2014;46(3):240. doi:10.1093/ABBS/GMT142
483. Neubert R, Nogueira AC, Neubert D. Thalidomide derivatives and the immune system. I. Changes in the pattern of integrin receptors and other surface markers on T lymphocyte subpopulations of marmoset blood. *Arch Toxicol*. 1993;67(1):1-17. doi:10.1007/BF02072029
484. Rieman DJ, McClung HA, Dodds RA, et al. Biosynthesis and processing of cathepsin K in cultured human osteoclasts. *Bone*. 2001;28(3):282-289. doi:10.1016/S8756-3282(00)00445-2
485. Duong LT, Lakkakorpi P, Nakamura I, Rodan GA. Integrins and signaling in osteoclast function. *Matrix Biology*. 2000;19(2):97-105. doi:10.1016/S0945-053X(00)00051-2
486. Horton MA, Helfrich MH. Integrins and Development: Integrins in Skeletal Cell Function and Development. Published online 2013. Accessed March 15, 2023. https://www.ncbi.nlm.nih.gov/books/NBK6331/
487. Bolzoni M, Storti P, Bonomini S, et al. Immunomodulatory drugs lenalidomide and pomalidomide inhibit multiple myeloma-induced osteoclast formation and the RANKL/OPG ratio in the myeloma microenvironment targeting the expression of adhesion molecules. *Exp Hematol*. 2013;41(4):387-397.e1. doi:10.1016/J.EXPHEM.2012.11.005
488. Breitkreutz I, Raab MS, Vallet S, et al. Lenalidomide inhibits osteoclastogenesis, survival factors and bone-remodeling markers in multiple myeloma. *Leukemia 2008 22:10*. 2008;22(10):1925-1932. doi:10.1038/leu.2008.174
489. Helfrich MH, Nesbitt SA, Lakkakorpi PT, et al. β1 integrins and osteoclast function: Involvement in collagen recognition and bone resorption. *Bone*. 1996;19(4):317-328. doi:10.1016/S8756-3282(96)00223-2
490. Ross FP, Chappel J, Alvarez JI, et al. Interactions between the bone matrix proteins osteopontin and bone sialoprotein and the osteoclast integrin alpha v beta 3 potentiate bone resorption. *Journal of Biological Chemistry*. 1993;268(13):9901-9907. doi:10.1016/S0021-9258(18)98430-9
491. Nesbitt S, Nesbit A, Helfrich M, Horton M. Biochemical characterization of human osteoclast integrins. Osteoclasts express alpha v beta 3, alpha 2 beta 1, and alpha v beta 1 integrins.

Journal of Biological Chemistry. 1993;268(22):16737-16745. doi:10.1016/S0021-9258(19)85479-0

492. Patil CR, Bhise SB. Preclinical evaluation of potential phytoconstituents in drug induced nephrotoxicity View project RE-EMERGENCE OF THALIDOMIDE. *Article in Indian Journal of Pharmacology*. 2003;35:204-212. Accessed March 14, 2023. https://www.researchgate.net/publication/267553297
493. Nianhang Chen, Lau H, Linghui Kong, et al. Pharmacokinetics of lenalidomide in subjects with various degrees of renal impairment and in subjects on hemodialysis. *J Clin Pharmacol*. 2007;47(12):1466-1475. doi:10.1177/0091270007309563
494. Bolomsky A, Schreder M, Meißner T, et al. Immunomodulatory drugs thalidomide and lenalidomide affect osteoblast differentiation of human bone marrow stromal cells invitro. *Exp Hematol*. 2014;42(7):516-525. doi:10.1016/j.exphem.2014.03.005
495. Chanan-Khan AA, Swaika A, Paulus A, et al. Pomalidomide: the new immunomodulatory agent for the treatment of multiple myeloma. *Blood Cancer J*. 2013;3(9):e143. doi:10.1038/BCJ.2013.38
496. Lacy MQ, McCurdy AR. Pomalidomide. *Blood*. 2013;122(14):2305-2309. doi:10.1182/BLOOD-2013-05-484782
497. Lacy MQ, Hayman SR, Gertz MA, et al. Pomalidomide (CC4047) plus low dose dexamethasone (Pom/dex) is active and well tolerated in lenalidomide refractory multiple myeloma (MM). *Leukemia : official journal of the Leukemia Society of America, Leukemia Research Fund, UK*. 2010;24(11):1934. doi:10.1038/LEU.2010.190
498. Dimopoulos M, Spencer A, Attal M, et al. Lenalidomide plus dexamethasone for relapsed or refractory multiple myeloma. *N Engl J Med*. 2007;357(21):2123-2132. doi:10.1056/NEJMOA070594
499. Weber DM, Chen C, Niesvizky R, et al. Lenalidomide plus dexamethasone for relapsed multiple myeloma in North America. *N Engl J Med*. 2007;357(21):2133-2142. doi:10.1056/NEJMOA070596
500. Mateos MV, Oriol A, Martínez-López J, et al. Bortezomib, melphalan, and prednisone versus bortezomib, thalidomide, and prednisone as induction therapy followed by maintenance treatment with bortezomib and thalidomide versus bortezomib and prednisone in elderly patients with untreated multiple myeloma: a randomised trial. *Lancet Oncol*. 2010;11(10):934-941. doi:10.1016/S1470-2045(10)70187-X
501. Rehman W, Arfons LM, Lazarus HM. The Rise, Fall and Subsequent Triumph of Thalidomide: Lessons Learned in Drug Development. *Ther Adv Hematol*. 2011;2(5):291. doi:10.1177/2040620711413165
502. Gao S, Wang S, Song Y. Novel immunomodulatory drugs and neo-substrates. *Biomark Res*. 2020;8(1):1-8. doi:10.1186/S40364-020-0182-Y/FIGURES/3

503. Yang K, Zhao Y, Nie X, Almodovar-Rivera CM, Xie H. A Cell-Based Target Engagement Assay for the Identification of Cereblon E3 Ubiquitin Ligase Ligands and Their Application in HDAC6 Degraders. *Cell Chem Biol*. 2020;27:866-876. doi:10.1016/j.chembiol.2020.04.008
504. Mundy GR. Role of cytokines in bone resorption. *J Cell Biochem*. 1993;53(4):296-300. doi:10.1002/JCB.240530405
505. Iwaszko M, Biały S, Bogunia-Kubik K. Significance of Interleukin (IL)-4 and IL-13 in Inflammatory Arthritis. *Cells*. 2021;10(11). doi:10.3390/CELLS10113000
506. Zheng WP, Flavell RA. The Transcription Factor GATA-3 Is Necessary and Sufficient for Th2 Cytokine Gene Expression in CD4 T Cells. *Cell*. 1997;89(4):587-596. doi:10.1016/S0092-8674(00)80240-8
507. Fallon PG, Ballantyne SJ, Mangan NE, et al. Identification of an interleukin (IL)-25-dependent cell population that provides IL-4, IL-5, and IL-13 at the onset of helminth expulsion. *J Exp Med*. 2006;203(4):1105-1116. doi:10.1084/JEM.20051615
508. Fort MM, Cheung J, Yen D, et al. IL-25 induces IL-4, IL-5, and IL-13 and Th2-associated pathologies in vivo. *Immunity*. 2001;15(6):985-995. doi:10.1016/S1074-7613(01)00243-6
509. Junttila IS. Tuning the cytokine responses: An update on interleukin (IL)-4 and IL-13 receptor complexes. *Front Immunol*. 2018;9(JUN):888. doi:10.3389/FIMMU.2018.00888/BIBTEX
510. Chomarat P, Banchereau J. Interleukin-4 and interleukin-13: their similarities and discrepancies. *Int Rev Immunol*. 1998;17(1-4):1-52. doi:10.3109/08830189809084486
511. Yamada A, Takami M, Kawawa T, et al. Interleukin-4 inhibition of osteoclast differentiation is stronger than that of interleukin-13 and they are equivalent for induction of osteoprotegerin production from osteoblasts. *Immunology*. 2007;120(4):573. doi:10.1111/J.1365-2567.2006.02538.X
512. Callard RE, Matthews DJ, Hibbert L. IL-4 and IL-13 receptors: are they one and the same? *Immunol Today*. 1996;17(3):108-110. doi:10.1016/0167-5699(96)80600-1
513. Bonecchi R, Facchetti F, Dusi S, et al. Induction of Functional IL-8 Receptors by IL-4 and IL-13 in Human Monocytes 1. Published online 2000. Accessed March 11, 2023. http://journals.aai.org/jimmunol/article-pdf/164/7/3862/1117976/3862.pdf
514. Moreno JL, Kaczmarek M, Keegan AD, Tondravi M. IL-4 suppresses osteoclast development and mature osteoclast function by a STAT6-dependent mechanism: irreversible inhibition of the differentiation program activated by RANKL. *Blood*. 2003;102(3):1078-1086. doi:10.1182/BLOOD-2002-11-3437
515. Munasinghe A, Lin P, Colina CM. Unraveling Binding Interactions between Human RANKL and Its Decoy Receptor Osteoprotegerin. *Journal of Physical Chemistry B*. 2017;121(39):9141-9148. doi:10.1021/ACS.JPCB.7B06687/ASSET/IMAGES/LARGE/JP-2017-06687J_0009.JPEG

516. Nelms K, Keegan AD, Zamorano J, Ryan JJ, Paul WE. The IL-4 receptor: signaling mechanisms and biologic functions. *Annu Rev Immunol*. 1999;17:701-738. doi:10.1146/ANNUREV.IMMUNOL.17.1.701
517. Goenka S, Kaplan MH. Transcriptional regulation by STAT6. *Immunol Res*. 2011;50(1):87-96. doi:10.1007/S12026-011-8205-2
518. Graber P, Gretener D, Herren S, et al. The distribution of IL-13 receptor > 1 expression on B cells, T cells and monocytes and its regulation by IL-13 and IL-4. doi:10.1002/(SICI)1521-4141(199812)28:12
519. Khurana Hershey GK. IL-13 receptors and signaling pathways: An evolving web. *Journal of Allergy and Clinical Immunology*. 2003;111(4):677-690. doi:10.1067/mai.2003.1333
520. IL-13R(alpha)2, a decoy receptor for IL-13 acts as an inhibitor of IL-4-dependent signal transduction in glioblastoma cells - PubMed. Accessed March 10, 2023. https://pubmed.ncbi.nlm.nih.gov/11861389/
521. De Vries JE. The role of IL-13 and its receptor in allergy and inflammatory responses. *Journal of Allergy and Clinical Immunology*. 1998;102(2):165-169. doi:10.1016/S0091-6749(98)70080-6
522 Hart PH, Ahern MJ, Smith MD, Finlay-Jones JJ. Regulatory effects of IL-13 on synovial fluid macrophages and blood monocytes from patients with inflammatory arthritis. *Clin Exp Immunol*. 1995;99(3):331. doi:10.1111/J.1365-2249.1995.TB05554.X
523. van der Velden VHJ, Naber BAE, Wierenga-Wolf AF, et al. Interleukin 4 receptors on human bronchial epithelial cells. An in vivo and in vitro analysis of expression and function. *Cytokine*. 1998;10(10):803-813. doi:10.1006/CYTO.1998.0365
524. Park MH, Kwon HJ, Kim JR, Lee B, Lee SJ, Bae YK. Elevated Interleukin-13 Receptor Alpha 1 Expression in Tumor Cells Is Associated with Poor Prognosis in Patients with Invasive Breast Cancer. *Ann Surg Oncol*. 2017;24(12):3780-3787. doi:10.1245/S10434-017-5907-2/TABLES/3
525. Shaik AP, Shaik AS, Al Majwal A, Al Faraj A. Blocking Interleukin-4 Receptor α Using Polyethylene Glycol Functionalized Superparamagnetic Iron Oxide Nanocarriers to Inhibit Breast Cancer Cell Proliferation. *Cancer Res Treat*. 2017;49(2):322-329. doi:10.4143/CRT.2016.091
526. Kang MA, Lee J, Ha SH, et al. Interleukin4Rα (IL4Rα) and IL13Rα1 Are Associated with the Progress of Renal Cell Carcinoma through Janus Kinase 2 (JAK2)/Forkhead Box O3 (FOXO3) Pathways. *Cancers 2019, Vol 11, Page 1394*. 2019;11(9):1394. doi:10.3390/CANCERS11091394
527. Papageorgis P, Ozturk S, Lambert AW, et al. Targeting IL13Ralpha2 activates STAT6-TP63 pathway to suppress breast cancer lung metastasis. *Breast Cancer Research*. 2015;17(1):1-15. doi:10.1186/S13058-015-0607-Y/FIGURES/6

528. Shi J, Song X, Traub B, Luxenhofer M, Kornmann M. Involvement of IL-4, IL-13 and Their Receptors in Pancreatic Cancer. *Int J Mol Sci*. 2021;22(6):1-16. doi:10.3390/IJMS22062998
529. Heller NM, Qi X, Junttila IS, et al. Type I IL-4 Receptors Selectively Activate IRS-2 to Induce Target Gene Expression in Macrophages. *Sci Signal*. 2008;1(51):ra17. doi:10.1126/SCISIGNAL.1164795
530. Trifunović J, Miller L, Debeljak Ž, Horvat V. Pathologic patterns of interleukin 10 expression – A review. *Biochem Med (Zagreb)*. 2015;25(1):36. doi:10.11613/BM.2015.004
531. Standiford TJ, Deng JC. INTERLEUKINS | IL-10. *Encyclopedia of Respiratory Medicine, Four-Volume Set*. Published online January 1, 2006:373-377. doi:10.1016/B0-12-370879-6/00480-4
532. Zhang JM, An J. Cytokines, Inflammation and Pain. *Int Anesthesiol Clin*. 2007;45(2):27. doi:10.1097/AIA.0B013E318034194E
533. Saraiva M, Vieira P, O'Garra A. Cytokines Focus: Biology and therapeutic potential of interleukin-10. *J Exp Med*. 2020;217(1). doi:10.1084/JEM.20190418
534. Iyer SS, Cheng G. Role of Interleukin 10 Transcriptional Regulation in Inflammation and Autoimmune Disease. *Crit Rev Immunol*. 2012;32(1):23. doi:10.1615/CRITREVIMMUNOL.V32.I1.30
535. Zhang Q, Chen B, Yan F, et al. Interleukin-10 Inhibits Bone Resorption: A Potential Therapeutic Strategy in Periodontitis and Other Bone Loss Diseases. *Biomed Res Int*. 2014;2014. doi:10.1155/2014/284836
536. Xu LX, Kukita T, Kukita A, Otsuka T, Niho Y, Iijima T. Interleukin-10 selectively inhibits osteoclastogenesis by inhibiting differentiation of osteoclast progenitors into preosteoclast-like cells in rat bone marrow culture system. *J Cell Physiol*. 1995;165(3):624-629. doi:10.1002/JCP.1041650321
537. Metzger CE, Gong S, Aceves M, Bloomfield SA, Hook MA. Osteocytes reflect a pro-inflammatory state following spinal cord injury in a rodent model. *Bone*. 2019;120:465-475. doi:10.1016/J.BONE.2018.12.007
538. Iyer SS, Cheng G. Role of Interleukin 10 Transcriptional Regulation in Inflammation and Autoimmune Disease. *Crit Rev Immunol*. 2012;32(1):23. doi:10.1615/CRITREVIMMUNOL.V32.I1.30
539. Porro C, Cianciulli A, Panaro MA. The Regulatory Role of IL-10 in Neurodegenerative Diseases. *Biomolecules 2020, Vol 10, Page 1017*. 2020;10(7):1017. doi:10.3390/BIOM10071017
540. Mosser DM, Zhang X. Interleukin-10: new perspectives on an old cytokine. *Immunol Rev*. 2008;226(1):205. doi:10.1111/J.1600-065X.2008.00706.X
541. Ferrao R, Wallweber HJA, Ho H, et al. The Structural Basis for Class II Cytokine Receptor Recognition by JAK1. *Structure*. 2016;24(6):897. doi:10.1016/J.STR.2016.03.023

542. Walter MR. The Molecular Basis of IL-10 Function: From Receptor Structure to the Onset of Signaling. *Curr Top Microbiol Immunol*. 2014;380:191. doi:10.1007/978-3-662-43492-5_9
543. Srinivasan L, Harris MC, Kilpatrick LE. Cytokines and Inflammatory Response in the Fetus and Neonate. *Fetal and Neonatal Physiology, 2-Volume Set*. Published online January 1, 2017:1241-1254.e4. doi:10.1016/B978-0-323-35214-7.00128-1
544. IL-10 induces the tyrosine phosphorylation of tyk2 and Jak1 and the differential assembly of STAT1 alpha and STAT3 complexes in human T cells and monocytes - PubMed. Accessed March 11, 2023. https://pubmed.ncbi.nlm.nih.gov/7543512/
545. Carey AJ, Tan CK, Ulett GC. Infection-induced IL-10 and JAK-STAT: A review of the molecular circuitry controlling immune hyperactivity in response to pathogenic microbes. *JAKSTAT*. 2012;1(3):159. doi:10.4161/JKST.19918
546. Wills-Karp M, Nathan A, Page K, Karp CL. New Insights Into Innate Immune Mechanisms Underlying Allergenicity. *Mucosal Immunol*. 2010;3(2):104. doi:10.1038/MI.2009.138
547. Iyer SS, Cheng G. Role of Interleukin 10 Transcriptional Regulation in Inflammation and Autoimmune Disease. *Crit Rev Immunol*. 2012;32(1):23. doi:10.1615/CRITREVIMMUNOL.V32.I1.30
548. Saxton RA, Tsutsumi N, Su LL, et al. Structure-based decoupling of the pro- and anti-inflammatory functions of interlukin-10. *Science*. 2021;371(6535). doi:10.1126/SCIENCE.ABC8433
549. Oft M. IL-10: Master Switch from Tumor-Promoting Inflammation to Antitumor Immunity. *Cancer Immunol Res*. 2014;2(3):194-199. doi:10.1158/2326-6066.CIR-13-0214
550. Jankovic D, Kugler DG, Sher A. IL-10 production by CD4+ effector T cells: a mechanism for self-regulation. *Mucosal Immunol*. 2010;3(3):239. doi:10.1038/MI.2010.8
551. Cyktor JC, Turner J. Interleukin-10 and Immunity against Prokaryotic and Eukaryotic Intracellular Pathogens. *Infect Immun*. 2011;79(8):2964. doi:10.1128/IAI.00047-11
552. Mogensen TH. Pathogen Recognition and Inflammatory Signaling in Innate Immune Defenses. *Clin Microbiol Rev*. 2009;22(2):240. doi:10.1128/CMR.00046-08
553. Houslay KF, Van Gijsel-Bonnello M, Petrova T, et al. IL-23 production is regulated via an MSK1/2-CREB dependent signalling pathway downstream of Toll like receptors. doi:10.1101/2020.07.07.189142
554. Ma X, Yan W, Zheng H, et al. Regulation of IL-10 and IL-12 production and function in macrophages and dendritic cells. *F1000Res*. 2015;4:1-13. doi:10.12688/F1000RESEARCH.7010.1
555. Kortylewski M, Xin H, Kujawski M, et al. Regulation of the IL-23 and IL-12 balance by Stat3 signaling in the tumor microenvironment. *Cancer Cell*. 2009;15(2):114-123. doi:10.1016/J.CCR.2008.12.018

556. Prêle CM, Keith-Magee AL, Yerkovich ST, Murcha M, Hart PH. Suppressor of cytokine signalling-3 at pathological levels does not regulate lipopolysaccharide or interleukin-10 control of tumour necrosis factor-α production by human monocytes. *Immunology*. 2006;119(1):8. doi:10.1111/J.1365-2567.2006.02383.X
557. Oft M. Immune regulation and cytotoxic T cell activation of IL-10 agonists – Preclinical and clinical experience. *Semin Immunol*. 2019;44:101325. doi:10.1016/J.SMIM.2019.101325
558. Evans KE, Fox SW. Interleukin-10 inhibits osteoclastogenesis by reducing NFATc1 expression and preventing its translocation to the nucleus. *BMC Cell Biol*. 2007;8:4. doi:10.1186/1471-2121-8-4
559. Yamada A, Takami M, Kawawa T, et al. Interleukin-4 inhibition of osteoclast differentiation is stronger than that of interleukin-13 and they are equivalent for induction of osteoprotegerin production from osteoblasts. *Immunology*. 2007;120(4):573. doi:10.1111/J.1365-2567.2006.02538.X
560. Zhu Y, Yao S, Chen L. CELL SURFACE SIGNALING MOLECULES IN THE CONTROL OF IMMUNE RESPONSES: A TIDE MODEL. *Immunity*. 2011;34(4):466. doi:10.1016/J.IMMUNI.2011.04.008

561. Thivierge M, Staňková J, Rola-Pleszczynski M. IL-13 and IL-4 Up-Regulate Cysteinyl Leukotriene 1 Receptor Expression in Human Monocytes and Macrophages. *The Journal of Immunology*. 2001;167(5):2855-2860. doi:10.4049/JIMMUNOL.167.5.2855
562. Aguilar-Hernandez MM, Blunt MD, Dobson R, et al. IL-4 enhances expression and function of surface IgM in CLL cells. *Blood*. 2016;127(24):3015-3025. doi:10.1182/BLOOD-2015-11-682906
563. Bonder CS, Finlay-Jones JJ, Hart PH. Interleukin-4 regulation of human monocyte and macrophage interleukin-10 and interleukin-12 production. Role of a functional interleukin-2 receptor γ-chain. *Immunology*. 1999;96(4):529. doi:10.1046/J.1365-2567.1999.00711.X
564. Yu M, Moreno JL, Stains JP, Keegan AD. Complex Regulation of Tartrate-resistant Acid Phosphatase (TRAP) Expression by Interleukin 4 (IL-4): IL-4 INDIRECTLY SUPPRESSES RECEPTOR ACTIVATOR OF NF-κB LIGAND (RANKL)-MEDIATED TRAP EXPRESSION BUT MODESTLY INDUCES ITS EXPRESSION DIRECTLY*. *J Biol Chem*. 2009;284(47):32968. doi:10.1074/JBC.M109.001016
565. Chaplin DD. Overview of the Immune Response. *J Allergy Clin Immunol*. 2010;125(2 Suppl 2):S3. doi:10.1016/J.JACI.2009.12.980
566. Zhang JM, An J. Cytokines, Inflammation and Pain. *Int Anesthesiol Clin*. 2007;45(2):27. doi:10.1097/AIA.0B013E318034194E
567. Yokota K. [Inflammation and osteoclasts]. *Nihon Rinsho Meneki Gakkai Kaishi*. 2017;40(5):367-376. doi:10.2177/JSCI.40.367

568. Epsley S, Tadros S, Farid A, Kargilis D, Mehta S, Rajapakse CS. The Effect of Inflammation on Bone. *Front Physiol*. 2021;11:1695. doi:10.3389/FPHYS.2020.511799/BIBTEX
569. Hofbauer LC, Lacey DL, Dunstan CR, Spelsberg TC, Riggs BL, Khosla S. Interleukin-1β and tumor necrosis factor-α, but not interleukin-6, stimulate osteoprotegerin ligand gene expression in human osteoblastic cells. *Bone*. 1999;25(3):255-259. doi:10.1016/S8756-3282(99)00162-3
570. Kobayashi K, Takahashi N, Jimi E, et al. Tumor Necrosis Factor α Stimulates Osteoclast Differentiation by a Mechanism Independent of the Odf/Rankl–Rank Interaction. *J Exp Med*. 2000;191(2):275. doi:10.1084/JEM.191.2.275
571. Grey A, Mitnick MA, Masiukiewicz U, et al. A role for interleukin-6 in parathyroid hormone-induced bone resorption in vivo. *Endocrinology*. 1999;140(10):4683-4690. doi:10.1210/ENDO.140.10.7036
572. Kasahara T, Imai S, Kojima H, et al. Malfunction of Bone Marrow Derived Osteoclasts and the Delay of Bone Fracture Healing in Diabetic Mice. *Bone*. 2010;47(3):617. doi:10.1016/J.BONE.2010.06.014
573. De Benedetti F, Rucci N, Del Fattore A, et al. Impaired skeletal development in interleukin-6-transgenic mice: a model for the impact of chronic inflammation on the growing skeletal system. *Arthritis Rheum*. 2006;54(11):3551-3563. doi:10.1002/ART.22175
574. Harmer D, Falank C, Reagan MR. Interleukin-6 interweaves the bone marrow microenvironment, bone loss, and multiple myeloma. *Front Endocrinol (Lausanne)*. 2019;10(JAN). doi:10.3389/FENDO.2018.00788/FULL
575. Ng PC, Li K, Wong RPO, et al. Proinflammatory and anti-inflammatory cytokine responses in preterm infants with systemic infections. *Arch Dis Child Fetal Neonatal Ed*. 2003;88(3):F209-F213. doi:10.1136/FN.88.3.F209
576. Romagnani S. T-cell subsets (Th1 versus Th2). *Ann Allergy Asthma Immunol*. 2000;85(1):9-18. doi:10.1016/S1081-1206(10)62426-X
577. Delaisse JM, Søe K, Andersen TL, Rojek AM, Marcussen N. The Mechanism Switching the Osteoclast From Short to Long Duration Bone Resorption. *Front Cell Dev Biol*. 2021;9:555. doi:10.3389/FCELL.2021.644503/BIBTEX
578. Asagiri M, Takayanagi H. The molecular understanding of osteoclast differentiation. *Bone*. 2007;40(2):251-264. doi:10.1016/J.BONE.2006.09.023
579. Feher J. Calcium and Phosphorus Homeostasis II: Target Tissues and Integrated Control. *Quantitative Human Physiology*. Published online January 1, 2017:933-945. doi:10.1016/B978-0-12-800883-6.00091-4
580. Straub RH, Cutolo M, Pacifici R. Evolutionary medicine and bone loss in chronic inflammatory diseases – a theory of inflammation-related osteopenia. *Semin Arthritis Rheum*. 2015;45(2):220. doi:10.1016/J.SEMARTHRIT.2015.04.014

581. Hardy R, Cooper MS. Bone loss in inflammatory disorders. *Journal of Endocrinology*. 2009;201(3):309-320. doi:10.1677/JOE-08-0568
582. Ginaldi L, Di Benedetto MC, De Martinis M. Osteoporosis, inflammation and ageing. *Immun Ageing*. 2005;2:14. doi:10.1186/1742-4933-2-14
583. Jung SM, Kim KW, Yang CW, Park SH, Ju JH, Mamura M. Cytokine-mediated bone destruction in rheumatoid arthritis. *J Immunol Res*. 2014;2014. doi:10.1155/2014/263625
584. Mbalaviele G, Novack D V., Schett G, Teitelbaum SL. Inflammatory osteolysis: a conspiracy against bone. *J Clin Invest*. 2017;127(6):2030-2039. doi:10.1172/JCI93356
585. Chen Z, Andreev D, Oeser K, et al. Th2 and eosinophil responses suppress inflammatory arthritis. *Nat Commun*. 2016;7. doi:10.1038/NCOMMS11596
586. Baba T, Miyazaki D, Inata K, et al. Role of IL-4 in bone marrow driven dysregulated angiogenesis and age-related macular degeneration. *Elife*. 2020;9:1-22. doi:10.7554/ELIFE.54257
587. Iwaszko M, Biały S, Bogunia-Kubik K. Significance of Interleukin (IL)-4 and IL-13 in Inflammatory Arthritis. *Cells*. 2021;10(11). doi:10.3390/cells10113000
588. Junttila IS. Tuning the cytokine responses: An update on interleukin (IL)-4 and IL-13 receptor complexes. *Front Immunol*. 2018;9(JUN):888. doi:10.3389/FIMMU.2018.00888/BIBTEX
589. Finkelman FD, Shea-Donohue T, Morris SC, et al. Interleukin-4- and interleukin-13-mediated host protection against intestinal nematode parasites. *Immunol Rev*. 2004;201:139-155. doi:10.1111/J.0105-2896.2004.00192.X
590. Borriello F, Longo M, Spinelli R, et al. IL-3 synergizes with basophil-derived IL-4 and IL-13 to promote the alternative activation of human monocytes. *Eur J Immunol*. 2015;45(7):2042. doi:10.1002/EJI.201445303
591. Doucet C, Brouty-Boyé D, Pottin-Clémenceau C, Canonica GW, Jasmin C, Azzarone B. Interleukin (IL) 4 and IL-13 act on human lung fibroblasts. Implication in asthma. *Journal of Clinical Investigation*. 1998;101(10):2129. doi:10.1172/JCI741
592. Pelaia C, Heffler E, Crimi C, et al. Interleukins 4 and 13 in Asthma: Key Pathophysiologic Cytokines and Druggable Molecular Targets. *Front Pharmacol*. 2022;13:756. doi:10.3389/FPHAR.2022.851940/BIBTEX
593. Gour N, Wills-Karp M. IL-4 and IL-13 Signaling in Allergic Airway Disease. *Cytokine*. 2015;75(1):68. doi:10.1016/J.CYTO.2015.05.014
594. Pålsson-McDermott EM, O'Neill LAJ. Targeting immunometabolism as an anti-inflammatory strategy. *Cell Research 2020 30:4*. 2020;30(4):300-314. doi:10.1038/s41422-020-0291-z
595. Guo L, Urban JF, Zhu J, Paul WE. Elevating Calcium in Th2 Cells Activates Multiple Pathways to Induce IL-4 Transcription and mRNA Stabilization. *The Journal of Immunology*. 2008;181(6):3984-3993. doi:10.4049/JIMMUNOL.181.6.3984

596. Park YG, Kang SK, Kim WJ, Lee YC, Kim CH. Effects of TGF-β, TNF-α, IL-β and IL-6 alone or in combination, and tyrosine kinase inhibitor on cyclooxygenase expression, prostaglandin E2 production and bone resorption in mouse calvarial bone cells. *International Journal of Biochemistry and Cell Biology*. 2004;36(11):2270-2280. doi:10.1016/j.biocel.2004.04.019
597. Yamada A, Takami M, Kawawa T, et al. Interleukin-4 inhibition of osteoclast differentiation is stronger than that of interleukin-13 and they are equivalent for induction of osteoprotegerin production from osteoblasts. *Immunology*. 2007;120(4):573. doi:10.1111/J.1365-2567.2006.02538.X
598. Palmqvist P, Lundberg P, Persson E, et al. Inhibition of hormone and cytokine-stimulated osteoclastogenesis and bone resorption by interleukin-4 and interleukin-13 is associated with increased osteoprotegerin and decreased RANKL and RANK in a STAT6-dependent pathway. *Journal of Biological Chemistry*. 2006;281(5):2414-2429. doi:10.1074/JBC.M510160200
599. Hong MH, Williams H, Jin CH, Pike JW. The inhibitory effect of interleukin-10 on mouse osteoclast formation involves novel tyrosine-phosphorylated proteins. *J Bone Miner Res*. 2000;15(5):911-918. doi:10.1359/JBMR.2000.15.5.911
600. Interleukin-10 selectively inhibits osteoclastogenesis by inhibiting differentiation of osteoclast progenitors into preosteoclast-like cells in rat bone marrow culture system - PubMed. Accessed March 10, 2023. https://pubmed.ncbi.nlm.nih.gov/7593242/
601. Xu LX, Kukita T, Kukita A, Otsuka T, Niho Y, Iijima T. Interleukin-10 selectively inhibits osteoclastogenesis by inhibiting differentiation of osteoclast progenitors into preosteoclast-like cells in rat bone marrow culture system. *J Cell Physiol*. 1995;165(3):624-629. doi:10.1002/JCP.1041650321
602. Evans KE, Fox SW. Interleukin-10 inhibits osteoclastogenesis by reducing NFATc1 expression and preventing its translocation to the nucleus. *BMC Cell Biol*. 2007;8:4. doi:10.1186/1471-2121-8-4
603. Liu D, Yao S, Wise GE. Effect of interleukin-10 on gene expression of osteoclastogenic regulatory molecules in the rat dental follicle. *Eur J Oral Sci*. 2006;114(1):42-49. doi:10.1111/J.1600-0722.2006.00283.X
604. Park-Min KH, Ji JD, Antoniv T, et al. IL-10 Suppresses Calcium-Mediated Costimulation of Receptor Activator NF-κB Signaling during Human Osteoclast Differentiation by Inhibiting TREM-2 Expression. *The Journal of Immunology*. 2009;183(4):2444-2455. doi:10.4049/JIMMUNOL.0804165Evans KE, Fox SW. Interleukin-10 inhibits osteoclastogenesis by reducing NFATc1 expression and preventing its translocation to the nucleus. *BMC Cell Biol*. 2007;8:4. doi:10.1186/1471-2121-8-4
605. Kitaura H, Marahleh A, Ohori F, et al. Osteocyte-Related Cytokines Regulate Osteoclast Formation and Bone Resorption. *Int J Mol Sci*. 2020;21(14). doi:10.3390/IJMS21145169

606. IL-10 modulates formation of osteoclasts in murine hemopoietic cultures - PubMed. Accessed March 10, 2023. https://pubmed.ncbi.nlm.nih.gov/8752948/ Lovibond AC, Haque SJ, Chambers TJ, Fox SW. TGF-β-induced SOCS3 expression augments TNF-α-induced osteoclast formation. *Biochem Biophys Res Commun*. 2003;309(4):762-767. doi:10.1016/J.BBRC.2003.08.068
607. Palmqvist P, Lundberg P, Persson E, et al. Inhibition of hormone and cytokine-stimulated osteoclastogenesis and bone resorption by interleukin-4 and interleukin-13 is associated with increased osteoprotegerin and decreased RANKL and RANK in a STAT6-dependent pathway. *J Biol Chem*. 2006;281(5):2414-2429. doi:10.1074/JBC.M510160200
608. Bendixen AC, Shevde NK, Dienger KM, Willson TM, Funk CD, Pike JW. IL-4 inhibits osteoclast formation through a direct action on osteoclast precursors via peroxisome proliferator-activated receptor γ1. *Proc Natl Acad Sci U S A*. 2001;98(5):2443. doi:10.1073/PNAS.041493198
609. Frost A, Jonsson KB, BrändstrÖm H, Ljunghall S, Nilsson O, Ljunggren O. Interleukin (IL)-13 and IL-4 inhibit proliferation and stimulate IL-6 formation in human osteoblasts: evidence for involvement of receptor subunits IL-13R, IL-13Ralpha, and IL-4Ralpha. *Bone*. 2001;28(3):268-274. doi:10.1016/S8756-3282(00)00449-X
610. Ahn JS, Agrawal B. IL-4 is more effective than IL-13 for in vitro differentiation of dendritic cells from peripheral blood mononuclear cells. *Int Immunol*. 2005;17(10):1337-1346. doi:10.1093/INTIMM/DXH312
611. Wills-Karp M, Finkelman FD. Untangling the Complex Web of IL-4– and IL-13–Mediated Signaling Pathways. *Sci Signal*. 2008;1(51):pe55. doi:10.1126/SCISIGNAL.1.51.PE55
612. van Helvoort EM, van der Heijden E, van Roon JAG, Eijkelkamp N, Mastbergen SC. The Role of Interleukin-4 and Interleukin-10 in Osteoarthritic Joint Disease: A Systematic Narrative Review. *Cartilage*. 2022;13(2). doi:10.1177/19476035221098167/ASSET/IMAGES/LARGE/10.1177_19476035221098167-FIG2.JPEG
613. van Helvoort EM, van der Heijden E, van Roon JAG, Eijkelkamp N, Mastbergen SC. The Role of Interleukin-4 and Interleukin-10 in Osteoarthritic Joint Disease: A Systematic Narrative Review. *Cartilage*. 2022;13(2). doi:10.1177/19476035221098167/ASSET/IMAGES/LARGE/10.1177_19476035221098167-FIG2.JPEG
614. Synergistic activity of interleukin-4 and interleukin-10 in suppression of inflammation and joint destruction in rheumatoid arthritis. Accessed March 8, 2023. https://onlinelibrary.wiley.com/doi/epdf/10.1002/1529-0131%28200101%2944%3A1%3C3%3A%3AAID-ANR2%3E3.0.CO%3B2-U

615. Lacraz S, Nicod LP, Chicheportiche R, Welgus HG, Dayer JM. IL-10 inhibits metalloproteinase and stimulates TIMP-1 production in human mononuclear phagocytes. *J Clin Invest*. 1995;96(5):2304-2310. doi:10.1172/JCI118286
616. Dechanet J, Rissoan MC, Banchereau J, Miossec P. Interleukin 4, but not Interleukin 10, Regulates the Production of Inflammation Mediators by Rheumatoid Synoviocytes. *Cytokine*. 1995;7(2):176-183. doi:10.1006/CYTO.1995.1024
617. Amanda Alexander AF, Kelsey I, Forbes H, Miller-Jensen Correspondence K, Alexander AF, Miller-Jensen K. Single-cell secretion analysis reveals a dual role for IL-10 in restraining and resolving the TLR4-induced inflammatory response ll Single-cell secretion analysis reveals a dual role for IL-10 in restraining and resolving the TLR4-induced inflammatory response. *CellReports*. 2021;36:109728. doi:10.1016/j.celrep.2021.109728
618. HEMPEL L, KÖRHOLZ D, BÖNIG H, et al. Interleukin-10 directly inhibits the interleukin-6 production in T-cells. *Scand J Immunol*. 1995;41(5):462-466. doi:10.1111/J.1365-3083.1995.TB03593.X
619. Kudo O, Fujikawa Y, Itonaga I, Sabokbar A, Torisu T, Athanasou NA. Proinflammatory cytokine (TNFα/IL-1α) induction of human osteoclast formation. *J Pathol*. 2002;198(2):220-227. doi:10.1002/PATH.1190
620. Azuma Y, Kaji K, Katogi R, Takeshita S, Kudo A. Tumor necrosis factor-α induces differentiation of and bone resorption by osteoclasts. *Journal of Biological Chemistry*. 2000;275(7):4858-4864. doi:10.1074/jbc.275.7.4858
621. Kobayashi K, Takahashi N, Jimi E, et al. Tumor Necrosis Factor α Stimulates Osteoclast Differentiation by a Mechanism Independent of the Odf/Rankl–Rank Interaction. *Journal of Experimental Medicine*. 2000;191(2):275-286. doi:10.1084/JEM.191.2.275
622. Guder C, Gravius S, Burger C, Wirtz DC, Schildberg FA. Osteoimmunology: A Current Update of the Interplay Between Bone and the Immune System. *Front Immunol*. 2020;11:58. doi:10.3389/FIMMU.2020.00058/BIBTEX
623. Bray MA, Singh S, Han H, et al. Cell Painting, a high-content image-based assay for morphological profiling using multiplexed fluorescent dyes. *Nat Protoc*. 2016;11(9):1757-1774. doi:10.1038/NPROT.2016.105
624. Riss TL, Moravec RA, Niles AL, et al. Cell Viability Assays. *Assay Guidance Manual*. Published online July 1, 2016. Accessed March 11, 2023. https://www.ncbi.nlm.nih.gov/books/NBK144065/
625. Single A, Beetham H, Telford BJ, Guilford P, Chen A. A comparison of real-time and endpoint cell viability assays for improved synthetic lethal drug validation. *J Biomol Screen*. 2015;20(10):1286-1293. doi:10.1177/1087057115605765
626. Opal SM, DePalo VA. Anti-Inflammatory Cytokines. *Chest*. 2000;117(4):1162-1172. doi:10.1378/CHEST.117.4.1162

627. Gogos CA, Drosou E, Bassaris HP, Skoutelis A. Pro- versus Anti-inflammatory Cytokine Profile in Patients with Severe Sepsis: A Marker for Prognosis and Future Therapeutic Options. *J Infect Dis*. 2000;181(1):176-180. doi:10.1086/315214
628. Ross FP, Teitelbaum SL. αvβ3 and macrophage colony-stimulating factor: partners in osteoclast biology. *Immunol Rev*. 2005;208(1):88-105. doi:10.1111/J.0105-2896.2005.00331.X
629. Faccio R, Takeshita S, Zallone A, Ross FP, Teitelbaum SL. c-Fms and the αvβ3 integrin collaborate during osteoclast differentiation. *Journal of Clinical Investigation*. 2003;111(5):749. doi:10.1172/JCI16924
630. Kitazawa S, Ross FP, McHugh K, Teitelbaum SL. Interleukin-4 induces expression of the integrin alpha v beta 3 via transactivation of the beta 3 gene. *J Biol Chem*. 1995;270(8):4115-4120. doi:10.1074/JBC.270.8.4115
631. García-Ortiz A, Rodríguez-García Y, Encinas J, et al. The Role of Tumor Microenvironment in Multiple Myeloma Development and Progression. *Cancers 2021, Vol 13, Page 217*. 2021;13(2):217. doi:10.3390/CANCERS13020217
632. Wei Q, Frenette PS. Niches for Hematopoietic Stem Cells and Their Progeny. *Immunity*. 2018;48(4):632-648. doi:10.1016/J.IMMUNI.2018.03.024
633. Cooper B. The origins of bone marrow as the seedbed of our blood: from antiquity to the time of Osler. *Proc (Bayl Univ Med Cent)*. 2011;24(2):115. doi:10.1080/08998280.2011.11928697
634. Carrancio S, Blanco B, Romo C, et al. Bone Marrow Mesenchymal Stem Cells for Improving Hematopoietic Function: An In Vitro and In Vivo Model. Part 2: Effect on Bone Marrow Microenvironment. *PLoS One*. 2011;6(10). doi:10.1371/JOURNAL.PONE.0026241
635. Bone marrow: Function, diseases, transplants, and donation. Accessed March 1, 2023. https://www.medicalnewstoday.com/articles/285666
636. Weiskopf K, Schnorr PJ, Pang WW, et al. Myeloid cell origins, differentiation, and clinical implications. *Microbiol Spectr*. 2016;4(5). doi:10.1128/MICROBIOLSPEC.MCHD-0031-2016
637. Kondo M, Wagers AJ, Manz MG, et al. Biology of hematopoietic stem cells and progenitors: implications for clinical application. *Annu Rev Immunol*. 2003;21:759-806. doi:10.1146/ANNUREV.IMMUNOL.21.120601.141007
638. Kondo M. Lymphoid and myeloid lineage commitment in multipotent hematopoietic progenitors. *Immunol Rev*. 2010;238(1):37. doi:10.1111/J.1600-065X.2010.00963.X
639. Lee N, Moon SY, Lee JH, et al. Discrepancies between the percentage of plasma cells in bone marrow aspiration and BM biopsy: Impact on the revised IMWG diagnostic criteria of multiple myeloma. *Blood Cancer J*. 2017;7(2). doi:10.1038/BCJ.2017.14
640. Kyle RA, Child JA, Anderson K, et al. Criteria for the classification of monoclonal gammopathies, multiple myeloma and related disorders: a report of the International

Myeloma Working Group. *Br J Haematol*. 2003;121(5):749-757. doi:10.1046/J.1365-2141.2003.04355.X

641. Wei Q, Frenette PS. Niches for Hematopoietic Stem Cells and Their Progeny. *Immunity*. 2018;48(4):632-648. doi:10.1016/J.IMMUNI.2018.03.024
642. Identification of a murine pan-T cell antigen which is also expressed during the terminal phases of B cell differentiation - PubMed. Accessed March 1, 2023. https://pubmed.ncbi.nlm.nih.gov/2897394/
643. Cyster JG. Homing of antibody secreting cells. *Immunol Rev*. 2003;194:48-60. doi:10.1034/J.1600-065X.2003.00041.X
644. Zhiming W, Luman W, Tingting Q, Yiwei C. Chemokines and receptors in intestinal B lymphocytes. *J Leukoc Biol*. 2018;103(5):807-819. doi:10.1002/JLB.1RU0717-299RR
645. O'Connor BP, Gleeson MW, Noelle RJ, Erickson LD. The rise and fall of long-lived humoral immunity: terminal differentiation of plasma cells in health and disease. *Immunol Rev*. 2003;194:61. doi:10.1034/J.1600-065X.2003.00055.X
646. Falank C, Fairfield H, Reagan MR. Reflections on Cancer in the Bone Marrow: Adverse Roles of Adipocytes. *Curr Mol Biol Rep*. 2017;3(4):254. doi:10.1007/S40610-017-0074-6
647. Lorusso G, Rüegg C. The tumor microenvironment and its contribution to tumor evolution toward metastasis. *Histochem Cell Biol*. 2008;130(6):1091-1103. doi:10.1007/S00418-008-0530-8/FIGURES/1
648. Fairfield H, Falank C, Avery L, Reagan MR. Multiple myeloma in the marrow: pathogenesis and treatments. *Ann N Y Acad Sci*. 2016;1364(1):32. doi:10.1111/NYAS.13038
649. Morgan GJ, Walker BA, Davies FE. The genetic architecture of multiple myeloma. *Nature Reviews Cancer 2012 12:5*. 2012;12(5):335-348. doi:10.1038/nrc3257
650. Grivennikov SI, Greten FR, Karin M. Immunity, Inflammation, and Cancer. *Cell*. 2010;140(6):883. doi:10.1016/J.CELL.2010.01.025
651. Pinho S, Frenette PS. Haematopoietic stem cell activity and interactions with the niche. *Nat Rev Mol Cell Biol*. 2019;20(5):303. doi:10.1038/S41580-019-0103-9
652. Chang MK, Raggatt LJ, Alexander KA, et al. Osteal Tissue Macrophages Are Intercalated throughout Human and Mouse Bone Lining Tissues and Regulate Osteoblast Function In Vitro and In Vivo. *The Journal of Immunology*. 2008;181(2):1232-1244. doi:10.4049/JIMMUNOL.181.2.1232
653. Lawson MA, McDonald MM, Kovacic N, et al. Osteoclasts control reactivation of dormant myeloma cells by remodelling the endosteal niche. *Nat Commun*. 2015;6. doi:10.1038/NCOMMS9983
654. McDonald MM, Khoo WH, Ng PY, et al. Osteoclasts recycle via osteomorphs during RANKL-stimulated bone resorption. *Cell*. 2021;184(5):1330. doi:10.1016/J.CELL.2021.02.002

655. Reagan MR, Rosen CJ. Navigating the bone marrow niche: translational insights and cancer-driven dysfunction. *Nat Rev Rheumatol*. 2016;12(3):154.
656. Young PP, Ardestani S, Li B. Myeloid Cells in Cancer Progression: Unique Subtypes and Their Roles in Tumor Growth, Vascularity, and Host Immune Suppression. *Cancer Microenvironment*. 2011;4(1):1. doi:10.1007/S12307-010-0045-4
657. Yan HH, Pickup M, Pang Y, et al. Gr-1+CD11b+ myeloid cells tip the balance of immune protection to tumor promotion in the premetastatic lung. *Cancer Res*. 2010;70(15):6139-6149. doi:10.1158/0008-5472.CAN-10-0706/656282/P/GR-1-CD11B-MYELOID-CELLS-TIP-THE-BALANCE-OF-IMMUNE
658. Yang L, DeBusk LM, Fukuda K, et al. Expansion of myeloid immune suppressor Gr+CD11b+ cells in tumor-bearing host directly promotes tumor angiogenesis. *Cancer Cell*. 2004;6(4):409-421. doi:10.1016/J.CCR.2004.08.031
659. Hiratsuka S, Nakamura K, Iwai S, et al. MMP9 induction by vascular endothelial growth factor receptor-1 is involved in lung-specific metastasis.
660. Hadjiaggelidou C, Katodritou E. Regulatory T-Cells and Multiple Myeloma: Implications in Tumor Immune Biology and Treatment. *J Clin Med*. 2021;10(19):4588. doi:10.3390/JCM10194588
661. Duque GA, Descoteaux A. Macrophage Cytokines: Involvement in Immunity and Infectious Diseases. *Front Immunol*. 2014;5(OCT). doi:10.3389/FIMMU.2014.00491
662. Liu Y, Zeng G. Cancer and Innate Immune System Interactions: Translational Potentials for Cancer Immunotherapy. *J Immunother*. 2012;35(4):299. doi:10.1097/CJI.0B013E3182518E83
663. Gonzalez H, Hagerling C, Werb Z. Roles of the immune system in cancer: from tumor initiation to metastatic progression. *Genes Dev*. 2018;32(19-20):1267. doi:10.1101/GAD.314617.118
664. Leivas A, Risueño RM, Guzmán A, et al. Natural killer cells efficiently target multiple myeloma clonogenic tumor cells. *Cancer Immunology, Immunotherapy*. 2021;70(10):2911. doi:10.1007/S00262-021-02901-Y
665. Moser-Katz T, Joseph NS, Dhodapkar M v., Lee KP, Boise LH. Game of Bones: How Myeloma Manipulates Its Microenvironment. *Front Oncol*. 2021;10. doi:10.3389/FONC.2020.625199/FULL
666. Hedvat C v., Comenzo RL, Teruya-Feldstein J, et al. Insights into extramedullary tumour cell growth revealed by expression profiling of human plasmacytomas and multiple myeloma. *Br J Haematol*. 2003;122(5):728-744. doi:10.1046/J.1365-2141.2003.04481.X
667. Štifter S, Babarović E, Valković T, et al. Combined evaluation of bone marrow aspirate and biopsy is superior in the prognosis of multiple myeloma. *Diagn Pathol*. 2010;5(1):30. doi:10.1186/1746-1596-5-30

668. Fujino M. The histopathology of myeloma in the bone marrow. *J Clin Exp Hematop*. 2018;58(2):61. doi:10.3960/JSLRT.18014
669. Fabian P, Moulis M. [Options for histological examination of bone marrow during diagnosis of multiple myeloma]. *Vnitr Lek*. 2006;52 Suppl 2(SUPPL. 2):66-70. Accessed February 4, 2023. https://europepmc.org/article/med/18175431
670. Singhal N, Singh T, Singh ZN, Shome DK, Gaiha M. Histomorphology of multiple myeloma on bone marrow biopsy. *Indian J Pathol Microbiol*. 2004;47(3):359-363. Accessed February 4, 2023. https://europepmc.org/article/med/16295424
671. Bone Marrow Tests for Multiple Myeloma | The IMF. Accessed February 4, 2023. https://www.myeloma.org/bone-marrow-tests
672. Bone Marrow Tests for Multiple Myeloma | The IMF. Accessed March 1, 2023. https://www.myeloma.org/bone-marrow-tests
673. Islam A. Bone marrow aspiration before bone marrow core biopsy using the same bone marrow biopsy needle: a good or bad practice? *J Clin Pathol*. 2007;60(2):212. doi:10.1136/JCP.2006.037341
674. Bone marrow test | Tests and scans | Cancer Research UK. Accessed February 4, 2023. https://www.cancerresearchuk.org/about-cancer/tests-and-scans/bone-marrow-test
675. What is myeloma? - Myeloma UK. Accessed February 4, 2023. https://www.myeloma.org.uk/understanding-myeloma/what-is-myeloma/
676. Li Y, Zheng Y, Li T, et al. Chemokines CCL2, 3, 14 stimulate macrophage bone marrow homing, proliferation, and polarization in multiple myeloma. *Oncotarget*. 2015;6(27):24218. doi:10.18632/ONCOTARGET.4523
677. Siddiqui JA, Partridge NC. CCL2/monocyte chemoattractant protein 1 and parathyroid hormone action on bone. *Front Endocrinol (Lausanne)*. 2017;8(MAR):49. doi:10.3389/FENDO.2017.00049/BIBTEX
678. Li X, Loberg R, Liao J, et al. A destructive cascade mediated by CCL2 facilitates prostate cancer growth in bone. *Cancer Res*. 2009;69(4):1685-1692. doi:10.1158/0008-5472.CAN-08-2164/654481/P/A-DESTRUCTIVE-CASCADE-MEDIATED-BY-CCL2-FACILITATES
679. Man JH, Choi SJ, Kurihara N, Koide M, Oba Y, David Roodman G. Macrophage inflammatory protein-1α is an osteoclastogenic factor in myeloma that is independent of receptor activator of nuclear factor κB ligand. *Blood*. 2001;97(11):3349-3353. doi:10.1182/blood.V97.11.3349
680. Homey B, Alenius H, Müller A, et al. CCL27-CCR10 interactions regulate T cell-mediated skin inflammation. *Nat Med*. 2002;8(2):157-165. doi:10.1038/NM0202-157
681. Cheng F, Yang SY, Fang XX, Wang X, Zhao FT. [Role of the CCL28-CCR10 pathway in monocyte migration in rheumatoid arthritis]. *Beijing da xue xue bao Yi xue ban = Journal of*

Peking University Health sciences. 2022;54(6):1074-1078. doi:10.19723/J.ISSN.1671-167X.2022.06.003

682. Yue Y, Zhang Q, Sun Z. CX3CR1 Acts as a Protective Biomarker in the Tumor Microenvironment of Colorectal Cancer. *Front Immunol*. 2022;12:1. doi:10.3389/FIMMU.2021.758040/FULL
683. Landsman L, Liat BO, Zernecke A, et al. CX3CR1 is required for monocyte homeostasis and atherogenesis by promoting cell survival. *Blood*. 2009;113(4):963-972. doi:10.1182/BLOOD-2008-07-170787
684. de Lau WBM, Kuipers J, Peters PJ, Lokhorsts HM, Clevers H, Bast BJEG. PUTATIVE MYELOMA PRECURSOR CELLS EXPRESSING 2,6 SIALIC ACID-MODIFIED ANTIGENS ACTUALLY BELONG TO THE ERYTHROID LINEAGE. *Leuk Res*. 1998;22(2):163-173.
685. Wei YY, Zhang XZ, Zhang F, et al. [Expression of CD71 on cell proliferation in hematologic malignancy and its correlation with Ki-67]. *Zhongguo Shi Yan Xue Ye Xue Za Zhi*. 2015;23(1):234-240. doi:10.7534/J.ISSN.1009-2137.2015.01.044
686. Mack EKM, Hartmann S, Ross P, et al. Monitoring multiple myeloma in the peripheral blood based on cell-free DNA and circulating plasma cells. *Ann Hematol*. 2022;101(4):811-824. doi:10.1007/S00277-022-04771-5/FIGURES/5
687. Tembhare PR, Sriram H, Khanka T, et al. Circulating Clonal Plasma Cells at Diagnosis and Peripheral Blood Measurable Residual Disease Assessment Provide Powerful Prognostication Biomarkers in Newly-Diagnosed Multiple Myeloma Patients Treated without Autologous Transplant. *Blood*. 2022;140(Supplement 1):1135-1136. doi:10.1182/BLOOD-2022-165715
688. Granell M, Calvo X, Garcia-Guiñón A, et al. Prognostic impact of circulating plasma cells in patients with multiple myeloma: implications for plasma cell leukemia definition. *Haematologica*. 2017;102(6):1099. doi:10.3324/HAEMATOL.2016.158303
689. Waldschmidt J, Wider D, Follo M, et al. Bone Marrow Interaction in Multiple Myeloma Pathogenesis: Phenotypical Analysis, Kinetics and Novel Therapy Approaches Based On CXCR4 Inhibition. *Blood*. 2012;120(21):2450-2450. doi:10.1182/BLOOD.V120.21.2450.2450
690. Kikuchi-Taura A, Okinaka Y, Takeuchi Y, et al. Bone Marrow Mononuclear Cells Activate Angiogenesis via Gap Junction-Mediated Cell-Cell Interaction. *Stroke*. Published online 2020:1279-1289. doi:10.1161/STROKEAHA.119.028072
691. Ożańska A, Szymczak D, Rybka J. Pattern of human monocyte subpopulations in health and disease. *Scand J Immunol*. 2020;92(1):e12883. doi:10.1111/SJI.12883
692. Drechsler M, Duchene J, Soehnlein O. Chemokines control mobilization, recruitment, and fate of monocytes in atherosclerosis. *Arterioscler Thromb Vasc Biol*. 2015;35(5):1050-1055. doi:10.1161/ATVBAHA.114.304649

693. Moser B, Willimann K. Chemokines: role in inflammation and immune surveillance. *Ann Rheum Dis*. 2004;63(suppl 2):ii84-ii89. doi:10.1136/ARD.2004.028316
694. el Arfani C, de Veirman K, Maes K, de Bruyne E, Menu E. Metabolic Features of Multiple Myeloma. *Int J Mol Sci*. 2018;19(4). doi:10.3390/IJMS19041200
695. Rizzieri D, Paul B, Kang Y. Metabolic alterations and the potential for targeting metabolic pathways in the treatment of multiple myeloma. *J Cancer Metastasis Treat*. 2019;5. doi:10.20517/2394-4722.2019.05
696. Yoo HC, Yu YC, Sung Y, Han JM. Glutamine reliance in cell metabolism. *Experimental & Molecular Medicine 2020 52:9*. 2020;52(9):1496-1516. doi:10.1038/s12276-020-00504-8
697. Yuan L, Sheng X, Willson AK, et al. Glutamine promotes ovarian cancer cell proliferation through the mTOR/S6 pathway. *Endocr Relat Cancer*. 2015;22(4):577-591. doi:10.1530/ERC-15-0192
698. Isoda A, Kaira K, Iwashina M, et al. Expression of L-type amino acid transporter 1 (LAT1) as a prognostic and therapeutic indicator in multiple myeloma. *Cancer Sci*. 2014;105(11):1496. doi:10.1111/CAS.12529
699. Bolzoni M, Chiu M, Accardi F, et al. Dependence on glutamine uptake and glutamine addiction characterize myeloma cells: a new attractive target. *Blood*. 2016;128(5):667-679. doi:10.1182/BLOOD-2016-01-690743
700. Cantor JM, Ginsberg MH. CD98 at the crossroads of adaptive immunity and cancer. *J Cell Sci*. 2012;125(6):1373. doi:10.1242/JCS.096040
701. Chen Y, Zhang J, Cui W, Silverstein RL. CD36, a signaling receptor and fatty acid transporter that regulates immune cell metabolism and fate. *J Exp Med*. 2022;219(6). doi:10.1084/JEM.20211314
702. Silverstein RL, Febbraio M. CD36, a Scavenger Receptor Involved in Immunity, Metabolism, Angiogenesis, and Behavior. *Sci Signal*. 2009;2(72):re3. doi:10.1126/SCISIGNAL.272RE3
703. Albert ML, Pearce SFA, Francisco LM, et al. Immature Dendritic Cells Phagocytose Apoptotic Cells via αvβ5 and CD36, and Cross-present Antigens to Cytotoxic T Lymphocytes. *J Exp Med*. 1998;188(7):1359. doi:10.1084/JEM.188.7.1359
704. Finnemann SC, Silverstein RL. Differential Roles of CD36 and αvβ5 Integrin in Photoreceptor Phagocytosis by the Retinal Pigment Epithelium. *J Exp Med*. 2001;194(9):1289. doi:10.1084/JEM.194.9.1289
705. Silverstein RL, Li W, Park YM, Rahaman SO. Mechanisms of Cell Signaling by the Scavenger Receptor CD36: Implications in Atherosclerosis and Thrombosis. *Trans Am Clin Climatol Assoc*. 2010;121:206. Accessed March 6, 2023. /pmc/articles/PMC2917163/
706. Wang H, Franco F, Tsui YC, et al. CD36-mediated metabolic adaptation supports regulatory T cell survival and function in tumors. *Nat Immunol*. 2020;21(3):298. doi:10.1038/S41590-019-0589-5

707. Prasanna SJ, Gopalakrishnan D, Shankar SR, Vasandan AB. Pro-Inflammatory Cytokines, IFNγ and TNFα, Influence Immune Properties of Human Bone Marrow and Wharton Jelly Mesenchymal Stem Cells Differentially. *PLoS One*. 2010;5(2):e9016. doi:10.1371/JOURNAL.PONE.0009016
708. Duque GA, Descoteaux A. Macrophage cytokines: Involvement in immunity and infectious diseases. *Front Immunol*. 2014;5(OCT):491. doi:10.3389/FIMMU.2014.00491/BIBTEX
709. Tsujimoto T, Lisukov IA, Huang N, Mahmoud MS, Kawano MM. Plasma Cells Induce Apoptosis of Pre-B Cells by Interacting With Bone Marrow Stromal Cells. *Blood*. 1996;87(8):3375-3383. doi:10.1182/BLOOD.V87.8.3375.BLOODJOURNAL8783375
710. Reagan MR, Kaplan DL. Mesenchymal Stem Cell Tumor-Homing: Detection Methods in Disease Model Systems. *Stem Cells*. 2011;29(6):920. doi:10.1002/STEM.645
711. Reagan MR, Ghobrial IM. Multiple Myeloma-Mesenchymal Stem Cells: Characterization, Origin, and Tumor-Promoting Effects. *Clinical Cancer Research*. 2012;18(2):342. doi:10.1158/1078-0432.CCR-11-2212
712. Webster JD, Vucic D. The Balance of TNF Mediated Pathways Regulates Inflammatory Cell Death Signaling in Healthy and Diseased Tissues. *Front Cell Dev Biol*. 2020;8:365. doi:10.3389/FCELL.2020.00365/BIBTEX
713. Lee C, Oh JI, Park J, et al. TNFα Mediated IL-6 Secretion Is Regulated by JAK/STAT Pathway but Not by MEK Phosphorylation and AKT Phosphorylation in U266 Multiple Myeloma Cells. *Biomed Res Int*. 2013;2013. doi:10.1155/2013/580135
714. Chen G, Goeddel D v. TNF-R1 signaling: A beautiful pathway. *Science (1979)*. 2002;296(5573):1634-1635. doi:10.1126/SCIENCE.1071924/ASSET/2858A14D-690B-4B8D-9F77-6815DF79FFBD/ASSETS/GRAPHIC/SE2120541001.JPEG
715. Aggarwal R, Ghobrial IM, Roodman GD. Chemokines in multiple myeloma. *Exp Hematol*. 2006;34(10):1289. doi:10.1016/J.EXPHEM.2006.06.017
716. Alexandrakis MG, Passam FH, Sfiridaki A, Kandidaki E, Roussou P, Kyriakou DS. Elevated serum concentration of hepatocyte growth factor in patients with multiple myeloma: correlation with markers of disease activity. *Am J Hematol*. 2003;72(4):229-233. doi:10.1002/AJH.10304
717. Lichtenstein A, Berenson J, Norman D, Chang M, Carlile A. Production of Cytokines by Bone Marrow Cells Obtained From Patients With Multiple Myeloma. *Blood*. 1989;74(4):1266-1273. doi:10.1182/BLOOD.V74.4.1266.1266
718. Confalone E, D'Alessio G, Furia A. IL-6 Induction by TNFα and IL-1β in an Osteoblast-Like Cell Line. *Int J Biomed Sci*. 2010;6(2):135. Accessed March 5, 2023. /pmc/articles/PMC3614745/

719. Karadag A, Oyajobi BO, Apperley JF, Graham R, Russell G, Croucher PI. Human myeloma cells promote the production of interleukin 6 by primary human osteoblasts. *Br J Haematol*. 2000;108(2):383-390. doi:10.1046/J.1365-2141.2000.01845.X
720. Tanaka T, Narazaki M, Kishimoto T. IL-6 in Inflammation, Immunity, and Disease. *Cold Spring Harb Perspect Biol*. 2014;6(10):a016295. doi:10.1101/CSHPERSPECT.A016295
721. Brocke-Heidrich K, Kretzschmar AK, Pfeifer G, et al. Interleukin-6–dependent gene expression profiles in multiple myeloma INA-6 cells reveal a Bcl-2 family–independent survival pathway closely associated with Stat3 activation. *Blood*. 2004;103(1):242-251. doi:10.1182/BLOOD-2003-04-1048
722. Frassanito MA, Cusmai A, Iodice G, Dammacco F. Autocrine interleukin-6 production and highly malignant multiple myeloma: relation with resistance to drug-induced apoptosis. *Blood*. 2001;97(2):483-489. doi:10.1182/BLOOD.V97.2.483
723. Kovacs E. Interleukin-6 leads to interleukin-10 production in several human multiple myeloma cell lines. Does interleukin-10 enhance the proliferation of these cells? *Leuk Res*. 2010;34(7):912-916. doi:10.1016/J.LEUKRES.2009.08.012
724. Brocke-Heidrich K, Kretzschmar AK, Pfeifer G, et al. Interleukin-6–dependent gene expression profiles in multiple myeloma INA-6 cells reveal a Bcl-2 family–independent survival pathway closely associated with Stat3 activation. *Blood*. 2004;103(1):242-251. doi:10.1182/BLOOD-2003-04-1048
725. Lee C, Oh JI, Park J, et al. TNFα Mediated IL-6 Secretion Is Regulated by JAK/STAT Pathway but Not by MEK Phosphorylation and AKT Phosphorylation in U266 Multiple Myeloma Cells. *Biomed Res Int*. 2013;2013. doi:10.1155/2013/580135
726. Portier M, Rajzbaum G, Zhang XG, et al. In vivo interleukin 6 gene expression in the tumoral environment in multiple myeloma. *Eur J Immunol*. 1991;21(7):1759-1762. doi:10.1002/EJI.1830210727
727. Matthes T, Manfroi B, Huard B. Revisiting IL-6 antagonism in multiple myeloma. *Crit Rev Oncol Hematol*. 2016;105:1-4. doi:10.1016/J.CRITREVONC.2016.07.006
728. Aggarwal R, Ghobrial IM, Roodman GD. Chemokines in multiple myeloma. *Exp Hematol*. 2006;34(10):1289. doi:10.1016/J.EXPHEM.2006.06.017
729. Alexandrakis MG, Passam FH, Sfiridaki A, Kandidaki E, Roussou P, Kyriakou DS. Elevated serum concentration of hepatocyte growth factor in patients with multiple myeloma: Correlation with markers of disease activity. *Am J Hematol*. 2003;72(4):229-233. doi:10.1002/AJH.10304
730. Thompson MA, Witzig TE, Kumar S, et al. Plasma levels of tumour necrosis factor alpha and interleukin-6 predict progression-free survival following thalidomide therapy in patients with previously untreated multiple myeloma. *Br J Haematol*. 2003;123(2):305-308. doi:10.1046/J.1365-2141.2003.04605.X

731. Zhu YX, Kortuem KM, Stewart AK. Molecular mechanism of action of immune-modulatory drugs thalidomide, lenalidomide and pomalidomide in multiple myeloma. *Leuk Lymphoma*. 2013;54(4):683-687. doi:10.3109/10428194.2012.728597
732. Muller GW, Chen R, Huang SY, et al. Amino-substituted thalidomide analogs: potent inhibitors of TNF-alpha production. *Bioorg Med Chem Lett*. 1999;9(11):1625-1630. doi:10.1016/S0960-894X(99)00250-4
733. Görgün G, Calabrese E, Soydan E, et al. Immunomodulatory effects of lenalidomide and pomalidomide on interaction of tumor and bone marrow accessory cells in multiple myeloma. *Blood*. 2010;116(17):3227. doi:10.1182/BLOOD-2010-04-279893
734. May RD, Fung M. Strategies targeting the IL-4/IL-13 axes in disease. *Cytokine*. 2015;75(1):89-116. doi:10.1016/J.CYTO.2015.05.018
735. Gour N, Wills-Karp M. IL-4 and IL-13 signaling in allergic airway disease. *Cytokine*. 2015;75(1):68-78. doi:10.1016/J.CYTO.2015.05.014
736. Bao K, Reinhardt RL. The differential expression of IL-4 and IL-13 and its impact on type-2 Immunity. *Cytokine*. 2015;75(1):25. doi:10.1016/J.CYTO.2015.05.008
737. Iwaszko M, Biały S, Bogunia-Kubik K. Significance of Interleukin (IL)-4 and IL-13 in Inflammatory Arthritis. *Cells*. 2021;10(11). doi:10.3390/CELLS10113000
738. Iwaszko M, Biały S, Bogunia-Kubik K. Significance of interleukin (IL)-4 and IL-13 in inflammatory arthritis. *Cells*. 2021;10(11). doi:10.3390/CELLS10113000
739. Miossec P, Briolay J, Dechanet J, Wijdenes J, Martinez-Valdez H, Banchereau J. Inhibition of the production of proinflammatory cytokines and immunoglobulins by interleukin-4 in an ex vivo model of rheumatoid synovitis. *Arthritis Rheum*. 1992;35(8):874-883. doi:10.1002/ART.1780350805
740. Zhang Y, Wang S, Liu Z, Yang L, Liu J, Xiu M. Increased Six1 expression in macrophages promotes hepatocellular carcinoma growth and invasion by regulating MMP-9. *J Cell Mol Med*. 2019;23(7):4523-4533. doi:10.1111/JCMM.14342
741. Quintero-Fabián S, Arreola R, Becerril-Villanueva E, et al. Role of Matrix Metalloproteinases in Angiogenesis and Cancer. *Front Oncol*. 2019;9:1370. doi:10.3389/FONC.2019.01370/BIBTEX
742. Egeblad M, Werb Z. New functions for the matrix metalloproteinases in cancer progression. *Nature Reviews Cancer 2002 2:3*. 2002;2(3):161-174. doi:10.1038/nrc745
743. Yabluchanskiy A, Ma Y, Iyer RP, Hall ME, Lindsey ML. Matrix metalloproteinase-9: Many shades of function in cardiovascular disease. *Physiology*. 2013;28(6):391-403. doi:10.1152/PHYSIOL.00029.2013/ASSET/IMAGES/LARGE/PHY0061301900006.JPEG
743. Müller-Quernheim J. MMPs are regulatory enzymes in pathways of inflammatory disorders, tissue injury, malignancies and remodelling of the lung. *European Respiratory Journal*. 2011;38(1):12-14. doi:10.1183/09031936.00079311

745. Page-McCaw A, Ewald AJ, Werb Z. Matrix metalloproteinases and the regulation of tissue remodelling. *Nat Rev Mol Cell Biol*. 2007;8(3):221-233. doi:10.1038/nrm2125
746. Löffek S, Schilling O, Franzke CW. Biological role of matrix metalloproteinases: a critical balance. *European Respiratory Journal*. 2011;38(1):191-208. doi:10.1183/09031936.00146510
747. Augoff K, Hryniewicz-Jankowska A, Tabola R, Stach K. MMP9: A Tough Target for Targeted Therapy for Cancer. *Cancers (Basel)*. 2022;14(7). doi:10.3390/CANCERS14071847/S1
748. Yang CC, Lin CC, Hsiao L der, Kuo JM, Tseng HC, Yang CM. Lipopolysaccharide-Induced Matrix Metalloproteinase-9 Expression Associated with Cell Migration in Rat Brain Astrocytes. *Int J Mol Sci*. 2020;21(1). doi:10.3390/IJMS21010259
749. de Pinho RT, da Silva WS, de Castro CÔrtes LM, da Silva Vasconcelos Sousa P, de Araujo Soares RO, Alves CR. Production of MMP-9 and inflammatory cytokines by Trypanosoma cruzi-infected macrophages. *Exp Parasitol*. 2014;147:72-80. doi:10.1016/J.EXPPARA.2014.09.003
750. Mostafa Mtairag E, Chollet-Martin S, Oudghiri M, et al. Effects of interleukin-10 on monocyte/endothelial cell adhesion and MMP-9/TIMP-1 secretion. *Cardiovasc Res*. 2001;49(4):882-890. doi:10.1016/S0008-6363(00)00287-X/2/49-4-882-GR6.GIF
751. Cathcart J, Pulkoski-Gross A, Cao J. Targeting matrix metalloproteinases in cancer: Bringing new life to old ideas. *Genes Dis*. 2015;2(1):26-34. doi:10.1016/J.GENDIS.2014.12.002
752. Lacraz S, Nicod LP, Chicheportiche R, Welgus HG, Dayer JM. IL-10 inhibits metalloproteinase and stimulates TIMP-1 production in human mononuclear phagocytes. *Journal of Clinical Investigation*. 1995;96(5):2304-2310. doi:10.1172/JCI118286
753. Lacraz S, Nicod L, Galve-de Rochemonteix B, Baumberger C, Dayer - JM, Welgus HG. Suppression of metalloproteinase biosynthesis in human alveolar macrophages by interleukin-4. *J Clin Invest*. 1992;90(2):382-388. doi:10.1172/JCI115872
754. Chizzolini C, Rezzonico R, de Luca C, Burger D, Dayer JM. Th2 Cell Membrane Factors in Association with IL-4 Enhance Matrix Metalloproteinase-1 (MMP-1) While Decreasing MMP-9 Production by Granulocyte-Macrophage Colony-Stimulating Factor-Differentiated Human Monocytes. *The Journal of Immunology*. 2000;164(11):5952-5960. doi:10.4049/JIMMUNOL.164.11.5952
755. Purwar R, Kraus M, Werfel T, Wittmann M. Modulation of keratinocyte-derived MMP-9 by IL-13: a possible role for the pathogenesis of epidermal inflammation. *J Invest Dermatol*. 2008;128(1):59-66. doi:10.1038/SJ.JID.5700940
756. Silbermann R, Bolzoni M, Storti P, et al. Bone Marrow Monocyte / Macrophage Derived Activin A Mediates the Osteoclastogenic Effect of IL-3 in Multiple Myeloma. *Leukemia*. 2014;28(4):951. doi:10.1038/LEU.2013.385

757. Wada A, Ito A, Iitsuka H, et al. Role of chemokine CX3CL1 in progression of multiple myeloma via CX3CR1 in bone microenvironments. *Oncol Rep*. 2015;33(6):2935-2939. doi:10.3892/OR.2015.3941
758. Y H, MM K, N H, et al. Identification of early plasma cells in peripheral blood and their clinical significance. *Br J Haematol*. 1996;92(1):184-191. doi:10.1046/J.1365-2141.1996.300835.X
759. Gupta S, Master S, Graham C. Extramedullary Multiple Myeloma: A Patient-Focused Review of the Pathogenesis of Bone Marrow Escape. *World J Oncol*. 2022;13(5):311. doi:10.14740/WJON1521
760. Kay NE, Leong T, Kyle RA, et al. Circulating Blood B Cells in Multiple Myeloma: Analysis and Relationship to Circulating Clonal Cells and Clinical Parameters in a Cohort of Patients Entered on the Eastern Cooperative Oncology Group Phase III E9486 Clinical Trial. *Blood*. 1997;90(1):340-345. doi:10.1182/BLOOD.V90.1.340
761. P. Leif Bergsagel AMS, Agnieszka Szczepek MJARB and LMP. In Multiple Myeloma, Clonotypic B Lymphocytes Are Detectable Among CD19+ Peripheral Blood Cells Expressing CD38, CD56, and Monotypic Ig Light Chain. *Blood*. 1995;85(2):436-447. doi:10.1182/BLOOD.V85.2.436.436
762. Pepino MY, Kuda O, Samovski D, Abumrad NA. Structure-function of CD36 and importance of fatty acid signal transduction in fat metabolism. *Annu Rev Nutr*. 2014;34:281-303. doi:10.1146/ANNUREV-NUTR-071812-161220
763. Cormerais Y, Giuliano S, LeFloch R, et al. Genetic Disruption of the Multifunctional CD98/LAT1 Complex Demonstrates the Key Role of Essential Amino Acid Transport in the Control of mTORC1 and Tumor Growth. *Cancer Res*. 2016;76(15):4481-4492. doi:10.1158/0008-5472.CAN-15-3376
764. Napolitano L, Scalise M, Galluccio M, Pochini L, Albanese LM, Indiveri C. LAT1 is the transport competent unit of the LAT1/CD98 heterodimeric amino acid transporter. *Int J Biochem Cell Biol*. 2015;67:25-33. doi:10.1016/J.BIOCEL.2015.08.004
765. Scalise M, Galluccio M, Console L, Pochini L, Indiveri C. The Human SLC7A5 (LAT1): The Intriguing Histidine/Large Neutral Amino Acid Transporter and Its Relevance to Human Health. *Front Chem*. 2018;6(JUN):243. doi:10.3389/FCHEM.2018.00243
766. Ma X, Xiao L, Liu L, et al. CD36-mediated ferroptosis dampens intratumoral CD8+ T cell effector function and impairs their antitumor ability. *Cell Metab*. 2021;33(5):1001-1012.e5. doi:10.1016/J.CMET.2021.02.015
767. Glatz JFC, Luiken JJFP. Thematic Review Series: Lipid Transfer Proteins: Dynamic role of the transmembrane glycoprotein CD36 (SR-B2) in cellular fatty acid uptake and utilization. *J Lipid Res*. 2018;59(7):1084. doi:10.1194/JLR.R082933
768. Bernstein ZS, Kim EB, Raje N. Bone Disease in Multiple Myeloma: Biologic and Clinical Implications. *Cells*. 2022;11(15). doi:10.3390/CELLS11152308

769. Edwards CM, Zhuang J, Mundy GR. The Pathogenesis of the Bone Disease of Multiple Myeloma. *Bone*. 2008;42(6):1007. doi:10.1016/J.BONE.2008.01.027
770. Kazandjian D. Multiple myeloma epidemiology and survival, a unique malignancy. *Semin Oncol*. 2016;43(6):676. doi:10.1053/J.SEMINONCOL.2016.11.004
771. Kumar SK, Rajkumar SV, Dispenzieri A, et al. Improved survival in multiple myeloma and the impact of novel therapies. *Blood*. 2008;111(5):2516. doi:10.1182/BLOOD-2007-10-116129
772. Giuliani N, Colla S, Rizzoli V. New insight in the mechanism of osteoclast activation and formation in multiple myeloma: focus on the receptor activator of NF-kappaB ligand (RANKL). *Exp Hematol*. 2004;32(8):685-691. doi:10.1016/J.EXPHEM.2004.03.015
773. Hideshima T, Anderson KC. Signaling Pathway Mediating Myeloma Cell Growth and Survival. *Cancers (Basel)*. 2021;13(2):1-17. doi:10.3390/CANCERS13020216
774. Musolino C, Allegra A, Innao V, Allegra AG, Pioggia G, Gangemi S. Inflammatory and Anti-Inflammatory Equilibrium, Proliferative and Antiproliferative Balance: The Role of Cytokines in Multiple Myeloma. *Mediators Inflamm*. 2017;2017. doi:10.1155/2017/1852517
775. Dessale M, Mengistu G, Mengist HM. Nanotechnology: A Promising Approach for Cancer Diagnosis, Therapeutics and Theragnosis. *Int J Nanomedicine*. 2022;17:3735. doi:10.2147/IJN.S378074
776. Moreno JL, Kaczmarek M, Keegan AD, Tondravi M. IL-4 suppresses osteoclast development and mature osteoclast function by a STAT6-dependent mechanism: irreversible inhibition of the differentiation program activated by RANKL. *Blood*. 2003;102(3):1078-1086. doi:10.1182/BLOOD-2002-11-3437
777. Musolino C, Allegra A, Innao V, Allegra AG, Pioggia G, Gangemi S. Inflammatory and Anti-Inflammatory Equilibrium, Proliferative and Antiproliferative Balance: The Role of Cytokines in Multiple Myeloma. *Mediators Inflamm*. 2017;2017. doi:10.1155/2017/1852517
778. Mocellin S, Marincola FM, Young HA. Interleukin-10 and the immune response against cancer: a counterpoint. *J Leukoc Biol*. 2005;78(5):1043-1051. doi:10.1189/JLB.0705358
779. Benjamin D, Park CD, Sharma V. Human B cell interleukin 10. *Leuk Lymphoma*. 1994;12(3-4):205-209. doi:10.3109/10428199409059591
780. Kovacs E. Interleukin-6 leads to interleukin-10 production in several human multiple myeloma cell lines. Does interleukin-10 enhance the proliferation of these cells? *Leuk Res*. 2010;34(7):912-916. doi:10.1016/J.LEUKRES.2009.08.012
781. Lu ZY, Zhang XG, Rodriguez C, et al. Interleukin-10 Is a Proliferation Factor But Not a Differentiation Factor for Human Myeloma Cells. *Blood*. 1995;85(9):2521-2527. doi:10.1182/BLOOD.V85.9.2521.BLOODJOURNAL8592521
782. Alexandrakis MG, Passam FH, Kyriakou DS, Dambaki K, Niniraki M, Stathopoulos E. Ki-67 Proliferation Index: Correlation with Prognostic Parameters and Outcome in Multiple

Myeloma. *American Journal of Clinical Oncology: Cancer Clinical Trials*. 2004;27(1):8-13. doi:10.1097/01.COC.0000045810.91816.41

783. Pappa C, Miyakis S, Tsirakis G, et al. Serum levels of interleukin-15 and interleukin-10 and their correlation with proliferating cell nuclear antigen in multiple myeloma. *Cytokine*. 2007;37(2):171-175. doi:10.1016/J.CYTO.2007.02.022
784. IL-10: a novel cytotoxic T cell differentiation factor - PubMed. Accessed March 28, 2023. https://pubmed.ncbi.nlm.nih.gov/1906502/
785. Takayanagi H. Osteoimmunology: shared mechanisms and crosstalk between the immune and bone systems. *Nature Reviews Immunology 2007 7:4*. 2007;7(4):292-304. doi:10.1038/nri2062
786. Ibáñez L, Abou-Ezzi G, Ciucci T, et al. Inflammatory Osteoclasts Prime TNFα-Producing CD4+ T Cells and Express CX3 CR1. *J Bone Miner Res*. 2016;31(10):1899-1908. doi:10.1002/JBMR.2868
787. Mori G, D'Amelio P, Faccio R, Brunetti G. The Interplay between the bone and the immune system. *Clin Dev Immunol*. 2013;2013. doi:10.1155/2013/720504

788. Musolino C, Allegra A, Innao V, Allegra AG, Pioggia G, Gangemi S. Inflammatory and Anti-Inflammatory Equilibrium, Proliferative and Antiproliferative Balance: The Role of Cytokines in Multiple Myeloma. *Mediators Inflamm*. 2017;2017. doi:10.1155/2017/1852517
789. Chauhan D, Singh A V., Brahmandam M, et al. Functional Interaction of Plasmacytoid Dendritic Cells with Multiple Myeloma Cells: A Novel Therapeutic Target. *Cancer Cell*. 2009;16(4):309. doi:10.1016/J.CCR.2009.08.019
790. Zhou A, Wu B, Yu H, et al. Current Understanding of Osteoimmunology in Certain Osteoimmune Diseases. *Front Cell Dev Biol*. 2021;9. doi:10.3389/FCELL.2021.698068
791. Galustian C, Meyer B, Labarthe MC, et al. The anti-cancer agents lenalidomide and pomalidomide inhibit the proliferation and function of T regulatory cells. *Cancer Immunol Immunother*. 2009;58(7):1033-1045. doi:10.1007/S00262-008-0620-4
792. Liu P, Jin Y, Sattar H, Liu H, Xie W, Zhou F. Natural killer cell immunotherapy against multiple myeloma: Progress and possibilities. *J Leukoc Biol*. 2018;103(5):821-828. doi:10.1002/JLB.2RU0517-176RR
793. Tsubaki M, Komai M, Itoh T, et al. Inhibition of the tumour necrosis factor-alpha autocrine loop enhances the sensitivity of multiple myeloma cells to anticancer drugs. *Eur J Cancer*. 2013;49(17):3708-3717. doi:10.1016/J.EJCA.2013.07.010
794. Jourdan M, Tarte K, Legouffe É, Brochier J, Rossi JF, Klein B. Tumor necrosis factor is a survival and proliferation factor for human myeloma cells. *Eur Cytokine Netw*. 1999;10(1):65. Accessed March 29, 2023. /pmc/articles/PMC2025696/

795. Nachbaur DM, Herold M, Maneschg A, Huber H. Serum levels of interleukin-6 in multiple myeloma and other hematological disorders: correlation with disease activity and other prognostic parameters. *Ann Hematol*. 1991;62(2-3):54-58. doi:10.1007/BF01714900/METRICS

796. Burger R. Impact of Interleukin-6 in Hematological Malignancies. *Transfusion Medicine and Hemotherapy*. 2013;40(5):336-343. doi:10.1159/000354194

Chapter Nine

Appendix

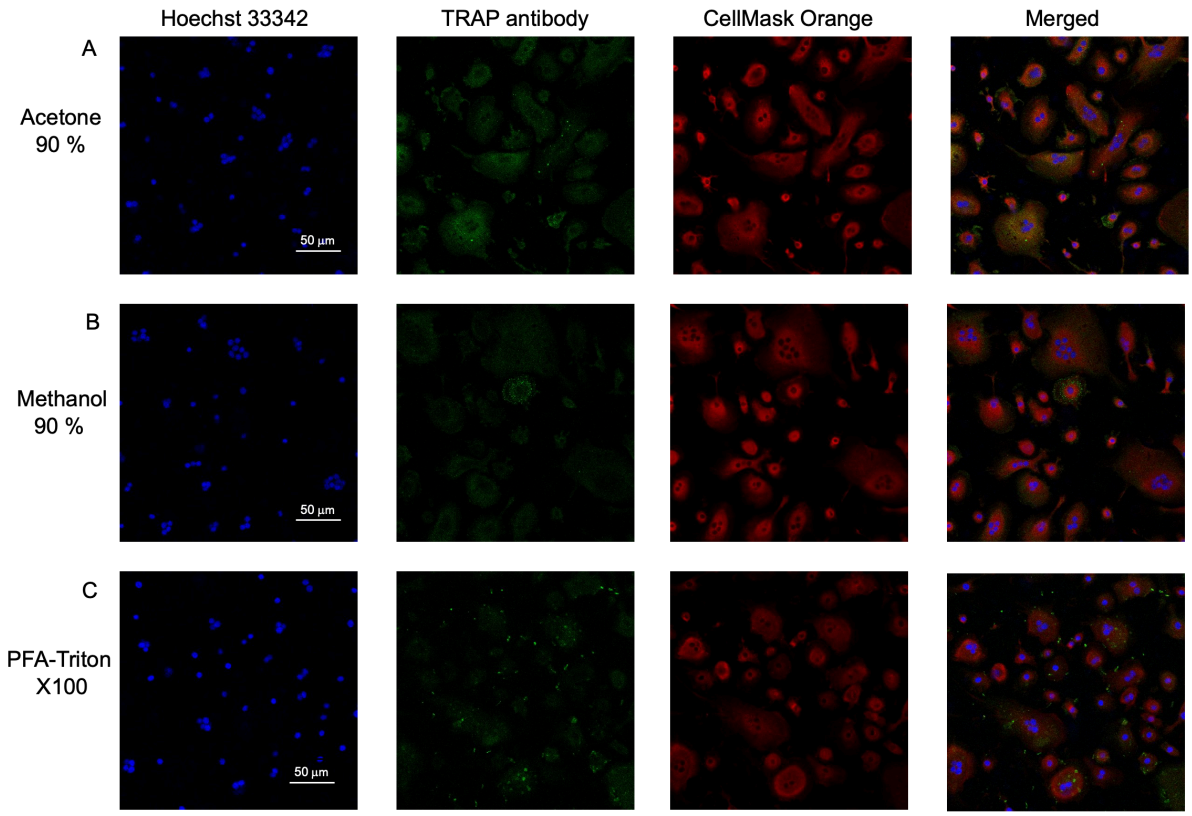

Appendix 9.1 The optimisation of the fixing technique on TRAP antibody expression on monocyte-derived osteoclasts differentiated with M-CSF and RANKL.

M-CSF and RANKL were used to drive the differentiation of monocytes isolated from healthy donors into osteoclasts. Confocal microscopy was used to determine the expression of TRAP on day 14. Different fixing techniques were tested multiple times before choosing the best method. These included: acetone 90 % (A), methanol 90% (B) and PFA-Triton-X100 (C). Nuclei were stained with Hoechst 33342 Solution and the plasma membrane was stained with CellMask™ Orange. TRAP was stained with FITC-labelled antibodies. Images were taken at X20 magnification and a 50 µm scale bar was included. Representative images from n= 4 experiments.

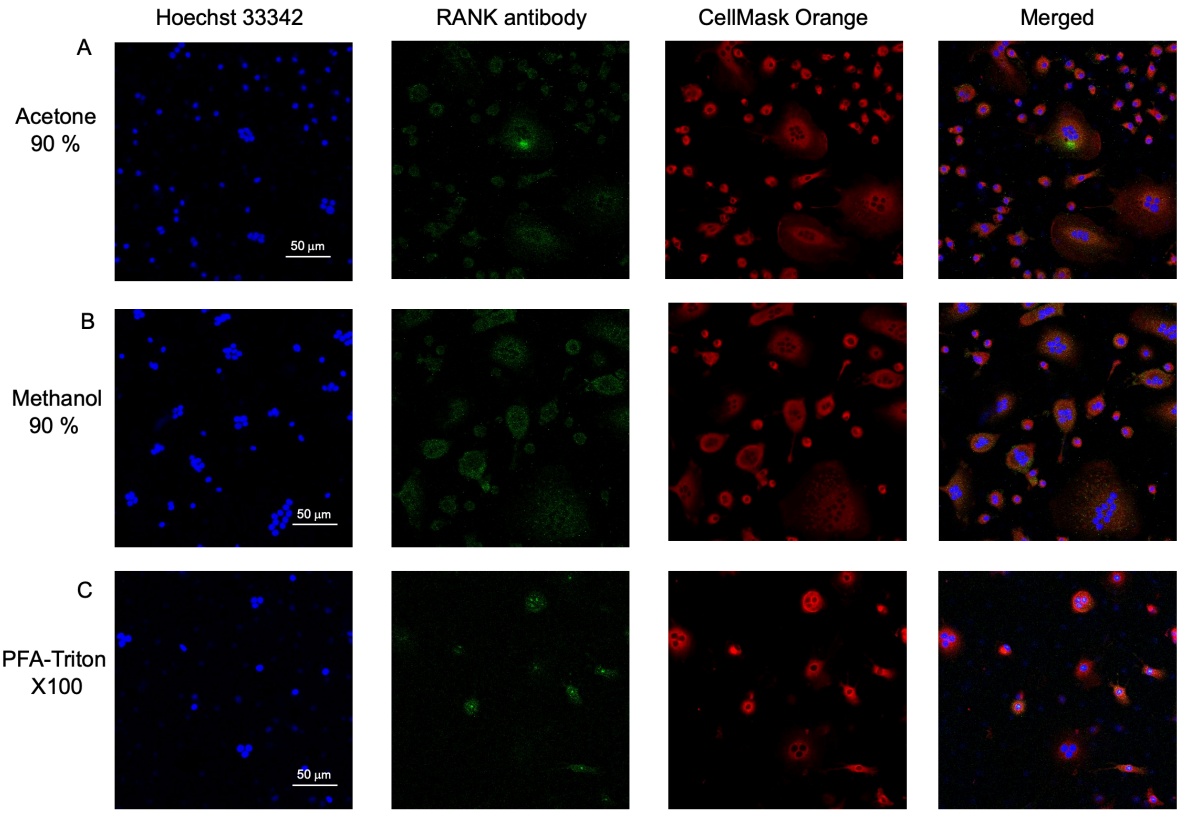

Appendix 9.2 The optimisation of the fixing technique on RANK antibody expression on monocyte-derived osteoclasts differentiated with M-CSF and RANKL.

M-CSF and RANKL were used to drive the differentiation of monocytes isolated from healthy donors into osteoclasts. Confocal microscopy was used to determine the expression of RANK on day 14. Different fixing techniques were tested before choosing the best method. These included: acetone 90 % (A), methanol 90% (B) and PFA-Triton-X100 (C). Nuclei were stained with Hoechst 33342 Solution and the plasma membrane was stained with CellMask™ Orange. RANK was stained with FITC-labelled antibodies. Images were taken at X20 magnification and a 50 µm scale bar was included. Representative images from n= 4 experiments.

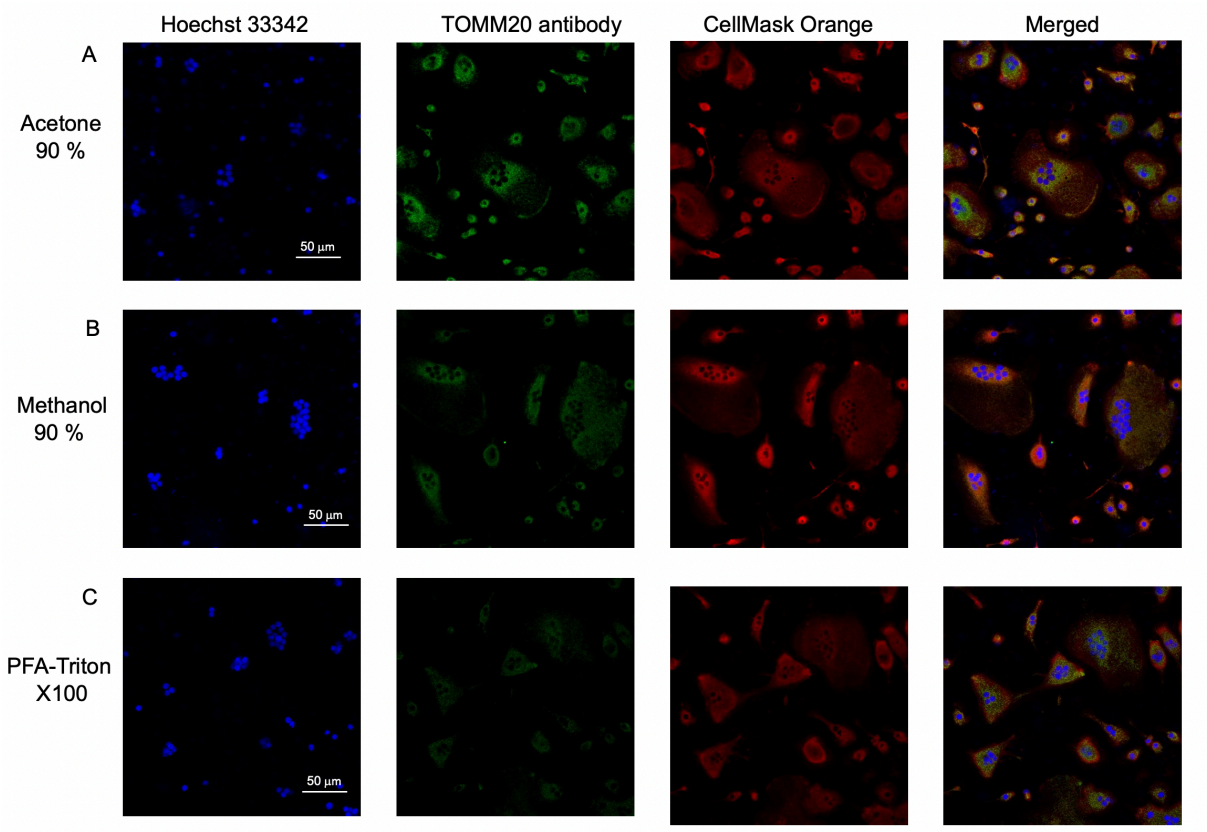

Appendix 9.3 The optimisation of the fixing technique on TOMM20 antibody expression on monocyte-derived osteoclasts differentiated with M-CSF and RANKL.

M-CSF and RANKL were used to drive the differentiation of monocytes isolated from healthy donors into osteoclasts. Confocal microscopy was used to determine the expression of TOMM20 on day 14. Different fixing techniques were tested before choosing the best method. These included: acetone 90 % (A), methanol 90% (B) and PFA-Triton-X100 (C). Nuclei were stained with Hoechst 33342 Solution and the plasma membrane was stained with CellMask™ Orange. TOMM20 was stained with FITC-labelled antibodies. Images were taken at X20 magnification and a 50 µm scale bar was included. Representative images from n= 4 experiments.

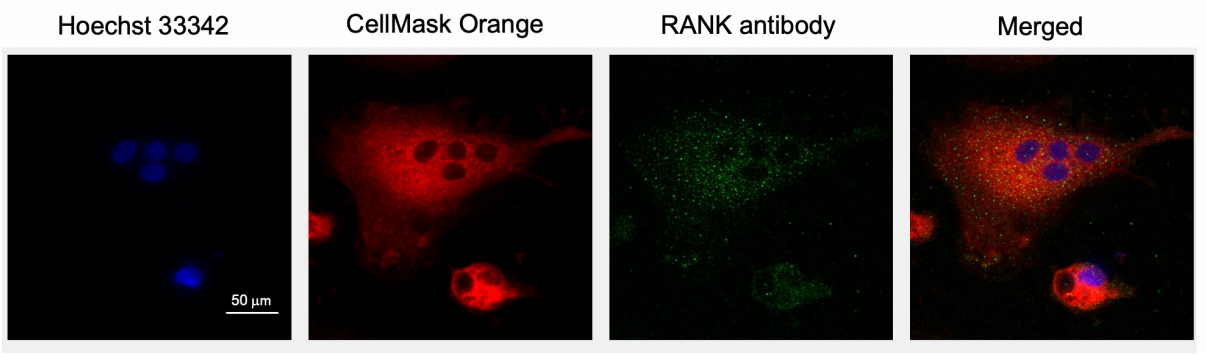

Appendix 9.4 RANK expression on monocyte-derived osteoclasts differentiated with M-CSF and RANKL.

M-CSF and RANKL were used to drive the differentiation of monocytes isolated from healthy donors into osteoclasts. Confocal microscopy was used to determine the expression of RANK on day 14. Nuclei were stained with Hoechst 33342 Solution and the plasma membrane was stained with CellMask™ Orange. RANK was stained with FITC-labelled antibodies. Images were taken at X63 magnification. Representative images from n= 6 experiments.

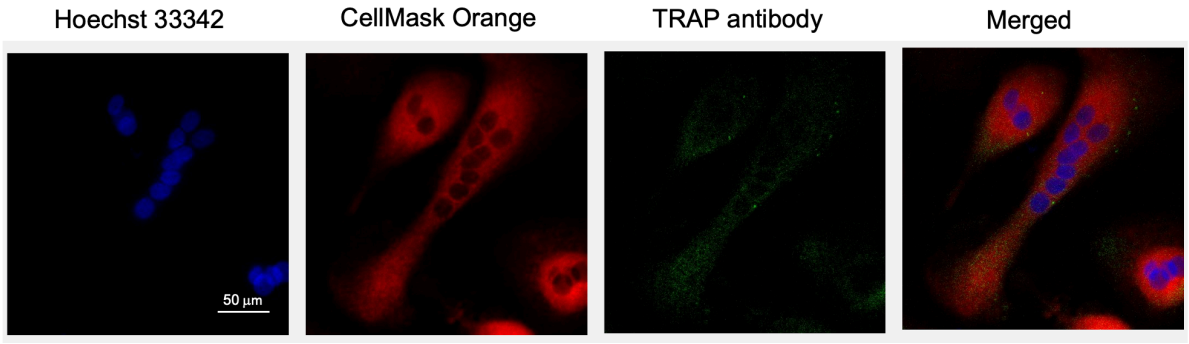

Appendix 9.5 TRAP expression on monocyte-derived osteoclasts differentiated with M-CSF and RANKL.

M-CSF and RANKL were used to drive the differentiation of monocytes isolated from healthy donors into osteoclasts. Confocal microscopy was used to determine the expression of TRAP on day 14. Nuclei were stained with Hoechst 33342 Solution and the plasma membrane was stained with CellMask™ Orange. TRAP was stained with FITC-labelled antibodies. Images were taken at X63 magnification. Representative images from n= 6 experiments.

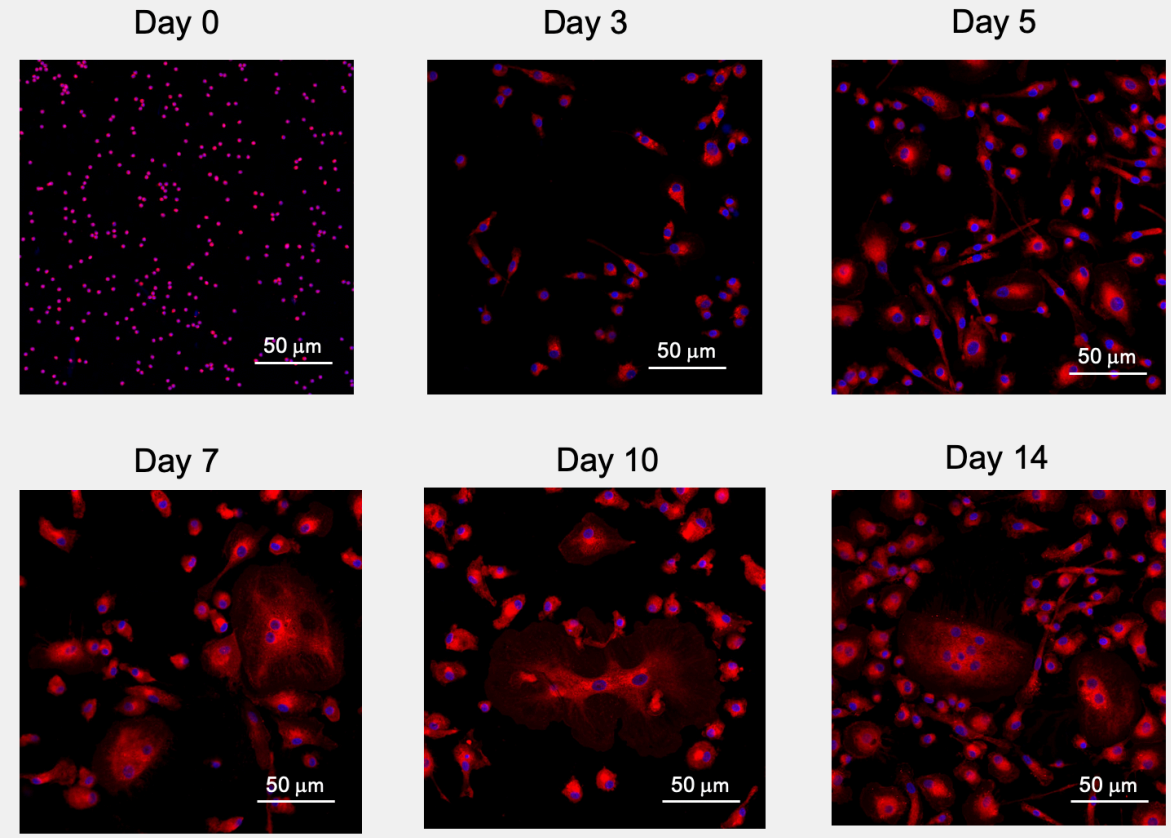

Appendix 9.6 Monocyte-derived osteoclasts differentiated with M-CSF and RANKL.

M-CSF and RANKL were used to drive the differentiation of monocytes isolated from healthy donors into osteoclasts. Confocal microscopy was used to determine the changes in morphology on day 0, 3, 7, 10, and 14. Nuclei were stained with Hoechst 33342 Solution and the plasma membrane was stained with CellMask™ Orange. Images were taken at X20 magnification. Representative images from n= 6 experiments.

Link to videos obtained from eSight RTCA:

https://swanseauniversity-my.sharepoint.com/:v:/g/personal/940266_swansea_ac_uk/ESbJCBrIAytNuB6kbPSI4fMBgoQUdK1XRNjRiFW26kAE5w?e=yCfgOr

Appendix 9.7 Monocyte-to-osteoclasts differentiation (100,000 cells). Video taken of osteoclast differentiation over 10/11 days using eSight RTCA

https://swanseauniversity-my.sharepoint.com/:v:/g/personal/940266_swansea_ac_uk/Ean107y9yeFJt1WlYBvJipMBJO1-UiIHeX2dO0UIFqck4w?e=ecOsHd

Appendix 9.8 Osteoclast differentiation in the presence of DMSO (VC) at 10μM. Video taken of osteoclast differentiation over 10/11 days using eSight RTCA

https://swanseauniversity-my.sharepoint.com/:v:/g/personal/940266_swansea_ac_uk/EYKg1ruXWw5Pnac8j9N8w60BvhgLnQeuvkebNQYYzec_sQ?e=KCm7Mk

Appendix 9.9 Osteoclast differentiation in the presence of lenalidomide at 10μM. Video taken of osteoclast differentiation over 10/11 days using eSight RTCA

https://swanseauniversity-my.sharepoint.com/:v:/g/personal/940266_swansea_ac_uk/EdVHGiQjQw1LoJzLzA2inqUBLx0x9K2XbXDVckDHSWn7nA?e=8hjUSc

Appendix 9.10 Osteoclast differentiation in the presence of pomalidomide at 10μM. Video taken of osteoclast differentiation over 10/11 days using eSight RTCA

https://swanseauniversity-my.sharepoint.com/:v:/g/personal/940266_swansea_ac_uk/EYjVb6iQUaJPoOfFZUHE7O4BdeGFGZ994B5OGs50MtJidQ?e=kryKeR

Appendix 9.11 Osteoclast differentiation in the presence of Thalidomide at 10μM. Video taken of osteoclast differentiation over 10/11 days using eSight RTCA